Application of the Moment Method to the Design of Slotted Waveguide Array Antennas

A.H.I. McCormick, M.Eng.

1988

Thesis submitted in fulfilment of the requirements for the degree of Doctor of Philosophy in the Department of Electrical and Electronic Engineering at Heriot-Watt University.

CONTENTS

LIST OF FIGURES

Figures are collected together at the end of each chapter.

Figure

LIST OF TABLES

8.4 Array Configuration Using Tuning Screws.

Acknowledgements

I would like to express my sincere thanks to Dr. A.J. Sangster for his guidance, encouragement and support throughout the course of this research. I would also like to thank Mr. D. Haldane and the staff of the departmental workshop, Mr. J. Tanner of Ferranti, Edinburgh Plc. for the care and effort he put into the near field measurements and my wife, Rona for assisting with the typing of this thesis. Finally, I wish to express my gratitude to the Science and Engineering Research Council for financing this research.

ABSTRACT

Slotted waveguide array antennas, which are widely used in radar systems, are becoming increasingly more amenable to computer aided design/synthesis procedures, since the scattering characteristics of a slot in a waveguide can be predicted to a high degree of accuracy. This thesis presents an improved theoretical CAD package to design arrays of this type. It differs from earlier such packages in that the reliance on measured data has been avoided with a theoretical technique termed the moment method being used to provide the self admittance data for the slots.

The efficient implementation of this package and in particular the incorporation of the moment method into it has been aided considerably by using this method to make a prior study of the nature of certain critical slot characteristics. Most of the more significant waveguide slot relationships have been discussed in the literature in one form or another except for those relating to slot width. A study employing the moment method has been carried out to eliminate this oversight and the functional relationship between this parameter and the slot resonance has been determined. The moment method solution has also been extended to permit the examination of round end slots, which are commonly used in practice, by developing a novel axial sectioning procedure.

The evolution of the computer aided array design package is described in some detail. The package has subsequently been employed to design array examples, one of which was constructed. The experimental and theoretical results for this antenna have been presented to

demonstrate the plausibility of this technique. Some less conventional array configurations have also been synthesised to demonstrate design flexibility.

CHAPTER 1

INTRODUCTION

Engineers have been familiar with the concept of a radiating slot in the wall of a waveguide for the last forty or so years and considerable effort has been directed towards solving the associated electromagnetic boundary value problem. Several analytical solutions have evolved with time, the sophistication of which have progressed concurrently with the advancements in computer technology. The availability of powerful, high speed computers has permitted more realistic mathematical models to be analysed and consequently, the accuracy of the theoretical solutions has improved. The moment method solution, which is presently the most accurate technique available, is capable of predicting to within experimental error (< 1%) the scattering characteristics of a slot of almost any length, located with little restriction in a waveguide wall of any thickness.

Antennas comprising of arrays of slots, appropriately positioned in the wall of a waveguide, are currently employed in both military and civilian microwave systems. This type of antenna has several advantages over the waveguide fed parabolic reflector antenna which dominated the market until the late 1950s. One of the main advantages is that the excitation distribution can readily be controlled over the array. Also, there is no problem with spillover or back radiation from the primary feed and the physical structure is more compact.

The task of designing slotted waveguide array antennas presents formidable analytical difficulties which have normally been overcome

by adopting certain simplifying assumptions. These simplifications have enabled antennas of this type to be designed with low side lobe levels, by employing accurately measured data for the self admittances of the individual slots, and by forming an equivalent dipole array, using Babinet's principle, to quantify the external mutual coupling. The internal mutual coupling is normally ignored as the effect is known to be negligible, as long as the height of the waveguide is not less than one quarter of its standard height. The reliance on measured data, however, restricts the array configurations which may be examined to those for which measured results exist. This restriction may be eased by incorporating an accurate analytical solution such as the moment method into the design procedure to provide theoretical self admittance data on the individual slots.

To accomplish a wholly theoretical design technique for tightly specified slotted waveguide antennas it is necessary, firstly to ensure that the analytical solution adopted is capable of accurately characterising a slot in a waveguide. Secondly, this solution must be incorporated into a synthesis program. This thesis represents a first attempt to do this. The moment method has been examined with a view to incorporating it into a design program for antennas of this type and considerable effort has been directed towards confirming that its theoretical predictions are of a sufficiently high standard (chapter 3). The analysis has also been extended to examine an axially sectioned slot with a view to improving the theoretical model to enable the effect of the round ends of the slots, which are actually used in practice, to be incorporated into the solution (chapter 4).

It is advantageous to have prior knowledge of the functional relationship between the slot characteristics and the dimensional parameters if a theoretical design procedure is to be implemented efficiently. These relationships have been comprehensively discussed in the literature with the exception of curiously the width parameter and therefore it was pertinent to examine this parameter. A study of the functional relationship between the slot width and the resonant behaviour of the slot has been carried out. The theoretical predictions obtained have been confirmed experimentally using an accurate waveguide bridge technique (chapters 4 & 5).

Once sufficient evidence had accrued to demonstrate clearly that the moment method solution was a suitable alternative to the measured data it was then incorporated into an array antenna design program (chapter 6). This procedure has been used to design various examples, one of which was constructed. Its radiation pattern has been examined on an accurate near field measurement system. The experimental and theoretical results, which have been presented, were used to assess the performance of the design approach (chapter 7). The flexibility of this procedure has also been examined and several less conventional array configurations were synthesised to demonstrate this (chapter 8).

CHAPTER 2

REVIEW OF THE LITERATURE

Slotted waveguide antennas have been topical in the literature since the 1940s and considerable effort has been directed towards developing efficient design/synthesis procedures. Inevitably, the procedures which evolved have been modified and refined over the intervening years, however, they still rely on measured data for the self admittance values of the individual slots in the array. This reliance on measured data restricts these techniques to examining array configurations for which measured results are available for the constituent slot radiators. In order to ease this restriction a synthesis procedure based on other than measured results is required. The obvious alternative is to theoretically evaluate the data and there are three predominant methods available for the analysis of apertures radiating through waveguide walls which may be used. These are the diffraction method originally propounded by Bethe [2.1], the variational method [2.2, 2.3, 2.4, 2.5] and the moment method [2.6, 2.7, 2.8]. The developments of these theoretical solutions have been comprehensively reviewed from the viewpoint of array synthesis in [2.9] and this is included in appendix 3. It is, however, worth re-examining briefly the development of these methods.

2.1 APERTURES IN INFINITE, THIN CONDUCTING SHEETS

The electromagnetic boundary value problem formed by an aperture in an infinite, thin conducting sheet is a prime slot radiation problem and it has been addressed by various investigators. Since the techniques which have arisen from these studies have often been applied to the slightly different problem of a slot radiating through

a waveguide wall, it is pertinent to consider the conducting screen case. However, our comments will be restricted to only a few of the more relevant papers and an exhaustive review of the literature has not been attempted here. The earliest paper on this subject dates back to the latter part of last century, when Lord Rayleigh [2.10] developed a theory for electrically small apertures. Around the same time, Kirchhoff presented an alternative theorem for large apertures (length > λ) and a good account of this is given by Stratton in [2.11]. However, Bethe [2.1] showed this solution to be in error as the boundary conditions were not satisfied on the conducting screen. He propounded an 'improved' solution which evaluated the scattering fields using the electric and magnetic dipole moments of the aperture. This method was capable of correctly predicting the far field radiation pattern of a short slot (length << λ). However, the predicted near field was incorrect and Bouwkamp [2.12] demonstrated this by showing the electric field to be discontinuous in the aperture due to an erroneous expression for the magnetic current density.

Levine and Schwinger [2.13] diversified and presented a solution based on the variational method to predict the fields scattered by an aperture in an infinite screen. This solution was capable of characterising slots with lengths up to and beyond resonance. An interesting graph was also presented in this paper which compared these techniques. This clearly demonstrated that the variational method was the only technique then available, which was capable of predicting acceptable results over the complete range of aperture sizes.

2.2 APERTURES RADIATING THROUGH WAVEGUIDE WALLS

The slotted waveguide antenna was initially developed during the Second World War for use in radar systems. Watson gives an interesting account of the early developments in [2.14] where extensive experimental investigations, to characterise a radiating slot in the wall of a waveguide, are reported. Stevenson published a theoretical solution based on Maxwell's equations in [2.15] which verified the results of these investigations. In this paper, which has been acknowledged as a classic in its field, he rigorously developed a set of equations for the conductance/resistance of a resonant slot in a waveguide.

Subsequently, these equations have been confirmed both experimentally and theoretically by Oliner in [2.3]. In this paper Oliner also extended the analysis to permit the impedance characteristics of non-resonant broadwall slots to be determined. His solution incorporated the work of several forerunners in the field, namely Marcuvitz and Schwinger [2.16] who addressed the problem of scattering from discontinuities in waveguides and Lewin [2.17] who examined slots radiating through the ends of waveguides. Equivalent circuits for the transverse, longitudinal and inclined slots were developed following the procedure described by Marcuvitz [2.18] and building on the variational solution detailed in [2.13]. Expressions to quantify the impedance values for each circuit were formulated using a sinusoidal trial function which modelled the field distribution in the slot.

The problem of the slot radiating through a waveguide wall which has finite thickness has also been addressed by Oliner and he modelled

this effect by considering the slot as a short transmission line in which only the TE_{10} mode was present. Experimental confirmation was produced by Oliner to demonstrate the effectiveness of this technique and his paper has been acknowledged as significantly advancing the slot antenna theory. It is worth pointing out that this solution is erroneous under certain conditions and this can be attributed to two main factors. Firstly, it was assumed that the slot would be positioned close to the centre of the waveguide and the Green's function was not summed for slots close to the side wall. Secondly, the effect of the slot thickness was dealt with in isolation and not included in the electromagnetic solution. However, in spite of these inadequacies, this solution has been universally employed to form the basis of analysis and synthesis of rectangular waveguide slot arrays. Consequently, it has with time been refined and extended to examine other slot arrangements. Larson and Powers [2.19] modified it to encompass dielectric filled waveguides, Bailey [2.20] used it to examine slots with dielectric coverings and Sangster and Hawkins [2.21, 2.4] extended it to characterise offset inclined slots.

An alternative variational solution was formulated by Das and Sanyal [2.5] using the reaction method [2.22] and the resulting predictions appear to be in slightly better agreement with experimental results, around resonance, than Oliner's results. This improvement can be attributed to the different trial function used to model the field in the slot.

The next major advancement in this field came in 1968 when Harrington [2.6] published his book 'Field Computation By Moment Methods', in which he detailed a moment method analysis of wire antennas. Vu Khac

and Carson [2.7, 2.23, 2.24, 2.25] have successfully applied this technique to the problem of apertures radiating through the waveguide wall. The effect of wall thickness was incorporated into the electromagnetic formulation of the problem and the resultant solution was capable of predicting slot characteristics which were in excellent agreement with experimental results. Vu Khac and Carson chose to adopt pulse basis functions to model the field distrubution in the slot instead of the conventional trignometric functions in this solution.

Lyon and Sangster [2.8] recognised the possibility of enhancing this solution by reverting back to trignometric basis functions and consequently, they developed a similar solution using sinusoidal basis functions. This solution was found to be computationally more efficient, with a single basis function reasonably emulating the field distribution in the slot compared to approximately 20 pulse functions and therefore this method avoided unnecessary manipulation of large matrices. The authors also extended the solution to characterise slots in bifurctated waveguide [2.26] and further work has been carried out to extend it to examine slots with dielectric coverings in [2.27].

Lyon and Hizal also pointed out in [2.27] that although the accuracy of the moment method predictions for slots was impressive, this could be improved upon by incorporating the effect of enhanced field strengths at the edges of the slot into the solution. This has been examined by various researchers; Stern and Elliott [2.28] presented both experimental and theoretical data for longitudinal shunt slots which demonstrated that the moment method can predict results

"comparable in accuracy to a carefully performed experiment" once this effect is incorporated into the solution. In this connection Park [2.29] also presents an interesting set of curves which shows moment method predictions with the edge enhancement included and excluded. An improvement of approximately 0.5% in accuracy for slots close to the waveguide centre line can be obtained.

While the analytical procedures for characterising slots in waveguides have progressed to the point were they can be realistically used in place of experimental results. The complexity exhibited by these techniques is such that a high power main frame computer is a pre-requisite if they are to be implemented. These solutions lost the simplicity of the earlier techniques which re-stimulated an interest in Bethe's [2.1] small aperture theorem around 1970. Consequently, effort was directed towards producing a simple closed form solution. Van Bladel [2.30, 2.31] developed equivalent circuits for various slots using Bethe's work and formulated closed form algebraic expressions to evaluate the component values. This enables small desk top computers to be used to characterise slots whose lengths are short with respect to a wavelength. Short slots are almost never used in practice and with this in mind Levy [2.32] extended the solution to characterise slots up to resonance. He also addressed, along with several other contributors, notably Cohn [2.33] and McDonald [2.34], the problem of evaluating the effect of finite wall thickness. The general approach has been to view the aperture as a short cut-off waveguide operating in its dominant mode (TE_{10}) and a correction factor has been introduced to compensate for this effect.

In a more recent paper Levy [2.35] highlights the fact that the condition of a uniform field across the aperture, which is strictly required by the small aperture solution, is not often satisfied and he formulated a set of correction factors which minimised this error by averaging the field over the aperture. The final modification to this method presently detailed in the literature adjusts the solution to satisfy the power conservation condition. This has been examined by both Collin [2.36] and Cheng [2.37] and correction factors are once again presented. Once all the modifications mentioned above have been incorporated into the analysis, this method may be employed to provide fast, reasonably accurate predictions of the slot characteristics up to resonance.

2.3 SLOTTED WAVEGUIDE ANTENNAS

The slotted waveguide antenna was first introduced by Watson [2.14] some 45 years ago and since then considerable attention has been paid to developing efficient design techniques. There are two physical considerations which must be taken account of in the design of an antenna of this type. Firstly, the amplitude and phase of the excitation distribution across the array must be determined for the desired far field pattern. Secondly, the physical array configuration must be such to correctly excite each slot in the array. The latter condition is inherently more difficult to satisfy. Before examining the methods available to accomplish this, it is worth mentioning some of the techniques available to evaluate the excitation distribution of an array.

The far field pattern of an antenna is usually characterised by an array factor which relates the radiation pattern to the excitations

of the individual elements in the array. This factor may readily be developed using vector algebra, however Schelkunoff [2.38] recognised that the vector format was not very convenient for design work and he developed an alternative solution which is almost always adopted in array design work. This solution converts the vector form of the array factor to a polynomial using Z transforms and the far field pattern can be shaped, with individual side lobes and/or groups of side lobes being raised or lowered, by appropriately positioning the roots of the polynomial in the complex Z plane. Perturbation techniques can readily be employed to correctly position the appropriate number of roots (zeros) to generate almost any desired far field pattern. Unfortunately, the excitation distributions cannot always be realised by slotted waveguide antennas due to the interdependence between the slot excitations and the physical array configuration. For example, the phase shift between slots is dependent on their position relative to each other, whereas, restrictions of this type do not occur for elements which can be fed independently. There are, however, at least three classical solutions detailed in the literature that are commonly employed for slotted waveguide antennas which should be mentioned.

Dolph recognised that the Chebyshev polynomial was ideally suited to generate a pattern with side lobes equal in magnitude and consequently, he developed a set of relationships in [2.39] to determine the root positions. This solution has been examined by many investigators in the intervening years and a number of revised algorithms based on Dolph's work have evolved [2.40, 2.41, 2.42, 2.43, 2.44, 2.45, 2.46, 2.47, 2.48].

The most significant extension of Dolph's solution was reported by Taylor [2.49] where it was adapted for continuous distributions. Taylor also slightly modified the solution to cause the outer side lobes to decay as a function of angular displacement from the main beam as he recognised the possibility of singularities in the Dolph solution. This solution may also be used to design arrays with discrete excitation distributions using a sampling technique.

The third solution to be mentioned is often employed in radar antennas to compensate range with elevation. It was developed by Woodward [2.50] and it shapes the pattern by filling in the nulls. This was achieved by superimposing a family of patterns so that the main beam of each successive partial pattern occurred at the first null of the preceding pattern. The heights of the main beams of each partial pattern were controlled to shape the pattern in accordance with the specification. This solution has also received considerable attention over the last 40 or so years due to its radar application and various refinements have been detailed in the literature [2.51, 2.52, 2.53, 2.54, 2.55, 2.56, 2.57].

There are numerous other solutions available in the literature, however, these are generally limited in their application as they have usually been formulated to solve specific problems. For example, Tsunoda and Goto [2.58] have presented a solution which employs resonant slots and adjusts the slot separation to correct the phase of the excitations. No attempt has been made to review these algorithms in this section.

Once the appropriate radiation pattern has been selected and the excitations of the elements in the array have been evaluated then the physical array configuration must be determined. Various investigators have examined this problem and, as mentioned previously, Watson was one of the earliest pioneer workers in this field. He addressed this problem in [2.14] and demonstrated experimentally the viability of employing slotted waveguides as antennas. In this paper both the resonant and travelling wave arrays were examined and procedures were developed for the design of these arrays with the additional option of either transverse or axial polarisation using longitudinal shunt slots or inclined sidewall slots respectively. Stevenson also briefly addressed this problem in [2.15] where he formulated expressions to evaluate the slot excitations in terms of the incident wave in the guide.

An interesting lecture was given by Fry [2.59] in 1946 which drew together much of the preceding work on slotted waveguide linear arrays. In this the implications of designing arrays of the type detailed by Watson were discussed and the concept of 'incremental conductance' was introduced. This is a conductance function which is evaluated experimentally in terms of both the slot separation and the slot inclination to compensate for the mutual coupling between edge slots. No such function was required for arrays comprising of longitudinal shunt slots as the mutual coupling is considerably less significant in this case.

At about the same time the literature suggests that attention was now being directed towards formulating efficient design procedures for slotted arrays and Kaminow and Stegen [2.60] developed solutions for

both resonant and non-resonant (travelling wave) arrays. While the design procedure for the resonant array was not too dissimilar to Watson's, that for the travelling wave array was much more complex with transmission line theory being employed to incorporate the reflection of each slot into the solution. Dion [2.61] developed a similar solution for a travelling wave array, which differed from reference [2.60] in that he assumed the coupling for each slot was small and therefore the array could be considered to be matched at every point. He demonstrated the validity of this simplifying assumption by using his method to design a 20 element array. This was constructed and the radiated pattern was found to be in reasonable agreement with the theoretical prediction. Dion also pointed out the need to control the spacing between slots to suppress second order beams and he formulated some relationships to determine the maximum spacing before these beams appeared.

The procedures outlined above have adopted the simplifying assumption that the mutual coupling between slots can be ignored. This enables them to be readily implemented to obtain array designs as long as the self admittance data for the individual slots is available. In this connection Jasik [2.62] has published an invaluable set of tables of self admittance data for a variety of slot displacements and frequencies. Crompton and Collin [2.63] have also examined the topic of slotted waveguide antennas, along with Brady [2.64] and interesting accounts of the relevant work have been elegantly drawn together and summarised in these extended texts.

During this period considerable effort has also been directed towards quantifying the mutual coupling between slots and three methods have

evolved to evaluate this. The periodic structure solution [2.65, 2.66], which is usually employed to characterise essentially infinite arrays, utilises the periodicity of the array and splits the array into unit cells. The complete admittance characteristics of the cell are then calculated and consequently, the mutual coupling is automatically taken into account. Vu Khac [2.7] developed an alternative solution which is more suited to slotted waveguide arrays. This is based on the moment method and evaluates the array problem as a single electromagnetic problem. This provides extremely accurate results, unfortunately, due to the excessive computational requirements it is presently impractical to implement this solution. An element by element solution is also available which is currently adopted in the design of most slotted waveguide arrays. This solution examines the mutual coupling for each element in the array separately and then applies superposition to determine the overall effect.

Initially, an experimental investigation was carried out by Ehrlich and Short [2.67] to examine the external mutual coupling between longitudinal slots and this indicated that this effect was comparable to that of waveguide tolerancing errors. The authors, therefore, concluded that the mutual coupling may be ignored in the design of linear arrays, of reasonable length, for side lobes set as low as -30 dBs. Kay and Simmons [2.68] also addressed this problem and they presented expressions for both internal and external mutual coupling between longitudinal slots radiating through the broadwall of a rectangular waveguide. The internal mutual effect was shown to be negligible in full height waveguide provided the slot separation was of the order of $\lambda_g/2$. It was sufficient to consider only the

external mutual coupling in the design of linear arrays even for arrays with the side lobe levels set lower than -30 dBs. Elliott [2.69] in a recent publication confirmed the findings on the internal mutual coupling and formulated expressions to evaluate the coupling due to the TE_{20} mode. The results presented show that the internal coupling can be neglected, unless the waveguide height is reduced to approximately one quarter of its standard height. An interesting pictorial representation has been presented in [2.70] which helps to enunciate clearly the relationship between the various scattering components of slots in an array environment.

The techniques mentioned so far to evaluate the mutual coupling are restricted in their application to resonant slots and therefore, they are not often employed in array design work. Instead Babinet's principle [2.71] is used to determine the coupling between slots by initially evaluating the equivalent mutual impedance between dipoles and then relating this to the slots. The initial investigations carried out to quantify the coupling between radiating dipoles date back to the work of Carter [2.72] in 1932 when he formulated an expression to characterise the mutual impedance between two dipoles. Since then this has been extended by several authors [2.73, 2.74, 2.75] to examine more complex configurations and consequently, the complexity of the equations has also increased. Baker and Lagrone [2.76] recognised that the introduction of numerical integration into the solution would considerably simplify the mathematics of the equations. Consequently, they formulated two relatively simple expressions to evaluate the mutual coupling and these are still currently used. Various investigators have examined this solution

and developed computationally more efficient algorithms [2.77, 2.78] to help minimise the processing requirements.

The next significant advance in this field came in 1978 when Elliott and Kurtz [2.79] presented a design procedure for slotted waveguide arrays which incorporated the external mutual coupling. This technique employed an equivalent dipole array to evaluate the mutual coupling along with Babinet's principle to transform these to equivalent slot values. It should be noted that this technique still relies on measured self admittance data to obtain a successful design. Elliott [2.80] extended the procedure to design travelling wave arrays in the following year and he presented a 21 element example designed by this routine. This was constructed and the experimental results were found to be in reasonable agreement with theory. In 1983 the dependence on the equivalent dipole array was removed and Elliott [2.81] presented a new 'improved technique' for the design of resonant arrays. The expression for the mutual coupling between slots was developed using a sinusoidal distribution to correctly model the field in the slot, resulting in a more complex solution involving a double integral compared to the previous dipole solution which required only a single integration. Malherbe and Davidson [2.82] recognised this and developed a correction factor to adjust Baker and Lagrone's work to provide results of similar accuracy while avoiding the complexity of the solution advocated by Elliott.

2.4 CONCLUSION

The electromagnetic boundary problem formed by a slot radiating through the wall of a waveguide has received considerable attention

in the literature, since introduction of slotted waveguide antennas during the Second World War. The sophistication of the analytical techniques to solve this problem have progressed concurrently with the advancements in computer technology. The availability of powerful computers has permitted more complex mathematical techniques to be adopted which has enabled more realistic models to be analysed. These have progressed to the point where the moment method is capable of accurately predicting experimental results, for commonly used slot examples.

Various techniques have also evolved over the years to design slotted waveguide array antennas. These procedures, however, have not advanced to the same extent as the single slot solutions. Presently they rely on accurately measured data for the self admittance of the individual slots and an equivalent dipole array to evaluate the mutual coupling between slots. Little or no effort appears to have been directed towards incorporating the accurate analytical solutions for slots into the design procedures. This can be attributed to the need to achieve practical processor times on presently available computing facilities.

CHAPTER 3

MOMENT METHOD ANALYSIS OF APERTURES IN RECTANGULAR WAVEGUIDE

The sophistication of the analytical techniques employed to solve the electromagnetic boundary value problem formed by radiating apertures in rectangular waveguide has progressed concurrently with advancements of computer technology. The availability of high speed main frame computers has permitted increasingly more complex mathematical techniques to be introduced, enabling more realistic models to be analysed. For example, the moment method can predict with some accuracy the behaviour of a slot of any length, located with little restriction, in a wall of any thickness. This technique basically reduces the electromagnetic scattering problem to a pair of simultaneous integral equations which can be arranged in matrix form and then solved by known techniques.

In this chapter it is convenient to restate the development of the moment method solutions for both the longitudinal and transverse slots, located in the broadwall of rectangular waveguides. However, it will suffice, to simply quote many of the results without reproducing the complex mathematics, as the technique is well documented in the literature [2.6, 2.7, 2.8, 2.27, 3.1].

3.1 FORMULATION OF THE INTEGRAL EQUATIONS

A diagram of the co-ordinate system used is illustrated in Figure (3.1) with an expanded view of the slot in Figure (3.2). For clarity the waveguide is designated region a, the slot region b and the half-space region c. The fields in regions a, b and c are ($\underline{E}_a + \underline{E}_i$, $\underline{H}_a + \underline{H}_i$), ($\underline{E}_b$, $\underline{H}_b$) and ($\underline{E}_c$, $\underline{H}_c$) respectively, where $\underline{E}_i$ and $\underline{H}_i$ are the

incident fields in the waveguide when the aperture is short-circuited. To satisfy the boundary conditions we require that, the tangential electric field is continuous over the upper and lower surfaces of the aperture (S′ and S):

$$\hat{\underline{n}} \times (\underline{E}_a - \underline{E}_b) = o \quad \text{on } S \tag{3.1a}$$

because

$$\hat{\underline{n}} \times \underline{E}_i = o \quad \text{here. Also}$$

$$\hat{\underline{n}}' \times (\underline{E}_c - \underline{E}_b) = o \quad \text{on } S' \tag{3.1b}$$

Applying the field equivalence principle, it is possible to replace an aperture by a short-circuit with a magnetic current $(\hat{\underline{n}} \times \underline{E})$ and $-(\hat{\underline{n}} \times \underline{E})$ on its upper and lower surfaces, respectively [2.3]. This converts the slotted waveguide problem into one comprising three connected regions, with known characteristics (waveguide, cavity and halfspace), which are excited by unknown currents at the position of the slot.

The tangential magnetic field must also be continuous so

$$\hat{\underline{n}} \times (\underline{H}_i + \underline{H}_a) = \hat{\underline{n}} \times \underline{H}_b \text{ on } S \tag{3.2a}$$

$$\hat{\underline{n}}' \times \underline{H}_c = \hat{\underline{n}}' \times \underline{H}_b \quad \text{on } S' \tag{3.2b}$$

and the fields must obey Maxwell's equations

$$\nabla \times \underline{E} = -j\omega\mu_o \underline{H} - \underline{J}_m$$

$$\nabla \times \underline{H} = j\omega\varepsilon_o \underline{E} \tag{3.3}$$

consequently, they also obey the wave equation

$$\nabla \times \nabla \times \underline{H} - k^2 \underline{H} = -j\omega\varepsilon_o \underline{J}_m \tag{3.4}$$

with $\hat{\underline{n}} \times \nabla \times \underline{H} = o$ on perfectly conducting surfaces.

If a Green's function $\underset{\sim}{G}(\underline{r}/\underline{r}_o)$, which satisfied the following equation:

$$\nabla \times \nabla \times \underset{\sim}{G}(\underline{r}/\underline{r}_o) - k^2 \underset{\sim}{G}(\underline{r}/\underline{r}_o) = - \underset{\sim}{I}\delta(\underline{r}/\underline{r}_o) \tag{3.5}$$

and the boundary condition $\hat{\underline{n}} \times \nabla \times \underset{\sim}{G}(\underline{r}/\underline{r}_o) = o$ on perfectly conducting surfaces, is introduced, it is possible to calculate the magnetic field in each region from [2.63]

$$\underline{H}(\underline{r}) = j\omega\varepsilon_o \iint_S \underset{\sim}{G}(\underline{r}/\underline{r}_o) \cdot \underline{J}_m(\underline{r}_o)\, dS_o \tag{3.6}$$

where $\underline{J}_m(\underline{r}_o)$ is a magnetic surface current.

Incorporating equation (3.6) into equation (3.2) results in a pair of simultaneous integral equations for $\hat{\underline{n}} \times \underline{E}$ and $\hat{\underline{n}}' \times \underline{E}'$

$$\hat{\underline{n}} \times \underline{H}_i(\underline{r}) = j\omega\varepsilon_o \hat{\underline{n}} \times \iint_S \{\underset{\sim}{G}_a(\underline{r}/\underline{r}_o) + \underset{\sim}{G}_b(\underline{r}/\underline{r}_o)\} \cdot$$

$$\{\hat{\underline{n}} \times \underline{E}(\underline{r}_o)\}dS_o + j\omega\varepsilon_o \hat{\underline{n}} \times \iint_{S'} \underset{\sim}{G}_b(\underline{r}/\underline{r}_o) \cdot$$

$$\{\hat{\underline{n}}' \times \underline{E}'(\underline{r}_o)\}dS_o \quad (\underline{r} \text{ on } S) \tag{3.7a}$$

$$0 = j\omega\varepsilon_o \hat{\underline{n}}' \times \iint_{S'} \{\underset{\sim}{G}_b(\underline{r}/\underline{r}_o) + \underset{\sim}{G}_c(\underline{r}/\underline{r}_o)\} \cdot$$

$$\{\hat{\underline{n}}' \times \underline{E}'(\underline{r}_o)\}dS_o + j\omega\varepsilon_o \hat{\underline{n}}' \times \iint_S \underset{\sim}{G}_b(\underline{r}/\underline{r}_o) \cdot$$

$$\{\hat{\underline{n}} \times \underline{E}(\underline{r}_o)\}dS_o \quad (\underline{r} \text{ on } S') \tag{3.7b}$$

where $\underset{\sim}{G}_{a,b,c}$ are the dyadic Green's function of the regions a, b and c respectively.

3.2 IMPLEMENTATION OF THE MOMENT METHOD

It is evident from the complexity of equations (3.7a and b) that they cannot be solved directly and an approximate mathematical procedure must be used. In the past variational techniques [2.3, 2.4, 2.5, 2.21] have been employed to solve such integral equations. These methods can predict reasonably accurately the scattering characteristics of slots radiating through waveguide walls of zero thickness for lengths up to and beyond resonance. However, the accuracy is limited somewhat as it is difficult to incorporate the effect of the finite slot thickness into these solutions. Therefore,

the method of moments [2.6] has been adopted which naturally incorporates this effect into the electromagnetic solution. It also has the added advantage that it may be applied directly to the integral equations without any rearrangement being required.

To enunciate this technique, consider the equation

$$Lf = g \tag{3.8}$$

where L is a known operator, g is a known function and f is the function to be determined. If f is approximated by a series of basis functions in the domain of L, as

$$f = \sum_{s=1}^{N} a_s f_s \tag{3.9}$$

it follows that

$$\sum_{s=1}^{N} a_s Lf_s = g \tag{3.10}$$

This may be converted into matrix form by defining a set of testing functions, h_1, h_2 ..... h_n, and taking a suitable inner product with each h_i.

$$\text{Hence } \sum_{s=1}^{N} A_s \langle h_i, Lf_s \rangle = \langle h_i, g \rangle \qquad i = 1, 2, 3 ..... N \tag{3.11}$$

which is equivalent to

$$[l_{is}]\ [a_s] = [g_i]$$

where $[l_{is}] =$

$$\begin{bmatrix} \langle h_1, Lf_2\rangle & \langle h_1, Lf_2\rangle & . & . & . & . \\ \langle h_2, Lf_2\rangle & \langle h_2, Lf_2\rangle & . & . & . & . \\ . & . & & & & \\ . & . & & & & \\ . & . & & & & \end{bmatrix}$$

$$[a_s] = \begin{bmatrix} a_1 \\ a_2 \\ . \\ . \\ . \end{bmatrix} \qquad [g_i] = \begin{bmatrix} \langle h_1, g\rangle \\ \langle h_2, g\rangle \\ . \\ . \\ . \end{bmatrix}$$

The basis and testing functions are chosen either as a good approximation to the solution or to reduce the matrix to a form which is easily solved.

In previous work on apertures in waveguide, trignometric basis functions have invariably proved to be computationally more efficient than pulse basis functions. A single sinusoidal function emulates

reasonably accurately the field distrubution in the slot, whereas approximately 20 pulse functions, using point matching, are required to model this. Consequently, we have chosen to proceed using sinusoidal basis functions to avoid unnecessary manipulation of large matrices. Referring to the slot co-ordinate system we therefore let

$$\hat{\underline{n}} \times \underline{E} = \hat{\underline{n}} \times \sum_{s=1}^{N} a_s f_s \hat{\underline{a}}_\eta \quad \text{on } S \tag{3.12}$$

and

$$\hat{\underline{n}}' \times \underline{E}' = \hat{\underline{n}}' \times \sum_{s=1}^{N} b_s f_s' \hat{\underline{a}}_\eta \text{ on } S' \tag{3.13}$$

where

$$f_s(\xi) = f_s'(\xi) = \sin \frac{s\pi(\xi + \frac{L}{2})}{L} \tag{3.14}$$

The method also requires the definition of a set of testing functions and an inner product. A considerable amount of work has been carried out on the evaluation of integral expressions of the type encountered in aperture problems [2.3], and, in order to build on this, the inner product chosen is

$$\iint_{S \text{ or } S'} p.q \, dS \tag{3.15}$$

and the testing functions will be of the same type as the basis functions, namely

$$f_i(\xi)\hat{\underline{a}}_\eta \qquad i = 1,2,3,\ldots\ldots, N \tag{3.16}$$

as in Galerkin's method [3.2, 3.3]. The procedure converts the integral equations into a matrix of the form

$$\begin{bmatrix} [A] & [C] \\ [D] & [B] \end{bmatrix} \begin{bmatrix} [a] \\ [b] \end{bmatrix} = \begin{bmatrix} [h] \\ [o] \end{bmatrix} \tag{3.17}$$

where

$$A_{i,s} = -j\omega\varepsilon_o \iint_S f_i \hat{\underline{a}}_\eta \cdot \{\hat{\underline{n}} \times \iint_S [\underset{\sim}{G}_a(\underline{r}/\underline{r}_o) + \underset{\sim}{G}_b(\underline{r}/\underline{r}_o)] \cdot f_s \hat{\underline{a}}_\xi \, dS_o\} \, dS \tag{3.18a}$$

$$B_{i,s} = -j\omega\varepsilon_o \iint_{S'} f'_i \hat{\underline{a}}_\eta \cdot \{\hat{\underline{n}}' \times \iint_{S'} [\underset{\sim}{G}_b(\underline{r}/\underline{r}_o) + \underset{\sim}{G}_c(\underline{r}/\underline{r}_o)] \cdot f'_s \hat{\underline{a}}_\xi \, dS_o\} \, dS \tag{3.18b}$$

$$C_{i,s} = j\omega\varepsilon_o \iint_S f'_i \hat{\underline{a}}_\eta \cdot \{\hat{\underline{n}} \times \iint_{S'} \underset{\sim}{G}_b(\underline{r}/\underline{r}_o) \cdot f_s \hat{\underline{a}}_\xi \, dS_o\} \, dS \tag{3.18c}$$

$$D_{i,s} = j\omega\varepsilon_o \iint_{S'} f_i \hat{\underline{a}}_\eta \cdot \{\hat{\underline{n}} \times \iint_S \underset{\sim}{G}_b(\underline{r}/\underline{r}_o) \cdot f'_s \hat{\underline{a}}_\xi \, dS_o\} \, dS \tag{3.18d}$$

$$h_i = - \iint_S f_i \hat{\underline{a}}_\eta \cdot \{\hat{\underline{n}} \times \underline{H}_i(r)\} \, dS \tag{3.18e}$$

When the integrals above have been evaluated and the matrix solved, the scattering parameters of the slot in question can be determined. The Green's function required (waveguide, cavity and halfspace) may be written down without difficulty.

3.3 EVALUATION OF THE MATRIX TERMS

The integrals in equation (3.18) have been rigorously evaluated in [3.1] and the mathematics is comprehensively documented there. Therefore the results will simply be quoted for completeness. However, a more detailed explanation of the significance of the ψ = constant mode (ψ mode) will be given as this mode was omitted from Lyon's solution.

The solution will be separated into the four components ie region a, b, c and the incident field, and the contribution of each component will be considered in turn.

3.3.1 FREE SPACE

The first region to be considered is free space and the Green's function is reproduced below [2.63]

$$\underset{\sim}{G}_c(\underline{r}/\underline{r}_o) = -\left(\underset{\sim}{I} + \frac{\nabla\nabla}{k^2}\right)\frac{e^{-jk|\underline{r}-\underline{r}_o|}}{2\pi|\underline{r}-\underline{r}_o|} \qquad (3.19)$$

On substituting this into equation (3.18b) the expression to be evaluated takes the form

$$j\omega\varepsilon_o \iint_{S'} f_i \iint_{S'} \left(1 + \frac{1}{k^2}\frac{d^2}{d\xi^2}\right)\frac{e^{-jk|\underline{r}-\underline{r}_o|}}{2\pi|\underline{r}-\underline{r}_o|}\, f_s\, dS_o\, dS \qquad (3.20)$$

The solution to the above expression naturally divides into two parts and the term relating to the imaginary component of the Green's function is as follows:

$$\frac{2W^2}{Z_o\lambda} \sum_{n=1}^{\infty} \sum_{p=1}^{n} \sum_{q=1}^{n-p+1} \frac{(-1)^{(n+p+q+2)_k} (2n-1)_L^{2n}}{(i\pi)^{2q-1} (S\pi)^{2p-1} (2n+1)}$$

$$\times \frac{[(-1)^i + (-1)^s - \delta_{q,\ n-p+1}\ ((-1)^{i+s} + 1)]}{(2n-1)\ (2n-2p-2q+2)!} \qquad (3.21)$$

The second component due to the real part of the Green's function results in a more complicated expression which is reproduced below:

$$\frac{j\omega\varepsilon_o}{4\pi k^2} \int_0^L \left\{ \begin{array}{l} \left(-\frac{1}{2}\ (1+(-1)^{(s-i)})\ \left(P_{is}((-1)^{(i-s)} \sin\frac{i\pi\Lambda}{L} - \sin\frac{s\pi\Lambda}{L}\right)\right. \\ \qquad \left[2\left(k^2 - \left(\frac{i\pi}{L}\right)^2\ (L-\Lambda)\ \cos\frac{i\pi\Lambda}{L}\right.\right. \\ \left.\left. -Q_{is}\ ((-1)^{(i+s)}\ \sin\frac{i\pi\Lambda}{L} + \sin\frac{s\pi\Lambda}{L})\right)\right] \end{array} \right\} \left\{ \begin{array}{l} (i \neq s) \\ (i = s) \end{array} \right.$$

$$\times \left(2W\ \left(\ln\ \left(W + (\Lambda^2 + W^2)^{\frac{1}{2}}\right) - \psi\ (\Lambda)\right)\right. \qquad (3.22)$$

$$\left. + \frac{2}{k}\ (\sin k\Lambda - \sin k\ (\Lambda^2 + W^2)^{\frac{1}{2}})\right) d\Lambda$$

$$+ \frac{j\omega\varepsilon_o W}{2\pi k^2}\ [(-1)^{(i-s)}\ \Delta_{is}\ ((P_{is} - Q_{is})(-1)^{(i-s)} \int_0^L \sin\frac{i\pi\Lambda}{L}\ \ln(\Lambda)\, d\Lambda$$

$$- (P_{is} + Q_{is}) \int_0^L \sin\frac{s\pi\Lambda}{L} \ln(\Lambda) d\Lambda) - 2\,\delta_{is}\,((\frac{L}{i\pi})^2\,(1-(-1)^i)$$

$$- \frac{L^2}{i\pi} si(i\pi) + (\frac{L}{i\pi}) \int_0^L \sin\frac{i\pi\Lambda}{L} \ln(\Lambda) d\Lambda)\,(k^2 - (\frac{i\pi}{L})^2)\,]$$

where

$$\Delta_{is} = \begin{cases} 0 & (i-s)\ \text{odd} \\ 1 & (i-s)\ \text{even} \end{cases} \tag{3.23}$$

$$\psi(\Lambda) = \int_0^W \frac{1 - \cos k\,(\Lambda^2+\sigma^2)^{\frac{1}{2}}\,d\sigma}{(\Lambda^2+\sigma^2)^{\frac{1}{2}}} \tag{3.24}$$

$$P_{is} = \begin{cases} k^2 - (si)\,(\frac{\pi}{L})^2\,\frac{2L}{\pi(i-s)} & i\neq s \\ 0 & i=s \end{cases} \tag{3.25}$$

$$Q_{is} = (k^2 + si\,(\frac{\pi}{L})^2)\,(\frac{2L}{\pi(i+s)}) \tag{3.26}$$

$$si(K) = \int_0^K \frac{\sin u}{u}\,du \tag{3.27}$$

3.3.2 CAVITY

The fields coupling to the surfaces of the slot due to the currents within the cavity contribute to each of the sub-matrices A, B, C and D. The integrals involved in evaluating these terms require the ξ component of the Green's function for the cavity, which is as follows:

$$\underset{\sim}{G}_b^{\xi\xi} = \sum_{l=o}^{\infty} \sum_{m=o}^{\infty} \sum_{n=o}^{\infty} \frac{\varepsilon_{lo}\, \varepsilon_{mo}\, \varepsilon_{no}}{WLT\ (k^2_{lmn} - k^2)} \left(\left(\frac{n\pi}{kL}\right)^2 - 1\right)$$

$$\times \cos \frac{l\pi(\eta + \frac{W}{2})}{W} \cos \frac{l\pi(\eta_o + \frac{W}{2})}{W} \cos \frac{m\pi(\zeta + T)}{T} \cos \frac{m\pi(\zeta_o + T)}{T}$$

$$\times \sin \frac{n\pi(\xi + \frac{L}{2})}{L} \sin \frac{n\pi(\xi_o + \frac{L}{2})}{L} \qquad (3.28)$$

where

$$k^2_{lmn} = \left(\frac{l\pi}{W}\right)^2 + \left(\frac{m\pi}{T}\right)^2 + \left(\frac{n\pi}{L}\right)^2 \qquad (3.29)$$

This may be simplified with a little mathematical manipulation and the application of the result quoted by Collin's [3.4]

$$\sum_{m=o}^{\infty} \frac{\varepsilon_{mo} \cos mx}{m^2 - a^2} = -\frac{\pi \cos (x-\pi)a}{a \sin \pi a} \quad \text{for } o \le x \le 2\pi \qquad (3.30)$$

to the following double summation

$$\underset{\sim}{G}_b^{\xi\xi}(\underline{r}/\underline{r}_o) = \sum_{l=o}^{\infty} \sum_{n=o}^{\infty} \frac{\varepsilon_{lo}\, \varepsilon_{no}}{WL} \cos \frac{l\pi(\eta + \frac{W}{2})}{W} \cos \frac{l\pi(\eta_o + \frac{W}{2})}{W}$$

$$\times \sin \frac{n\pi(\xi + \frac{L}{2})}{L} \sin \frac{n\pi(\xi_o + \frac{L}{2})}{L} \frac{(1 - (\frac{n\pi}{kL})^2)}{k_g \sin k_g T}$$

$$\times \begin{cases} \cos k_g\zeta \cos k_g(\zeta_o + T) \\ \cos k_g(\zeta + T) \cos k_g\zeta_o \end{cases} \quad \zeta \gtrless \zeta_o \qquad (3.31)$$

where

$$k_g^2 = k^2 - \left(\frac{i\pi}{L}\right)^2 \qquad (3.32)$$

The self coupling and mutual coupling terms for the sub-matrices can now be determined by substituting equation (3.31) into equation (3.18) and evaluating the integrals.

The self coupling expression for the lower surface of the slots, which appears in $A_{i,s}$ can be reduced to

$$j \frac{WL}{2} \frac{1}{kZ_o T} \frac{k_g T}{\tan k_g T} \delta_{is} \qquad (3.33a)$$

and similarly the expression for the self coupling of the upper surface (equation (3.18b)) is

$$- j \frac{WL}{2} \frac{1}{kZ_o T} \frac{k_g T}{\tan k_g T} \delta_{is} \qquad (3.33b)$$

The mutual coupling term $C_{i,\,s}$ and $D_{i,\,s}$ were also evaluated to give

$$C_{i,\,s} = - D_{i,\,s} = - j \frac{WL}{2} \frac{1}{kZ_o T} \frac{k_g T}{\sin k_g T} \delta_{is} \qquad (3.33c)$$

3.3.3 WAVEGUIDE

The general integral equation (3.7) permits any slot orientations to be analysed. However, this involves integration of more than one

component of the waveguide Green's function and each component comprises of a double infinite summation. Therefore, the analysis has been restricted to the transverse and longitudinal slots.

3.3.3a THE TRANSVERSE SLOT

The component of the waveguide Green's function required in equation (3.18a) for the transverse slot is given by

$$\underset{\sim}{G}_a^{xx}(\underline{r}/\underline{r}_o) = \frac{1}{2j\omega\varepsilon_o} \sum_{n=1}^{\infty}\sum_{m=1}^{\infty} e^{-\Gamma_{nm}|z - z_o|} B_{nm}^2 \left(\frac{m\pi}{b}\right)^2 (\omega\varepsilon_o)^2$$

$$\times \sin\frac{n\pi x}{a} \sin\frac{n\pi x_o}{a} \cos\frac{m\pi y}{b} \cos\frac{m\pi y_o}{b} \qquad (3.34)$$

$$- \sum_{n=o}^{\infty}\sum_{m=o}^{\infty} e^{-\Gamma_{nm}|z - z_o|} A_{nm}^2 \Gamma_{nm}^2 \left(\frac{n\pi}{a}\right)^2$$

$$n\neq m=o$$

$$\times \sin\frac{n\pi x}{a} \sin\frac{n\pi x_o}{a} \cos\frac{m\pi y}{b} \cos\frac{m\pi y_o}{b}$$

where

$$A_{nm}^2 = \frac{\varepsilon_{on}\,\varepsilon_{om}}{j\omega\mu_o\,\Gamma_{nm}\,k^2\,ab} \qquad (3.35a)$$

$$B_{nm}^2 = \frac{4}{j\omega\varepsilon_o\,\Gamma_{nm}\,k^2\,ab} \qquad (3.35b)$$

$$k^2 = \left(\frac{n\pi}{a}\right)^2 + \left(\frac{m\pi}{b}\right)^2 \qquad (3.35c)$$

and when this is substituted into equation (3.18a) and evaluated the expression reduces to:

$$\frac{2j\omega\varepsilon_o}{k^2 ab} \sum_{n=1}^{\infty} \sigma(i,n)\sigma(s,n)\left(U_n W + \frac{e^{-\Gamma_{no}W} - 1}{\Gamma_{no}} + 2\Gamma_{no}^2\right.$$

$$\left. \times \left\{\left(\frac{b}{\pi}\right)^3 \left(\frac{1}{2}\frac{j}{\rho_n^3} + \frac{1}{\rho_n^2}\right) + \sum_{m=1}^{\infty} \frac{e^{-\Gamma_{nm}W}}{\Gamma_{nm}^3}\right\}\right) \qquad (3.36)$$

where

$$\sigma(i,n) = \begin{cases} \begin{cases} \dfrac{2L}{i\pi}\dfrac{1}{\alpha^2-1}\sin\dfrac{\alpha i\pi}{2}\cos\dfrac{n\pi x_1}{a} & \alpha \neq 1 \\ \dfrac{L}{2}(-1)^{i/2}\cos\dfrac{n\pi x_1}{a} & \alpha = 1 \end{cases} & i \text{ even} \\ \begin{cases} \dfrac{2L}{i\pi}\dfrac{1}{1-\alpha^2}\cos\dfrac{\alpha i\pi}{2}\sin\dfrac{n\pi x_1}{a} & \alpha \neq 1 \\ \dfrac{L}{2}(-1)^{\frac{i-2}{2}}\sin\dfrac{n\pi x_1}{a} & \alpha = 1 \end{cases} & i \text{ odd} \end{cases} \qquad (3.37)$$

and $$\alpha = \frac{nL}{ia} \qquad (3.38)$$

$$U_n = \begin{cases} \dfrac{\pi\rho_n \cos \pi\rho_n}{\sin \pi\rho_n} & n = 1 \\ \dfrac{\pi\rho_n \cosh \pi\rho_n}{\sinh \pi\rho_n} & n > 1 \end{cases} \qquad (3.39)$$

$$\rho_n = b\sqrt{(\frac{k}{\pi})^2 - (\frac{n}{a})^2} \tag{3.40}$$

3.3.3b THE LONGITUDINAL SLOT

The summation of the H modes for the Green's function for the longitudinal slot is found to contain a term which results in the expression being divergent [3.5]. Therefore, an alternative solution employing a vector potential is preferred and the integral in equation (3.18a) is replaced by the equivalent integral.

$$\iint_S f_i \underline{\hat{a}}_x \cdot (-\underline{\hat{a}}_y \times \underline{H}_z)\, dS \tag{3.41}$$

where

$$\underline{H} = -j\omega \underline{A}_m + \frac{\nabla\nabla \cdot \underline{A}_m}{j\omega\mu_o\varepsilon_o} \tag{3.42}$$

$$\underline{A}_m = \varepsilon_o \iint_S \underline{J}_m(\underline{r}) \cdot \underline{\underline{G}}_m (\underline{r}/\underline{r}_o)\, dS_o \tag{3.43}$$

$$\underline{J}_m = \underline{\hat{a}}_z \sin\{\frac{s\pi(Z_o + \frac{L}{2})}{L}\} \tag{3.44}$$

Rahmat-Samii [3.6] in the course of his work developed the following expression for $\underline{\underline{G}}_m^{ZZ}$

$$G_m^{ZZ} = \sum_{n=o}^{\infty}\sum_{m=o}^{\infty} \frac{\varepsilon_{no}\varepsilon_{mo}}{2ab\Gamma_{nm}} e^{-\Gamma_{nm}|Z-Z_o|} \cos\frac{n\pi x}{a} \cos\frac{n\pi x_o}{a} \sin\frac{m\pi y}{b} \sin\frac{m\pi y_o}{b} \tag{3.45}$$

which used in conjunction with equations (3.42) to (3.44) enabled equation (3.41) to be solved giving

for n = o

$$- \frac{j\omega\varepsilon_o}{ab}[W^2 \{(\frac{1}{k^2} + (1 - (\frac{s\pi}{kL})^2)(\frac{b}{\pi})^2\gamma(n,s))\}L\delta_{is} + (si)\ (\frac{\pi}{kL})^2$$

$$\times \{1 + (-1)^{(i+s)}\} \sum_{m=1}^{\infty} \frac{\varepsilon_{om}(1-(-1)^i e^{-\Gamma_{nm}L})\ \{1 + (\frac{k}{\Gamma_{nm}})\}^2}{\Gamma_{nm}^3 \{1 + (\frac{s\pi}{\Gamma_{nm}L})^2\}\{1 + (\frac{i\pi}{\Gamma_{nm}L})^2\}}] \qquad (3.46a)$$

and for n ≠ o

$$\frac{-j\omega\varepsilon_o}{2ab} \sum_{n=1}^{\infty} [(\frac{a}{n\pi})^2\ (\sin\frac{n\pi(x_1 + \frac{W}{2})}{a} - \sin\frac{n\pi(x_1 - \frac{W}{2})}{a})^2$$

$$\times \{(1 - (\frac{s\pi}{kL})^2)(\frac{b}{\pi})^2\gamma(n,s)\}L\delta_{is} + (si)\ (\frac{\pi}{kL})^2\ \{1 + (-1)^{(i+s)}\}$$

$$\times \sum_{m=o}^{\infty} \frac{\varepsilon_{om}(1-(-1)^i e^{-\Gamma_{nm}L})\ \{1 + (\frac{k}{\Gamma_{nm}})\}^2}{\Gamma_{nm}^3 \{1 + (\frac{s\pi}{\Gamma_{nm}L})^2\}\{1 + (\frac{i\pi}{\Gamma_{nm}})^2\}}] \qquad (3.46b)$$

where

$$\gamma(n,s) = \frac{-\pi^2 \cos b\sqrt{k^2 - \{(\frac{s\pi}{L})^2 + (\frac{n\pi}{a})^2\}}}{b\sqrt{k^2 - \{(\frac{s\pi}{L})^2 + (\frac{n\pi}{a})^2\}}\ \sin b\sqrt{k^2 - \{(\frac{s\pi}{L})^2 + (\frac{n\pi}{a})^2\}}} \qquad (3.47)$$

The above solution developed by Lyon does not include the contribution of the ψ = constant mode (m=o, n=o). This must be incorporated into the solution to correctly characterise the stored energy in the waveguide. In fact, Vu Khac and Carson [3.7] have demonstrated from the mathematics, that if this mode is omitted from the solution then there arises a small but definite discontinuity in H_z in the source free region, which is clearly incorrect. This additional mode is produced by a magnetic current source lying in the direction of propagation and consequently it is only excited by a longitudinal shunt slot. This can be understood qualitatively by examining Figure (3.3) which shows the equivalent TEM (TM_{oo}) mode, propagating sideways in parallel plate waveguide, coupling to a longitudinal slot. It is also suggested in [3.7] that the reason why this mode has been neglected in the past is probably because the stored energy for a longitudinal slot has usually been calculated from a transverse slot [2.3] which does not excite this mode.

An additional term must be incorporated into the above solution to account for this mode and this can be evaluated as follows: the H field component of the ψ_o mode for a slot of infinite length is given by the last term of equation (27) in [3.8]. That is

$$H_z|_{\psi_o} = -\frac{1}{j\omega\mu_o S_c} \int_C (\hat{\underline{n}} \times \underline{E}) \cdot \hat{\underline{a}}_z \, dC \qquad (3.48)$$

where C is the contour and S_c is the cross sectional area of the waveguide. However, for a slot of finite length the surface magnetic current $(\hat{\underline{n}} \times \underline{E})$, which is not uniform, must be averaged over its length to permit evaluation of the integral.

$$H_z|_{\psi_o} = \frac{-W\,((-1)^s - 1)}{j\omega\mu_o\, ab\, s\pi} \tag{3.49}$$

This is then substituted into equation (3.41) and after a little manipulation the required term is found to be:

$$\frac{-W^2\, L(1-(-1)^i)\,\,(1-(-1)^s)}{j\omega\mu_o\, ab\, s\, i\, \pi^2} \tag{3.50}$$

3.3.4 CONTRIBUTION OF INCIDENT FIELD

Before determining vectors a and b the contribution of the incident fields must be evaluated, this is given by:

$$h_i = -\iint_S f_i\, \hat{\underline{a}}_z \cdot \{\underline{n} \times \underline{H}_i(\underline{r})\}\, dS \tag{3.51}$$

which depends on the slot orientation. The incident fields are given by

$$E_y^+ = -j\omega\mu_o\, \phi \sin\frac{\pi x}{a}\, e^{-j\beta_g z}\, \hat{\underline{A}}_y \tag{3.52}$$

$$H_x^+ = j\,\beta_g\, \phi \sin\frac{\pi x}{a}\, e^{-j\beta_g z}\, \hat{\underline{A}}_x \tag{3.53}$$

$$H_z^+ = \frac{\pi}{a}\phi \cos\frac{\pi x}{a}\, e^{-j\beta_g z}\, \hat{\underline{A}}_z \tag{3.54}$$

$$\text{where} \quad \phi = (kZ_o\, \beta_g\, ab)^{-\frac{1}{2}} \tag{3.55}$$

Substituting equations (3.52), (3.53) and (3.54) into equation (3.51) gives, for a transverse slot

$$h_i = 2j\phi\ \sigma(i,1)\ \sin\frac{\beta_g W}{2} \tag{3.56}$$

where $\sigma(i, 1)$ is defined in equation (3.37).

For a longitudinal slot

$$h_i = \phi\ [\sin\frac{\pi(X_1 + \frac{W}{2})}{a} - \sin\frac{\pi(X_1 - \frac{W}{2})}{a}]$$

$$\times \frac{\frac{i\pi}{L}}{(\frac{i\pi}{L})^2 - \beta_g{}^2} \begin{cases} 2\cos\beta_g\frac{L}{2} & i \text{ odd} \\ 2j\sin\beta_g\frac{L}{2} & i \text{ even} \end{cases} \tag{3.57}$$

3.4 SUMMARY OF MATRIX ENTRIES

All the components of the matrix have now been defined so it is possible to determine the transverse electric fields on both the upper and lower surfaces of the slot by matrix manipulation and hence evaluate the transmission and reflection coefficients of the slot. However, before proceeding it is beneficial to pause for a moment and summarise the equations in each sub-matrix

$$A_{i,s} = \text{Eqn (3.36) or (Eqn (3.46) + Eqn (3.50)) + Eqn (3.33a)}$$

$$B_{i,s} = \text{Eqn (3.21) + Eqn (3.22) + Eqn (3.33b)}$$

$$C_{i,s} = \text{Eqn (3.33c)} \tag{3.58}$$

$D_{i,s}$ = - Eqn (3.33c)

h_i = Eqn (3.54) or Eqn (3.57).

3.5 CALCULATION OF TRANSMISSION AND REFLECTION COEFFICIENTS

The scattering fields for the aperture must initially be calculated to enable the transmission and reflection coefficients to be determined. The tangential field on the inner surface of the slot is given by:

$$\hat{\underline{n}} \times \underline{E}\ (\underline{r}) = \sum_{s=1}^{N} a_s\ f_s\ \hat{\underline{a}}_\xi \qquad (3.59)$$

where

$$f_s = \sin \frac{s\pi\ (\xi + \frac{L}{2})}{L} \qquad -\frac{L}{2} < \xi < \frac{L}{2} \qquad (3.60)$$

and when this is substituted back into equation (3.6) and evaluated for the dominant mode of the appropriate Green's function then the scattering fields may be determined. The scattering parameters can then be obtained without difficulty. For the transverse slot,

$$S_{11} = \frac{A_{10}\ \sqrt{2}\ \pi}{a} \sin\ (\beta_g\ \tfrac{W}{2}) \sum_{s=1}^{N} a_s\ \sigma\ (s,\ 1) \qquad (3.61)$$

$$S_{21} = 1 - S_{11} \qquad (3.62)$$

where A_{nm} and σ (i, n) are defined in equations (3.35) and (3.37) respectively, and for the longitudinal slot,

$$S_{11} = \frac{A_{10}\,\pi}{j\sqrt{2}a}\left(\sin\frac{\pi(x_1+\frac{W}{2})}{a} - \sin\frac{\pi(x_1-\frac{W}{2})}{a}\right)$$

$$\times \sum_{s=1}^{N}\left(a_s \frac{\frac{s\pi}{L}}{(\frac{s\pi}{L})^2 - \beta_g^2}\right)\begin{cases} 2\cos\beta_g\frac{L}{2} & s \text{ odd} \\ 2j\sin\beta_g\frac{L}{2} & s \text{ even} \end{cases} \qquad (3.63)$$

$$S_{21} = 1 - (-1)^s S_{11} \qquad (3.64)$$

3.6 DISCUSSION ON TECHNIQUE

A moment method solution to the integral equations (3.7a and b) for the transverse and longitudinal slots radiating through the broadwall of rectangular waveguide is presented, based on the work of Lyon [3.1]. The ψ = constant mode is incorporated into the solution and computed results are presented in Figure (3.4) and Figure (3.5). In Figure (3.4) the resonant length of a square ended longitudinal slot is illustrated as a function of offset from the guide centre line. The results suggest that the resonant length is under-estimated by approximately 3% when this mode is ignored and this is confirmed by experimental data [2.28] on square ended longitudinal slots. The normalised power radiated is plotted against slot length in Figure (3.5) which also clearly shows the theoretical shift of resonance due to the more accurate prediction of the stored energy in the waveguide.

There is, however, a residual error between the theoretical and experimental results in Figure (3.4) which can primarily be attributed to the omission of the field enhancement at the edges of the slot (see Figure (3.6)). Park in his work on slots presented a

set of curves in [2.29] to illustrate the effect of incorporating this mode. His results show a reduction in the predicted resonant length by approximately 0.5% for low offsets and approximately 0.2% for large offsets which almost exactly compensates for the error in Figure (3.4).

Although the solution predicts accurately the slot characteristics it is worth mentioning the main shortcomings of the technique.

(a) The field enhancement at the edge of the slot has been omitted as the effect is negligible for slots radiating through waveguides of standard wall thickness. Note the experimental results shown in Figure (3.3) are for slots radiating through a thin walled waveguide (0.1 of standard walled thickness).

(b) The slots used in practice usually exhibit a large length to width ratio and therefore the cross-polar or longitudinally directed E field component within the slots is so small it can safely be ignored [3.9, 3.10]. There are nevertheless some applications for wide slots and in these instances a more complex basis function is required in the analysis [3.11].

(c) The theoretical solution presented in this chapter has been restricted to characterising square ended slots, however, in practice such slots are almost never used due to manufacturing difficulties. Round ended slots are far more common. This gives rise to an additional discrepancy between

theory and practice and therefore correction factors, based on equal perimeter/area rules, must be employed to compensate for this error [3.10, 3.12].

3.7 CONCLUSION

The advancement of computers has allowed approximate solutions, such as the moment method to be developed, which are able to predict to within experimental error the characteristics of a slot radiating through the wall of a waveguide. This technique was initially limited to the transverse and longitudinal slots as discussed in this chapter, however, recently the method has been extended to allow a slot of any orientation to be analysed [3.13].

It has also been suggested in [2.79] that the moment method solution is capable of characterising a slot with sufficient accuracy to use it as an alternative to the measured data currently relied upon for the design of slotted waveguide antennas. It is therefore pertinent to investigate this further and a purely theoretical computer aided design/synthesis package based on this method has been developed and is described later on in this thesis.

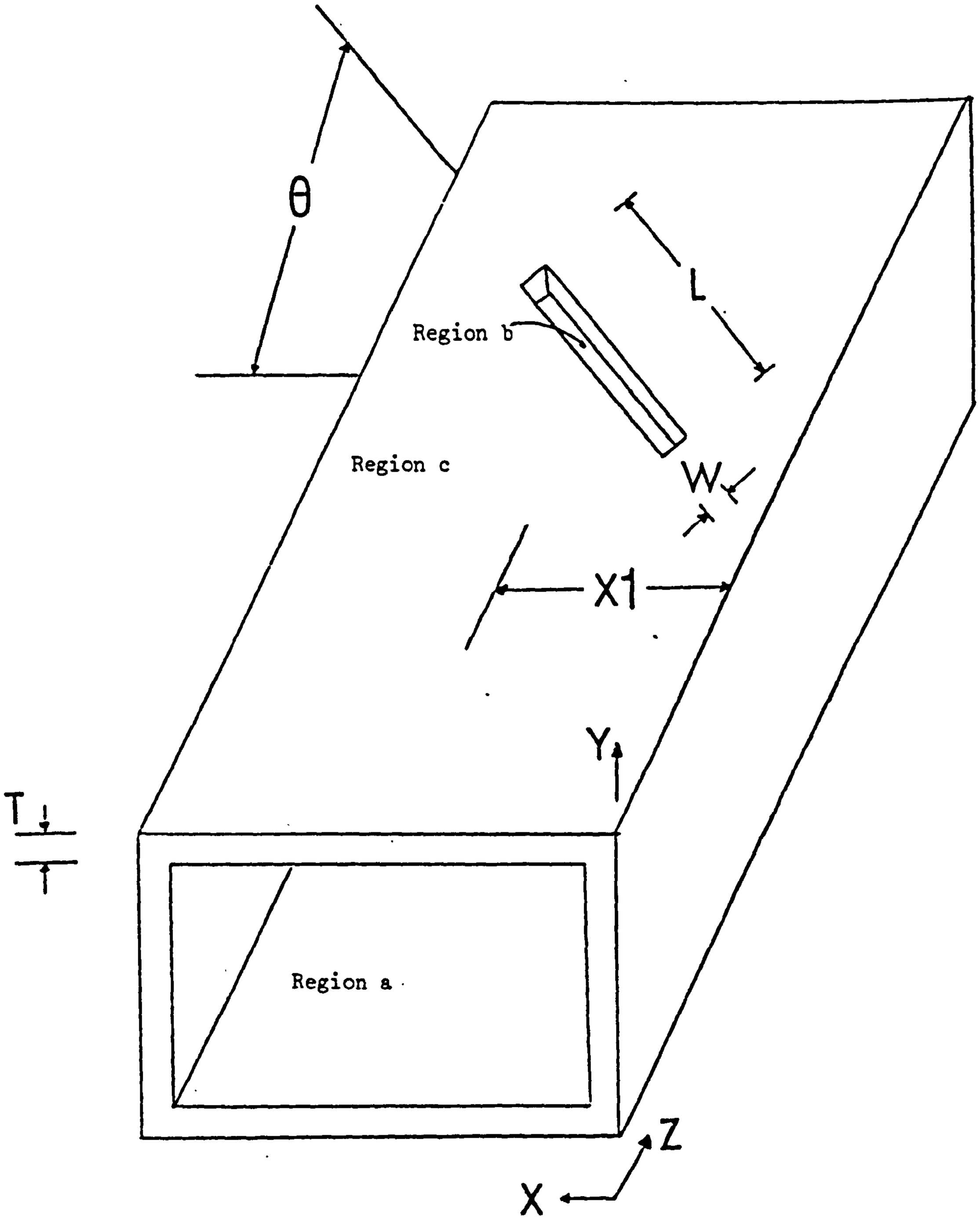

Figure 3.1

Co-ordinate System of Slotted Waveguide

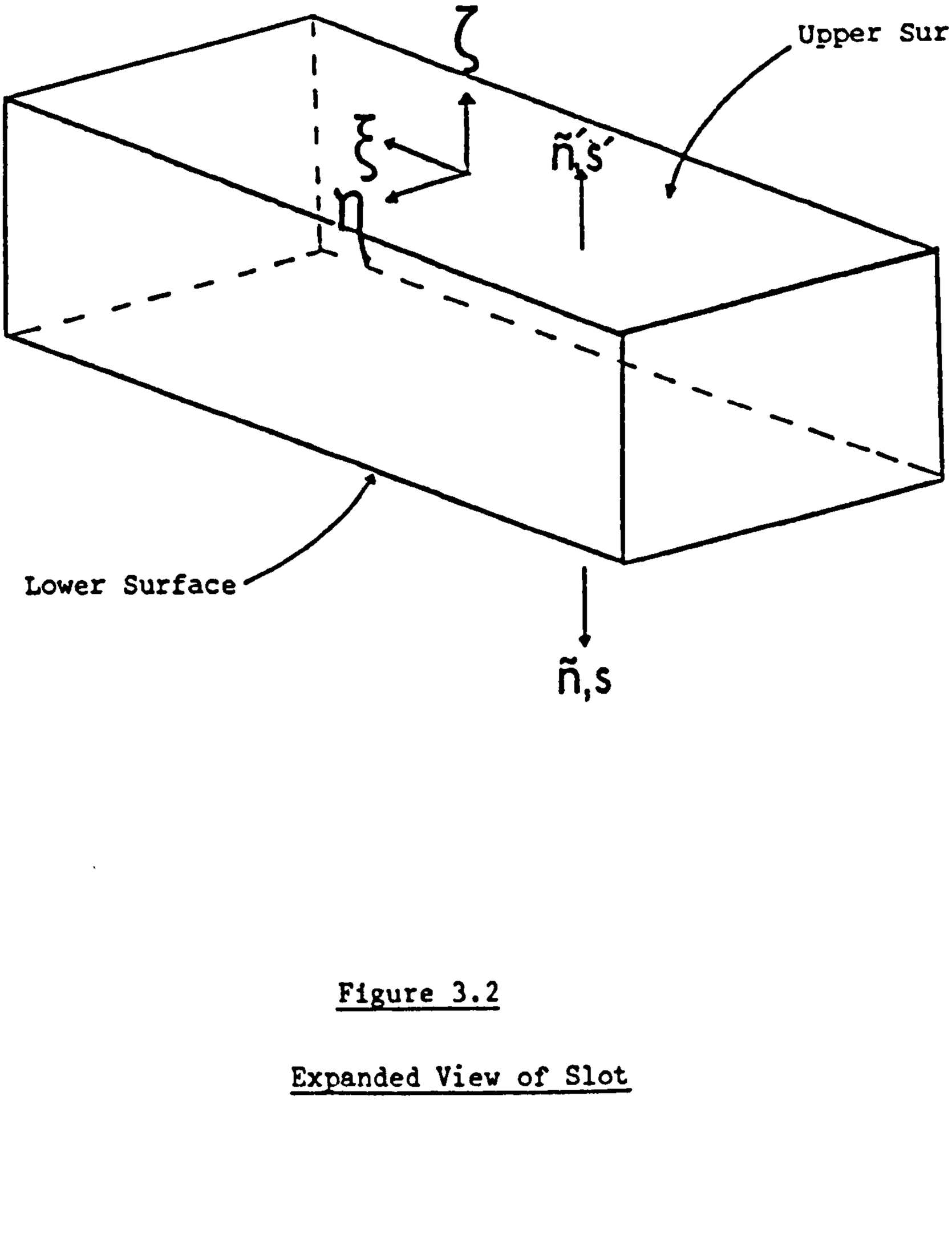

Figure 3.2

Expanded View of Slot

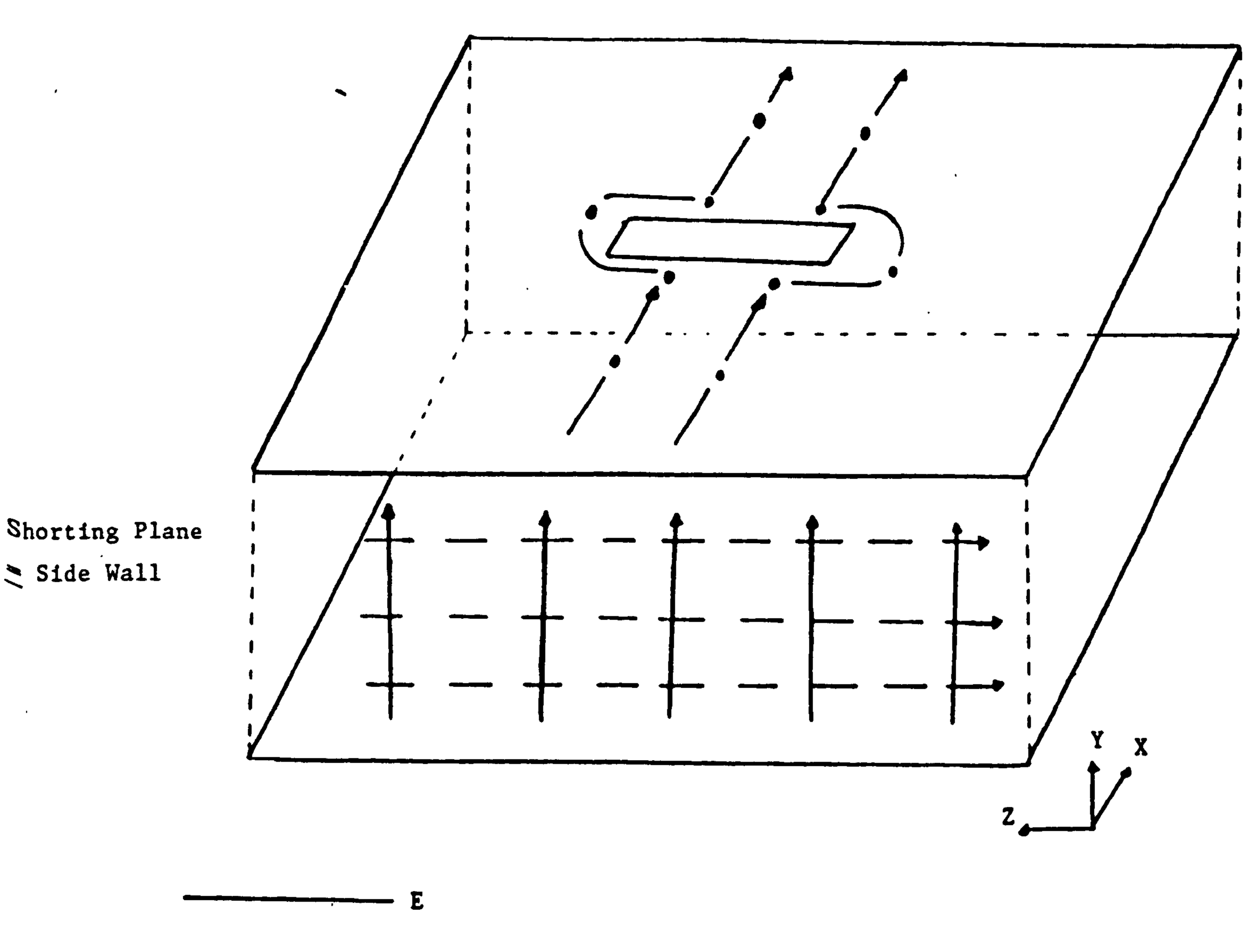

Figure 3.3

Equivalent TEM (TMoo) Mode in Parallel Plate Waveguide

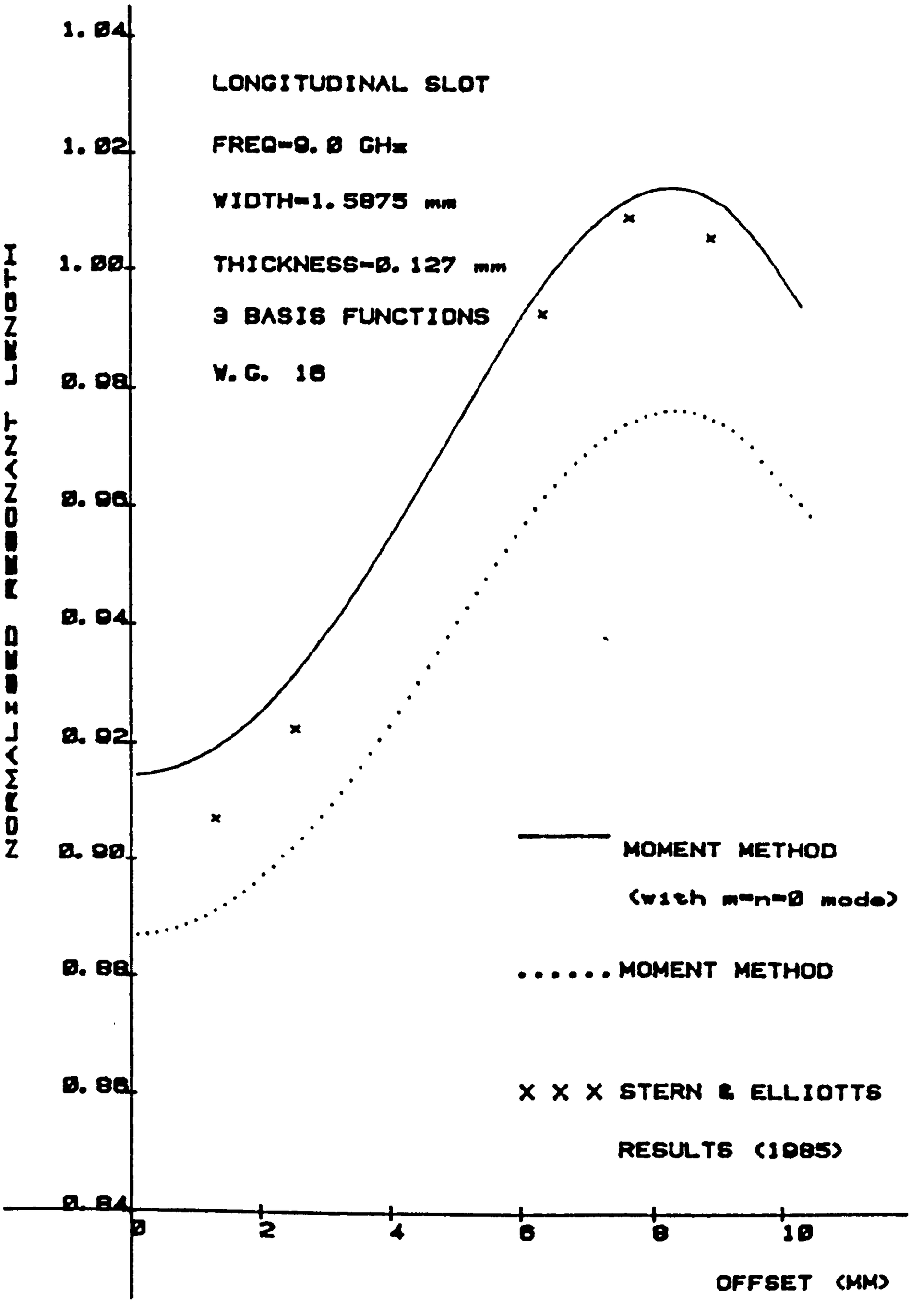

Figure 3.4

Resonant Length as a Function of Offset
for a Rectangular Longitudinal Slot

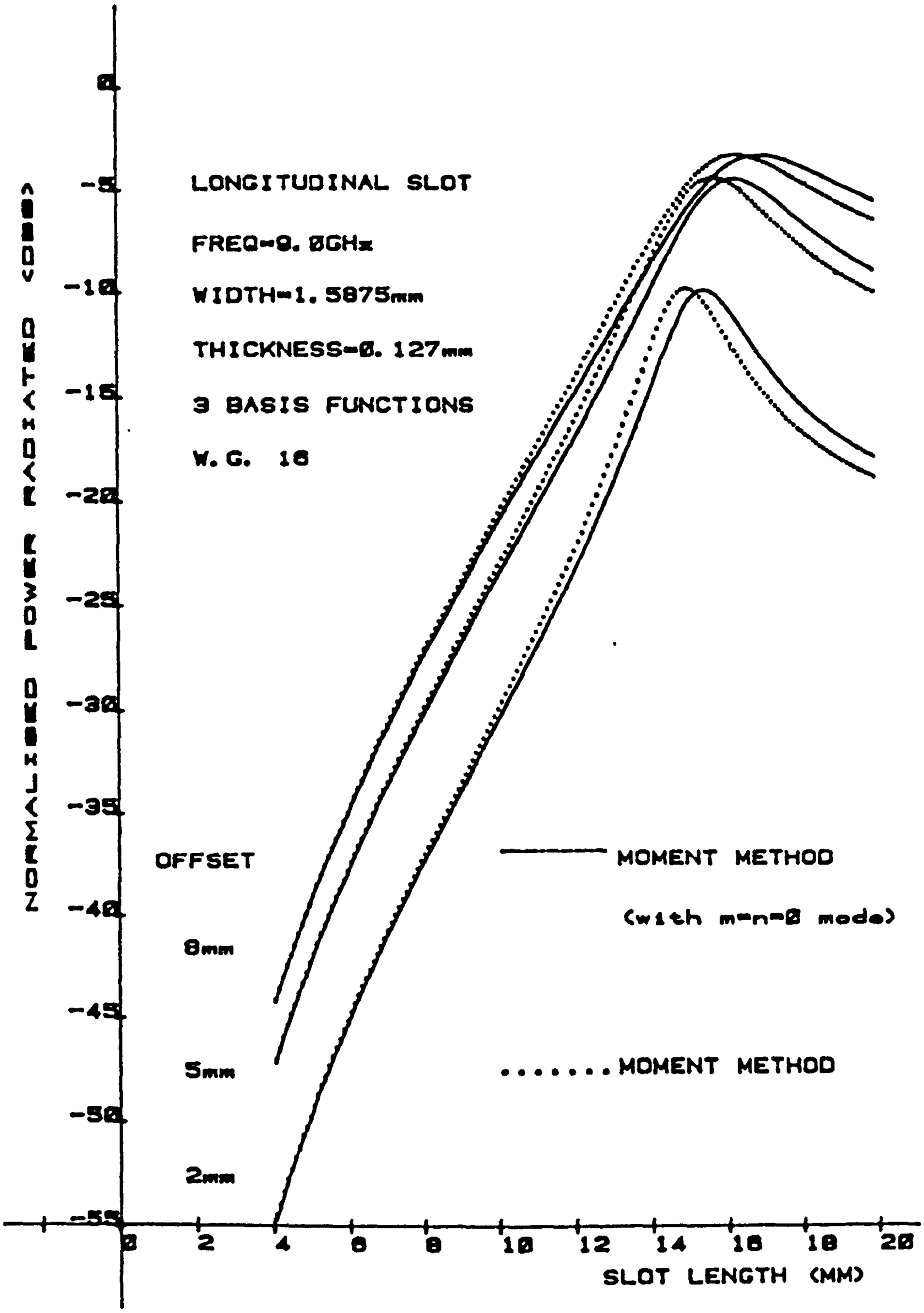

Figure 3.5

Normalised Power Radiated Versus Slot Length
for a Rectangular Longitudinal Slot

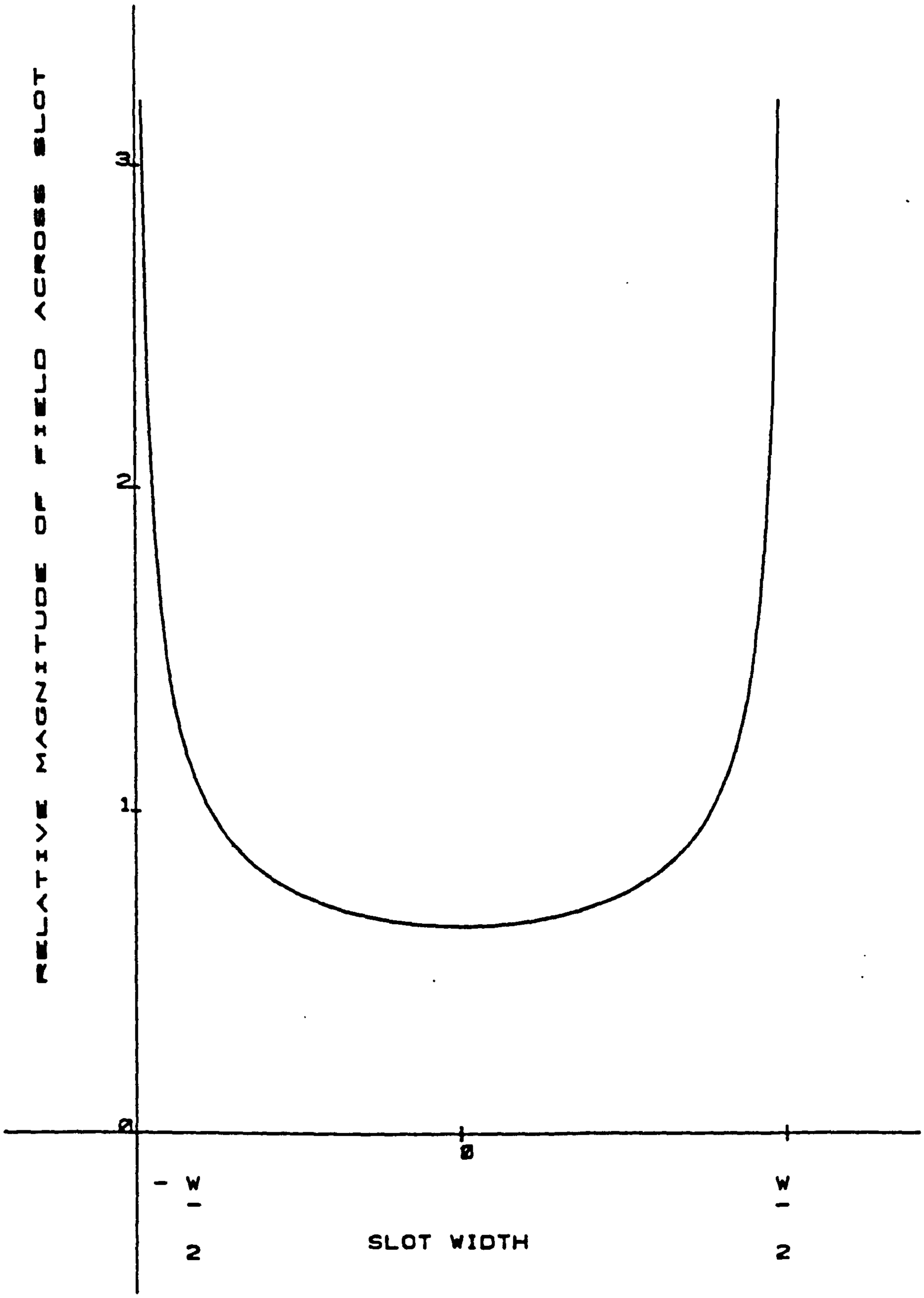

Figure 3.6

A Graph of the Relative Magnitude of the Field Across the Slot

CHAPTER 4

A STUDY OF SLOT RADIATORS USING THE MOMENT METHOD

The previous chapter described an effective method of analysing longitudinal and transverse slots in the broadwall of a rectangular waveguide. This analysis is extended to an axially sectioned slot in which the sections may have different lengths to model the round end and the field within the sections can be weighted to crudely emulate the edge effect. Theoretical results have been presented to enable an assessment of the viability of the improved model to be made. The contents of this section have been described in reference [4.1] which is included in Appendix 3.

Also it was noted that the predictions obtained from the moment method were sufficiently accurate for it to form the basis of a purely theoretical computer aided design/synthesis package for slotted waveguide array antennas. However, the efficient implementation of such a package can be considerably aided if some prior knowledge of the functional relationship between the slot scattering, or admittance characteristics and its dimensional parameters are available. These relationships have been discussed in the literature [2.7, 2.8, 2.25, 3.1, 4.1], for all dimensional parameters, except curiously the width parameter. Some limited studies of the width have been reported by Putman [4.2] and Crompton [4.3] but these apply to an isolated slot in a conducting ground plane. These studies show that for slots of this category the resonant frequency decreases slowly and almost linearly with width. On the basis of a simplistic area or perimeter rule [3.12], this result is not unexpected. This kind of behaviour has also been

demonstrated by Watson [4.4] in curves which are reproduced in Silver [3.9] for a longitudinal offset slot radiator in rectangular waveguide.

Using computations based on the method of moments it is shown that this 'expected' resonant frequency versus width relationship does not always occur for slots in waveguide, and this is particularly so in the case of longitudinal shunt slots which in fact for large offsets exhibit an increasing resonant frequency with width. The reasons for this reversal of the 'usual' trend are discussed in the latter part of this chapter. The contents of this section have been described in reference [4.5] along with the experimental results detailed in the next chapter.

4.1 MODIFIED FORMULATION FOR SECTIONED SLOT

A round end slot can be modelled using the moment method by considering that the slot comprises of rectangular slices as illustrated, for n = 3, in Figure (4.1c). The essence of the modification in mathematical terms then lies in calculating the self coupling for each section and the mutual coupling between the sections.

Before detailing the development of the mathematics, the algorithm for determining the section lengths shall be stated:-

1. Set the length of the middle section equal to the length of the round ended slot.

2. Calculate the remaining length by setting the section width equal to W/3 and matching the area to that of the round ended slot.

3. Calculate the length of the equivalent square ended slot having the same width (W) and perimeter as the given round ended slot.

From the above, the following formulae are obtained

$$\text{Length of section 1, 3} = \text{L equivalent} + (\frac{1}{2} - \frac{\pi}{8})W \qquad (4.1)$$

$$\text{Length of section 2} = \text{L equivalent} + (2 - \frac{\pi}{2})W \qquad (4.2)$$

In the current analysis the above sectioned slot modification is applied to the inner surface of the slot only. The cavity and its outer surface are set equal to the length of the middle section. This minimises the computation yet provides sufficient evidence to demonstrate the effectiveness of this procedure. In principle however, the modification should be applied to both inner and outer surfaces of the slot 'cavity' and to the cavity itself, in a 'thick' wall example.

4.1.1 TRANSVERSE SLOT

For the transverse slot the introduction of a 3-section slot model entails some modification to the A sub-matrix of equation (3.17). However, only that portion of $A_{i,s}$ (equation (3.18a)) which contains the waveguide Green's function is involved. It is reproduced below:

$$j\omega\varepsilon_o \iint_S f_i \iint_S \underset{\sim}{G}_a^{xx} f_s \, dS_o dS \tag{4.3}$$

where $\underset{\sim}{G}_a^{xx}$ is the x component of $\underset{\sim}{G}_a$.

In the conventional analysis this component of $A_{i,s}$ describes the self coupling, whereas for a 3-slot model the modification must include all three self coupling terms and the six mutual coupling terms. Hence, this term must be expanded to:-

$$\sum_{p=1}^{3} \sum_{q=1}^{3} j\omega\varepsilon_o \iint_{S_{p,q}} f_i \iint_{S_{p,q}} \underset{\sim}{G}_a^{xx} f_s \, dS_o dS \tag{4.4}$$

The evaluation of the integrals in term (4.4) largely follows the procedure described in reference [3.1] and therefore the solution is simply outlined below with a full description of the mathematics being restricted to the Appendices.

On substituting f_i, f_s and $\underset{\sim}{G}_a(\underline{r}/\underline{r}_o)$ into the integral expression (4.4) we obtain

$$\sum_{p=1}^{3} \sum_{q=1}^{3} \frac{j\omega\varepsilon_o}{k_c^2 ab} \int_{z_p - \frac{W_1}{2}}^{z_p + \frac{W_1}{2}} \int_{x_1 - \frac{L_p}{2}}^{x_1 + \frac{L_p}{2}} \sin \frac{s\pi(x_o - x_1 + \frac{L_p}{2})}{L_p}$$

$$\times \int_{z_q - \frac{W_1}{2}}^{z_q + \frac{W_1}{2}} \int_{x_1 - \frac{L_q}{2}}^{x_1 + \frac{L_q}{2}} \sin \frac{s\pi(x_o - x_1 + \frac{L_q}{2})}{L_q}$$

$$\times \left(\sum_{n=1}^{\infty} \sum_{m=0}^{\infty} \varepsilon_{0m} \, e^{-\Gamma_{nm}|z - z_o|} \right.$$

$$\times \left[\frac{\Gamma_{nm}}{k^2}\left(\frac{n\pi}{a}\right)^2 - \frac{1}{\Gamma_{nm}}\left(\frac{m\pi}{b}\right)^2\right] \sin\frac{n\pi x}{a} \sin\frac{n\pi x_o}{a}$$

$$\times \cos\frac{m\pi y}{b} \cos\frac{m\pi y_o}{b}) dx_o dz_o dx dz \qquad (4.5)$$

where $W_1 = W/3$

L_p, L_q is the section slot length dependent on p and q

Z_p, Z_q are the respective displacements from the centre of the slot to the centre of the sections

and $$\varepsilon_{0j} = \begin{cases} 1 \text{ for } j = 0 \\ 2 \text{ for } j \neq 0 \end{cases}$$

The integral breaks down into three sections

1. The self coupling term for the middle section.
2. The self coupling terms of the outer sections.
3. The mutual coupling terms.

The solution for the self coupling term for the middle section can be reduced to

$$\frac{2j\omega\varepsilon_o}{k_c^2 ab} \sum_{n=1}^{\infty} \sigma(i,n)\sigma(s,n)\left(U_n W_1 + \frac{e^{-\Gamma_{n0}W_1} - 1}{\Gamma_{n0}} + 2\Gamma_{no}^2\right.$$

$$\left.\times \left\{\left(\frac{b}{\pi}\right)^3 \left(\frac{1}{2}\frac{j}{\rho_n^3} + \frac{1}{\rho_n^2}\right) + \sum_{m=1}^{\infty} \frac{e^{-\Gamma_{nm}W_1}}{\Gamma_{nm}^3}\right\}\right) \qquad (4.6)$$

where

$$\sigma(i,n) = \begin{cases} \begin{cases} \dfrac{\frac{2L}{i\pi}}{\alpha^2-1} \sin\dfrac{\alpha i\pi}{2} \cos\dfrac{n\pi x_1}{a} & \alpha \neq 1 \\ \dfrac{L}{2}(-1)^{i/2} \cos\dfrac{n\pi x_1}{a} & \alpha = 1 \end{cases} & i \text{ even} \\ \begin{cases} \dfrac{\frac{2L}{i\pi}}{1-\alpha^2} \cos\dfrac{\alpha i\pi}{2} \sin\dfrac{n\pi x_1}{a} & \alpha \neq 1 \\ \dfrac{L}{2}(-1)^{\frac{i-2}{2}} \sin\dfrac{n\pi x_1}{a} & \alpha = 1 \end{cases} & i \text{ odd} \end{cases} \tag{4.7}$$

and $$\alpha = \frac{nL}{ia} \tag{4.8}$$

$$U_n = \begin{cases} \dfrac{\pi\rho_n \cos \pi\rho_n}{\sin \pi\rho_n} & n = 1 \\ \dfrac{\pi\rho_n \cosh \pi\rho_n}{\sinh \pi\rho_n} & n > 1 \end{cases} \tag{4.9}$$

$$\rho_n = b\sqrt{\left(\frac{k}{\pi}\right)^2 - \left(\frac{n}{a}\right)^2} \tag{4.10}$$

and L is the length of the middle section.

Solving for the self coupling term of the outer section gives

$$\frac{2j\omega\varepsilon_o}{k_c^2 ab} \sum_{n=1}^{\infty} \sigma(i,n)\, \sigma(s,n) \sum_{m=0}^{\infty} \varepsilon_{0m}\left[1 - \left(\frac{m\pi}{\Gamma_{nm} b}\right)^2\right] e^{-\Gamma_{nm} z_1}$$

$$\times \left[Z_1\left(e^{-\Gamma_{nm}W_1} - 1\right) + W_1 + \frac{1}{\Gamma_{nm}}\left(e^{-\Gamma_{nm}W_1} - 1\right)\right] \qquad (4.11)$$

where Z_1 is the magnitude of the displacement from the centre line to the centre of the outer section.

Note: The length used is now that of the outer section.

Solving for the mutual coupling term produces

$$\frac{j\omega\varepsilon_o}{k_c^2 ab} \sum_{n=1}^{\infty} \sigma(i,n)\sigma(s,n) \sum_{m=0}^{\infty} - \frac{\varepsilon_{om}}{\Gamma_{nm}}\left[1 - \left(\frac{m\pi}{\Gamma_{nm} b}\right)^2\right]$$

$$\times \left[2e^{-\Gamma_{nm}Z} - e^{-\Gamma_{nm}(Z+W_1)} - e^{-\Gamma_{nm}(Z-W_1)}\right] \qquad (4.12)$$

where Z is the displacement between the appropriate sections.

Note: The lengths used in $\sigma(i,n)$ and $\sigma(s,n)$ may differ depending on which sections are coupling.

4.1.2 LONGITUDINAL SLOT

For the longitudinal slot geometry the field solutions require to satisfy the Maxwell divergence relation for $\underline{H}$ and this calls for a slightly different treatment. Equation (3.41) gives the mathematical relationships describing the self-coupling processes within a single (ie individual) slot. For a sectioned slot comprising of three equal width elements this term can be re-expressed as

$$\sum_{p=1}^{3}\sum_{q=1}^{3}\iint_{S_{p,q}} f_i \hat{\underline{a}}_x \cdot (-\hat{\underline{a}}_y \times \underline{H}_{z\,p,q})\,ds \tag{4.13}$$

where

$$\underline{H} = -j\omega\underline{A}_m + \frac{\nabla\nabla\cdot\underline{A}_m}{j\omega\mu_o\varepsilon_o} \tag{4.14}$$

$$\underline{A}_m = \varepsilon_o \iint_{S_{p,q}} \underline{J}_m(\underline{r}) \cdot \underset{\sim}{G}_m\,(\underline{r}/\underline{r}_o)\,dS_o \tag{4.15}$$

$$\underline{J}_m = -\hat{\underline{a}}_z \sin\left\{\frac{s\pi(Z_o + \frac{L}{2})}{L}\right\} \tag{4.16}$$

and

$$\underset{\sim}{G}_m = \sum_{n=o}^{\infty}\sum_{m=o}^{\infty} \frac{\varepsilon_{on}\varepsilon_{om}}{2ab\Gamma_{nm}} e^{-\Gamma_{nm}|Z-Z_o|} \cos\frac{n\pi x}{a} \cos\frac{n\pi x_o}{a} \sin\frac{m\pi y}{b} \sin\frac{m\pi y_o}{b} \tag{4.17}$$

The integrals in term (4.13) can be evaluated following procedures previously detailed in reference [3.1] and once more the solution will be simply outlined below with a full mathematical description being restricted to the appendices.

The integrals involved in expression (4.13) are conveniently divided into two types; those associated with the self coupling terms and the mutual coupling terms for sections of equal length, and those associated with the mutual coupling terms for sections of unequal length.

In the former case, the integral (4.13) may be solved in conjunction with (4.14) to (4.17) to give, after some mathematics, terms of the following form:

for n = 0

$$- \frac{j\omega\varepsilon_o}{ab}\Big[W_1^2 \left\{\left(\frac{1}{k^2} + \left(1 - \left(\frac{s\pi}{kL}\right)^2\right)\left(\frac{b}{\pi}\right)^2\gamma(n,s)\right)\right\}L\delta_{is} + (si)\ \left(\frac{\pi}{kL}\right)^2$$

$$\times \left\{1 + (-1)^{(i+s)}\right\} \sum_{m=1}^{\infty} \frac{\varepsilon_{om}\left(1-(-1)^i\, e^{-\Gamma_{nm}L}\right)\left\{1 + \left(\frac{k}{\Gamma_{nm}}\right)^2\right\}}{\Gamma_{nm}^3\left\{1 + \left(\frac{s\pi}{\Gamma_{nm}L}\right)^2\right\}\left\{1 + \left(\frac{i\pi}{\Gamma_{nm}L}\right)^2\right\}}\Big] \qquad (4.18a)$$

and for n ≠ 0

$$\frac{-j\omega\varepsilon_o}{2ab} \sum_{n=1}^{\infty}\Big[\left(\frac{a}{n\pi}\right)^2 \left(\sin\frac{n\pi\left(x_a + \frac{W_1}{2}\right)}{a} - \sin\frac{n\pi\left(x_a - \frac{W_1}{2}\right)}{a}\right)$$

$$\times \left(\sin\frac{n\pi\left(x_b + \frac{W_1}{2}\right)}{a} - \sin\frac{n\pi\left(x_b - \frac{W_1}{2}\right)}{a}\right) \qquad (4.18b)$$

$$\times \left\{\left(1 - \left(\frac{s\pi}{kL}\right)^2\right)\left(\frac{b}{\pi}\right)^2\gamma(n,s)\right\}L\delta_{is} + (si)\ \left(\frac{\pi}{kL}\right)^2\left\{1 + (-1)^{(i+s)}\right\}$$

$$\times \sum_{m=o}^{\infty} \frac{\varepsilon_{om}\left(1-(-1)^i\, e^{-\Gamma_{nm}L}\right)\left\{1 + \left(\frac{k}{\Gamma_{nm}}\right)^2\right\}}{\Gamma_{nm}^3\left\{1 + \left(\frac{s\pi}{\Gamma_{nm}L}\right)^2\right\}\left\{1 + \left(\frac{i\pi}{\Gamma_{nm}}\right)^2\right\}}\Big]$$

where

$$\gamma(n,s) = \frac{-\pi^2 \cos b\sqrt{k^2 - \{(\frac{s\pi}{L})^2 + (\frac{n\pi}{a})^2\}}}{b\sqrt{k^2 - \{(\frac{s\pi}{L})^2 + (\frac{n\pi}{a})^2\}} \sin b\sqrt{k^2 - \{(\frac{s\pi}{L})^2 + (\frac{n\pi}{a})^2\}}}$$

and x_a, x_b are the offsets for the sections in question.

In the latter case equation (4.13) is solved with different limits of integration due to the differing section lengths, and produces terms which are typically of the form:

for n = 0

$$\frac{-j\omega\varepsilon_o}{ab} W_1^2 [\frac{2(\frac{iL_a}{s^2\pi L_b})^2}{[1 - (\frac{i\,L_a}{s\,L_b})^2]} ((-1)^i \sin \frac{s\pi(\frac{L_a}{2} + \frac{L_b}{2})}{L_a}$$

$$- \sin \frac{s\pi\,(\frac{L_a}{2} - \frac{L_b}{2})}{L_a}) [\frac{1}{k^2} + (\frac{b}{\pi})^2 [1 - (\frac{s\pi}{kL_a})^2] \gamma(n,s)]$$

$$+ (\frac{si\pi^2}{L_a L_b}) \sum_{m=1}^{\infty} \frac{\varepsilon_{om}[1 + (\frac{\Gamma_{nm}}{k})^2]}{\Gamma_{nm}^5 [1 + (\frac{s\pi}{\Gamma_{nm}L_a})^2][1 + (\frac{i\pi}{\Gamma_{nm}L_b})^2]}$$

$$\times [(e^{-\Gamma_{nm}(\frac{L_a}{2} - \frac{L_b}{2})} - (-1)^i e^{-\Gamma_{nm}(\frac{L_a}{2} + \frac{L_b}{2})})$$

$$- (-1)^s (e^{-\Gamma_{nm}(\frac{L_a}{2} + \frac{L_b}{2})} - (-1)^i e^{-\Gamma_{nm}(\frac{L_a}{2} - \frac{L_b}{2})})]] \qquad (4.19a)$$

and for $n \neq 0$

$$\frac{-j\omega\varepsilon_o}{2ab} \sum_{n=1}^{\infty} \left(\frac{a}{n\pi}\right)^2 \left(\sin \frac{n\pi\left(x_a + \frac{W_1}{2}\right)}{a} - \sin \frac{n\pi\left(x_a - \frac{W_1}{2}\right)}{a}\right)$$

$$\times \left(\sin \frac{n\pi\left(x_b + \frac{W_1}{2}\right)}{a} - \sin \frac{n\pi\left(x_b - \frac{W_1}{2}\right)}{a}\right)$$

$$\times \left[\frac{2\left(\frac{iL_a}{2}\right)^2}{\left[1 - \left(\frac{i}{s}\frac{L_a}{L_b}\right)^2\right]} \frac{s^2\pi L_b}{}\right] \left((-1)^i \sin \frac{s\pi\left(\frac{L_a}{2} + \frac{L_b}{2}\right)}{L_a} - \sin \frac{s\pi\left(\frac{L_a}{2} - \frac{L_b}{2}\right)}{L_a}\right)$$

$$\times \left(\frac{b}{\pi}\right)^2 \left[1 - \left(\frac{s\pi}{kL_a}\right)^2\right] \gamma(n,s)$$

$$+ \left(\frac{si\pi^2}{L_a L_b}\right) \sum_{m=o}^{\infty} \frac{\varepsilon_{om}\left[1 + \left(\frac{\Gamma_{nm}}{k}\right)^2\right]}{\Gamma_{nm}^5 \left[1 + \left(\frac{s\pi}{\Gamma_{nm}L_a}\right)^2\right]\left[1 + \left(\frac{i\pi}{\Gamma_{nm}L_b}\right)^2\right]}$$

$$\times \left[\left(e^{-\Gamma_{nm}\left(\frac{L_a}{2} - \frac{L_b}{2}\right)} - (-1)^i e^{-\Gamma_{nm}\left(\frac{L_a}{2} + \frac{L_b}{2}\right)}\right)\right.$$

$$\left. - (-1)^s \left(e^{-\Gamma_{nm}\left(\frac{L_a}{2} + \frac{L_b}{2}\right)} - (-1)^i e^{-\Gamma_{nm}\left(\frac{L_a}{2} - \frac{L_b}{2}\right)}\right)\right] \qquad (4.19b)$$

where L_a, L_b are the lengths of the appropriate sections.

The Ψ = constant mode must also be included in the complete solution for the longitudinal slot. This mode may be modified as follows for the sectional slot.

$$\frac{-3W_1^{\,2}\,(1-(-1)^{i})(1-(-1)^{s})}{j\,\omega\,\mu_o\,ab\,i\,s\,\pi^2}\;\times\;(L_1+2L_2) \qquad (4.20)$$

Where L_1 and L_2 are the lengths of the middle section and outer section respectively.

The complete solution for integral expression (4.13) is

$$\Sigma \text{ term } (4.18) + \Sigma \text{ term } (4.19) + \text{term } (4.20) \qquad (4.21)$$

The summation of term (4.18) includes all self coupling terms and mutual coupling terms for sections with the same length. The summation of term (4.19) includes all mutual coupling terms for differing lengths.

4.1.3 CONTRIBUTION OF THE INCIDENT FIELD

The contribution of the incident field remains to be calculated for the new slot arrangement, this is given by

$$h_i = -\iint_S f_i\;\hat{\underline{a}}_z\;.\;\{\underline{n}\;x\;\underline{H}_i(r)\}\;dS \qquad (4.22)$$

and depends on the slot orientation. The incident fields are given by

$$E_y^+ = -j\omega\mu_o\;\phi\;\sin\frac{\pi x}{a}\;e^{-j\beta_g z}\;\hat{\underline{A}}_y \qquad (4.23)$$

$$H_x^+ = j\;\beta_g\;\phi\;\sin\frac{\pi x}{a}\;e^{-j\beta_g z}\;\hat{\underline{A}}_x \qquad (4.24)$$

$$H_z^+ = \frac{\pi}{a} \phi \cos \frac{\pi x}{a} e^{-j\beta_g z} \hat{A}_z \qquad (4.25)$$

where $$\phi = (k Z_o \beta_g a b)^{-\frac{1}{2}} \qquad (4.26)$$

Substituting equations (4.23), (4.24), (4.25) into equation (4.22) gives, for a transverse slot

$$h_i = \sum_{D=1}^{3} 2j\phi \sigma(i,1) \sin \frac{\beta_g W_1}{2} e^{-j\beta_g Z_D} \qquad (4.27)$$

where Z_D is the offset from the centre of the slot to the centre of the section being summed.

For a longitudinal slot

$$h_i = \sum_{D=1}^{3} \phi \left[\sin \frac{\pi(X_D + \frac{W_1}{2})}{a} - \sin \frac{\pi(X_D - \frac{W_1}{2})}{a} \right]$$

$$\times \frac{\frac{i\pi}{L_D}}{(\frac{i\pi}{L_D})^2 - \beta_g^2} \begin{cases} 2 \cos \beta_g L_{D/2} & i \text{ odd} \\ 2j \sin \beta_g L_{D/2} & i \text{ even} \end{cases} \qquad (4.28)$$

where X_D is the offset to the centre line of the section, and L_D is the length of the section.

4.1.4 EDGE EFFECT

The sectioned model may also be employed to simulate the enhanced field strengths at the slot edges. A functional relationship for the field profile across the slot in the presence of the edge enhancement

has been formulated by Park [2.29] and is reproduced below. For clarity this function is also illustrated in Figure (4.2) (solid curve).

$$\frac{W}{\pi\sqrt{\left(\frac{W}{2}\right)^2 - (\eta)^2}} \qquad (4.29)$$

This effect can be incorporated into the model by averaging the above function over the n(=3) sections of the slot. The averaged values are shown in Figure (4.2) (dashed line). These values are used to adjust the self coupling and mutual coupling terms in the moment method analysis.

4.2 DISCUSSION OF RESULTS

A computer program has been written to accommodate the analysis described in the preceding sections which is capable of predicting the radiation or scattering characteristics, in S-matrix or equivalent circuit form, for any longitudinal or transverse slot in the broadwall of rectangular waveguide. The program has been used to generate theoretical results, firstly, to assess the viability of the sectioned slot and secondly, to develop an understanding of the relationship between the slot scattering and the width parameter. The latter study has been restricted to the longitudinal slot due to its application to array antennas.

4.2.1 SECTIONED SLOT

The sectioned slot has been assessed by examining two particularly interesting cases, namely the resonance behaviour of a longitudinal

slot as a function of its offset from the waveguide centre line and the power radiated by a transverse slot as a function of its length.

In Figure (4.3) computer predictions are presented of the resonant length of a square ended longitudinal slot as a function of its offset from the guide centre line. Two cases are presented, namely a conventional result and a sectioned result. Both cases use three trignometric basis functions. It can be seen that for the square ended slot example sectioning has very little effect on the computed results. Clearly, therefore, there is little to be gained by sectioning for square ended slots. Both curves show a deviation of at worst approximately 1% from the measured results of Stern and Elliott [2.28].

However, in practical slotted waveguide antennas square ended slots are almost never used. Round ended slots are much more common. It is pertinent, therefore, to attempt to model the round ended slots as discussed earlier and some results from this modelling are shown in Figure (4.4). This figure also contains some measured results due to Stegen [4.6] to assist in the assessment of the computer predictions. Two theoretical cases are shown each of which is intended to model the Stegen experiment. These are, firstly a square ended slot model and secondly a three sectioned slot model. The figure clearly demonstrates that the sectioned slot provides an improvement of approximately 1% on the conventional square ended model for small offsets. However, at approximately 6 mm offset the model breaks down and the theoretical curves cross with the solution for the conventional slot shifting closer to the Stegen result. This

crossover can be attributed to the crudeness of the model with the sectioning being applied to only the inner surface of the slot.

Further evidence that slot sectioning, even when very coarse, can improve agreement between theory and experiment for round ended slots is illustrated in Figure (4.5). Here models which are intended to represent a round ended transverse slot in the broadwall of rectangular waveguide are examined. Firstly, a simple square ended slot model equal in length to the round ended slot, which it is intended to represent, provides an over estimate of the power radiated by such a slot. The lowest curve provides a lower limit to power radiated being that of an equivalent length (perimeter rule) square ended slot which is known to under-estimate the radiation strength of its round ended counterpart. The three sectioned slot model predicts radiation strengths for the round ended slot which lie nicely between these limiting cases up to resonance confirming sectioning can provide some improvement in accuracy for the moment method. The model breaks down at resonance and this can once again be attributed to its crudeness.

The edge effect has also been incorporated into the sectioned model and results for the transverse and longitudinal slots are presented in Figures (4.5) and (4.6) respectively. Unfortunately it is virtually impossible to distinguish between the results which demonstrates that this model is too simplistic to accurately predict the effect of the enhanced fields at the edges of the slots.

4.2.2 WIDTH PARAMETER

Preliminary theoretical studies of the influence of the slot width on the resonant length of longitudinal offset slots were carried out using simple trignometric basis functions. This choice of basis function is adequate provided the field enhancement within the slot due to the edge effect is not significant. This assumption is reasonable if the waveguide wall is not too thin (ie less than 0.05a where a is the guide width) otherwise a more complex basis function must be adopted [3.11]. The width to length ratio has also been restricted to values for which any cross-polar component within the slot can safely be neglected [3.9, 3.10].

In Figure (4.7) computer predictions are presented of the resonant length of a conventional square ended longitudinal slot as a function of offset from the waveguide centre line. Three cases are presented each using three trignometric basis functions. It can be seen for offsets in excess of 5 mm the resonant length becomes an increasing function of slot width whereas it is a decreasing function of width for small offsets. The curves also show that over the Stegen offset range (2 to 6 mm) the computed results differ from that of the typical slot (W = 1.5875 mm) by at most 1%, even for relatively wide slots for which W = 2.5 mm.

To understand how this contrasting resonant behaviour comes about, reference must be made to the susceptance characteristics of such slots. This is illustrated in Figure (4.8) in which shunt slot susceptance is plotted against slot length for two particular offsets, namely 4 mm and 8 mm. The lower set of curves (4 mm) show largely the same trends as some familiar susceptance curves produced

by Watson. In particular they show that for small offsets shunt slots display a region where susceptance is almost independent of width and this region is in the negative susceptance range. By contrast for a large offset (8 mm) this region of width independent susceptance moves into the positive susceptance range. It is this movement of the width independent region which results in the contrasting resonant frequency behaviour described earlier.

Susceptance has also been plotted as a function of offset in Figures (4.9) and (4.10) for two slot examples. In Figure (4.9) a 15.8 mm slot which resonates at a large offset has been chosen, while in Figure (4.10) a 15.3 mm slot is employed to ensure resonance occurs at a small offset. In both cases comparison is made between a 1.5875 mm and a 2.5 mm wide slot. Resonance occurs when the total susceptance crosses the zero axis and the figures show that this coincides with balancing of the parts of susceptance associated with energy storage within the guide and the part associated with storage of energy within the slot itself and on its outer surface. When these partial susceptances are compared between the two figures it is noticeable that while the inner surface susceptance differs only slightly, the cavity plus outer surface susceptance curves are markedly different in form with a reversal of the order of curves. Also for the shorter slot (Figure (4.10)) the susceptance of the cavity and the outer surface is much more sensitive to width. Both of these factors contribute to the differing resonance characteristics which the two slots exhibit.

Figures (4.11) to (4.14) demonstrate very similar behaviour for a shunt slot located in a 'thin walled' waveguide, namely 0.127 mm.

The extent of the comparison between thick and thin walled examples suggests that storage of energy in the vicinity of the slot is not too sensitive to wall thickness. However, this observation is made in the knowledge that field enhancement at the slot edges has not been incorporated into the model.

The second phenomenon observed is the bandwidth improvement. This is illustrated in Figures (4.15) and (4.16) where the normalised power radiated is plotted as a function of slot length. Two sets of results are presented to demonstrate this effect for contrasting values of slot offset. For slots which are at, or close to, resonance the width variation is seen to have little effect on the power radiated. However, for slots off resonance the effect is significant with the wider slot having a flatter response. It is this flattening of response which gives rise to the bandwidth improvement.

4.3 CONCLUSION

The moment method of analysis of radiating slots in rectangular waveguide has conventionally been applied to square ended slots. This analysis has been extended to round ended slots by employing slot sectioning on the inner surface of the slot. The slot cavity and outer surface are adjusted to accommodate this modification. This technique is clearly more demanding in computational terms but not excessively so if trignometric basis functions are employed. Improvements in accuracy of the order of 1% are observed for the predicted resonant length of longitudinal slots with low offsets. However, the model breaks down under certain conditions due to its simplicity. Unfortunately any attempt to increase the sophistication

of the model by for example applying sectioning to the cavity and outer surface of the slot and/or incorporating more than three sections leads to dramatic increases in computational effort which are difficult to justify.

The moment method analysis for conventional slots has also been used to examine the resonant characteristics of shunt slots exhibiting width to length ratios in the range of $0.1 < W/L < 0.25$. Such slots are used to achieve improved bandwidth performance and/or power handling capacity for longitudinal shunt slot arrays.

The computations indicate that the relationship between resonant length and slot width differs markedly for slots which are close to the centre of the waveguide and those nearer the side wall. This difference in behaviour has been discussed and explained in terms of changes in slot susceptance.

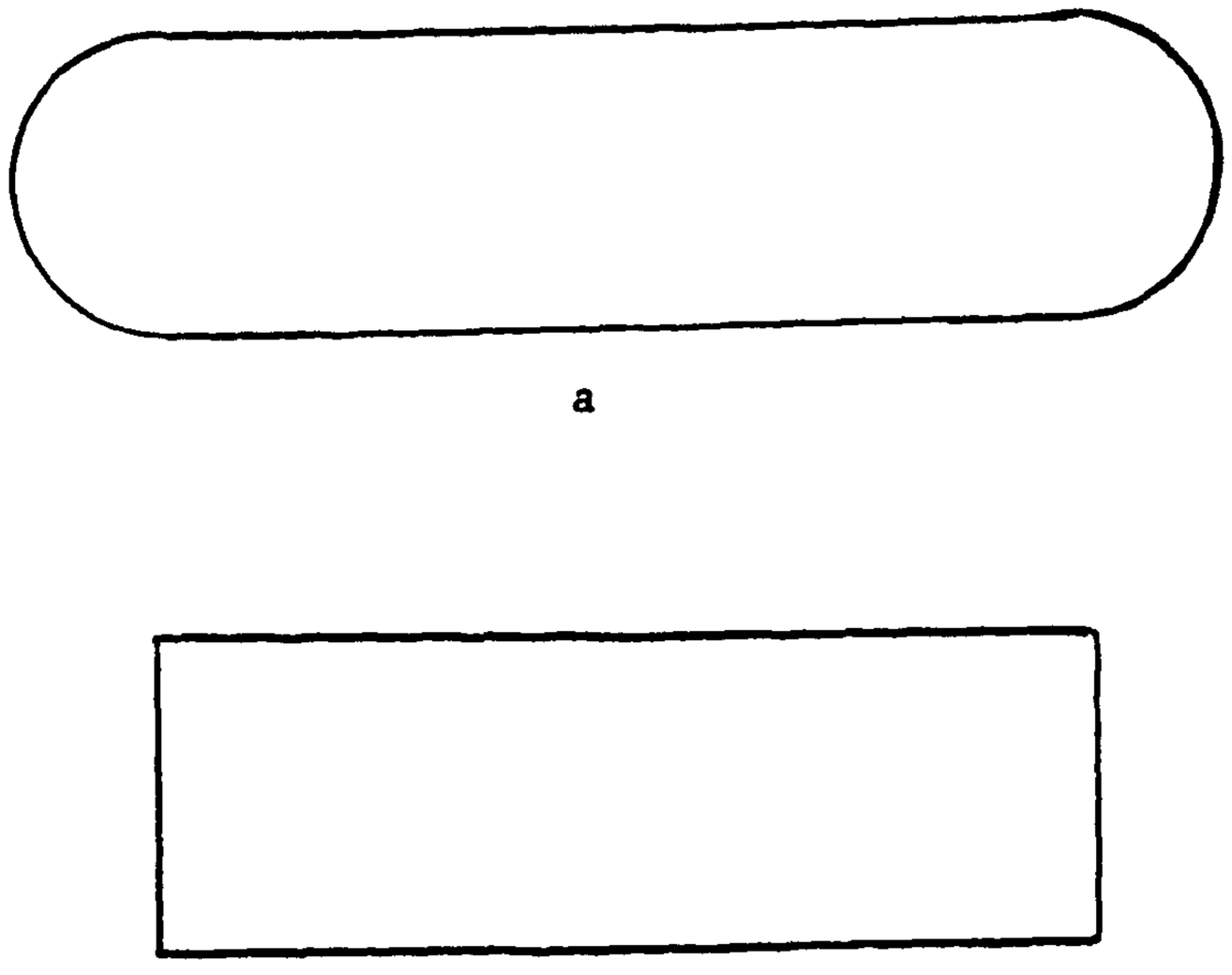

View of (a) Round ended slot

(b) Equivalent length rectangular slot

(c) Sectioned slot

Figure 4.1

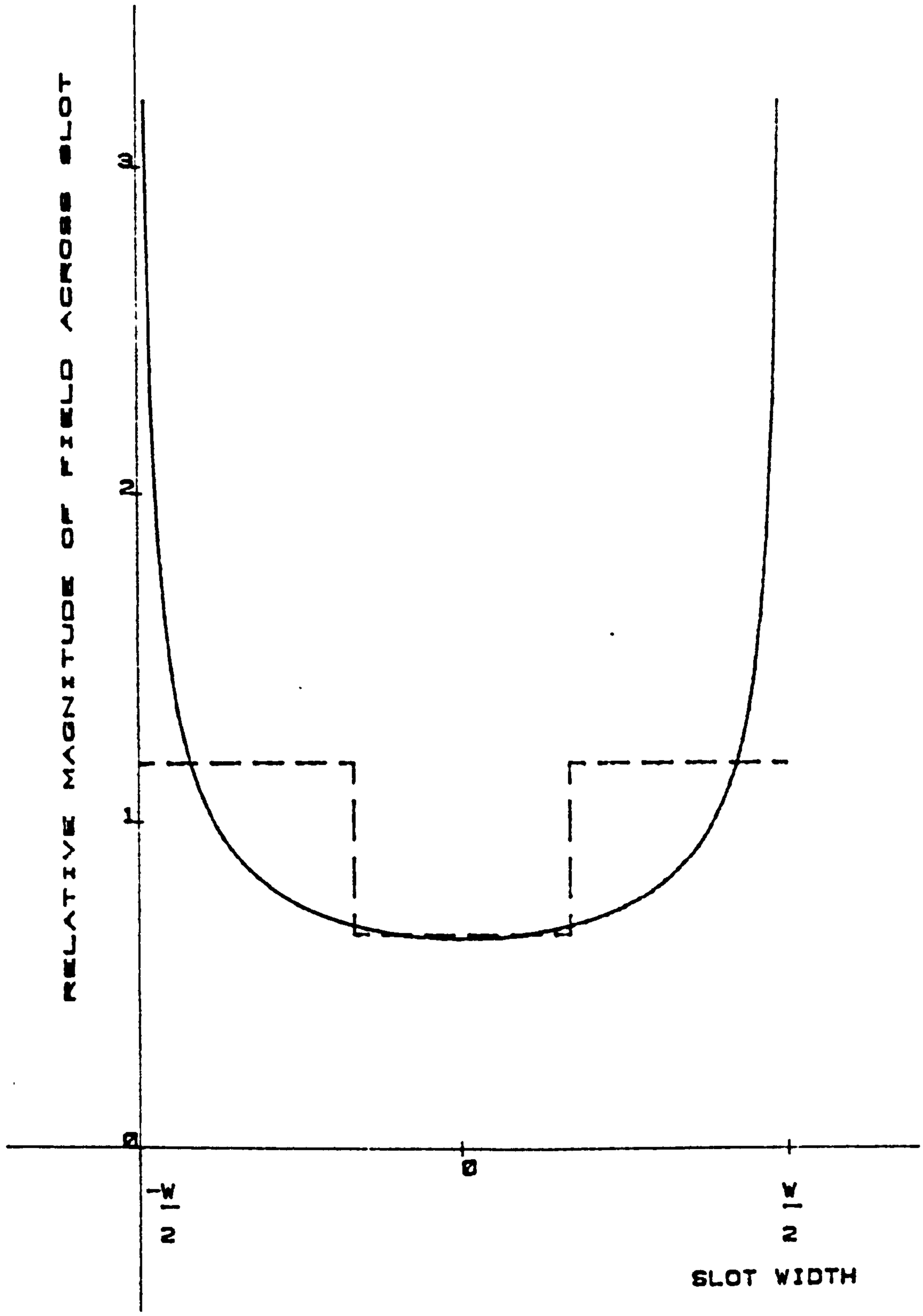

Figure 4.2

A Graph of the Relative Magnitude of the Field across the Slot

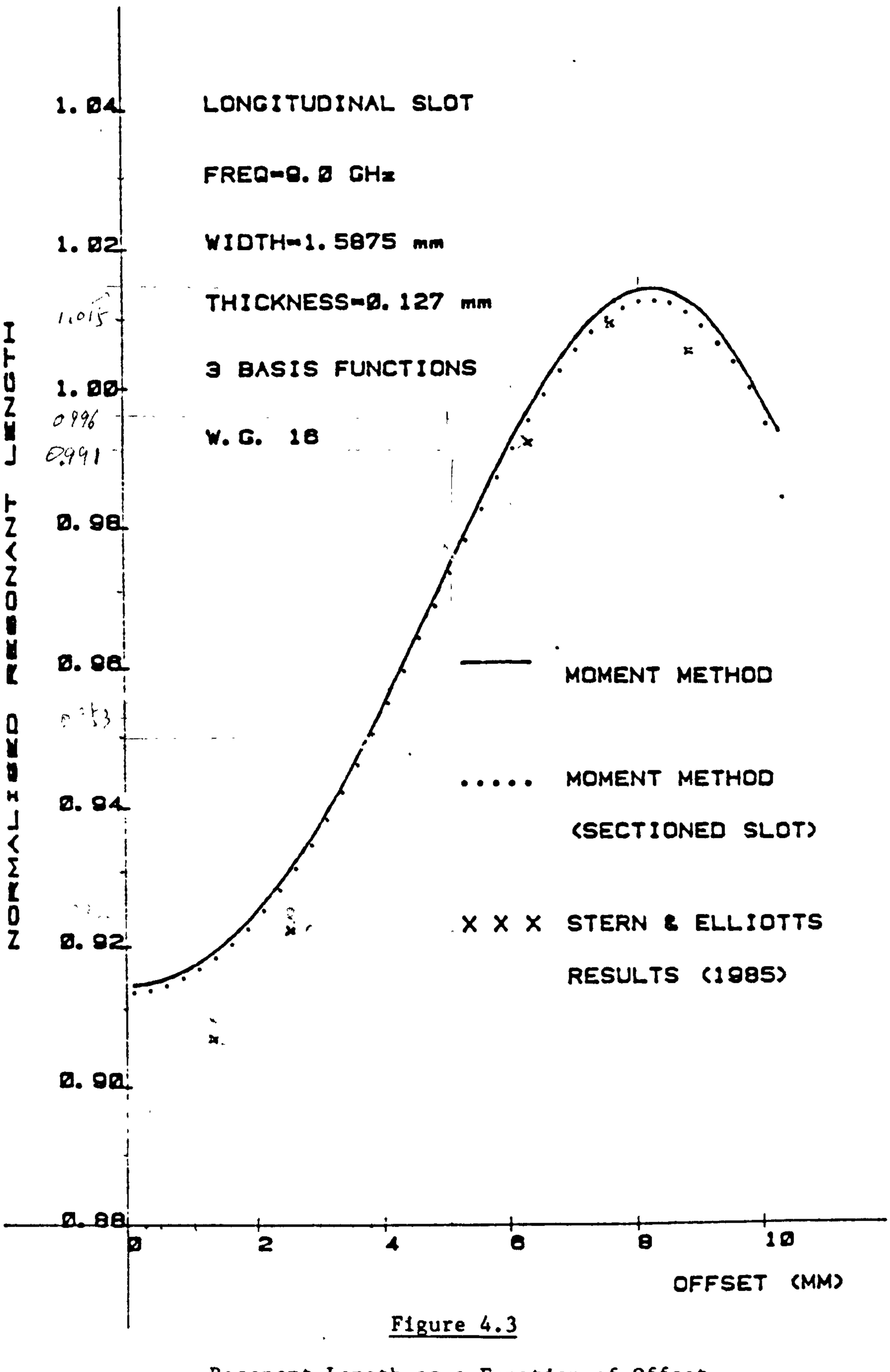

Figure 4.3

Resonant Length as a Function of Offset
for Various Rectangular Longitudinal Slots

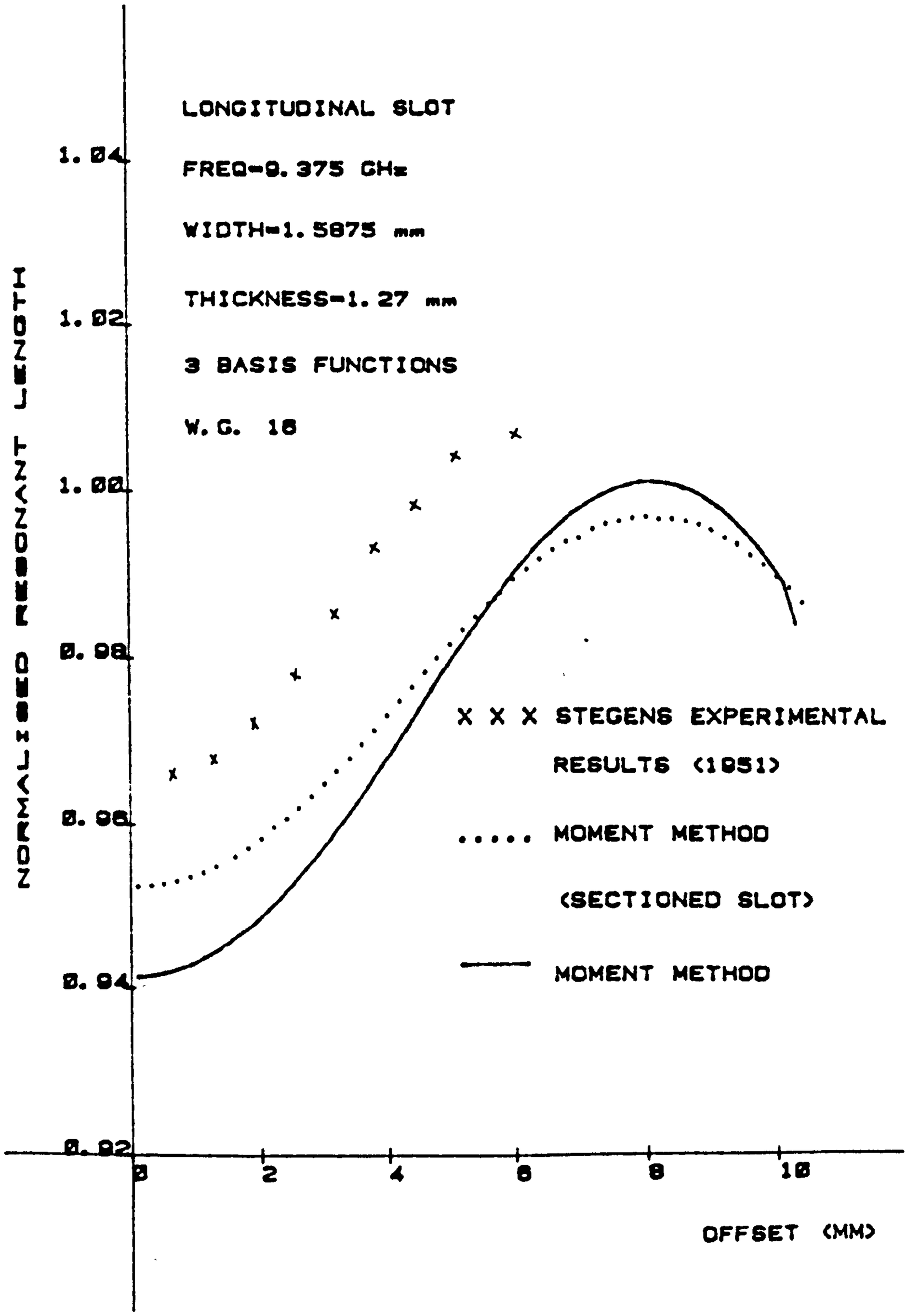

Figure 4.4

Resonant Length as a Function of Offset
for Various Longitudinal Slots

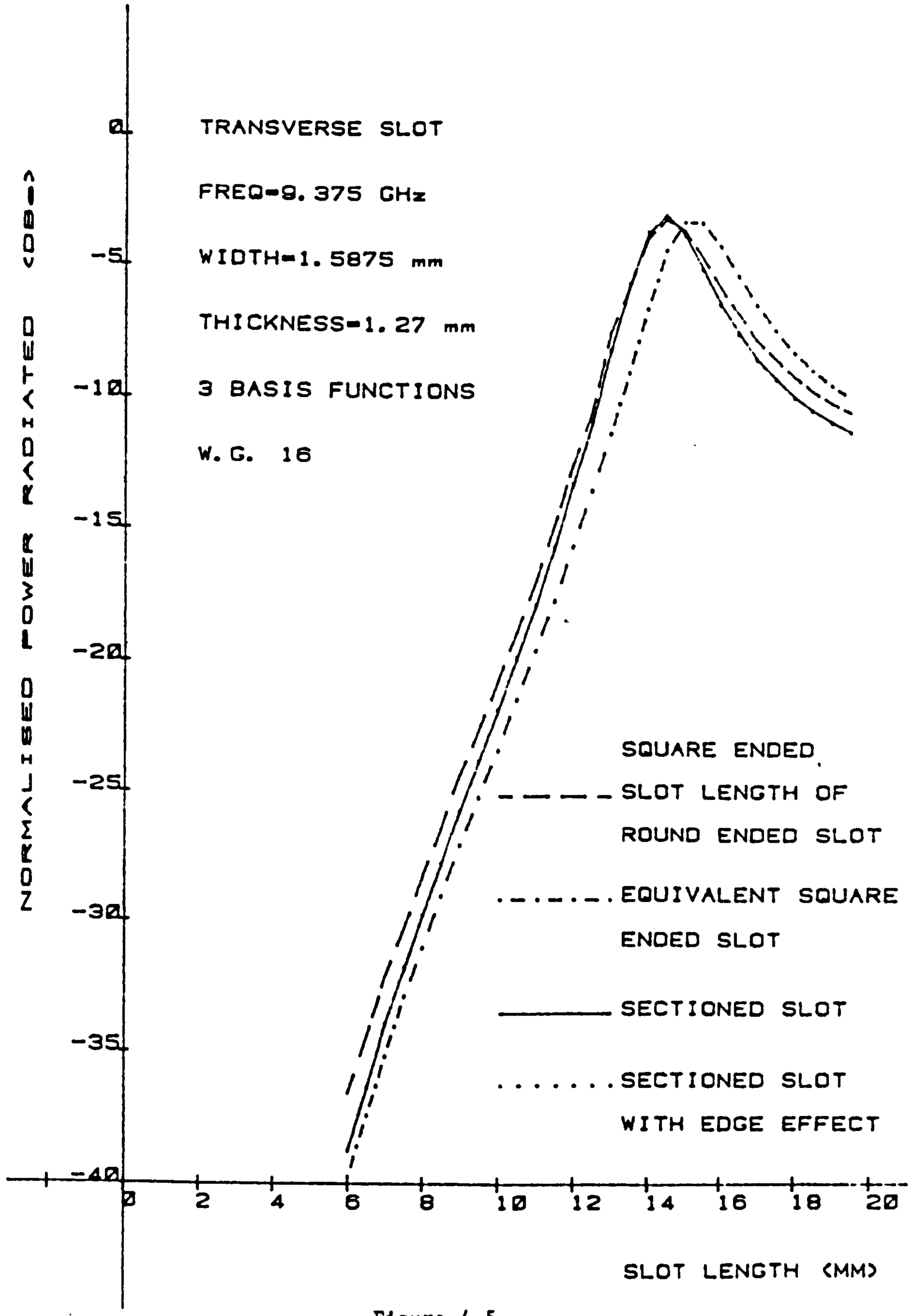

Figure 4.5

Normalised Power Radiated versus Slot Length
for various Transverse Slots

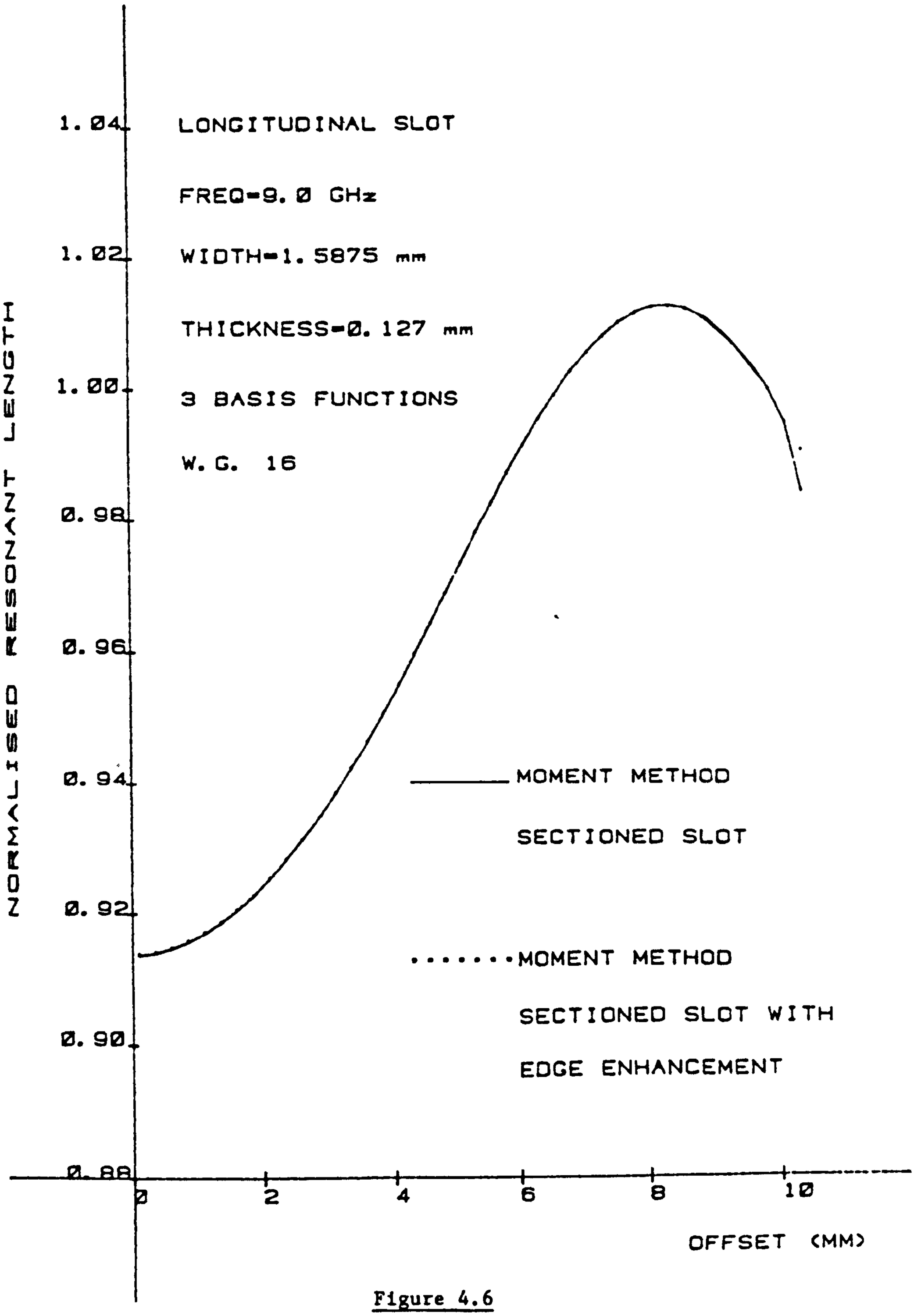

Figure 4.6

Resonant Length as a Function of Offset for a Sectioned Rectangular Longitudinal Slot

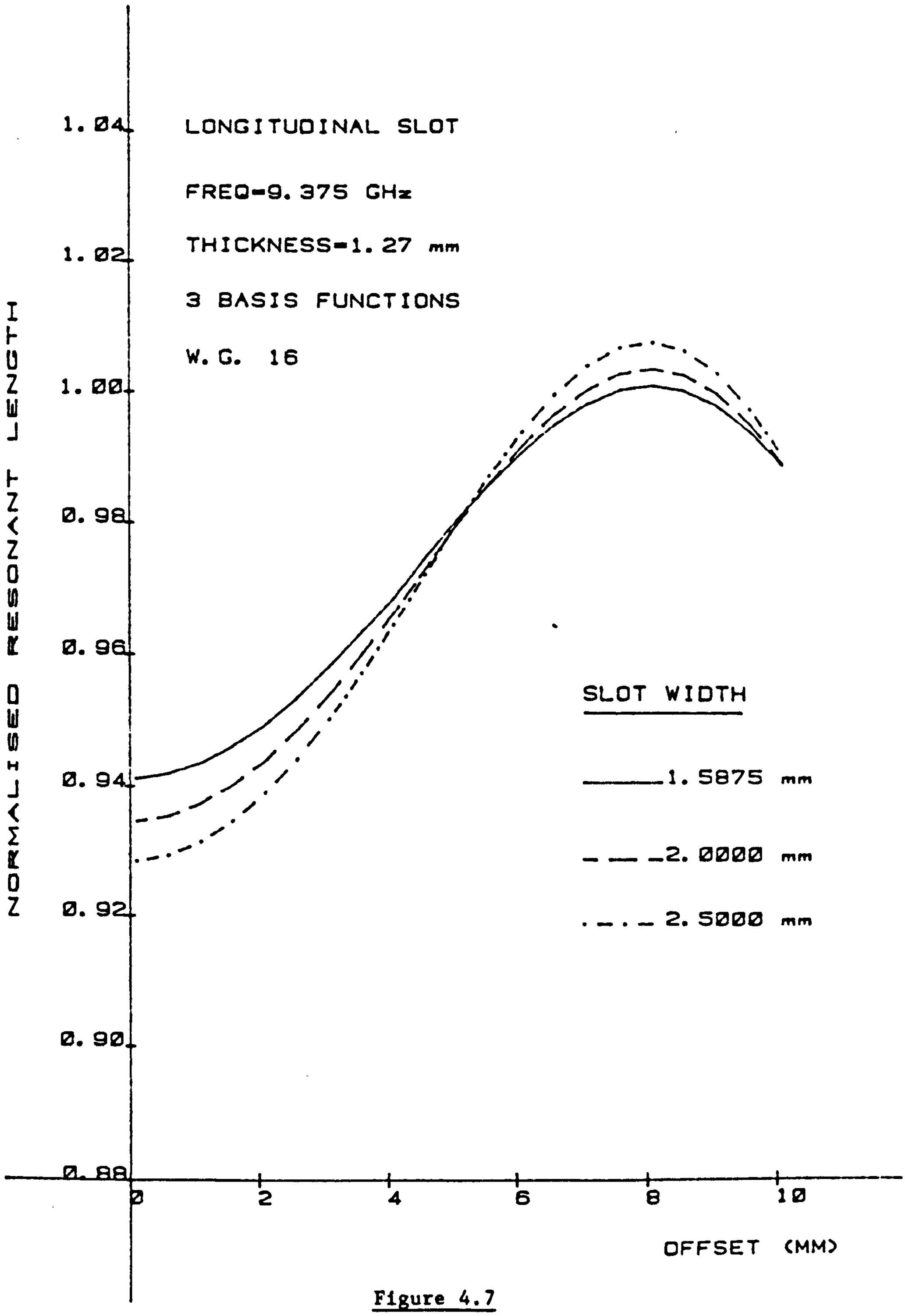

Figure 4.7

Resonant Length as a Function of Offset for various Longitudinal Slots - Thick Walled Case

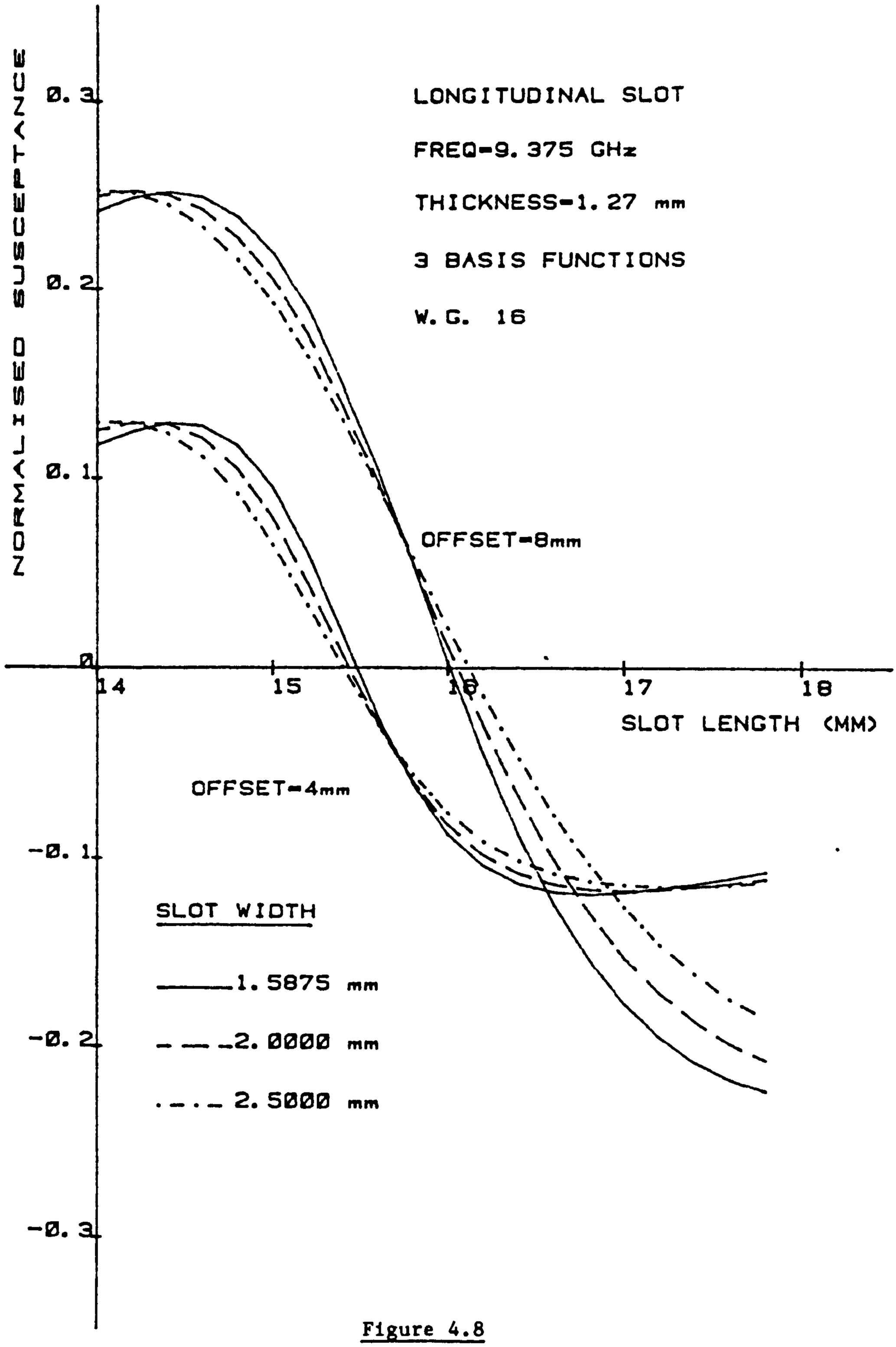

Figure 4.8

Normalised Susceptance as a Function of Slot Length for a Longitudinal Slot

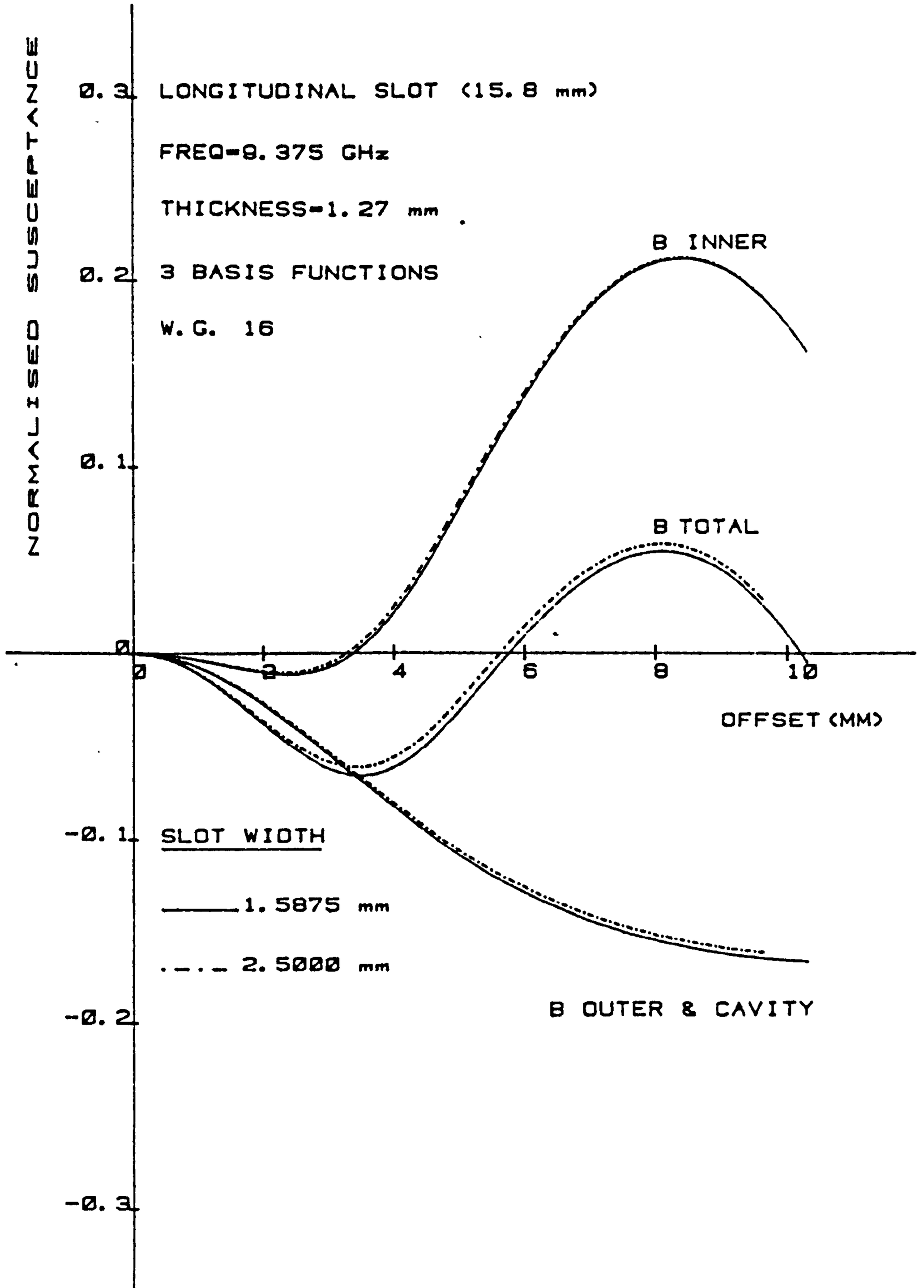

Figure 4.9

Normalised Susceptance as a Function of Offset for a Longitudinal Slot (15.8 mm)

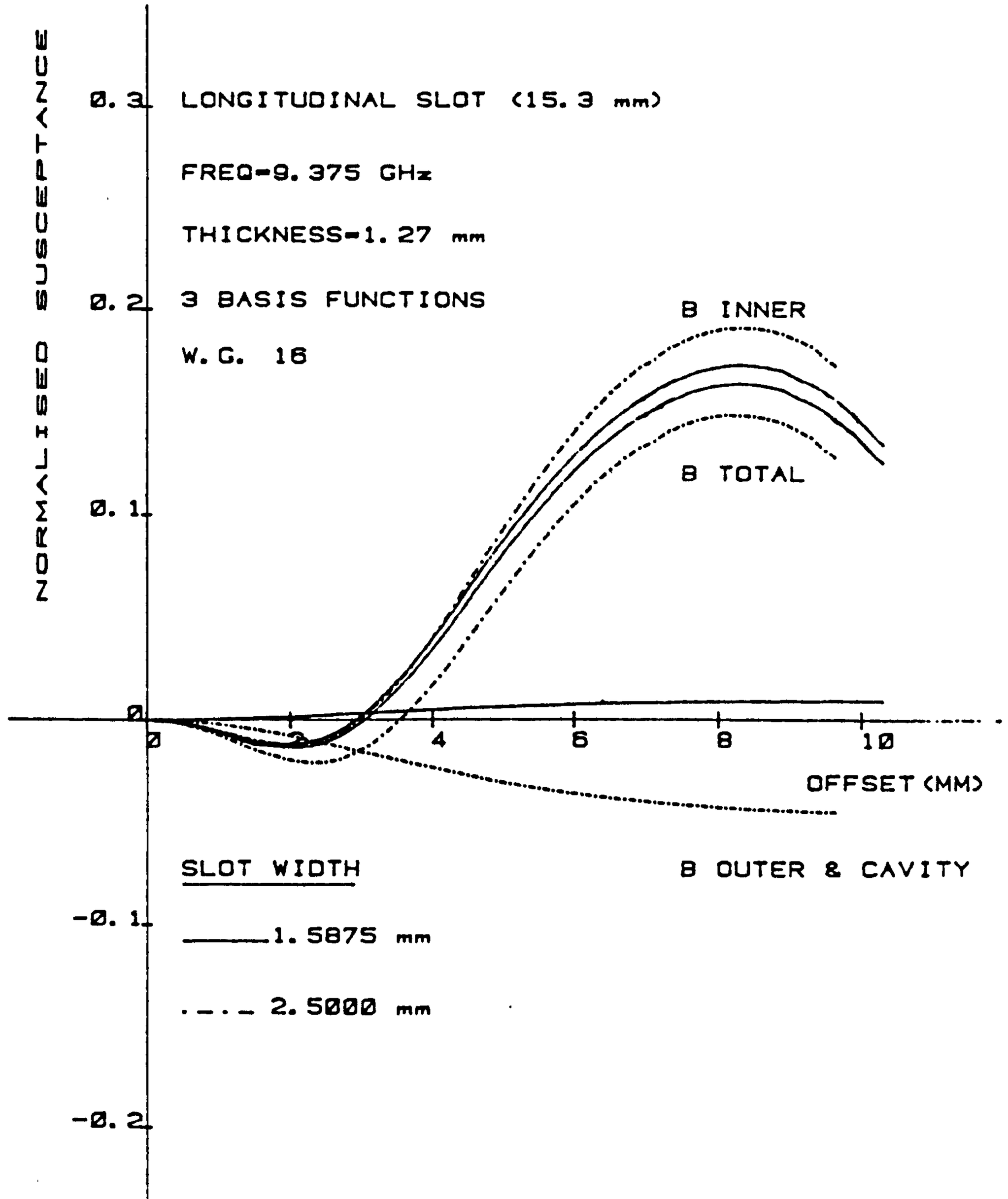

Figure 4.10

Normalised Susceptance as a Function of Offset
for a Longitudinal Slot (15.3 mm)

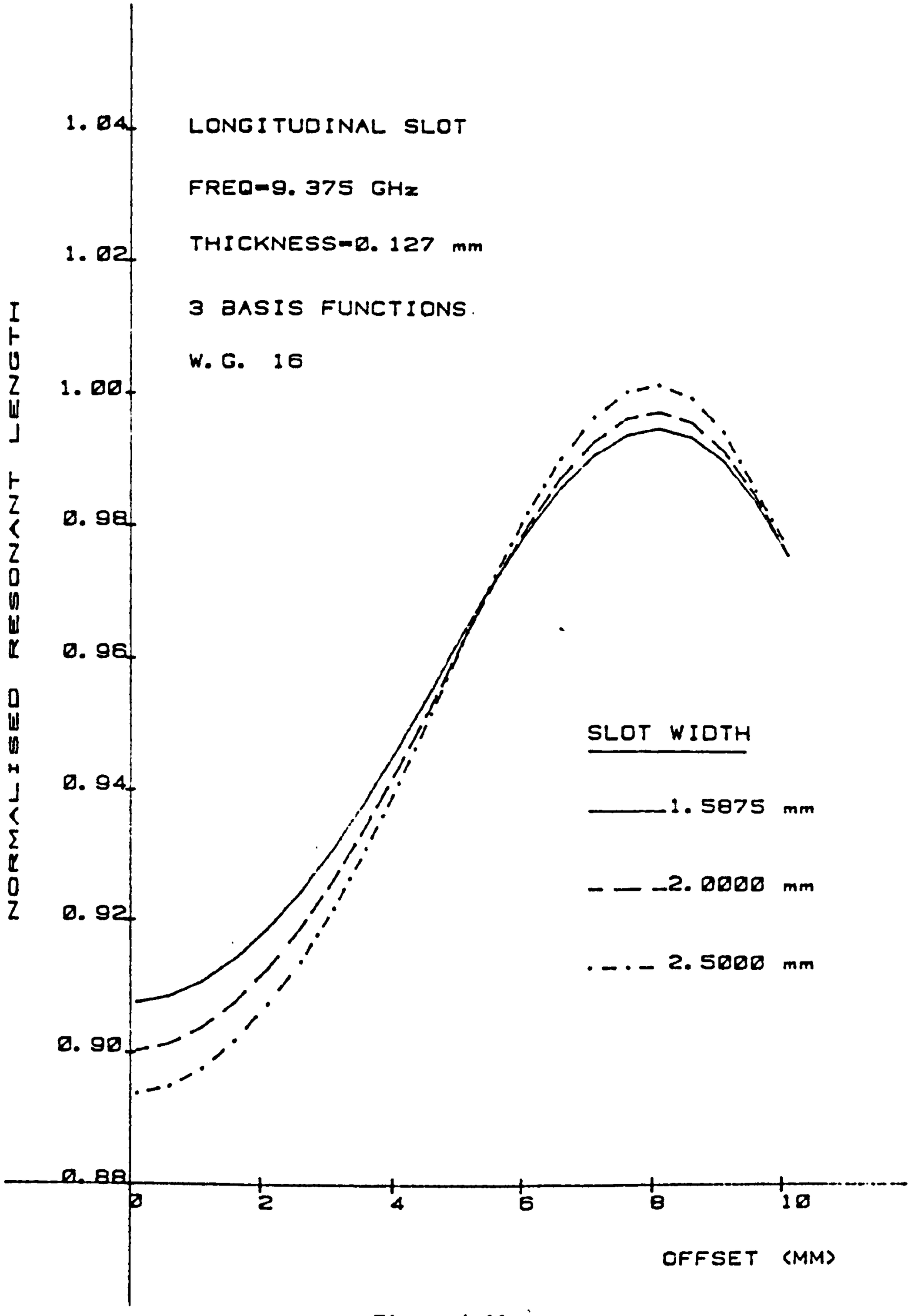

Figure 4.11

Resonant Length as a Function of Offset for Various Longitudinal Slots - Thin Walled Case

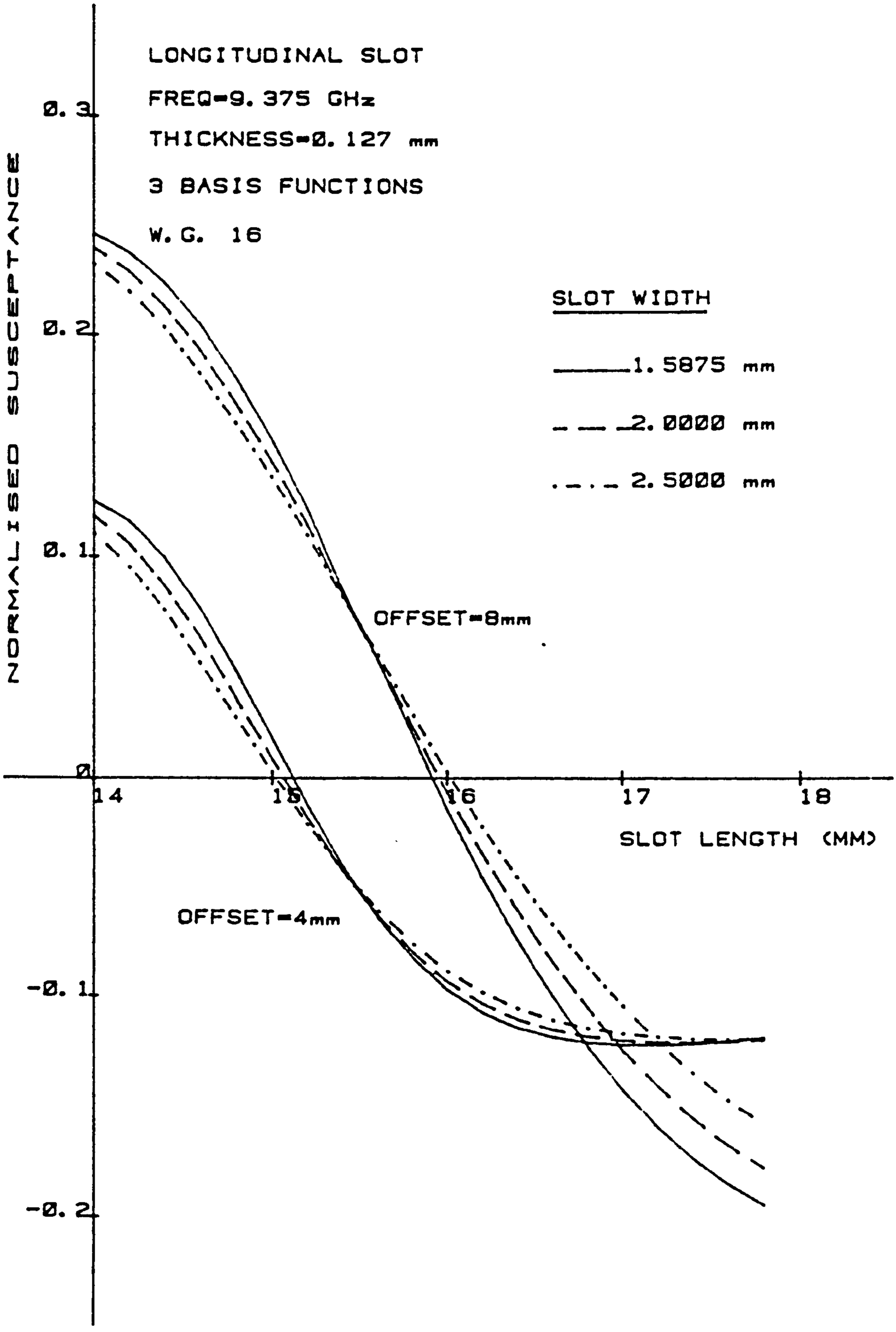

Figure 4.12

Normalised Susceptance as a Function of Slot Length for a Longitudinal Slot

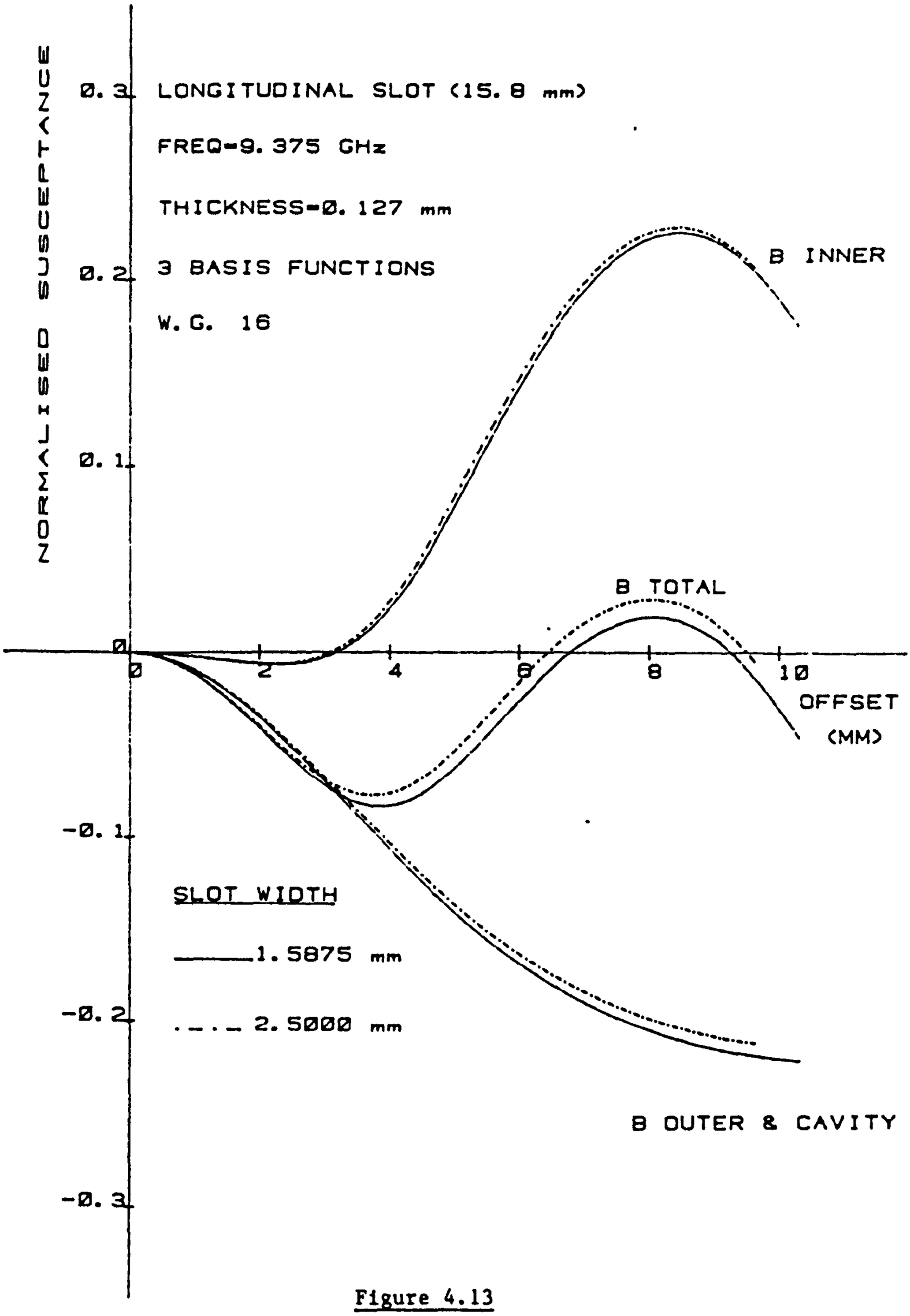

Figure 4.13

Normalised Susceptance as a Function of Offset
for a Longitudinal Slot (15.8 mm)

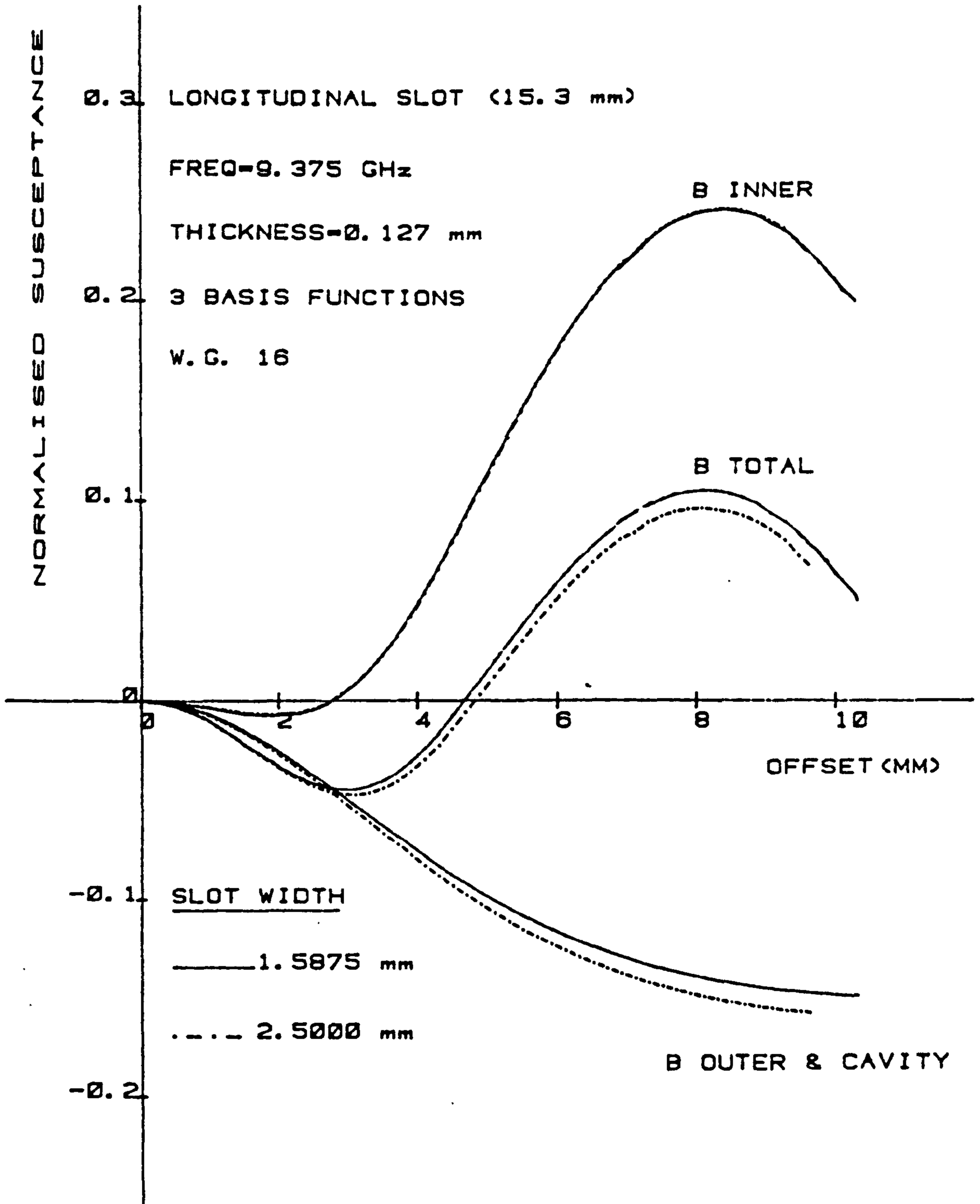

Figure 4.14

Normalised Susceptance as a Function of Offset for a Longitudinal Slot (15.3 mm)

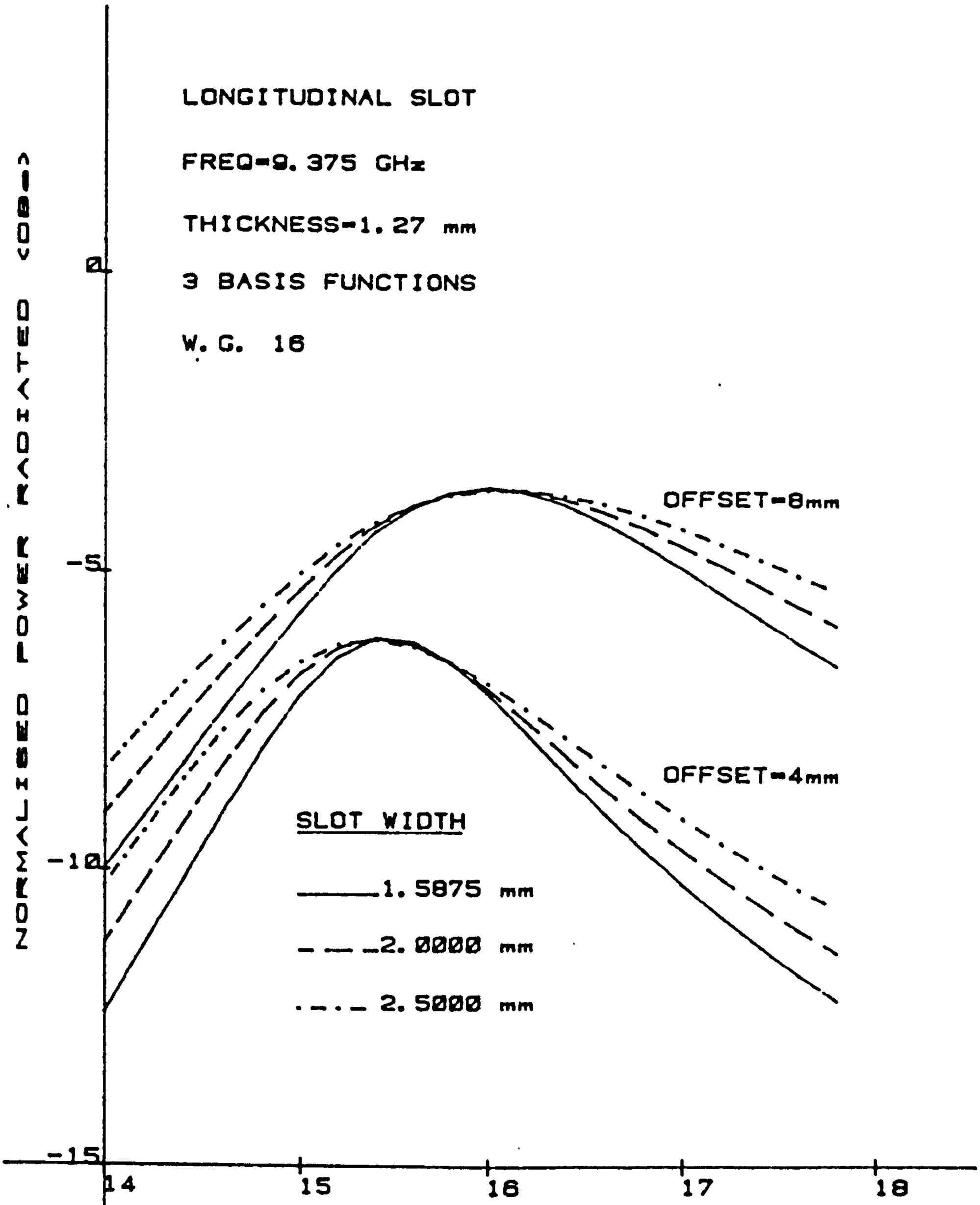

Figure 4.15

Normalised Power Radiated as a Function of Slot Length for a Longitudinal Slot - Thick Walled Case

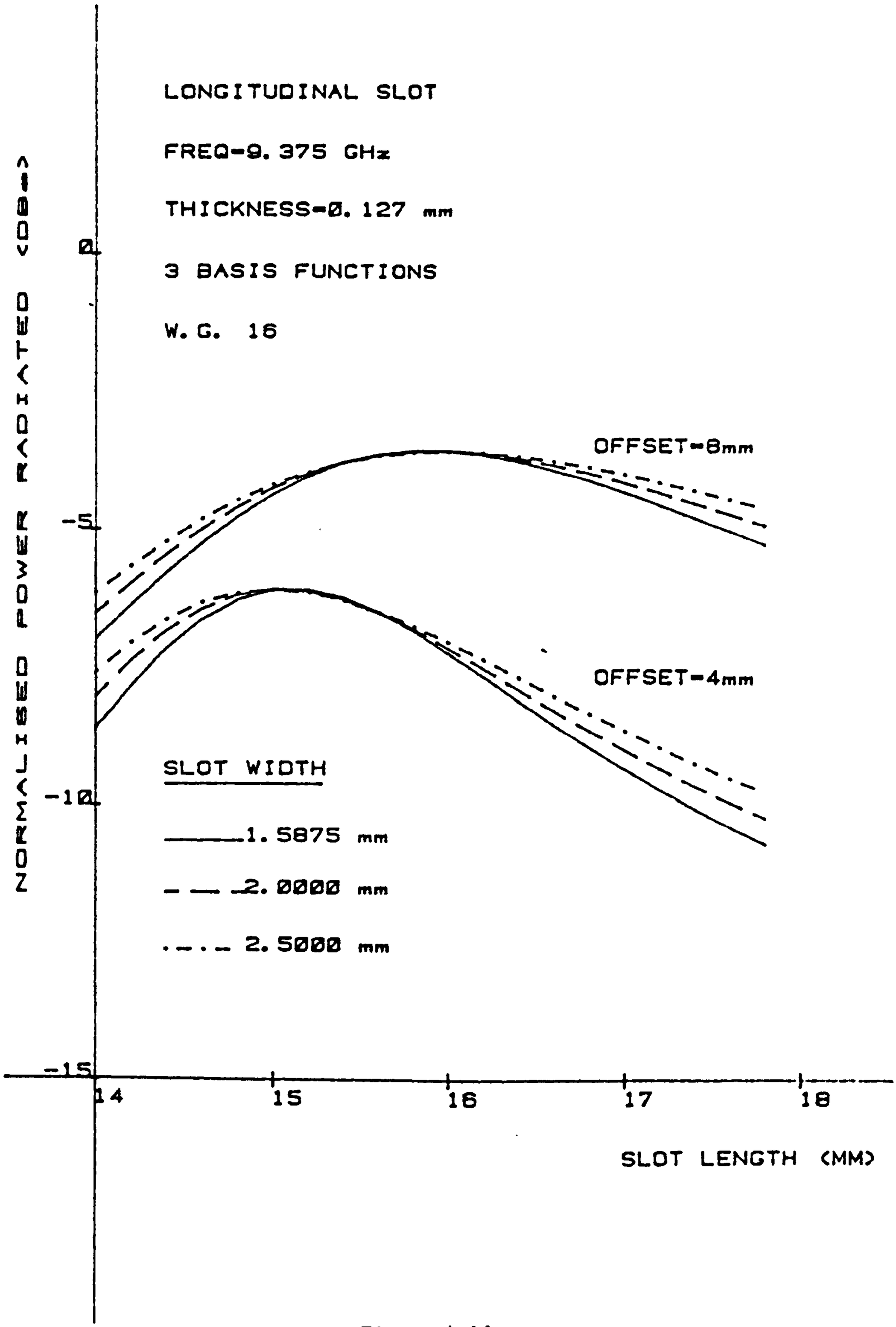

Figure 4.16

Normalised Power Radiated as a Function of Slot Length for a Longitudinal Slot - Thin Walled Case

CHAPTER 5

EXPERIMENTAL CONFIRMATION OF WIDTH DEPENDENT CHARACTERISTICS OF A LONGITUDINAL SLOT

The theoretical study based on the method of moments in the preceding chapter has produced data on the functional relationship between the resonant length and the width parameter of a longitudinal shunt slot. The measurements described in this chapter confirm the predicted relationship and once more demonstrate the suitability of this analysis technique for CAD work.

Unfortunately, the traditional measurement techniques are unable to provide the experimental data for longitudinal slots over the required offset range. Therefore, a new measurement technique has been developed using a precision waveguide bridge in conjunction with an r.f. source synchronised to an accurate frequency counter. However, before discussing this set-up in detail, it is worth digressing slightly and outlining the techniques currently available.

5.1 COMPARISON OF MEASUREMENT TECHNIQUES

There are three measurement techniques available to characterise slots in waveguides. The simplest of these measures the transmission and reflection coefficients of the slotted waveguide section using the arrangements illustrated in Figures (5.1) and (5.2) respectively. This method provides reasonable results for slots which couple strongly to the incident fields. However, if the slot coupling drops below -10 dBs then this technique is difficult to implement as the transmission and reflection coefficients become virtually indistinguishable from one and zero respectively.

Watson [4.5] postulated an alternative, more sensitive technique which was capable of characterising slots with radiated power levels down to approximately -20 dBs. A schematic diagram of this measurement system is illustrated in Figure (5.3). This measurement involves initially determining the position of the short circuit which effectively shorts the slot and permits no power to radiate. The short circuit is then moved $\lambda_g/4$ and the input VSWR is measured which enables the slot to be characterised using transmission line theory.

A third technique based on a resonant cavity has also been reported in [5.1] which was later refined by McGrane [5.2]. This technique is capable of characterising a slot which radiates power levels down to around -30 dBs and operates on the principle that the introduction of a slot into a resonant cavity perturbs the 'Q' and the resonant frequency, which in turn affects the transmission through the cavity. The measurement system has been illustrated in Figure (5.1). Most of the components in this figure are self explanatory, however, it is worth mentioning the construction of the cavity which comprises of a length of waveguide which is resonated between two irises. The slot is characterised using this technique by measuring the power coupled through the cavity, the change in coupled power (once the slot is introduced) and the shift in resonant frequency. Also, the transmission characteristics of the irises must be measured over the experimental frequency range. Once this data has been collected then the scattering parameters of the slot may be evaluated in terms of the transmission coefficients of the cavity. A short fortran program has been detailed in [5.2] to process these results.

McGrane suggests that the length of the waveguide section should be approximately ten times the free space wavelength of the lowest operating frequency to yield sufficient resonances within the cavity to plot a curve of slot coupling against frequency. However, this must be lengthened if the resonant frequency of a longitudinal slot is to be determined accurately. Even then it is extremely difficult to obtain the required accuracy as the experimental data is only actually available at the resonant frequencies of the cavity. Consequently, interpolation is required to determine the resonant frequency of the slot. A second drawback of this technique is its inability to characterise slots which are close to resonance exhibiting large offsets as most of the power is absorbed in the slots. This results in the cavity being damped and consequently, the relevant data cannot be measured.

5.2 WAVEGUIDE BRIDGE TECHNIQUE

An alternative measurement system has been developed which measures the phase and magnitude of the reflection coefficient of a slot in a waveguide and is capable of accurately determining the resonant frequency of a longitudinal slot of any width and offset. A schematic diagram of this measurement system is presented in Figure (5.5). As mentioned earlier this uses a precision waveguide bridge in conjunction with an r.f. source, which is synchronised to an accurate frequency counter to control the input signal to within 10 kHz. This system operates by splitting the input signal and feeding two channels: a test channel and a reference channel. The slotted waveguide section is connected to the test channel and terminated in a matched load via a three stub tuner which can be adjusted to optimise the match at each operating frequency. A variable short

circuit is used to terminate the reference channel. This is driven by a high precision micrometer to locate the short at a position which is electrically equivalent to the centre of the slot. The reflected signals from both the slot and the short circuit are then processed by a network analyser and the reflection coefficient of the slot is displayed on a magnitude/phase meter and a polar display.

Various steps have been taken to optimise this measurement system. For example, the set-up has been mounted inside an anechoic chamber to minimise the back-scattering that occurs when the slot radiates and the slotted waveguide section has been embedded in a ground plane (27 x 30 cm) which was edged with lossy r.f. absorbent material to suppress edge diffraction. Care has also been taken to ensure that stable temperature conditions prevail during each measurement. This has been achieved by running the system continuously, for several hours, prior to performing a measurement. High precision components have also been used to enhance the accuracy of this measurement and the result is a system that is capable of determining the resonant frequency of a slot to an accuracy of better than 0.2%.

A series of measurements was carried out on various round end slots cut in standard X-band waveguide. However, before discussing the results it is worth detailing the experimental procedure. The set-up was initially calibrated with the test channel terminated in a fixed short circuit and the reference channel in a variable short circuit. Care was taken to ensure that any differences in electrical length between the two channels over the operating frequency range were determined and compensated for. These differences were quantitatively determined by adjusting the variable short circuit

until the two signals entering the network analyser were identical and the bridge balanced. This was repeated for each operating frequency and the short circuit position was recorded. The set-up was then re-arranged and the slotted waveguide section was connected to the test channel and terminated in a matched load via a stub tuner. An additional section of waveguide was introduced into the reference channel and the short circuit was adjusted to locate it at exactly the same electrical position as the centre of the slot. The precision insert, which was manufactured to short the slot on the inner surface of the waveguide, was then placed in the slot and the stub tuner was adjusted to optimise the match. On removal of the insert the reflection coefficient was displayed on the network analyser and if the imaginary component was not equal to zero then the operating frequency, and consequently, the short circuit and the stub tuner were adjusted until the resonant frequency was found.

5.3 EXPERIMENTAL RESULTS

The measured results for W ≈ 1.6 mm, obtained using the technique described above, extends the Stegen curve [4.6] to an offset of 9.51 mm. It is important to note that the measurement system determines the frequency of resonance of a slot cut to a pre-determined size and therefore the resonant frequency may differ slightly from the desired Stegen value of 9.375 GHz.

SLOT	OFFSET (mm)	WIDTH (mm)	LENGTH (mm)	AVERAGED F_o (GHz)
1	1.94	2.56	15.27	9.421
2	2.00	1.54	15.49	9.399

3	5.79	1.58	16.83	9.027
4	7.85	2.06	16.60	9.396
5	8.02	1.60	16.76	9.166
6	8.09	2.53	16.68	9.409
7	9.51	1.57	16.64	9.107

Table (5.1)

Physical Parameters And Resonant Frequencies

Of Round Ended Longitudinal Slots.

The deviations in frequency and slot width are quite apparent in Table (5.1) and the moment method has been employed to quantify the errors associated with these. The errors have been evaluated by determining the theoretical resonant lengths of each slot for the frequencies and slot widths tabulated above and also for Stegen's frequency (9.375 GHz) and width (1.5875 mm) where applicable. The differences between the normalised resonant lengths were then taken and used to estimate the errors. It should be noted that the calculations were actually carried out for square ended slots, however, it has been assumed that they provide a good estimation of the errors for the corresponding round ended slots. The results have been tabulated in Table (5.2) and these suggest that the error associated with the frequency and width deviations are small.

SLOT	$\frac{2L}{\lambda_o}$ Actual Freq.	$\frac{2L}{\lambda_o}$ Stegen's Freq.	Deviation
1	0.936	0.937	0.001
2	0.949	0.948	-0.001
3	0.995	0.988	-0.007
4	1.003	1.004	0.001
5	1.008	1.001	-0.007
6	1.006	1.008	0.002
7	1.004	0.995	-0.009

Table (5.2)

Estimated Error In Normalised Resonant Length

Note: The above estimates are for equivalent square ended slots.

The measured results are presented in Figure (5.6) where they are compared with Stegen's experimental results and corrected moment method predictions. The moment method results have been corrected using an equal area rule, which was developed by Josefsson [3.18] for slots with a W/L ratio of 0.1, to compensate for the square ends of the theoretical slots.

For large offsets > 6.0 mm the moment method computations suggest that the resonant length of a shunt slot continues to increase as the offset is enlarged up to approximately 8.0 mm, whereupon it decreases until the slot meets the side wall. It is clear from the figure that the measured results are in good agreement with the theoretical predictions. There is however a discrepancy between the measured

results and Stegen's results. Stegen's suggest the resonant length increases more slowly for offsets in excess of 5 mm, whereas Figure (5.6) shows the length increasing steadily up to 8 mm which is consistent with the results reported by Stern and Elliott in [3.15]. The reason for the difference can be attributed to the limited offset range Stegen employed, and to a possible error in his last measured point giving rise to the observed discrepancy.

Also shown in Figure (5.6) are three measured points for wider than 'normal' shunt slots. These show that for a large offset (8 mm) the resonant length of a shunt slot increases with width and for a small offset (2 mm) the length decreases with width as predicted by the moment method computations. However the measured change in resonant length with increasing width is somewhat larger than the theoretical estimate (Figure (5.7)). This difference can mainly be attributed to the fact that the measured slots were round ended while the theory applies to square ended slots. The W/L ratios for these slots are too large to accommodate the Josefsson [3.18] correction.

5.4 CONCLUSION

An experimental technique has been detailed in this chapter which is able to provide extremely accurate measured data on the resonant frequency of a longitudinal slot radiating through the broadwall of a rectangular waveguide. The measured results obtained confirm that the method of moments correctly predicts the functional relationship between the slot scattering and the width parameter. Therefore this method may be employed to characterise square ended slots exhibiting a W/L ratio of up to 0.25 with some confidence.

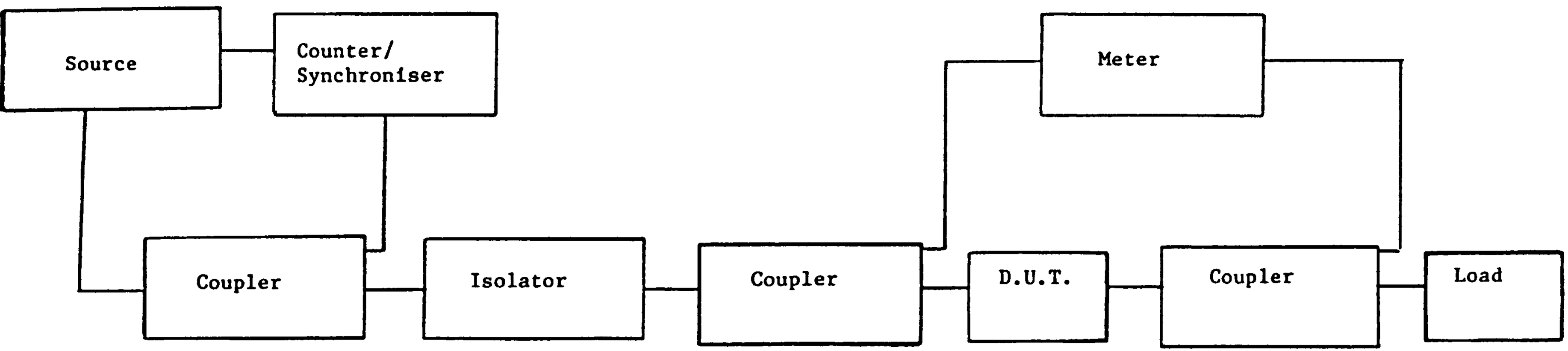

Figure 5.1

Schematic Diagram of Transmission Coefficient Measurement System

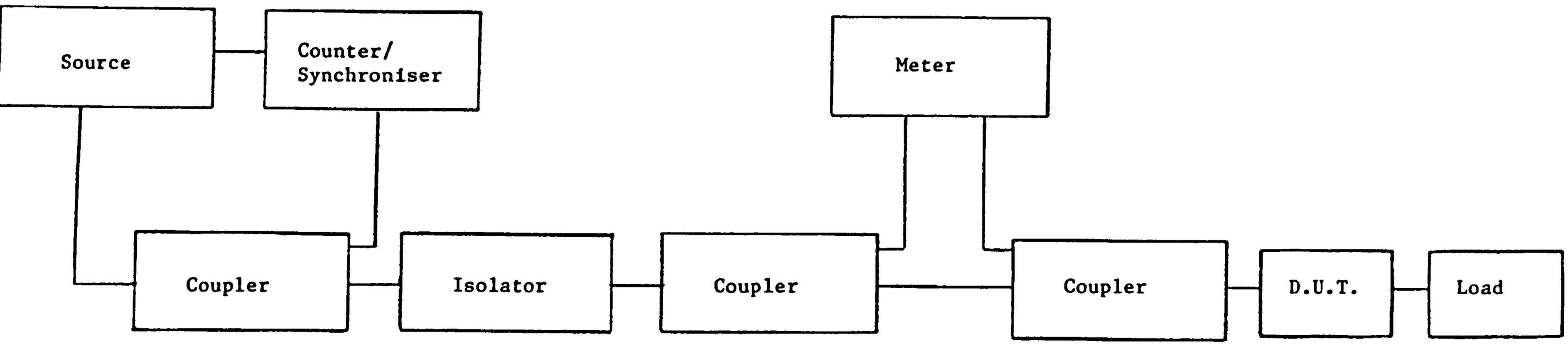

Figure 5.2

Schematic Diagram of Reflection Coefficient Measurement System

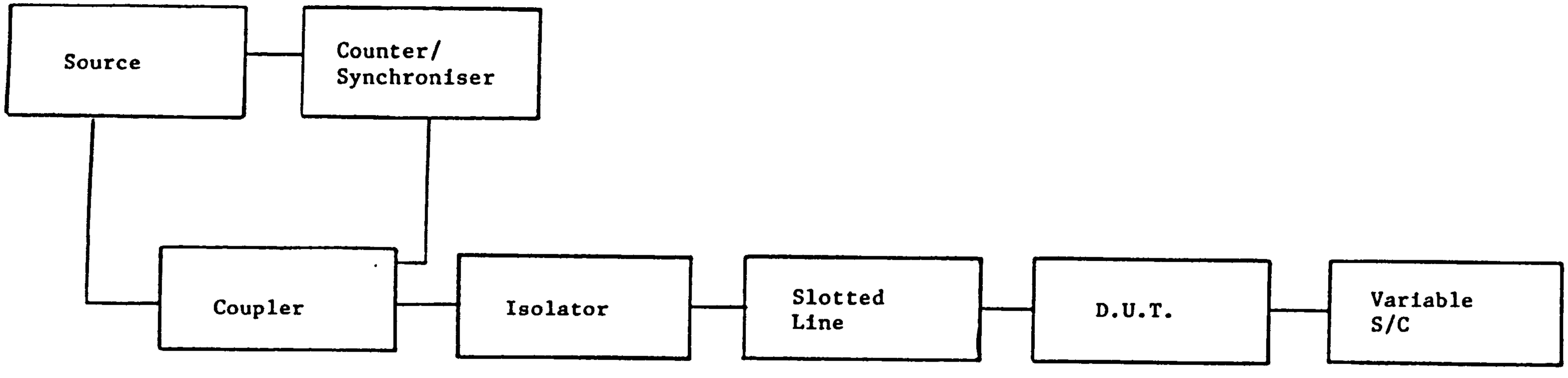

Figure 5.3

Schematic Diagram of Short Circuit Measurement System

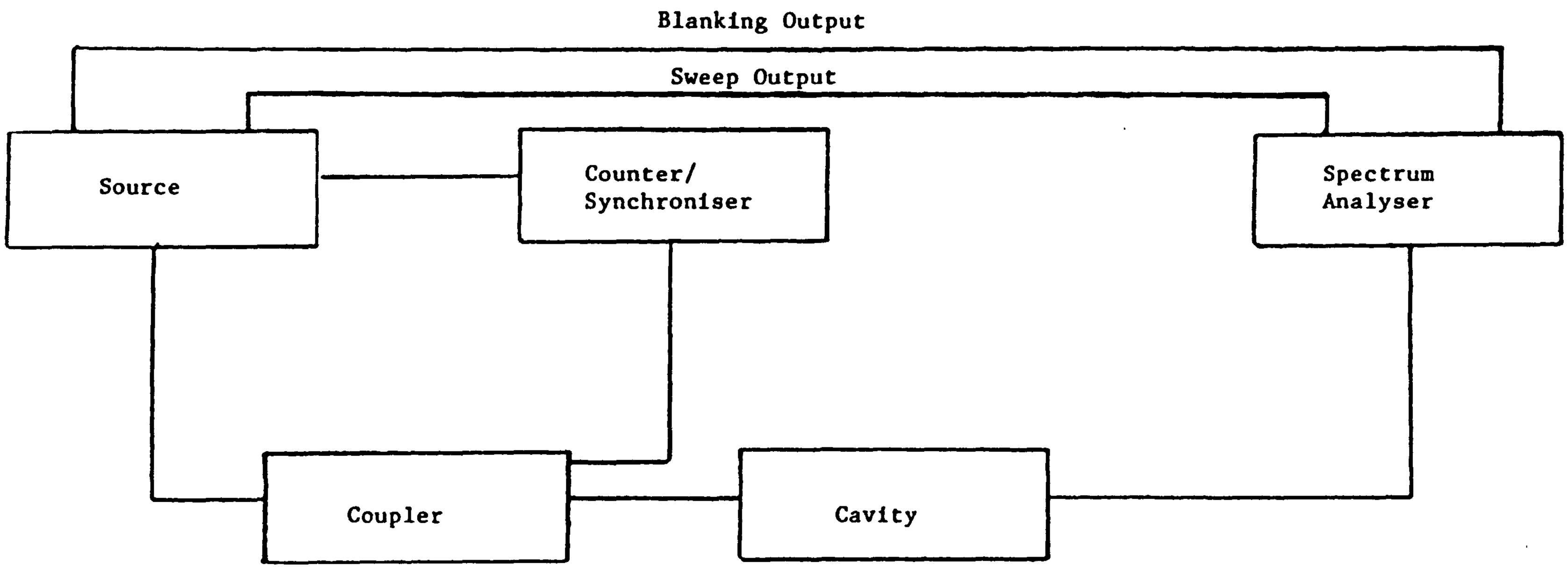

Figure 5.4

Schematic Diagram of Resonant Cavity Measurement System

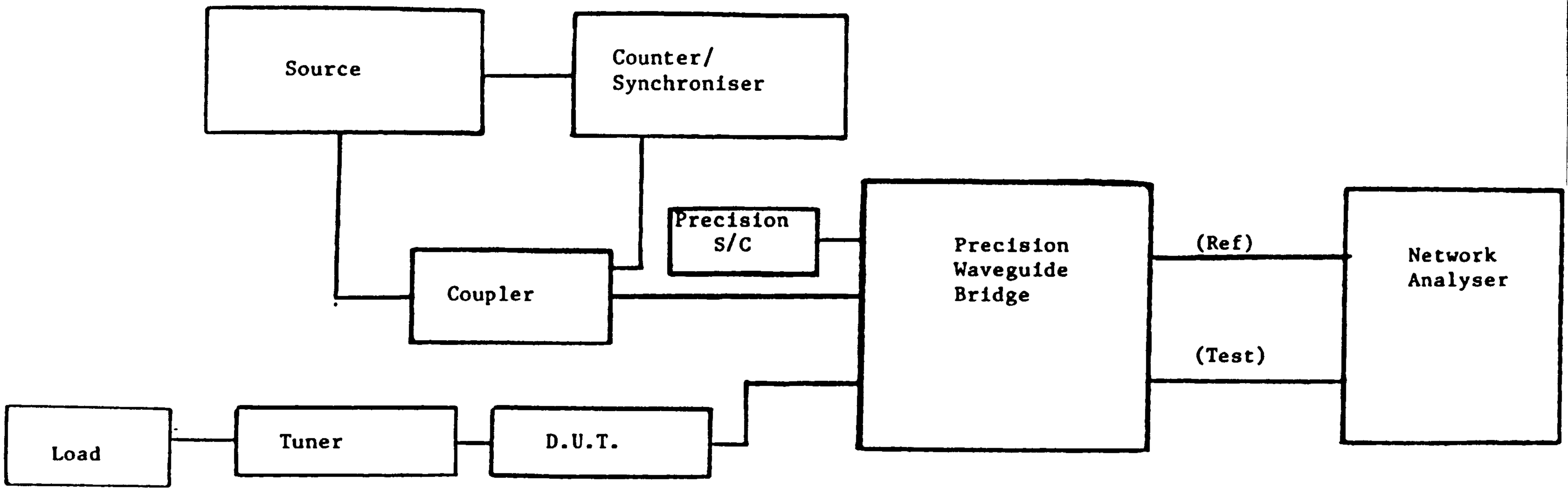

Figure 5.5

Schematic Diagram of Waveguide Bridge Measurement System

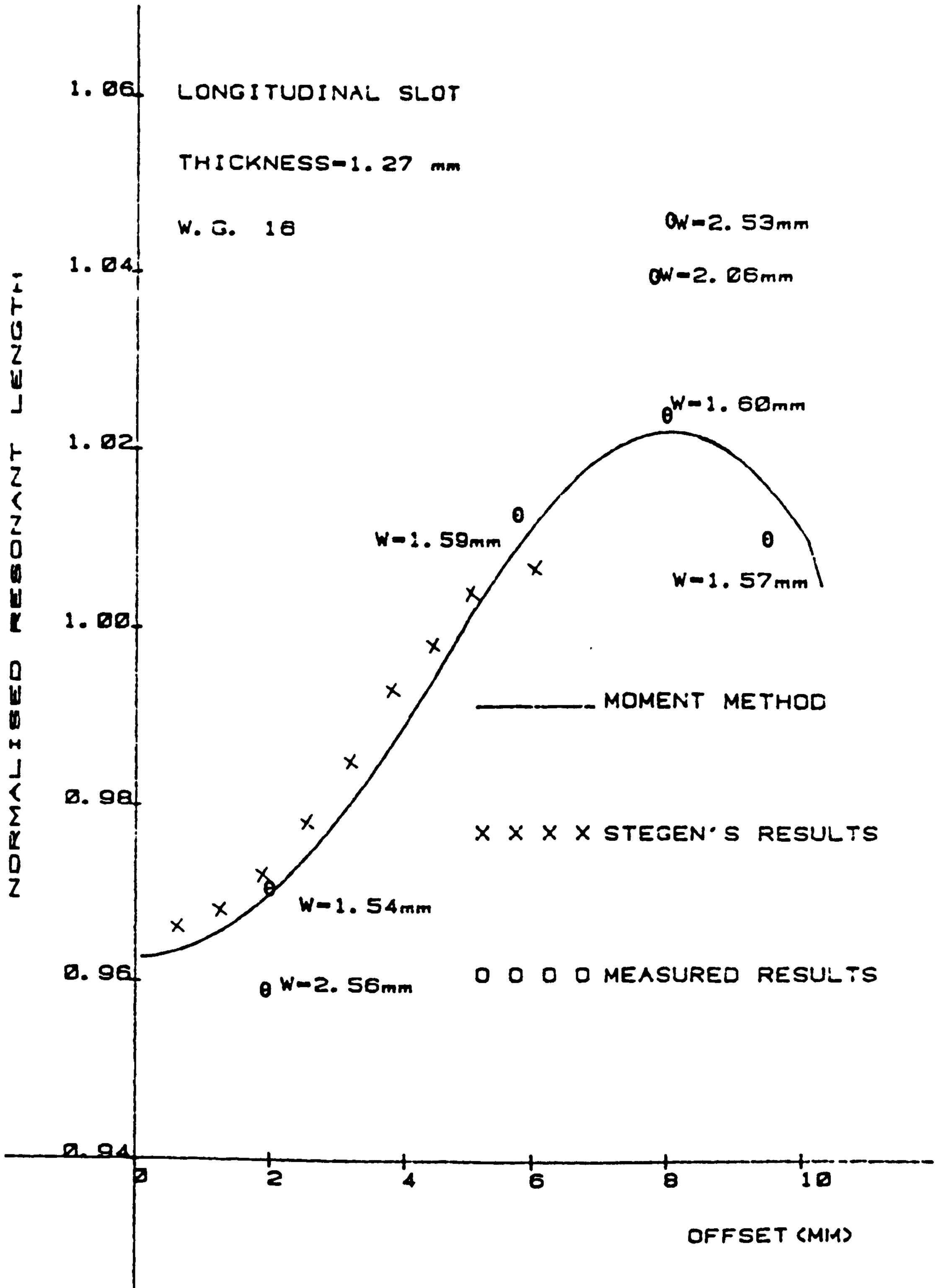

Figure 5.6

Comparison of Measured and Theoretical
Results for the Resonant Length of Longitudinal Slots

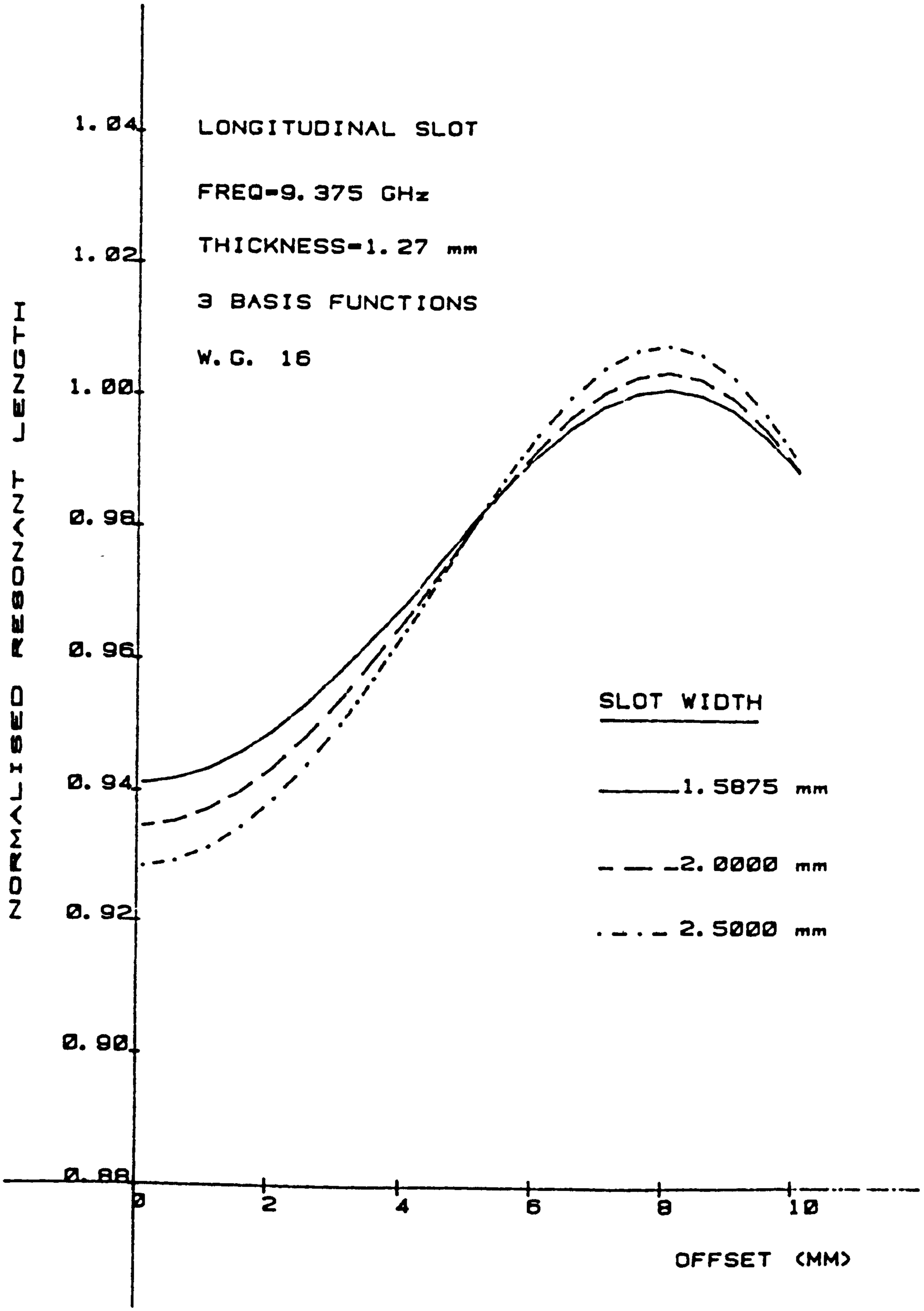

Figure 5.7

Resonant Length as a Function of Offset
for Various Longitudinal Slots

CHAPTER 6

THE DEVELOPMENT OF A PURELY THEORETICAL DESIGN/SYNTHESIS CAD PACKAGE FOR SLOTTED WAVEGUIDE ARRAYS

Design methods for slotted waveguide array antennas have been evolving since the Second World War. The early developments were largely aimed at understanding and formulating methods for calculating the scattering characteristics of individual apertures in waveguide. This has progressed until solutions such as the moment method described in chapter 3, have evolved which can predict accurately experimental results, for commonly used slot examples. In parallel with these aperture investigations, effort has also been directed towards evolving procedures for forming arrays of such apertures [2.63, 2.79, 3.9, 4.4, 6.1, 6.2] and in particular at methods accommodating the mutual effect [2.76] which is important for low side lobe level design. The outcome of this work has been the formulation of a relatively sophisticated synthesis procedure for slotted waveguide array antennas [2.79].

However, the synthesis techniques referred to above, which require that the self admittances of the individual slots in the array be known to a high degree of accuracy, have generally been implemented using measured data for the self admittances. This, of course, implies that it is only possible to synthesis arrays for which measured results are available for the constituent slot radiators. This is an unnecessary restriction as modern high speed computers permit the incorporation of the moment method solution into such synthesis procedures to provide accurate theoretical data on the self

admittances of the individual slots. This chapter details the development of a purely theoretical synthesis procedure.

6.1 SYNTHESIS OF SLOTTED WAVEGUIDE ARRAY ANTENNA

The synthesis procedure described in this section is based to a large extent on the method described by Elliott and Kurtz [2.79] but it incorporates a number of essential modifications to accommodate the inclusion of the moment method which has been introduced to compute the self admittances of the individual apertures. Without these modifications the resultant Computer Aided Design package would require excessive computer processing time.

The procedure has initially been limited to the design of a uniform linear travelling wave array comprising of longitudinal shunt slots. The required excitation levels of the array elements, to meet the prescribed far field pattern, are determined using a standard technique. Such techniques are available in the literature [6.3, 6.4, 6.5] and exhibit varying degrees of sophistication depending on the pattern constraints and array geometry. However, for the purpose of demonstrating the principle of slotted waveguide array synthesis using the moment method, a relatively simple far field pattern is assumed which can be represented by a Dolph-Chebyshev [2.39] function. The Schelkunoff [2.38] unit circle technique is used in conjunction with this function to determine the number of slots required to satisfy the specification. The array factor is then deduced from the roots, and hence the active scattering parameters

for each slot can be evaluated. These parameters accommodate both the self effect for any given slot and the mutual effect of its neighbours.

In traditional slotted waveguide array synthesis programs, the self effect, which is usually presented as a self admittance value, is extracted from measured data. Whereas here, the measured data is replaced by theoretical values, obtained using the method of moments, which are computed as and when the synthesis program requires them. Consequently, the program contains essentially three components, namely the formulation of the active admittances of the slots, the calculation of the mutual admittances and finally the calculation of the self admittances. The techniques employed to determine the respective values are detailed in the following three sections.

6.2 ACTIVE ADMITTANCE

The active admittances of the elements in the array may be determined in a straightforward manner once the array factor is defined. This factor relates the far field pattern to the element excitations and typically takes the following form for a n-element array.

$$f(\psi) = [1 + C_1 e^{j\psi} + C_2 e^{j2\psi} ..... C_{n-1} e^{j(n-1)\psi}] \qquad (6.1)$$

where

$\psi = [\beta d \cos \phi + \alpha]$

α is the progressive phase shift between elements

β is the phase constant ($2\pi/\lambda$)

d is the element spacing

ϕ is the angle relative to the array

C_{n-1} is the coefficient of the n^{th} element.

The roots of this polynomial are determined from the Dolph-Chebyshev solution using the following relationships:

$$T_n(x) = \begin{cases} (-1)^n \cosh(n \cosh^{-1}|x|) & x < -1 \\ \cos(n \cos^{-1} x) & |x| < 1 \\ \cosh(n \cos^{-1} x) & x > 1 \end{cases} \qquad (6.2)$$

where

n is the number of roots

$x = x_o \cos(\psi/2)$

$x_o = \cosh\left(\frac{\cosh(SLR)}{n}\right)$

SLR is the side lobe ratio.

Once the array factor is generated then the active admittances may be determined by realising that the weighting of the coefficients is the same as the weighting of the slot voltages across the array. The equivalent circuit for a travelling wave array is illustrated in Figure (6.1) where Y_L is the load admittance, and Y_1 to Y_N are the respective slot admittances.

The admittance values are determined by applying power conservation which enables the following equations to be generated.

$$(1 - |\rho_n|)^2 \, A_n^2 = A_{n+1}^2 \tag{6.3}$$

$$(1 - |\rho_n|^2 - (1 - |\rho_n|)^2)^2 \, A_n^2 = P_n \tag{6.4}$$

where

ρ_n is the reflection coefficients of the n^{th} slot.

A_n is the amplitude of the incident signal of the n^{th} section.

P_n is the power radiated through the n^{th} aperture, as dictated by the array factor.

These equations permit the reflection coefficient of each element to be evaluated once the power dissipated in the load is defined. Consequently, if the scattering levels at each slot are small, as they are except for very short arrays, then the active admittances are given by:

$$Y_n^A = \frac{-2\rho_n}{1 + \rho_n} \tag{6.5}$$

The calculation is iterated for varying amounts of power dissipated in the load and the admittances are recalculated using the above formula until an acceptable input match is obtained. These admittance values comprise of both a self scattering effect and a mutual effect. The relationship between these components has been developed by Elliott and Kurtz in [2.79] and has the following form:

$$Y_n^A = Y_n + \sum_{\substack{m=1 \\ m \neq n}}^{N} \frac{V_m}{V_n} Y_{mn} \qquad (6.6)$$

where

Y_n^A is the active admittance

Y_n is the self admittance

V_m is the mode voltage of the m^{th} slot

V_n is the mode voltage of the n^{th} slot

Y_{mn} is the mutual impedance between the m and n^{th} slots.

To help enunciate this relationship Das' [2.70] pictorial representation of the equivalent impedance form of equation (6.6) has been reproduced in Figure (6.2) along with the equivalent admittance circuit in Figure (6.3). These figures clearly illustrate how the components interact and equation (6.6) may be generated using simple circuit theory.

The mode voltages used in this expression are calculated from transmission line theory which produces the following relationships:

$$V_n = V_{n+1} (\cos \beta d + j Y_{n+1} \sin \beta d) \qquad (6.7)$$

where

$$Y_{n+1} = Y^{A}_{n+1} + \frac{Y_{n+2} \cos \beta d + j \sin \beta d}{\cos \beta d + j\, Y_{n+2} \sin \beta d} \tag{6.8}$$

except for the slot nearest the load where

$$\frac{Y_{n+1}}{G_o} = \frac{Y^{A}_{n+1}}{G_o} + 1 \tag{6.9}$$

6.3 MUTUAL COMPONENT

The mutual scattering between slots is usually determined by applying Babinet's principle [2.71] which equates the slot array to an equivalent dipole array. The mutual impedances between the equivalent dipoles can then be evaluated using the work of Baker and Lagrone [2.76] and these are related to the other scattering components using the following expression developed by Elliott [2.80] which equates the components of equation (6.6) to equivalent dipole impedances.

$$Z^{A}_{n} = Z_{nn} + \sum_{\substack{m=1 \\ m \neq n}}^{N} \frac{V_m^{s}}{V_n^{s}} Z_{mn} \tag{6.10}$$

where

Z_n^{A} is the active equivalent dipole impedance

Z_{nn} is the loaded self impedance of the dipole

Z_{mn} is the mutual impedance of the dipoles

V_m^{s} is the slot voltage of the m^{th} slot

V_n^s is the slot voltage of the n^{th} slot

However, before this can be implemented an expression relating the admittance of a waveguide fed slot to the impedance of an equivalent dipole is required. This has been developed in [6.1] and for completeness a brief description of the main steps involved in the development of this expression will be given; the mathematics will not be reproduced as it is well documented by Elliott.

An initial assumption is made that the waveguide array is embedded in an infinite, perfectly conducting ground plane to enable an interim two wire fed slotted array to be introduced. The same electric field distributions are set up across both arrays and this results in identical radiation patterns in half space. However, the admittance characteristics are different, as higher order modes scatter off the waveguide fed slot, giving rise to an additional susceptance component. This component is also dependent on the slot offset from the waveguide centre line. The two wire fed slot, therefore, requires an additional load to be placed across its terminals to correctly model this admittance characteristic.

The complementary dipole array is now introduced and the complex power flow of the three equivalent arrays can be evaluated using Booker's [2.71] relationship. These are equated to ensure that each array exhibits the same radiation patterns and admittance characteristics. This results in the following expression relating the dipole impedance to the waveguide fed slot admittance being generated:

$$Y_n^A = \frac{73}{Z_n^A} \left[\frac{4(a/b)}{0.61\pi(\beta/k)} \left(\frac{\cos 2\beta L_n - \cos 2kL_n}{\sin 2kL_n}\right)^2 \times \sin\left(\frac{\pi X_n}{a}\right)^2\right] \quad (6.11)$$

where

Z_n^A is the active impedance of the equivalent n^{th} dipole.

L_n is the length of the n^{th} slot.

X_n is the slot offset from the guide centre line.

The above equation may also be used to relate the self admittance of a slot to the equivalent loaded dipole impedance by replacing Y_n^A and Z_n^A by Y_n and Z_{nn} respectively.

The mutual impedance Z_{mn} between a pair of dipoles still remains to be calculated and this can be determined using the Induced EMF Method. This method assumes a current distribution in the first dipole, which induces a potential along the second dipole and hence the mutual impedance can be defined as:

$$Z_{21} = \frac{-V_{21}}{I_1} \quad (6.12)$$

The following expressions have been developed in [2.76] using this technique.

$$R_{21} = \frac{-30}{\sin\frac{kL_1}{2}\sin\frac{kL_2}{2}} \int_{-\frac{L_2}{2\lambda}}^{\frac{L_2}{2\lambda}} \left[2\,\frac{\sin(kr)\,\cos(k\frac{L_1}{2})}{r} - \frac{\sin kr_1}{r_1} \right.$$

$$\left. - \frac{\sin kr_2}{r_2} \right] \sin[k\,(\tfrac{L_2}{2} - |s|]\quad d(\tfrac{s}{\lambda}) \qquad (6.13)$$

$$X_{21} = \frac{-30}{\sin\frac{kL_1}{2}\sin\frac{kL_2}{2}} \int_{-\frac{L_2}{2\lambda}}^{\frac{L_2}{2\lambda}} \left[2\,\frac{\cos(kr)\,\cos(\frac{L_1}{2})}{r} \right.$$

$$\left. - \frac{\cos kr_1}{r_1} - \frac{\cos kr_2}{r_2} \right] \sin[k(\tfrac{L_2}{2} - |s|)]\quad d(\tfrac{s}{\lambda}) \qquad (6.14)$$

where

$$r = \sqrt{x_o^2 + (z_o + s)^2}$$

$$r_1 = \sqrt{x_o^2 + (z_o + s + \tfrac{L_1}{2})^2}$$

$$r_2 = \sqrt{x_o^2 + (z_o + s - \tfrac{L_1}{2})^2}$$

The array geometry is illustrated in Figure (6.4).

The above expressions must be adjusted by the following correction factor

$$[1 - 2.4\,(0.5 - \frac{L_1}{\lambda})] \qquad (6.15)$$

to compensate for the difference between the field distribution of a dipole and the distribution in a slot as suggested in reference [2.82]. This method provides a satisfactory solution without resorting to the more complex expressions advocated in [2.81].

To implement these mutual impedance expressions preliminary knowledge of the slot spacings and offsets is required. These initial values need not be particularly accurate, so approximate spacings are deduced from the array factor and Stevenson's [2.15] resonant conductance formula is used to provide trial offsets for the shunt slot array with the lengths all set to $\lambda/2$.

$$g = 2.09 \frac{\lambda_g}{\lambda} \frac{a}{b} \cos^2\left(\frac{\pi\lambda}{2\lambda_g}\right) \sin^2\left(\frac{\pi x}{a}\right) \qquad (6.16)$$

The self scattering may now be evaluated. However, before proceeding it is worth noting that the internal mutual coupling has been omitted from the solution as its effect is known to be negligible in full height waveguide [2.69].

6.4 SELF ADMITTANCE

The self admittance values of the waveguide fed slots may be evaluated either as slot admittances using equation (6.6) or as equivalent dipole impedances using equation (6.10). Both methods will be addressed here.

Firstly, consider the method using slot admittances. Equation (6.6) requires the dipole mutual impedance to be transformed to equivalent

slot admittances. This is achieved by partitioning equation (6.11) as detailed in [6.6] to give:

$$\frac{Y_{mn}^2}{Y'_n \; Y'_m} = \frac{Z_{mn}^2}{Z_{nn} \; Z_{mm}} \qquad (6.17)$$

where Y'_n can be related to Y_{self} using the following relationship along with equation (6.11)

$$Y'_n = \frac{\frac{4(a/b)}{0.61\pi(\beta/k)} \left(\frac{\cos 2\beta L_n - \cos 2kL_n}{\sin 2kL_n}\right)^2 \sin^2\left(\frac{\pi x_n}{a}\right)}{(Z_{nn}/73) - \sum_{m=1}^{N} (Z_{mn}/73)^2/(Zmm/73)} \qquad (6.18)$$

Note: The m=n term is not included in the above summation.

The physical relationship between Y'_n and Y_{self} has been defined in [2.79]. Y'_n is the self admittance of the n^{th} slot with theoretical short circuits placed λ_g away from the centre of the neighbouring slots and Y_{self} is simply the self admittance of the n^{th} slot with no other slots present.

The self admittances of the individual slots may now be evaluated using equations (6.6), (6.11), (6.17) and (6.18).

The second method is slightly more elegant and is based on equation (6.10). The active admittances of the slots are initially transformed to equivalent dipole impedances which are in turn substituted along with the appropriate mutual impedances into equation (6.10) to give the self impedance values. These values are

then transformed to equivalent slot admittances using equation (6.11) and (6.18).

The latter method is computationally more efficient and it helps the synthesis procedure converge more rapidly on a stable solution. Therefore this method has been preferred and is incorporated into the synthesis program. However, for the first pass through the program a simpler technique is employed and equation (6.6) is used along with the approximation presented below to provide a fast approximate solution for the self admittances.

$$Y_{mn} = \frac{Y_n^A Z_{mn}}{73} \qquad (6.19)$$

Once a set of self admittances for the slot array has been determined the new slot lengths (L_n) and slot offsets (X_n) can then be deduced using a two stage process. This involves the variational method [2.3], which generates rapidly calculable closed-form solutions followed by the use of the moment method solution. This two stage approach is dictated by the need to include the moment method into a corrected Gauss-Newton root-finding routine which searches for the slot length and slot offset appropriate to any given value of self admittance. In order that this process should not be excessively demanding in computing time in a multi-slot array design, it is imperative that 'good' trial values for slot length and slot offset are available.

For the first pass through the program sufficiently 'good' trial values for L_n and X_n can be computed relatively quickly using the

closed-form variational equations for the first two slots. These have been corrected for wall thickness using reference [2.32]. The procedure adopted in the program, first converts the self admittances to equivalent impedances, as this is a more convenient form for the variational technique. Then the offset term X_n is eliminated from the resistive expression and a bisectional root-finding routine is used to determine the appropriate slot lengths with the offsets being evaluated by substitution. The equations used are as follows:

$$R = \frac{\frac{8\pi a^3 b}{3\lambda^3 \lambda_g}\left[1 - \left(\frac{2L}{\lambda_g}\right)^2\right]^2\left[1 - 0.374\left(\frac{L}{\lambda}\right)^2 + 0.130\left(\frac{L}{\lambda}\right)^4\right] C_T^2}{\cos^2\left(\frac{\pi L}{\lambda_g}\right)}$$

$$\times \left(\frac{2a}{\lambda_g}\right)^2 \left|\frac{\cos\frac{\pi L}{2a}\left(1 - \left(\frac{2L}{\lambda_g}\right)^2\right)}{\cos\frac{\pi L}{\lambda_g}\left(1 - \left(\frac{L}{a}\right)^2\right)}\right|^2 \frac{B}{X} \qquad (6.20)$$

$$\text{Offset} = \frac{a}{\pi} \sin^{-1}\left[\left(\frac{2a}{\lambda_g}\right)^2 \left|\frac{\cos\frac{\pi L}{2a}\left(1 - \left(\frac{2L}{\lambda_g}\right)^2\right)}{\cos\frac{\pi L}{\lambda_g}\left(1 - \left(\frac{L}{a}\right)^2\right)}\right|^2 \frac{B}{X}\right]^{\frac{1}{2}} \qquad (6.21)$$

where X is the reactive component of the self impedance

C_T is the thickness correction term

$$B = \frac{1}{2} B_t + \frac{B_{rj}}{n_j^2} + \frac{2b}{\lambda_g}\left[\ln 2 + \frac{\pi W}{6b} + \frac{3}{2}\left(\frac{b}{\lambda_g}\right)^2\right] \qquad (6.22)$$

$$B_t = \frac{4b}{\lambda_g}\left\{-\ln\left(\sin\left(\frac{\pi W}{2b}\right)\right) + \frac{1}{2}\left(\frac{b}{\lambda_g}\right)^2\cos^4\left(\frac{\pi W}{2b}\right)\right\}$$

$$- \frac{4b}{\lambda_g}\left(\frac{\lambda_g}{\lambda_{g3}}\right)^2\left[\frac{\cos\left(\frac{3\pi L}{2a}\right)}{\cos\left(\frac{\pi L}{2a}\right)} \cdot \frac{1 - \left(\frac{L}{a}\right)^2}{1 - 9\left(\frac{L}{a}\right)^2}\right]^2$$

$$\times \left[1 + \left(\frac{\pi W}{2\lambda_{g3}}\right)^2\right] \ln\left(\frac{4\lambda_{g3}}{\pi\gamma W}\right) \qquad (6.23)$$

$$\frac{1}{n_j^2} = \frac{ab}{WL}\left[\frac{\pi}{4}\frac{1 - \left(\frac{L}{a}\right)^2}{\cos\left(\frac{\pi L}{2a}\right)}\right]^2 \qquad (6.24)$$

$$B_{rj} = \frac{4w\lambda_g}{\lambda^2}\left\{\left(\frac{k'}{k_o}\right)^2\left[C + \frac{3}{2} - \ln\left(\gamma|k'|w\right)\right] + \frac{\sin k_o L}{k_o L}\right.$$

$$\left. + \left[1 + \left(\frac{\lambda}{2L}\right)^2\right]S_- - \frac{2}{3}\frac{W}{L}\left(\frac{\lambda}{2L}\right)^2\right\} \qquad (6.25)$$

Also $\quad k' = \sqrt{k_o^2 - \left(\frac{\pi}{L}\right)}; \quad k_o = \frac{2\pi}{\lambda}; \quad \gamma = 1.781$

$$\lambda_{g3} = \frac{\lambda}{\left|1 - \left(\frac{3\lambda}{2a}\right)^2\right|^{\frac{1}{2}}}$$

and $\quad C = \dfrac{Ci(k_o L + \pi) + Ci|k_o L - \pi|}{2}$

where Ci is the cosine integral; $\quad Ci(x) = \int_{\infty}^{x} \frac{\cos t}{t}\, dt$

$$S_- = \frac{Si(k_o L + \pi) - Si(k_o L - \pi)}{2\pi}$$

where Si is the sine integral; $Si(x) = \int_{o}^{x} \frac{\sin t}{t}\, dt$

The values of L_n and X_n determined from the above expressions are, as indicated above, used as trial values in the more accurate root-finding routine which incorporates the moment method. The moment method has been implemented using a single trignometric basis function. While this involves a slight sacrifice of accuracy (Figures (6.5) and (6.6)), the time savings which accrue are very significant.

In addition the moment method equations presented in chapter 3 clearly display a considerable degree of repetitiveness which can be eliminated to further enhance the computational speeds. For example, the solution for a typical slot involves equation (3.18) being summed over approximately 2500 modes. Many of the modal characteristics need only be calculated once as they are invariant from slot to slot and they can be stored for use as and when required. The efficiency is also enhanced by efficiently testing the summations for convergence. In fact, if care is taken to store data and efficient test procedures are adopted then an improvement of between 300 and 400% is gained over a program in which the mathematics are programmed directly from the equations.

The moment method equations are then incorporated into a corrected Gauss-Newton root-finding routine which determines the improved values for L_n and X_n. However rather than searching for the slot self admittance in this routine, it has been found that searching for the reflection coefficient ρ is more effective. This is because with ρ it is easier to separate the effect of slot length from that of slot offset as a result of the differing ways in which these

dimensions influence the magnitude and the phase of ρ, (Figures (6.7), (6.8), (6.9) and (6.10)). More particularly, the program makes use of the observation that the magnitude of ρ is almost linearly dependent on offset, while its argument is almost linearly dependent on slot length for small changes in these dimensions near resonance.

Once the new improved values of L_n and X_n are determined the program is then iterated until a stable solution is obtained. That is the mutual scattering is recalculated which in turn results in an adjustment in the self admittance terms and hence a set of slightly different L_n's and X_n's are found; the process is repeated until a satisfactory solution is found.

The final adjustment to the solution is to correct for the radiated and transmitted phase deviations caused by the slots. The mathematics of the moment method naturally evaluates these phase shifts and this enables them to be compensated for. Figure (6.11) illustrates this effect and the separation between the slots is adjusted to correct for the transmission phase shift for the slot in question and the difference between the radiated phase shifts of the present slot and adjacent slot on the load side. Ideally this effect should be corrected for while the solution is being iterated, however, the effect is small and therefore it is sufficient to simply incorporate this adjustment at the end of the array design [6.7].

6.5 DESCRIPTION OF COMPUTER PROGRAM

A fortran program has been written incorporating the procedures discussed in the preceding sections to enable a purely theoretical

design of a travelling wave array to be carried out. A flow chart showing the basic steps in the synthesis program is illustrated below.

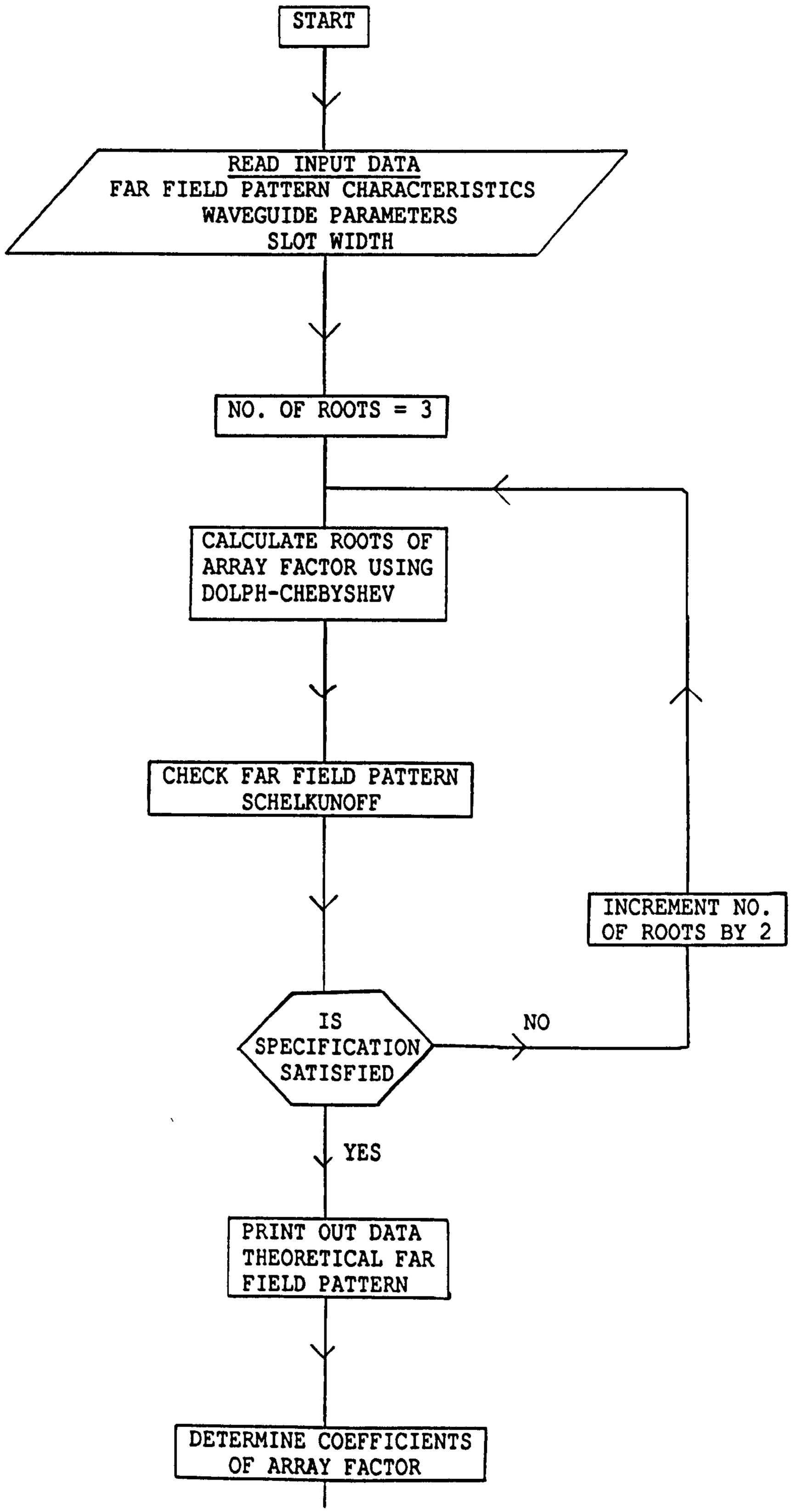
START
READ INPUT DATA
FAR FIELD PATTERN CHARACTERISTICS
WAVEGUIDE PARAMETERS
SLOT WIDTH
NO. OF ROOTS = 3
CALCULATE ROOTS OF ARRAY FACTOR USING DOLPH-CHEBYSHEV
CHECK FAR FIELD PATTERN SCHELKUNOFF
INCREMENT NO. OF ROOTS BY 2
IS SPECIFICATION SATISFIED
NO
YES
PRINT OUT DATA THEORETICAL FAR FIELD PATTERN
DETERMINE COEFFICIENTS OF ARRAY FACTOR

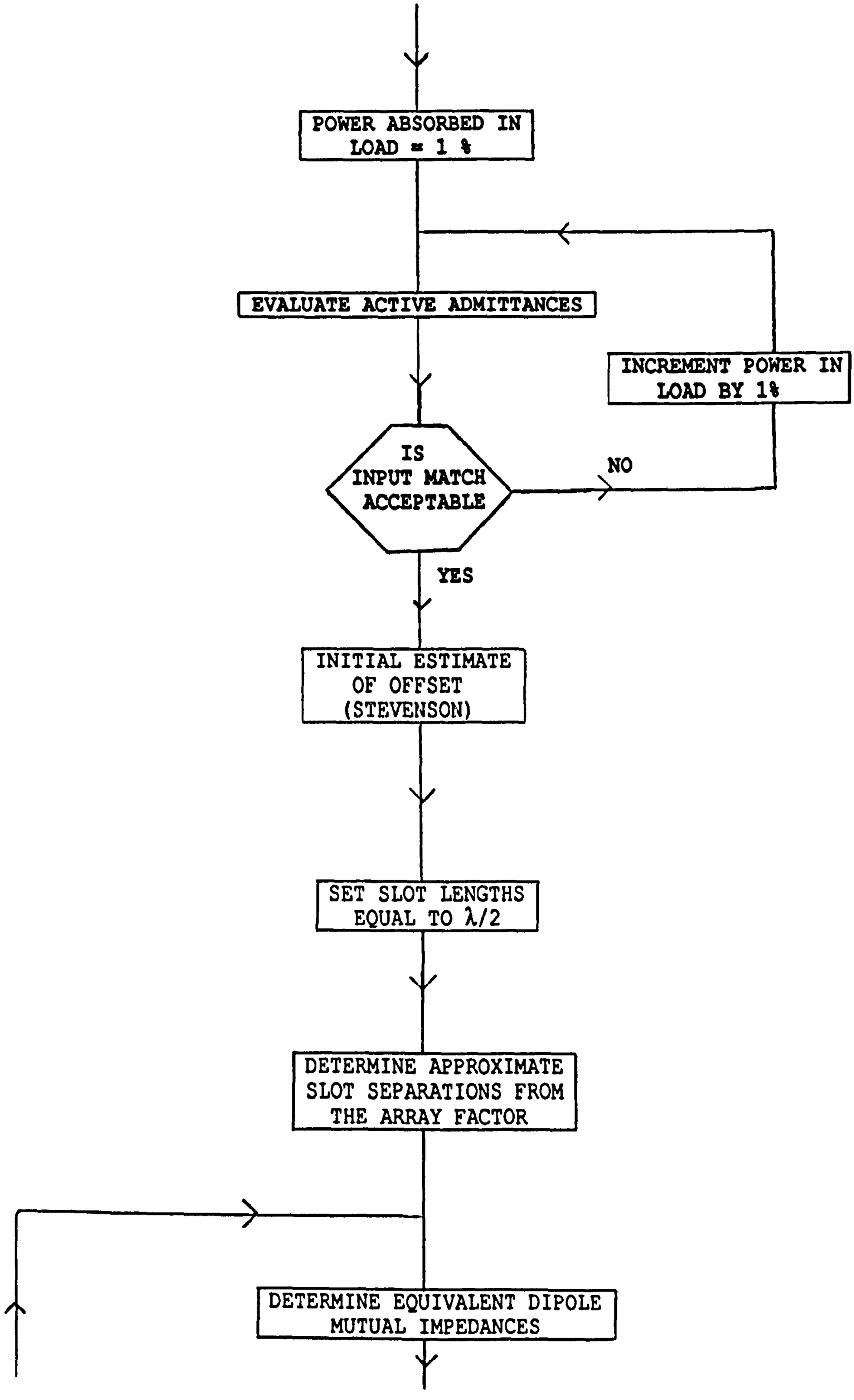
POWER ABSORBED IN LOAD = 1 %
EVALUATE ACTIVE ADMITTANCES
INCREMENT POWER IN LOAD BY 1%
IS INPUT MATCH ACCEPTABLE
NO
YES
INITIAL ESTIMATE OF OFFSET (STEVENSON)
SET SLOT LENGTHS EQUAL TO λ/2
DETERMINE APPROXIMATE SLOT SEPARATIONS FROM THE ARRAY FACTOR
DETERMINE EQUIVALENT DIPOLE MUTUAL IMPEDANCES

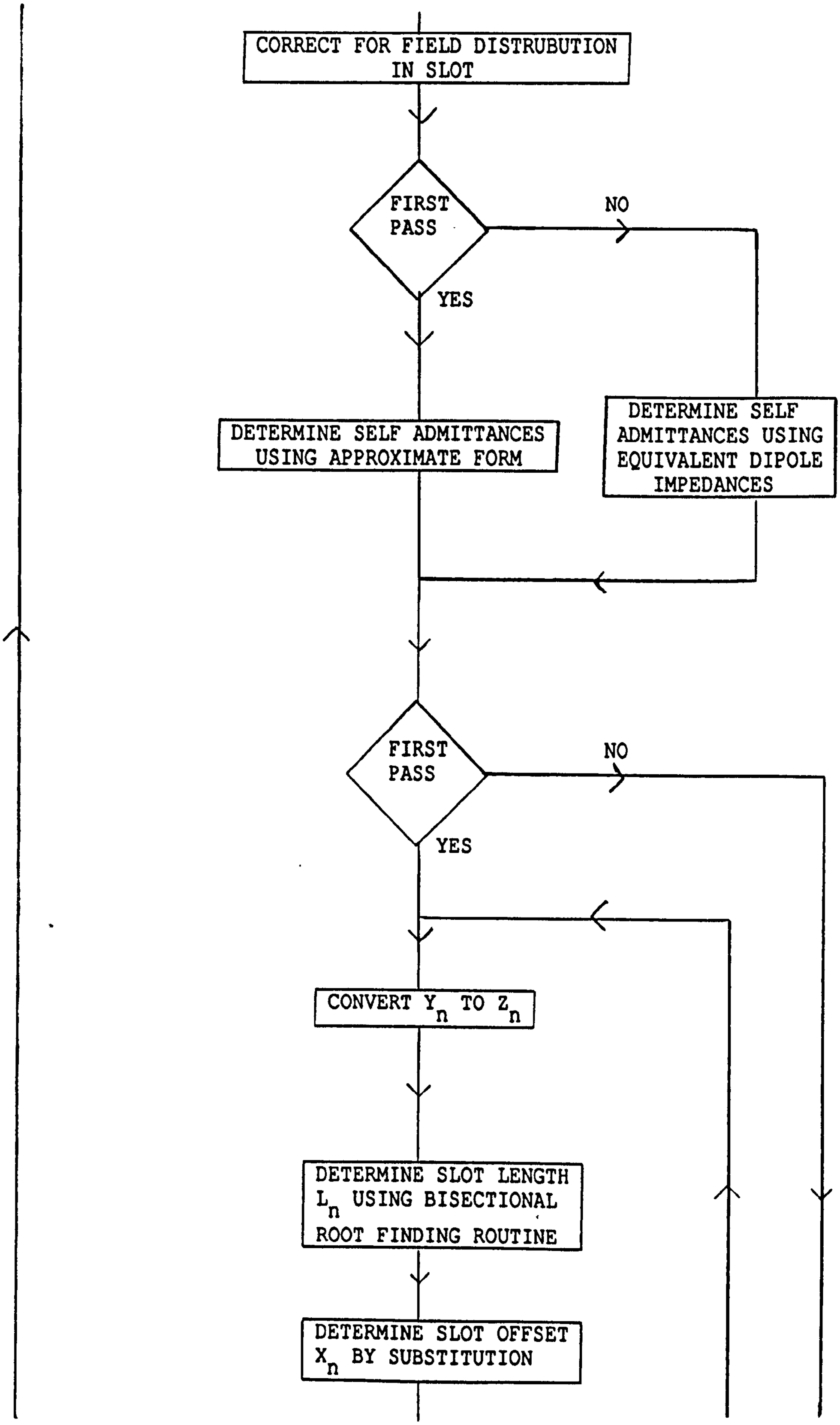
CORRECT FOR FIELD DISTRUBUTION IN SLOT
FIRST PASS
NO
YES
DETERMINE SELF ADMITTANCES USING APPROXIMATE FORM
DETERMINE SELF ADMITTANCES USING EQUIVALENT DIPOLE IMPEDANCES
FIRST PASS
NO
YES
CONVERT Y_n TO Z_n
DETERMINE SLOT LENGTH L_n USING BISECTIONAL ROOT FINDING ROUTINE
DETERMINE SLOT OFFSET X_n BY SUBSTITUTION

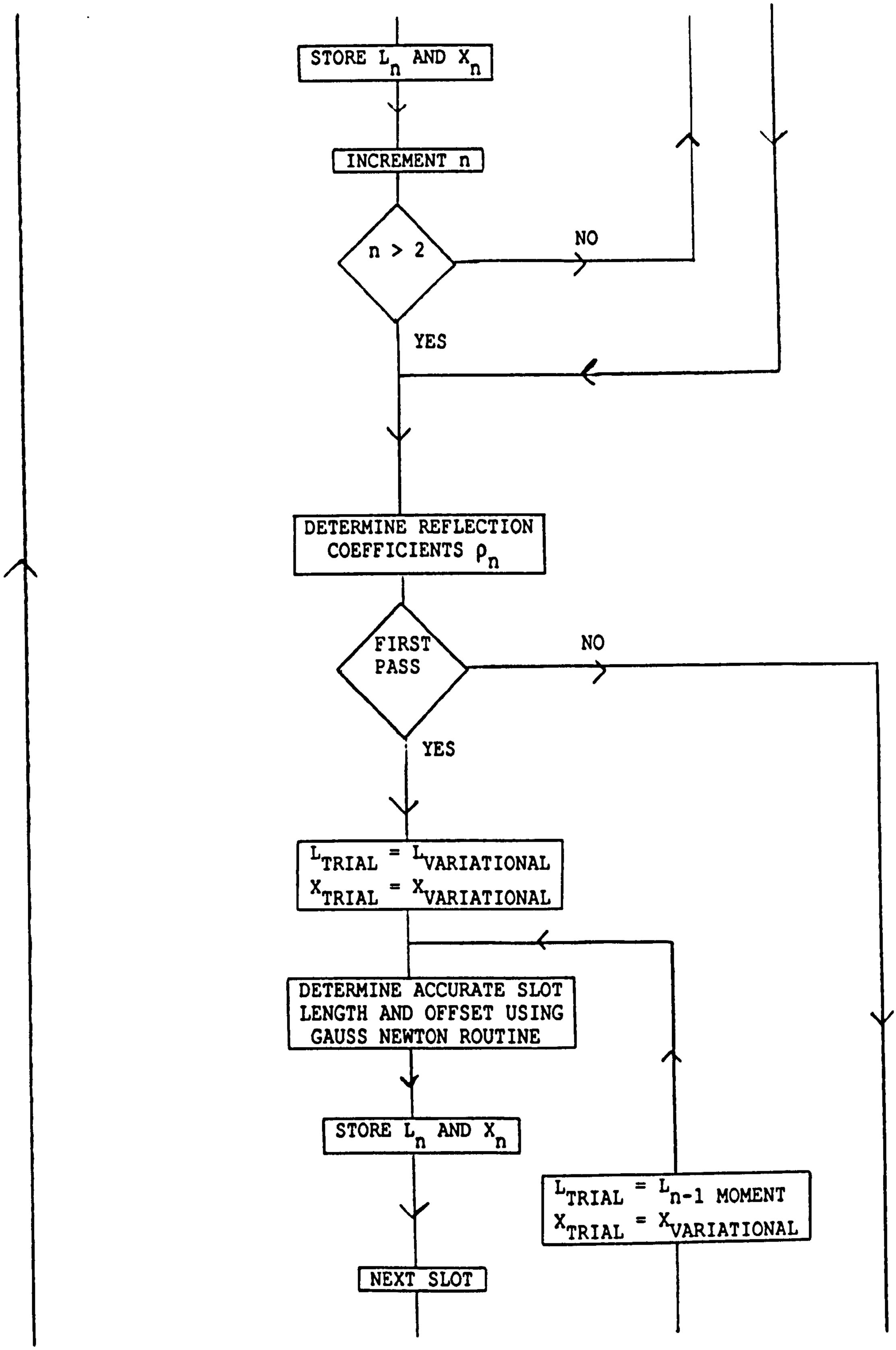
STORE L_n AND X_n
INCREMENT n
n > 2
NO
YES
DETERMINE REFLECTION COEFFICIENTS ρ_n
FIRST PASS
NO
YES
$L_{TRIAL} = L_{VARIATIONAL}$
$X_{TRIAL} = X_{VARIATIONAL}$
DETERMINE ACCURATE SLOT LENGTH AND OFFSET USING GAUSS NEWTON ROUTINE
STORE L_n AND X_n
NEXT SLOT
$L_{TRIAL} = L_{n-1}$ MOMENT
$X_{TRIAL} = X_{VARIATIONAL}$

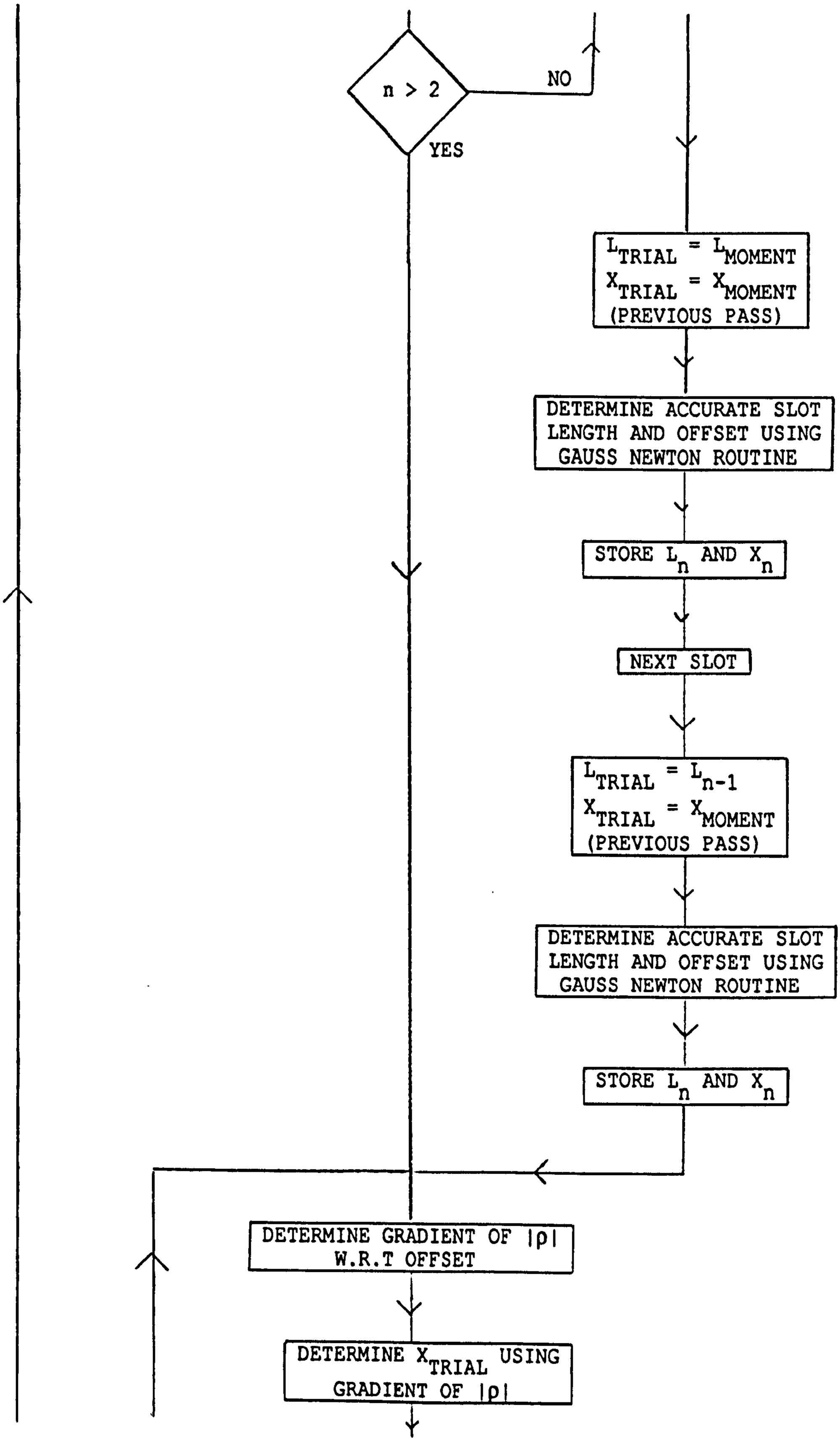
n > 2
NO
YES
$L_{TRIAL} = L_{MOMENT}$
$X_{TRIAL} = X_{MOMENT}$
(PREVIOUS PASS)
DETERMINE ACCURATE SLOT LENGTH AND OFFSET USING GAUSS NEWTON ROUTINE
STORE L_n AND X_n
NEXT SLOT
$L_{TRIAL} = L_{n-1}$
$X_{TRIAL} = X_{MOMENT}$
(PREVIOUS PASS)
DETERMINE ACCURATE SLOT LENGTH AND OFFSET USING GAUSS NEWTON ROUTINE
STORE L_n AND X_n
DETERMINE GRADIENT OF |ρ| W.R.T OFFSET
DETERMINE X_{TRIAL} USING GRADIENT OF |ρ|

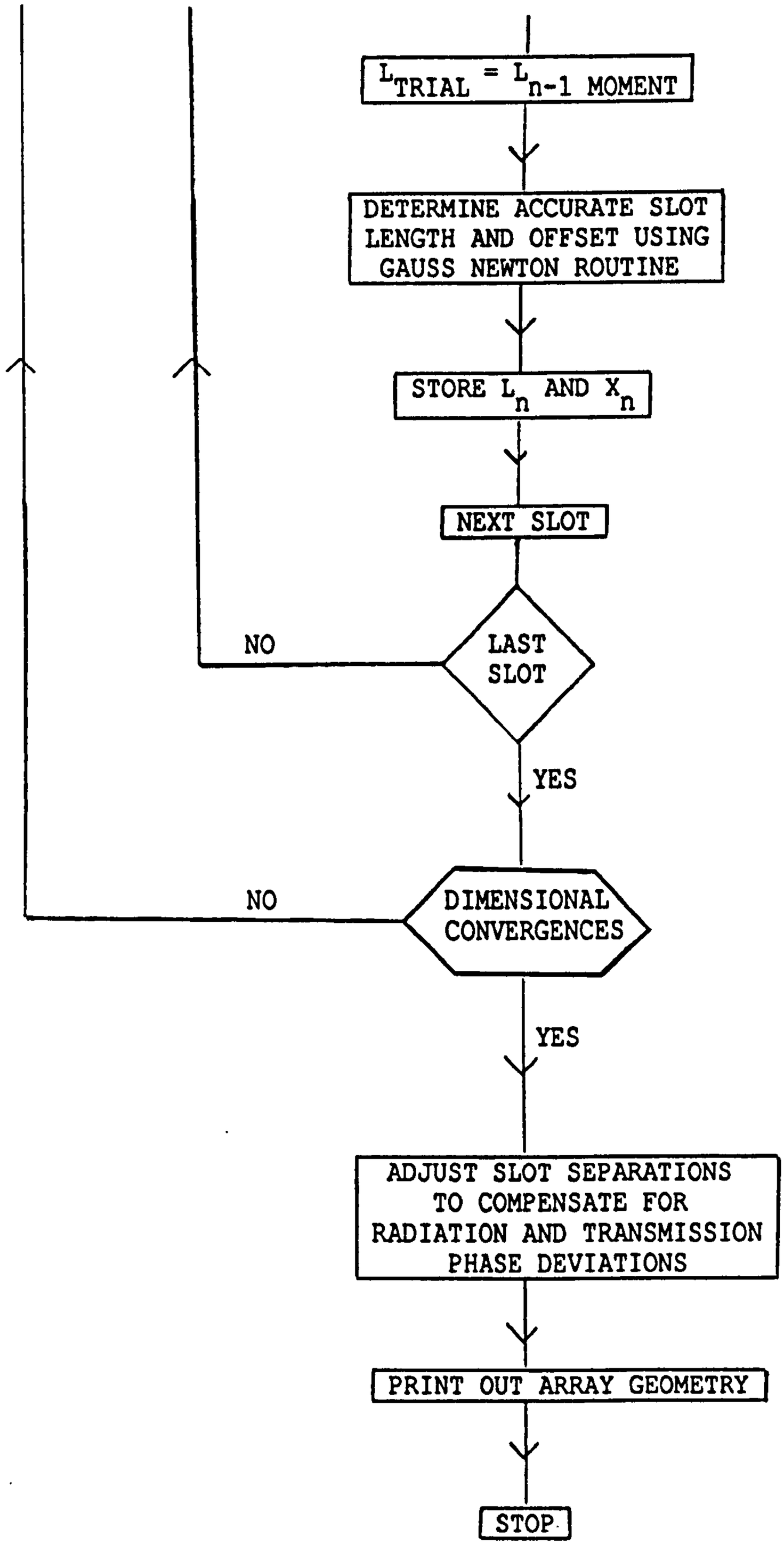
$L_{TRIAL} = L_{n-1}$ MOMENT
DETERMINE ACCURATE SLOT LENGTH AND OFFSET USING GAUSS NEWTON ROUTINE
STORE L_n AND X_n
NEXT SLOT
LAST SLOT
NO
YES
DIMENSIONAL CONVERGENCES
NO
YES
ADJUST SLOT SEPARATIONS TO COMPENSATE FOR RADIATION AND TRANSMISSION PHASE DEVIATIONS
PRINT OUT ARRAY GEOMETRY
STOP

The flow chart has been simplified considerably for clarity and most of the steps shown are reasonably self explanatory. However, it is perhaps pertinent to highlight some aspects of the chart which have been successful in promoting computational efficiency. As mentioned earlier particular attention has been paid to enhancing the efficiency of the latter part of the program, as the majority of the processing time is required to accurately locate the individual slots and determine their lengths. On the other hand the mathematics involved in calculating the admittance components are relatively straightforward and do not require much processing time. Therefore, the subroutines employed to evaluate these terms have been programmed, more or less, directly from the mathematics without paying special attention to improving the efficiency.

In order that the slots of appropriate lengths may be located accurately and efficiently in the top wall of the waveguide, care is needed to ensure that the trial values of L and X, required for the Gauss-Newton root-finding, are as accurate as possible. This is achieved by employing the variational method to provide an initial set of trial values for the first slot. Note, the equations used in this routine have been restricted to Oliner's solution along with a thickness correction factor. There are other enhancements to this technique suggested in the literature [3.12] but these have been omitted to minimise the complexity of the mathematics. The trial values obtained from this method are modified slightly to improve their accuracy with the length being adjusted to 98% of its original length and the offset from the guide centre line being increased by 2%. The adjustment factors have been determined intuitively after running the program several times. These trial values are then used

in the Gauss-Newton root-finding routine which incorporates the moment method to determine the improved values for L_1 and X_1. This routine accesses the moment method many times during the design of an array and it is therefore, imperative that this solution is efficiently programmed. Especially, as it is known to posses a high degree of repetitiveness with many of the modal characteristics being invariant from slot to slot. Consequently, care has been taken to ensure that these characteristics are only evaluated once with the data being stored in either global arrays or common memory blocks in a form which may be readily accessed as and when the program requires it.

The trial values for the second slot are set up in a slightly different manner with the 'improved' length of the first slot being used as the trial length as it provides a more accurate starting point than the variational result. The offset is set equal to the adjusted variational result for the second slot and once more the improved values for L and X are evaluated using the Gauss-Newton root-finding routine.

The trial values for the remaining slots are all set in a similar manner. The length is set equal to the improved length of the previous slot and the offset is deduced by interpolation using the gradient of the magnitude of the reflection coefficient with respect to the slot offset from the guide centre line. Note, the gradient is evaluated each time from the previous two slots to optimise the accuracy of the trial offsets. Once these enhancements have been

incorporated then the trial values and the 'improved' slot positions differ only slightly and therefore the processing time required for the Gauss-Newton routine is minimised.

This is repeated until a complete set of L's and X's are obtained, then the program is iterated with the mutual coupling being recalculated etc. Note; the variational solution is not required in the subsequent passes as the array configuration is known to change only slightly and therefore, the 'improved' lengths and offsets evaluated during the previous pass can be used as trial values in place of the variational data.

The computations are repeated, as indicated on the flow chart, until the values of L_n and X_n differ from the values of the previous pass by less than realistic fabrication tolerances (approximately 0.05 mm in our case). It was found that usually 3 to 4 passes were sufficient to achieve this.

6.6 CONCLUSION

A computer aided design package for the synthesis of rectangular waveguide broadwall arrays comprising of shunt slots has been described. The package differs from preceding contributions in this area in that the self admittances of the slots are computed, rather than taken from a data bank of measured values. The self admittance computations rely on the use of the moment method which is known to be potentially as accurate as the best measurements in evaluating slot self scattering effects. To accommodate the moment method, which does not unfortunately yield rapidly calculable closed form expressions for the scattering parameters of a slot, considerable

care has been exercised in developing time saving computational procedures.

Some continuing limitations in the CAD package have also been identified, but these can readily be eliminated once computational speeds permit. For example the use of a more elaborate basis function in the moment method would improve the basic accuracy of the program as would a more direct method of calculating the mutual impedance between slots.

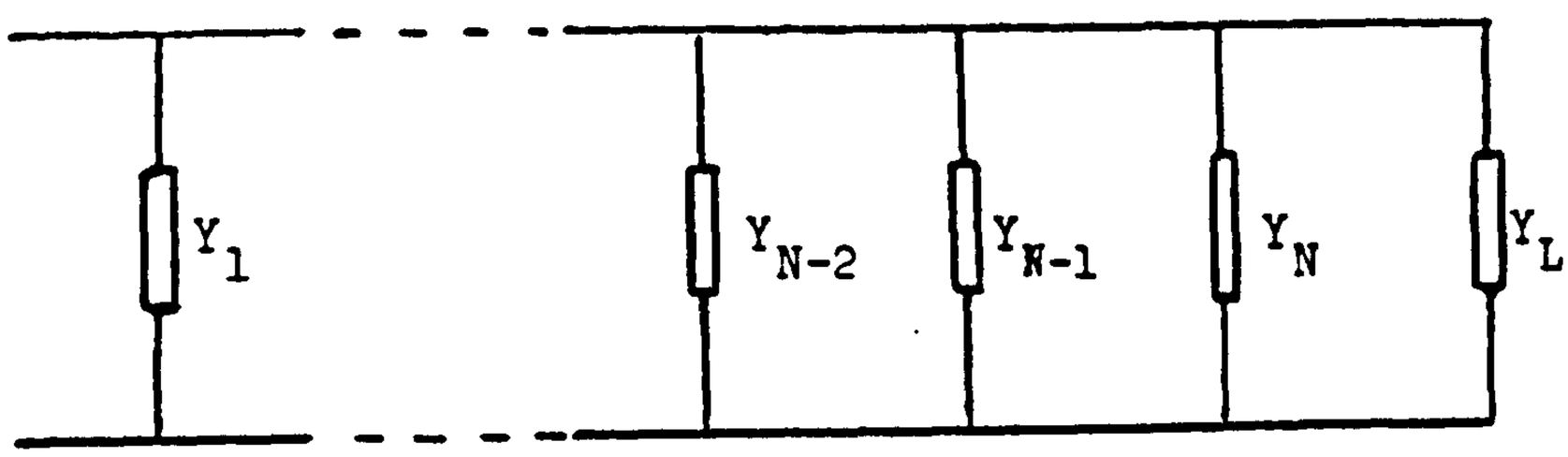

Figure 6.1

Equivalent Circuit for Travelling Wave Array

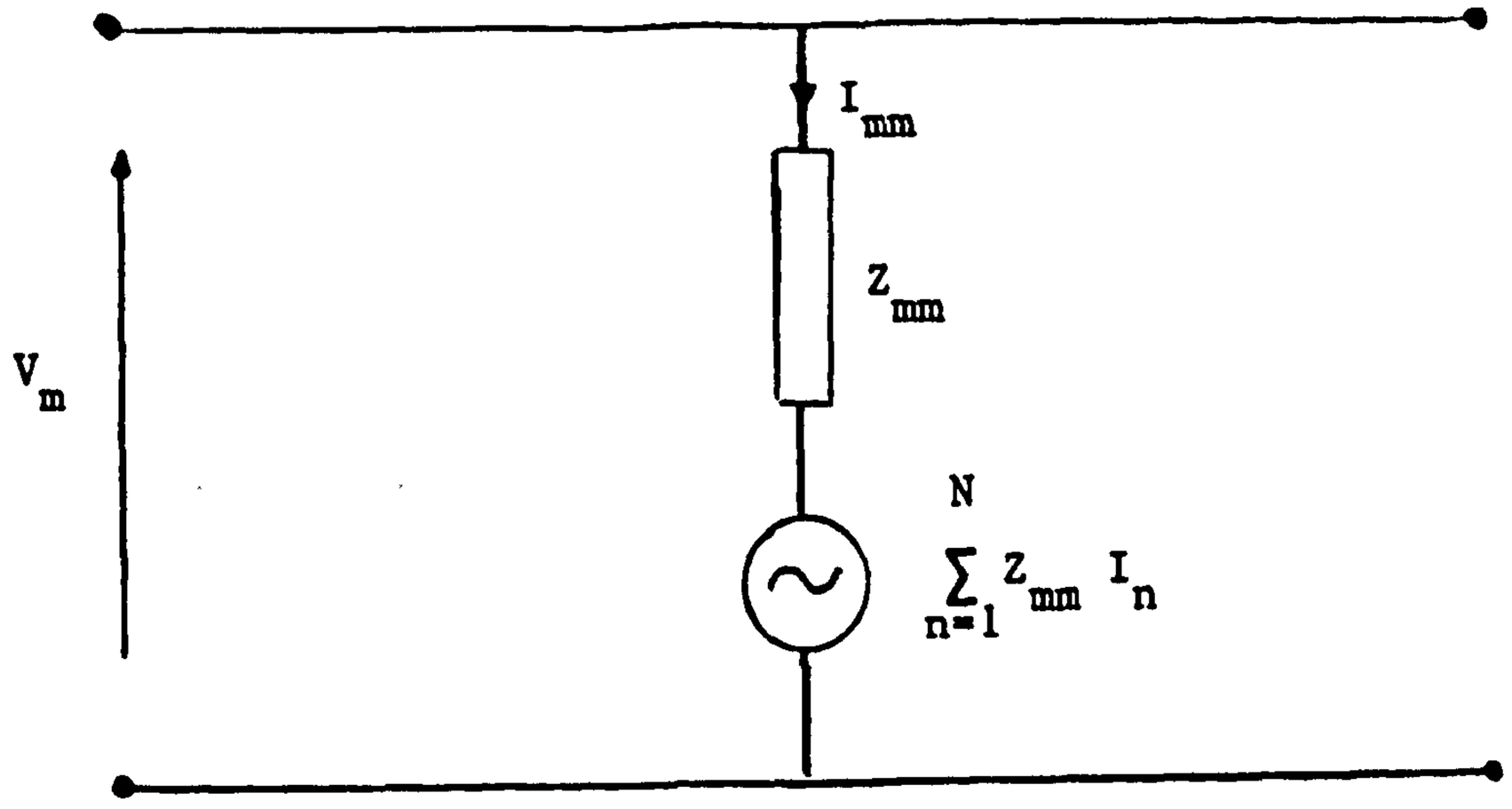

Figure 6.2

Das' Pictorial Representation of Equation (6.6)

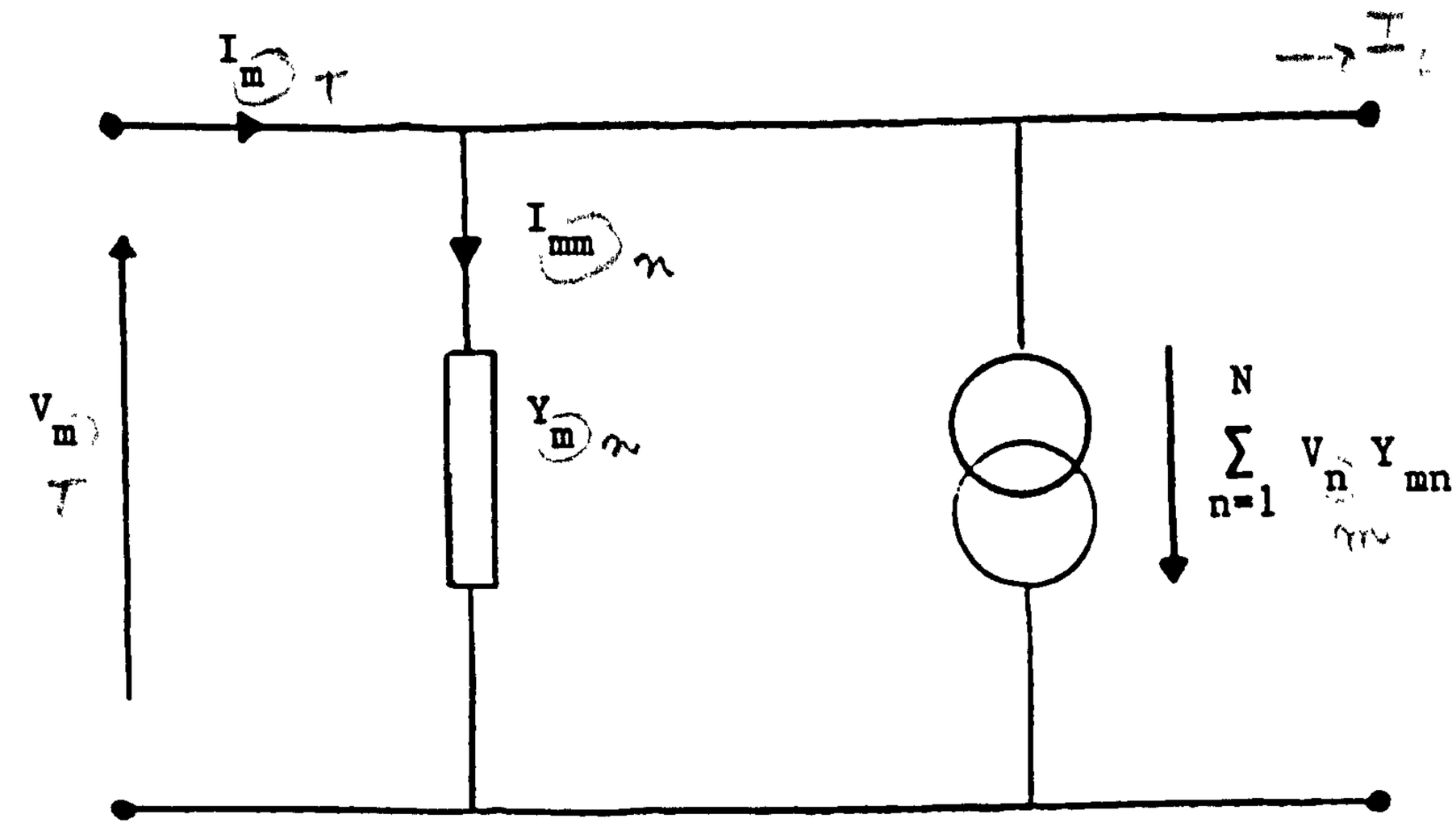

Figure 6.3

Equivalent Admittance Circuit for Equation (6.6)

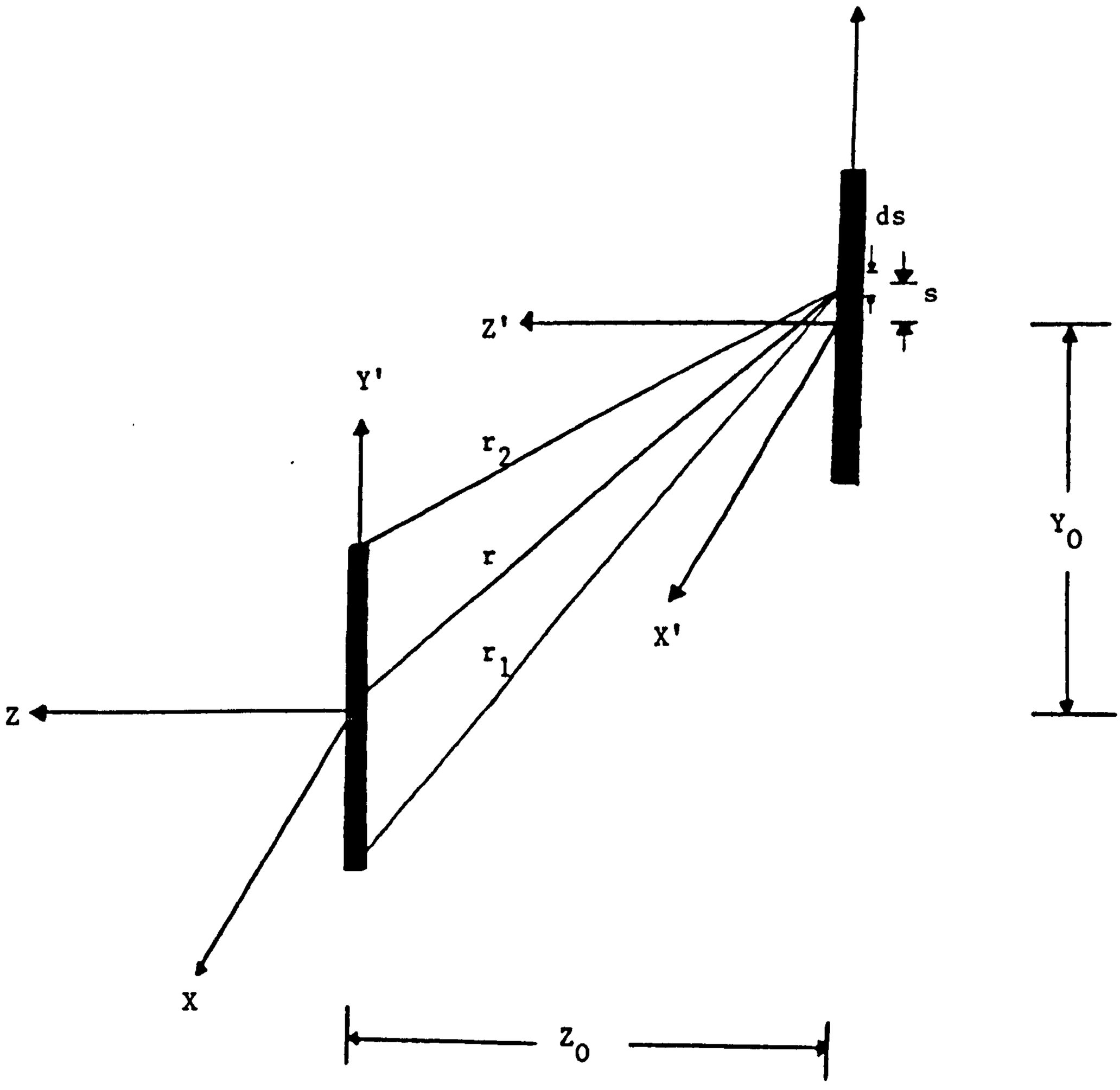

Figure 6.4

Equivalent Dipole Geometry

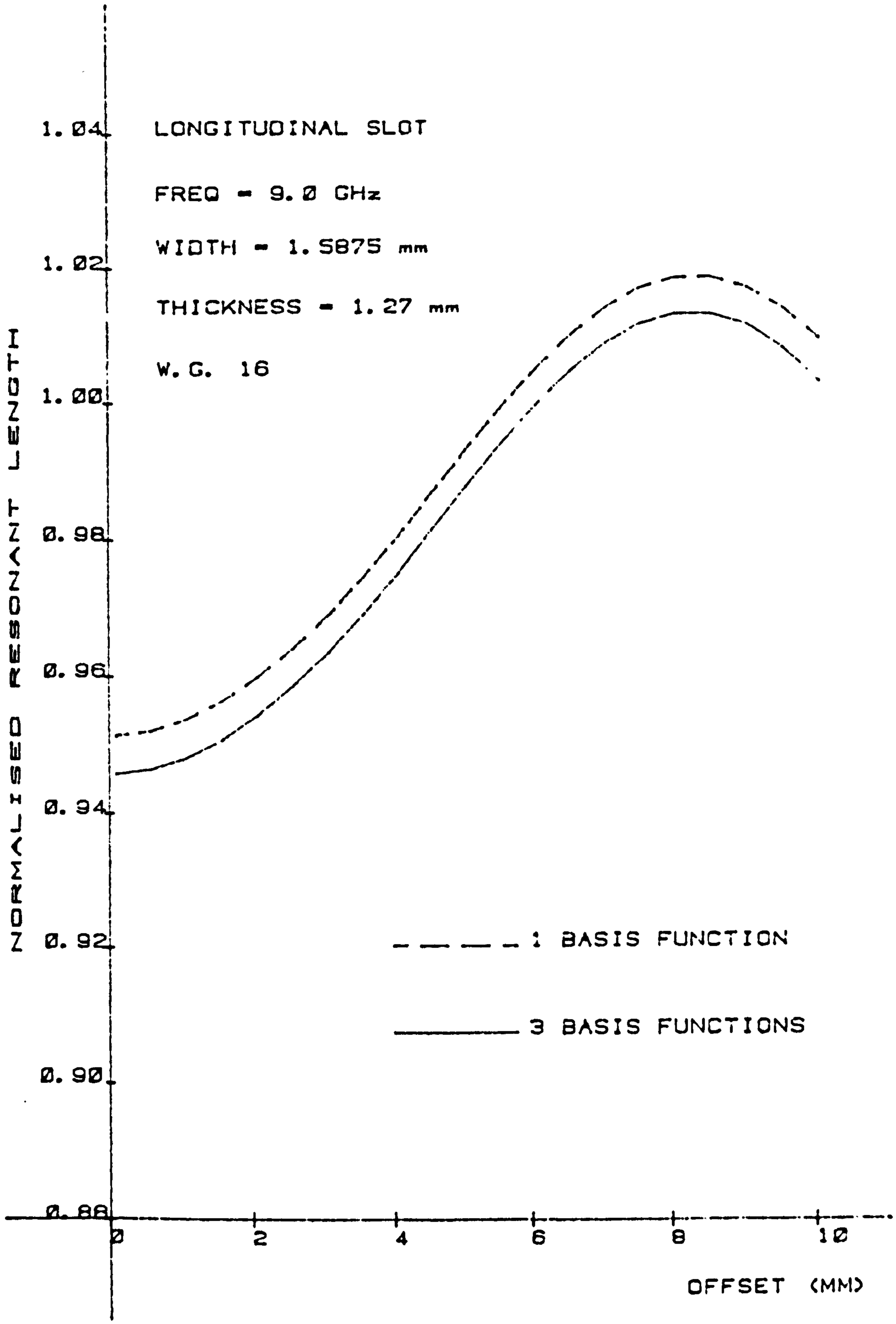

Figure 6.5a

A Graph of the Resonant Length as a Function of Offset for Various Longitudinal Slots - Thick-Walled Case

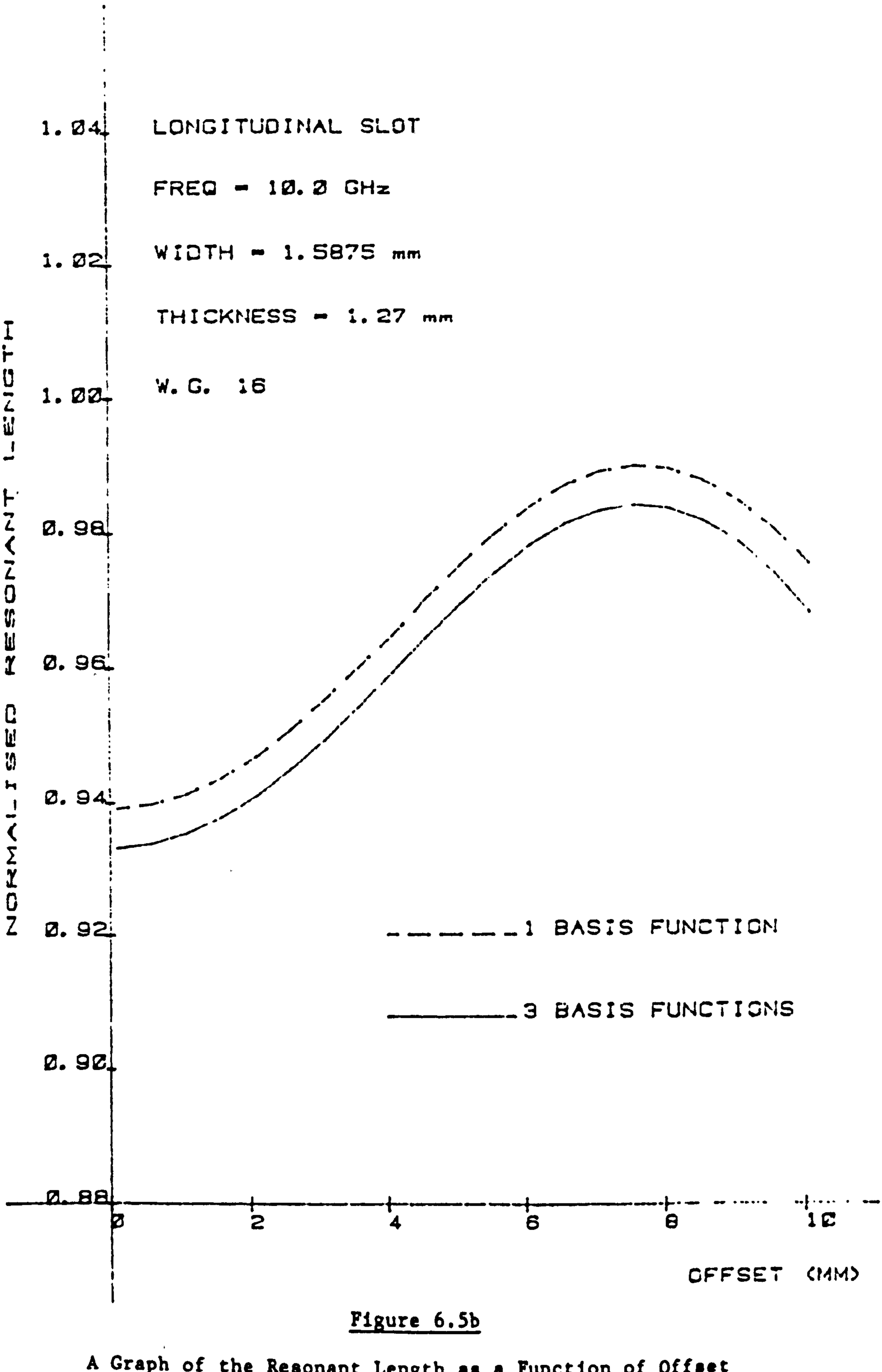

Figure 6.5b

A Graph of the Resonant Length as a Function of Offset for Various Longitudinal Slots - Thick-Walled Case

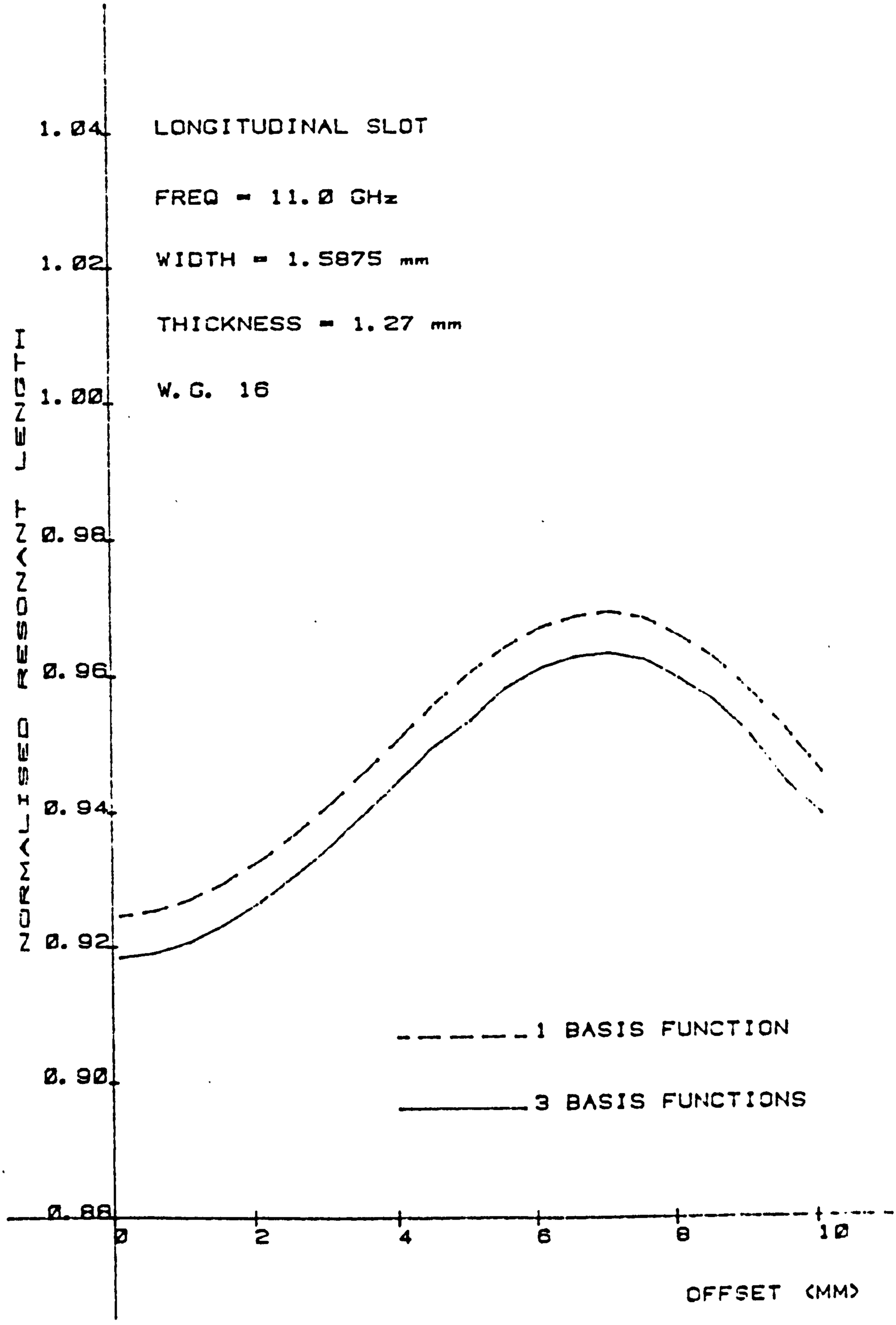

Figure 6.5c

A Graph of the Resonant Length as a Function of Offset for Various Longitudinal Slots - Thick-Walled Case

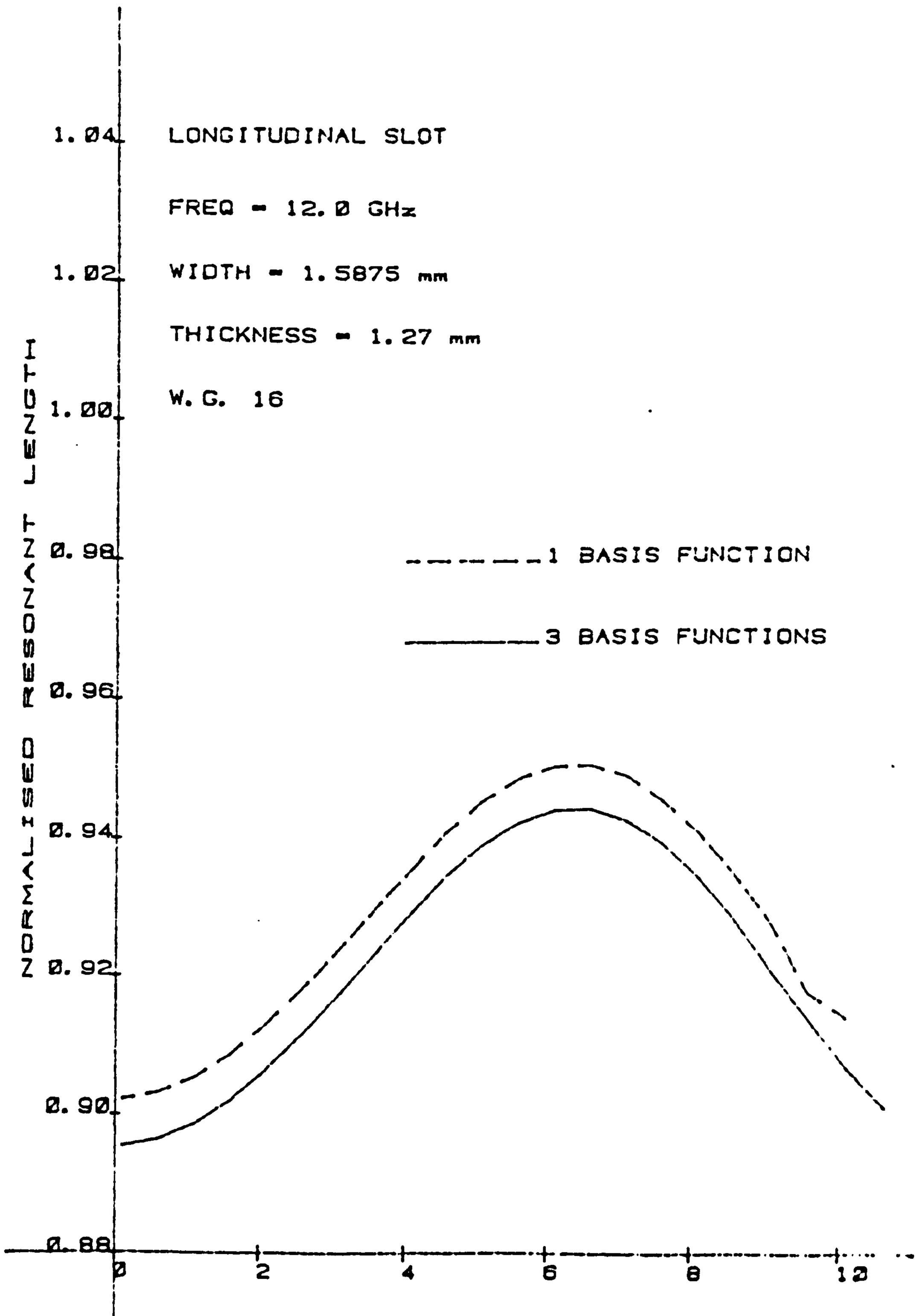

Figure 6.5d

A Graph of the Resonant Length as a Function of Offset for Various Longitudinal Slots - Thick-Walled Case

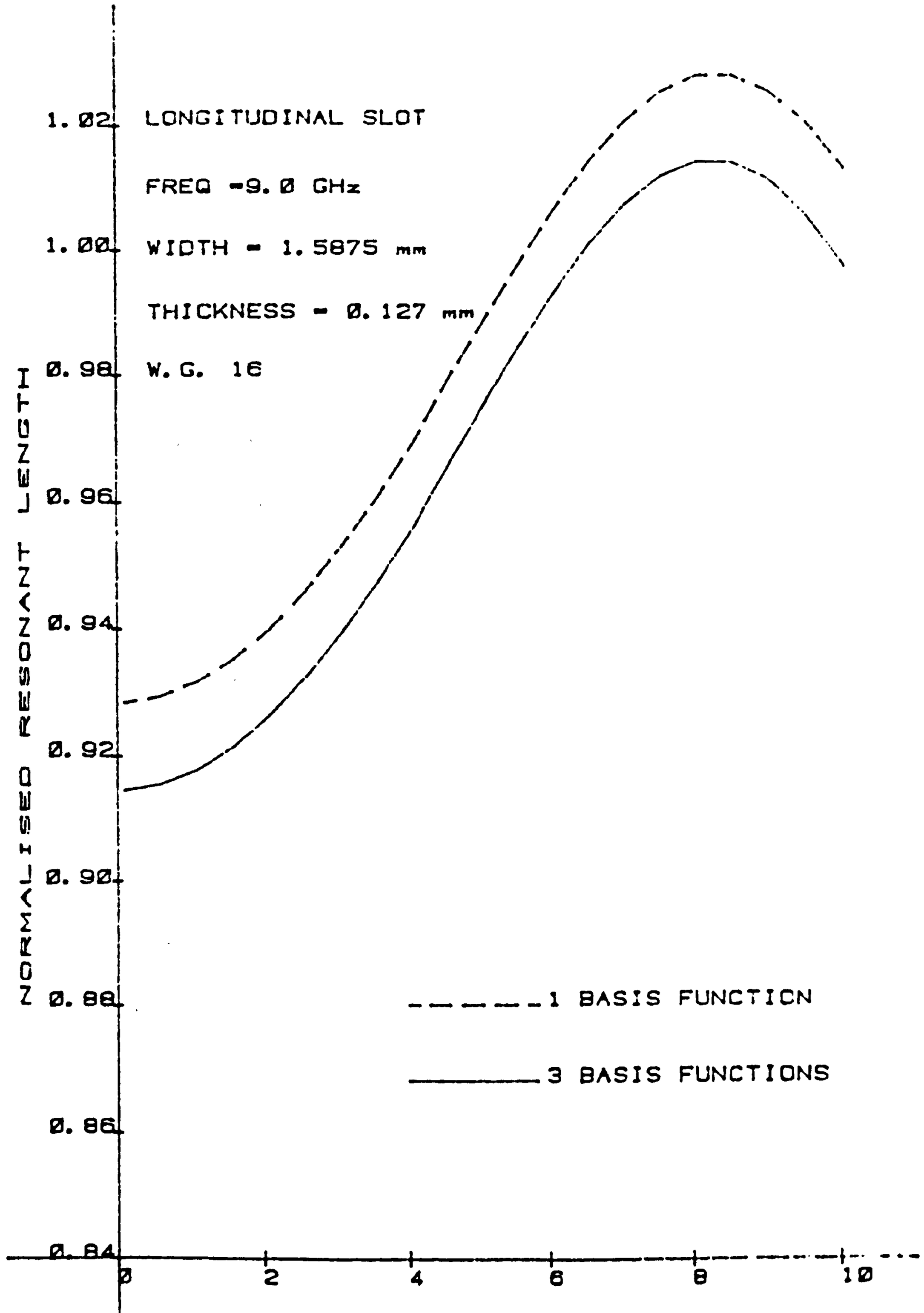

Figure 6.6a

A Graph of the Resonant Length as a Function of Offset for Various Longitudinal Slots - Thin-Walled Case

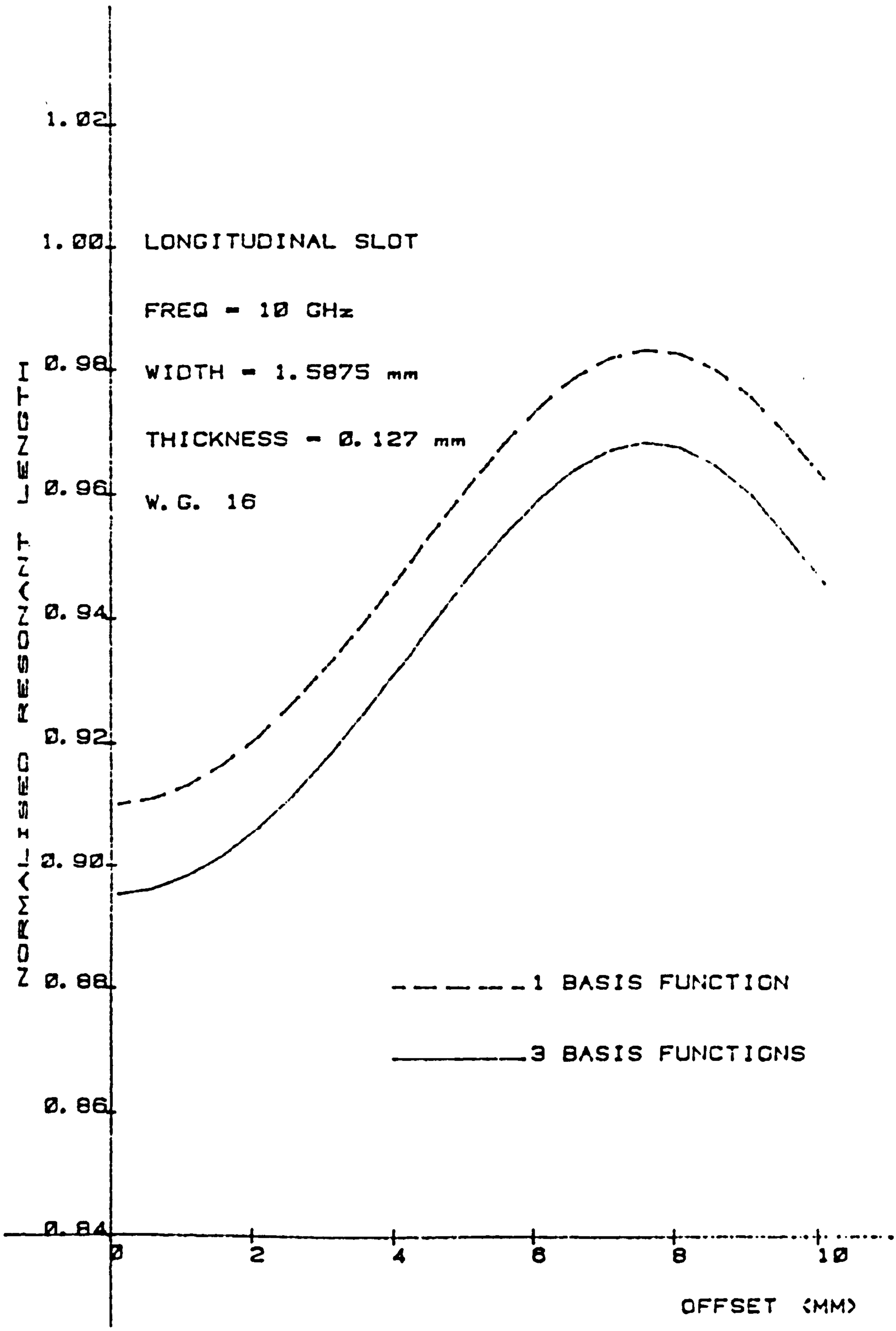

Figure 6.6b
A Graph of the Resonant Length as a Function of Offset for Various Longitudinal Slots - Thin-Walled Case

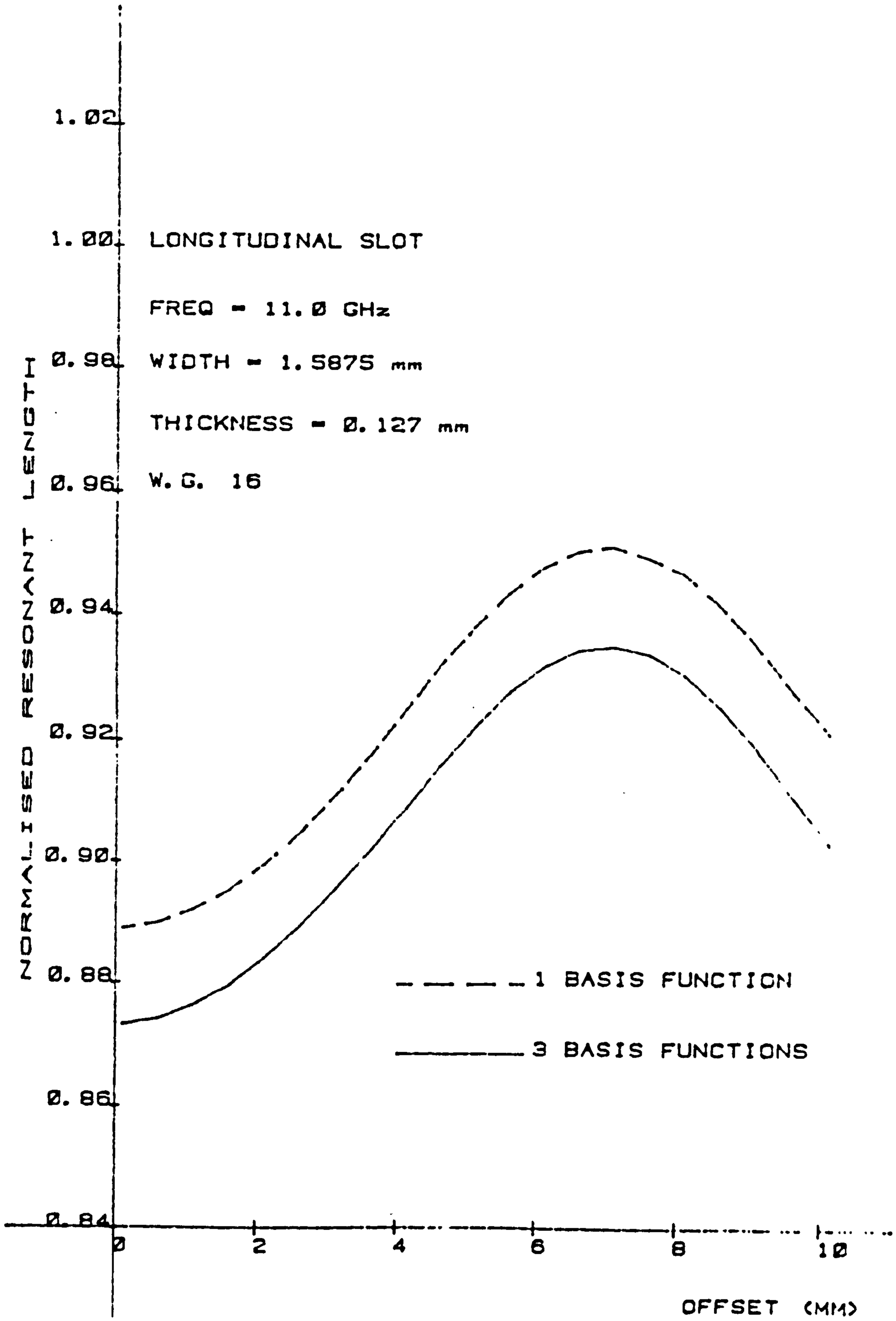

Figure 6.6c

A Graph of the Resonant Length as a Function of Offset for Various Longitudinal Slots - Thin-Walled Case

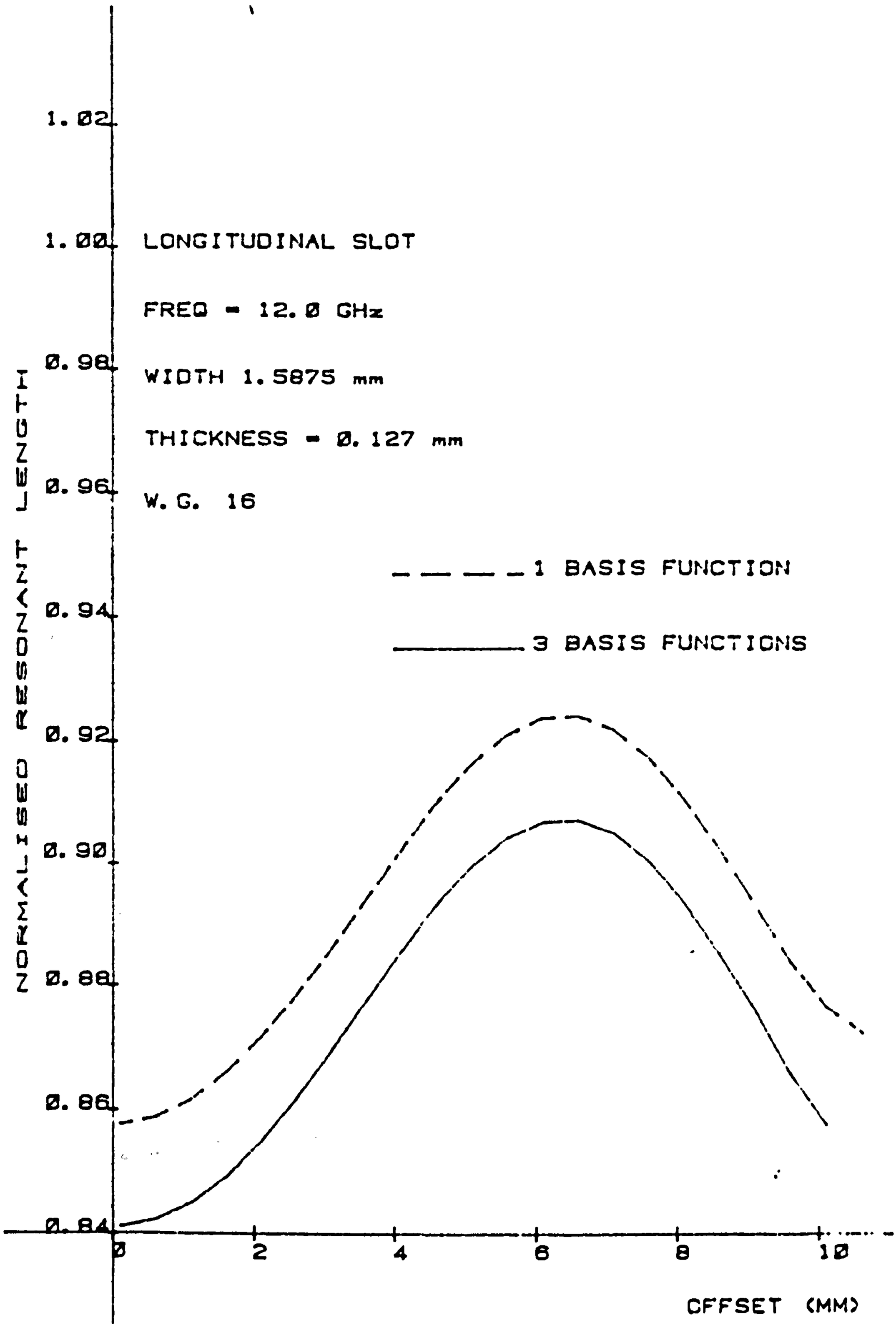

Figure 6.6d

A Graph of the Resonant Length as a Function of Offset for Various Longitudinal Slots - Thin-Walled Case

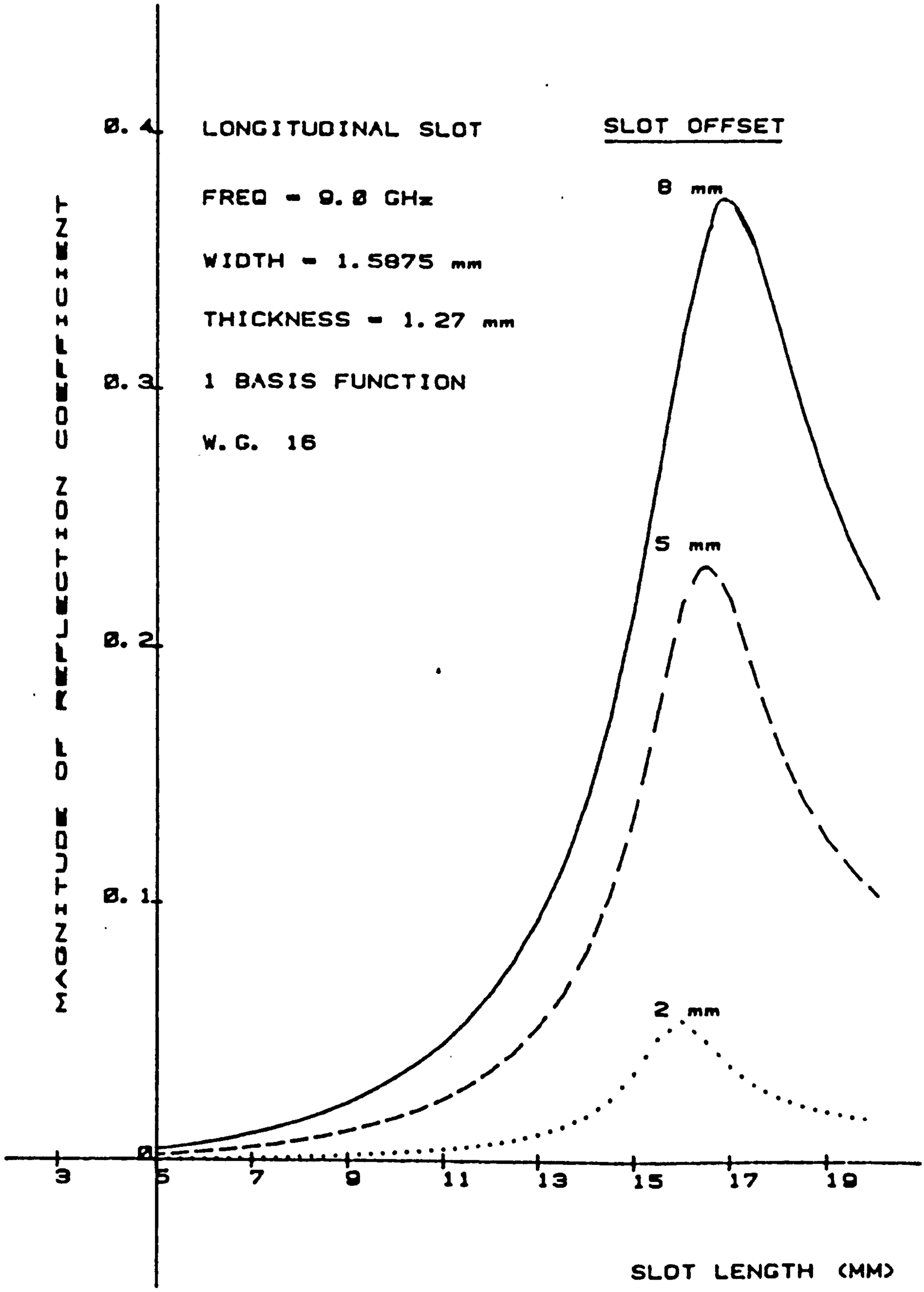

Figure 6.7a

A Graph of the Magnitude of the Reflection Coefficient Versus Slot Length for Various Longitudinal Slots

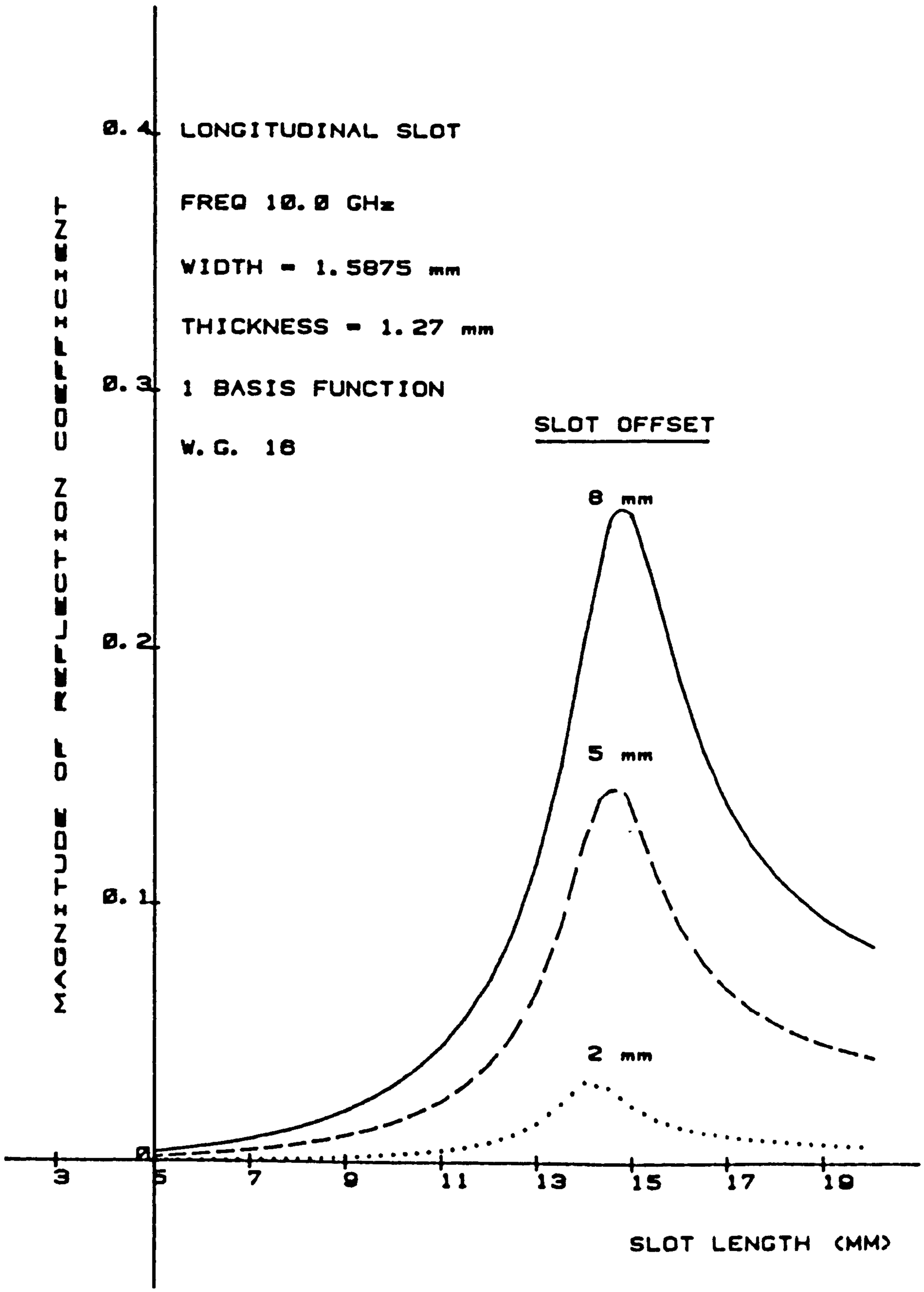

Figure 6.7b

A Graph of the Magnitude of the Reflection Coefficient Versus Slot Length for Various Longitudinal Slots

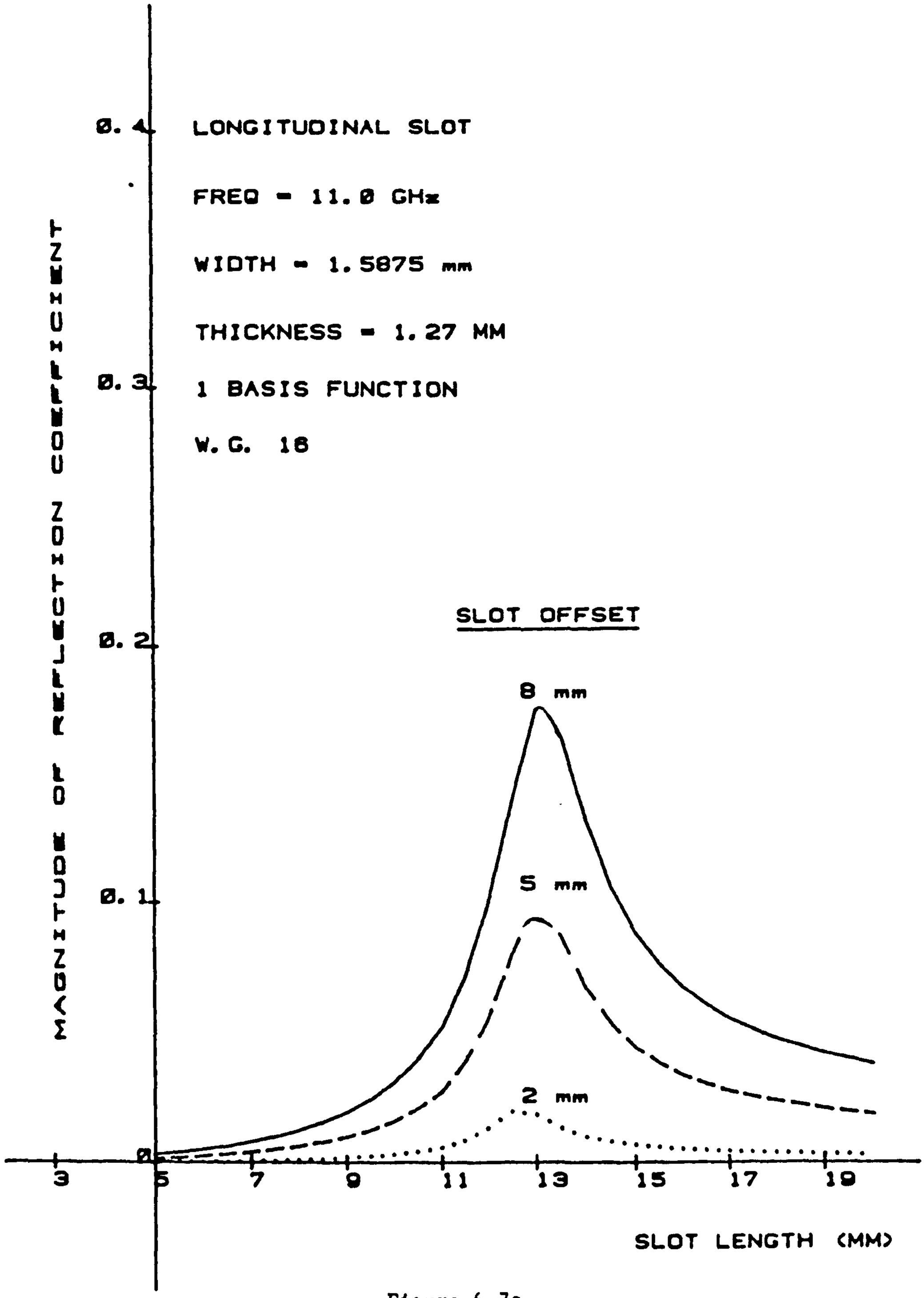

Figure 6.7c

A Graph of the Magnitude of the Reflection Coefficient Versus Slot Length for Various Longitudinal Slots

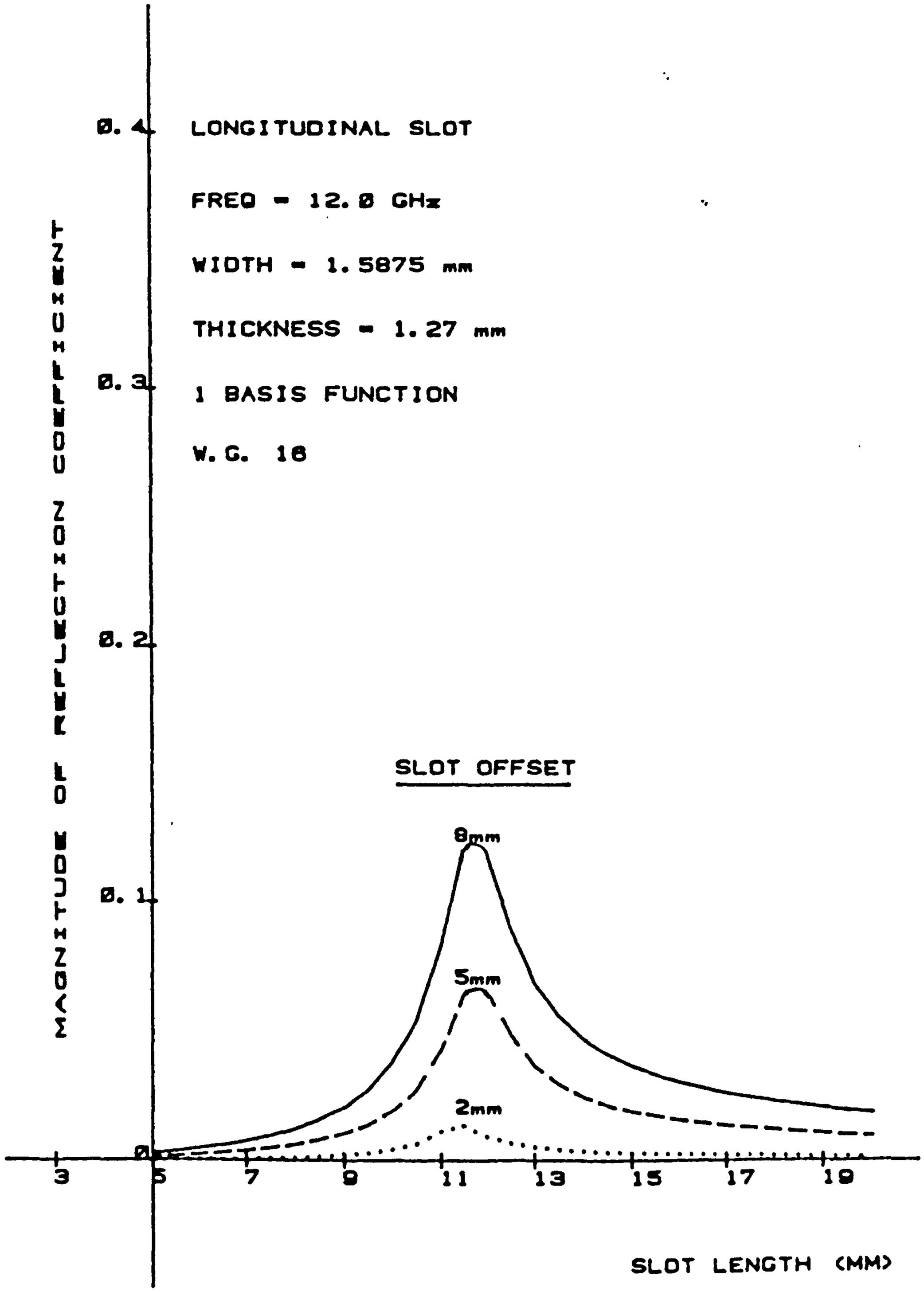

Figure 6.7d

A Graph of the Magnitude of the Reflection Coefficient Versus Slot Length for Various Longitudinal Slots

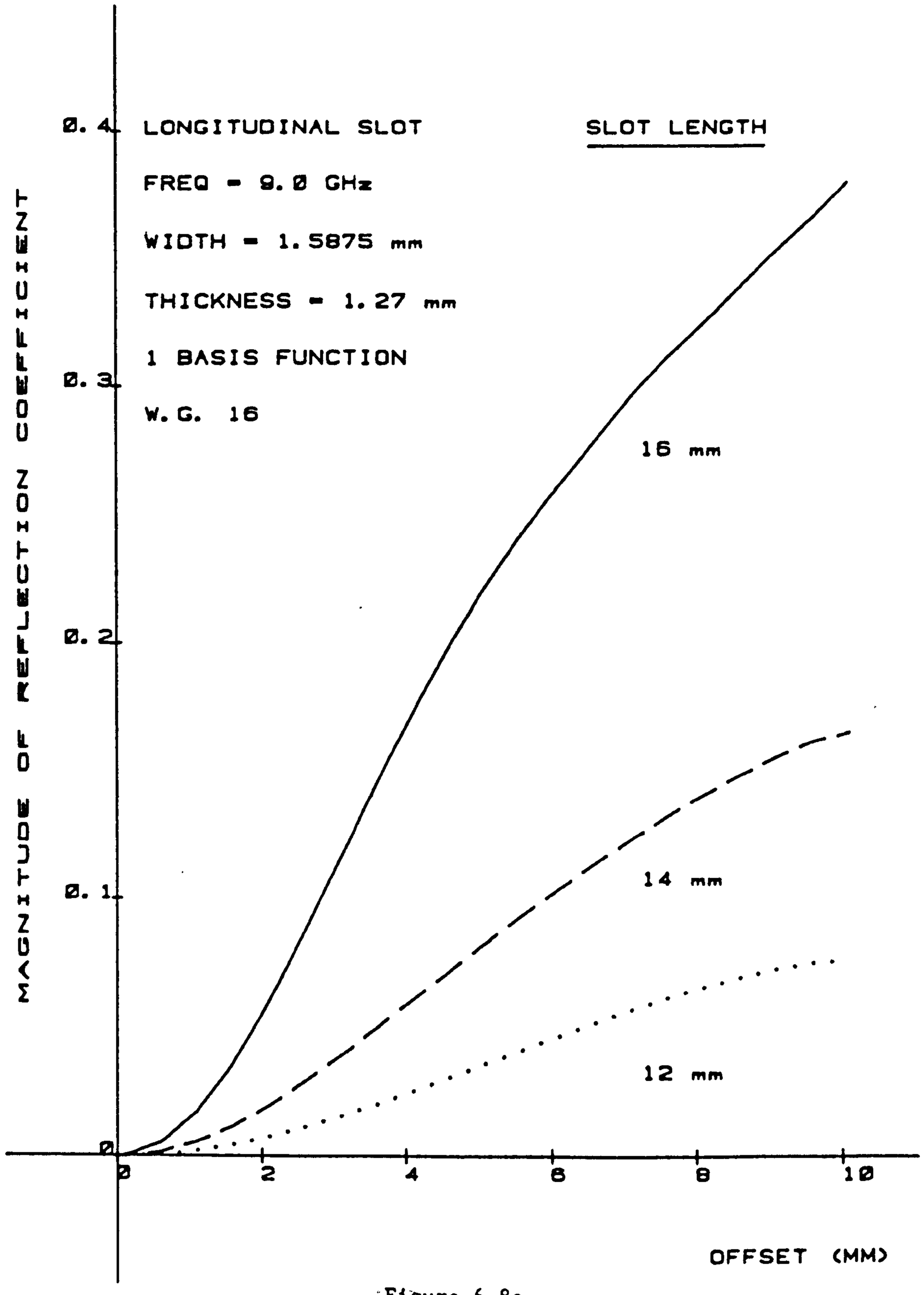

Figure 6.8a

A Graph of the Phase of the Reflection Coefficient Versus Slot Length for Various Longitudinal Slots

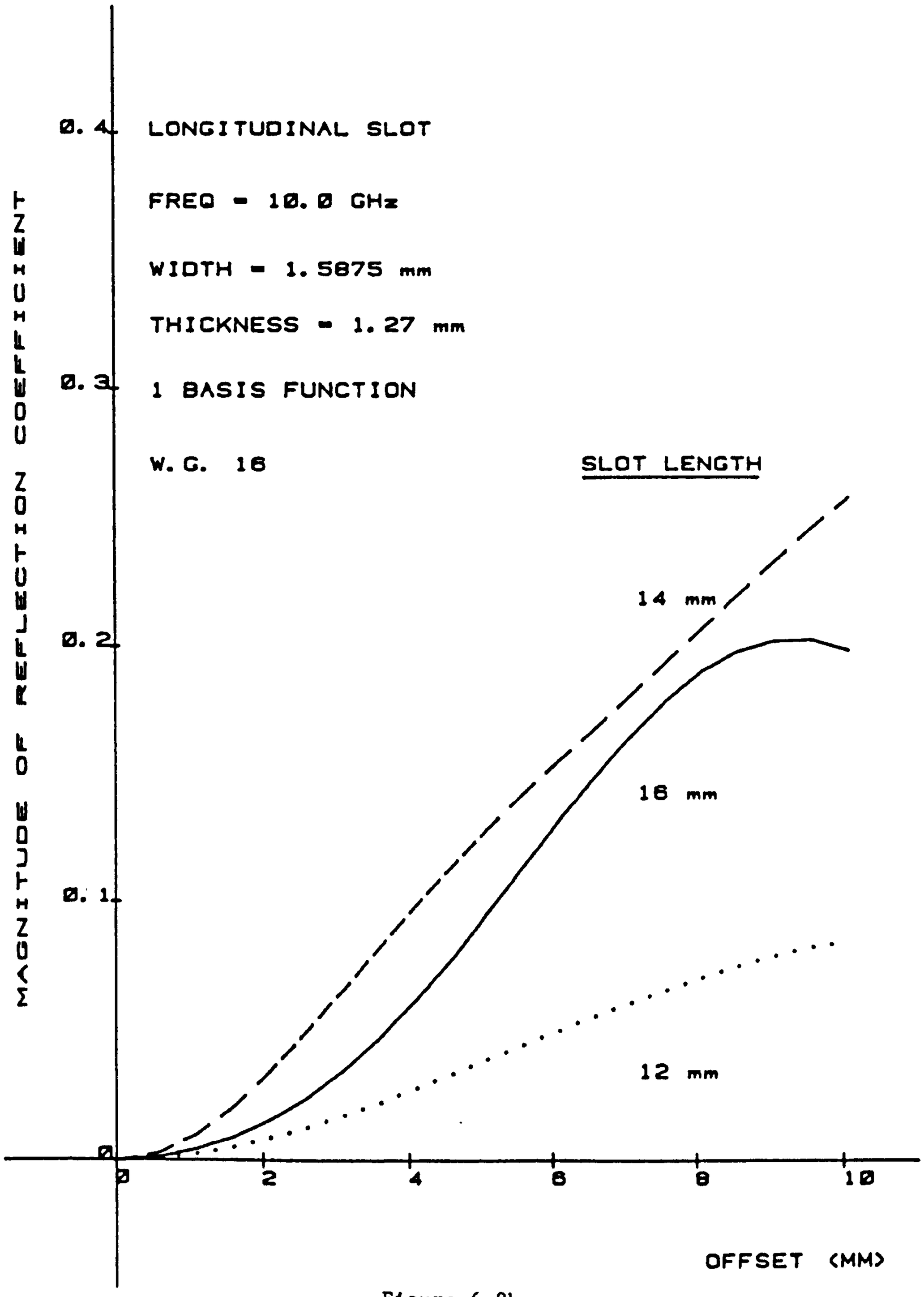

Figure 6.8b

A Graph of the Phase of the Reflection Coefficient Versus Slot Length for Various Longitudinal Slots

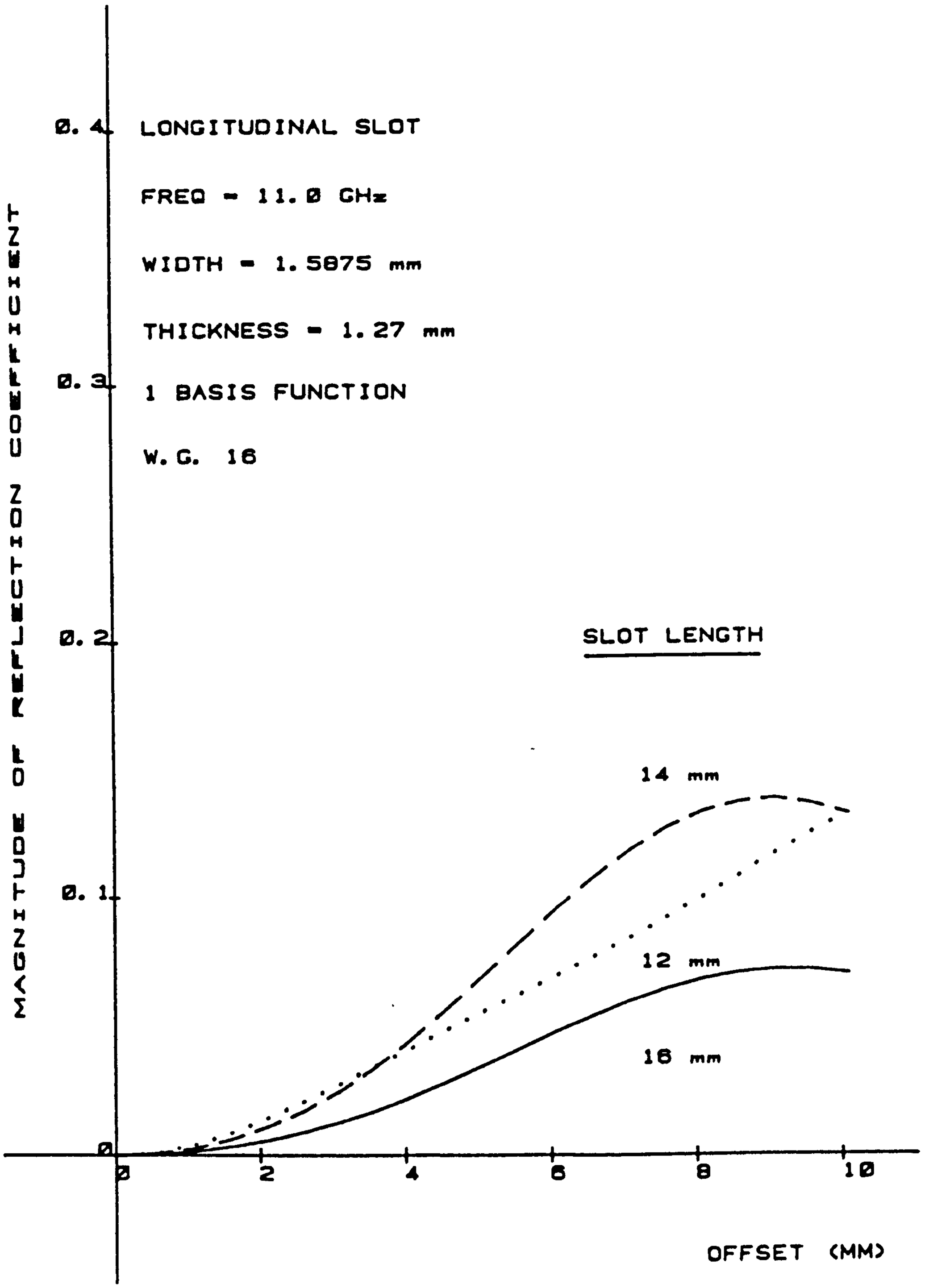

Figure 6.8c

A Graph of the Phase of the Reflection Coefficient Versus Slot Length for Various Longitudinal Slots

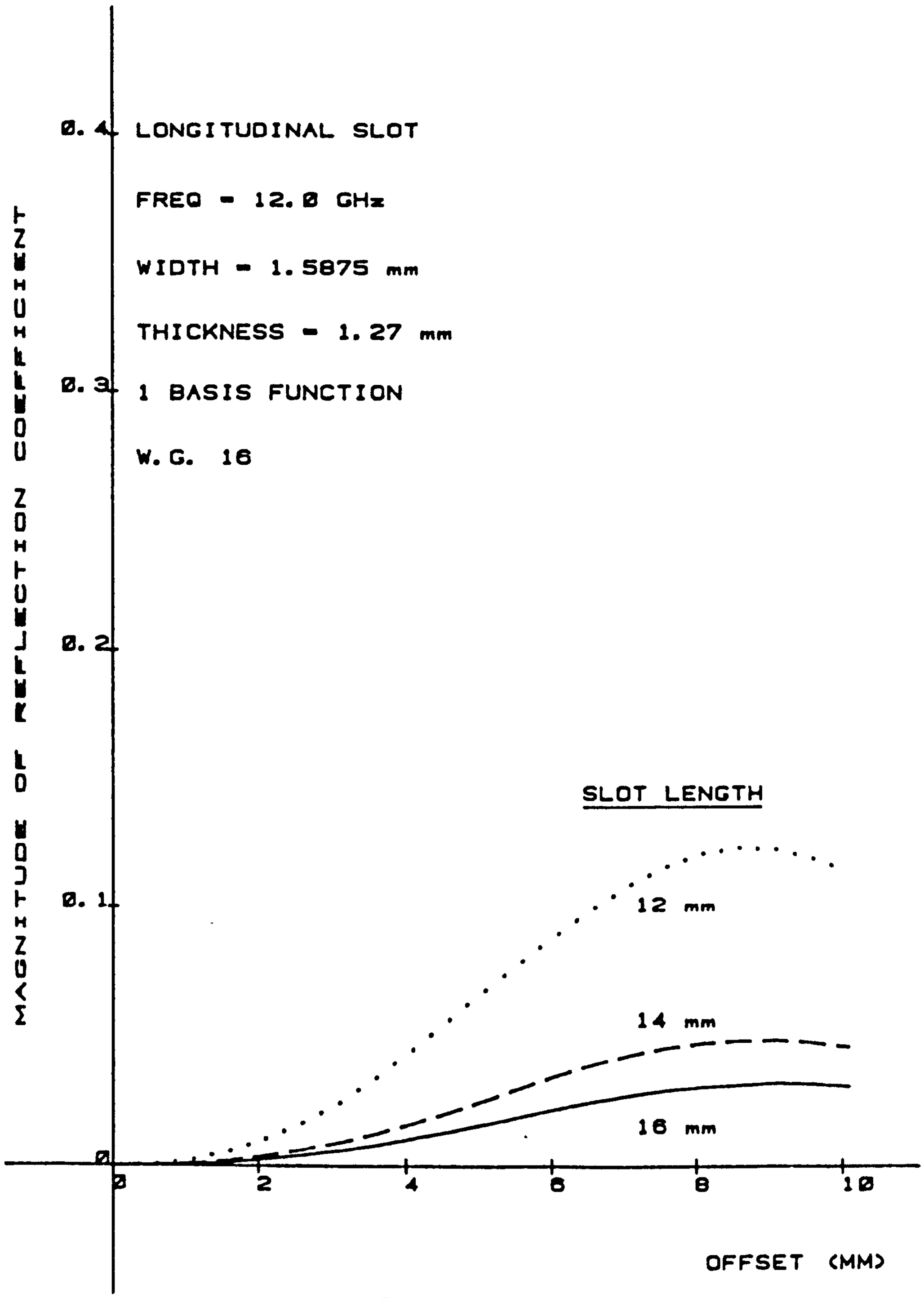

Figure 6.8d

A Graph of the Phase of the Reflection Coefficient Versus Slot Length for Various Longitudinal Slots

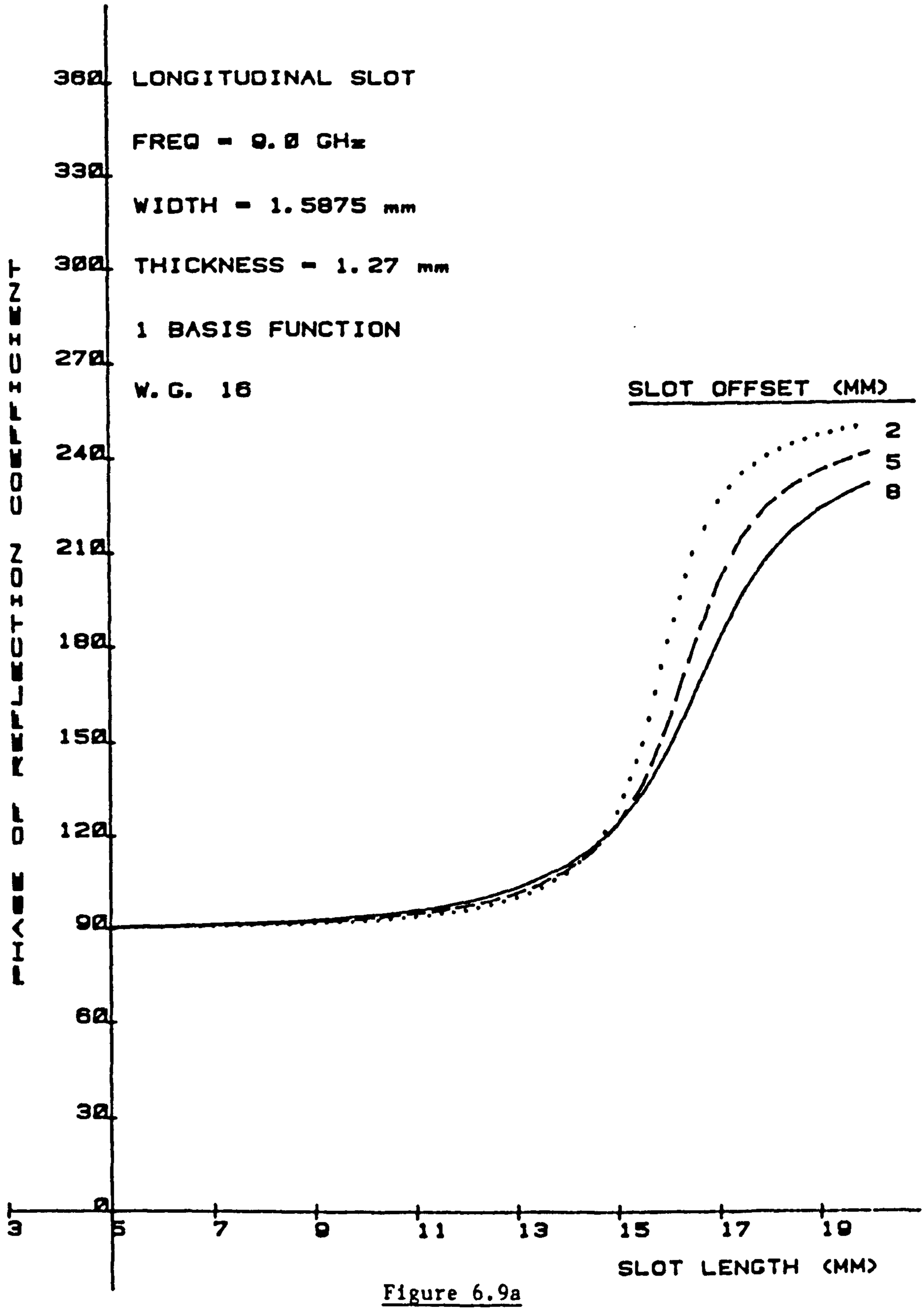

Figure 6.9a

A Graph of the Magnitude of the Reflection Coefficient as a Function of Slot Offset from the Waveguide Centre Line for Various Longitudinal Slots

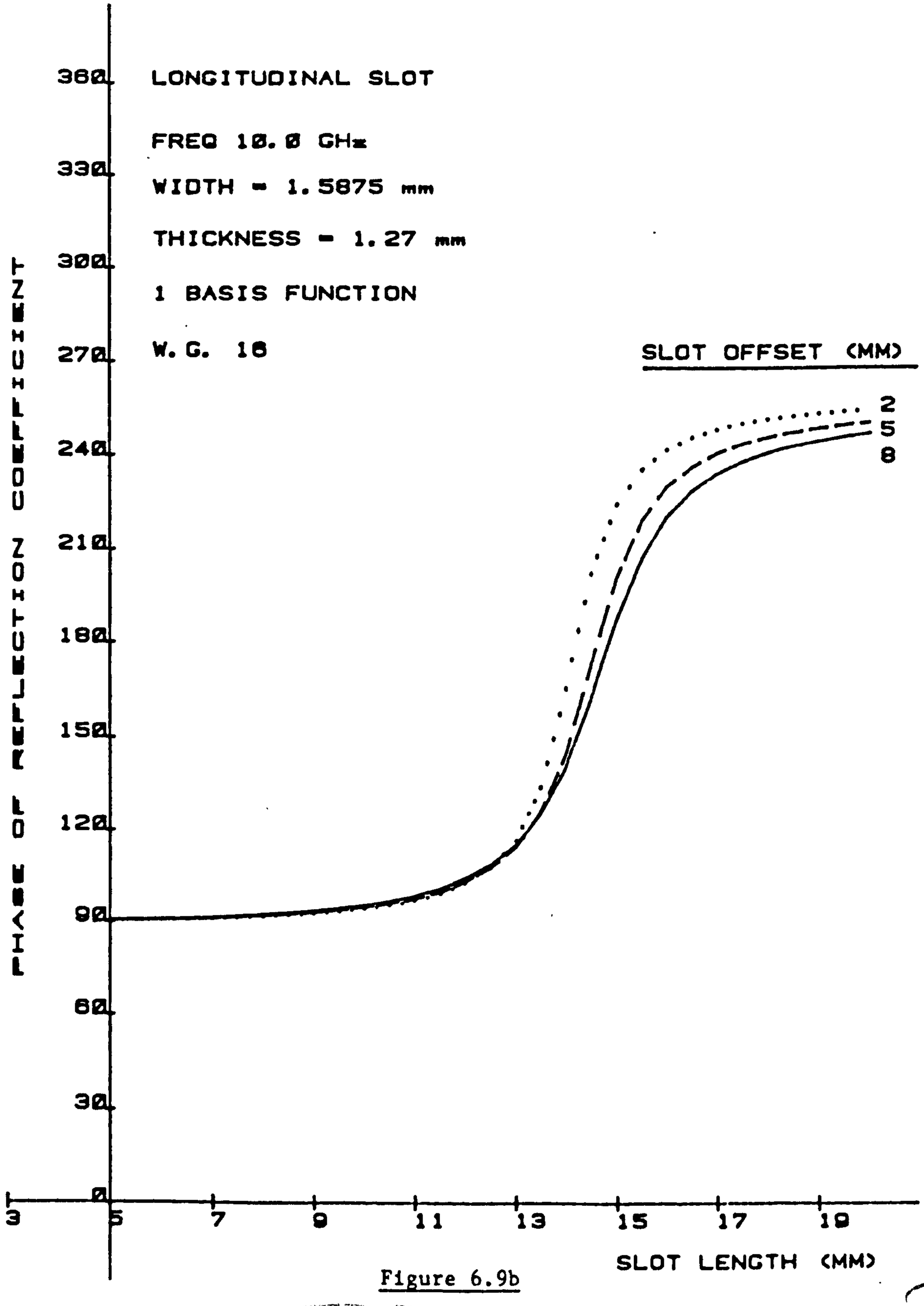

Figure 6.9b

A Graph of the Magnitude of the Reflection Coefficient as a Function of Slot Offset from the Waveguide Centre Line for Various Longitudinal Slots

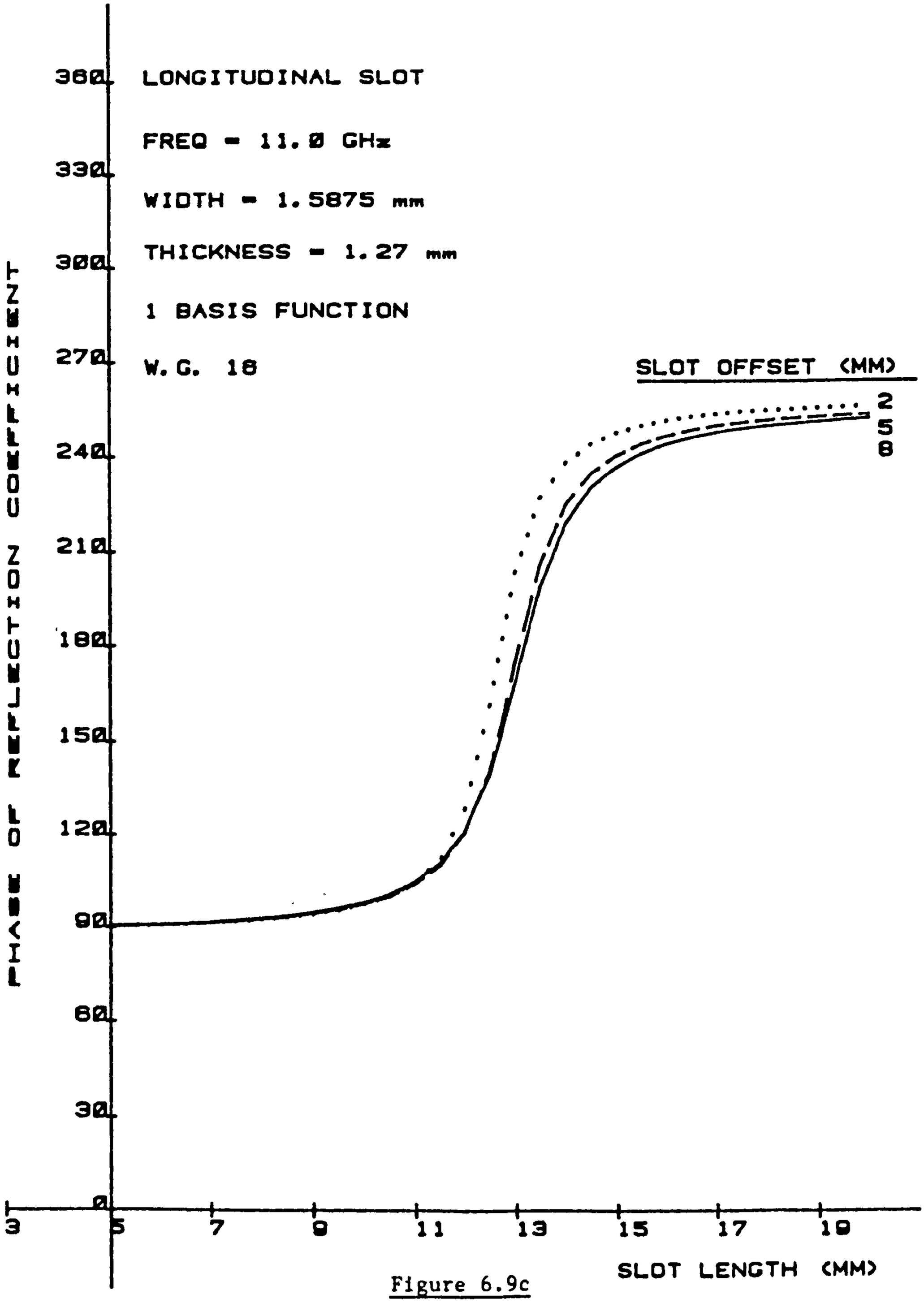

Figure 6.9c

A Graph of the Magnitude of the Reflection Coefficient as a Function of Slot Offset from the Waveguide Centre Line for Various Longitudinal Slots

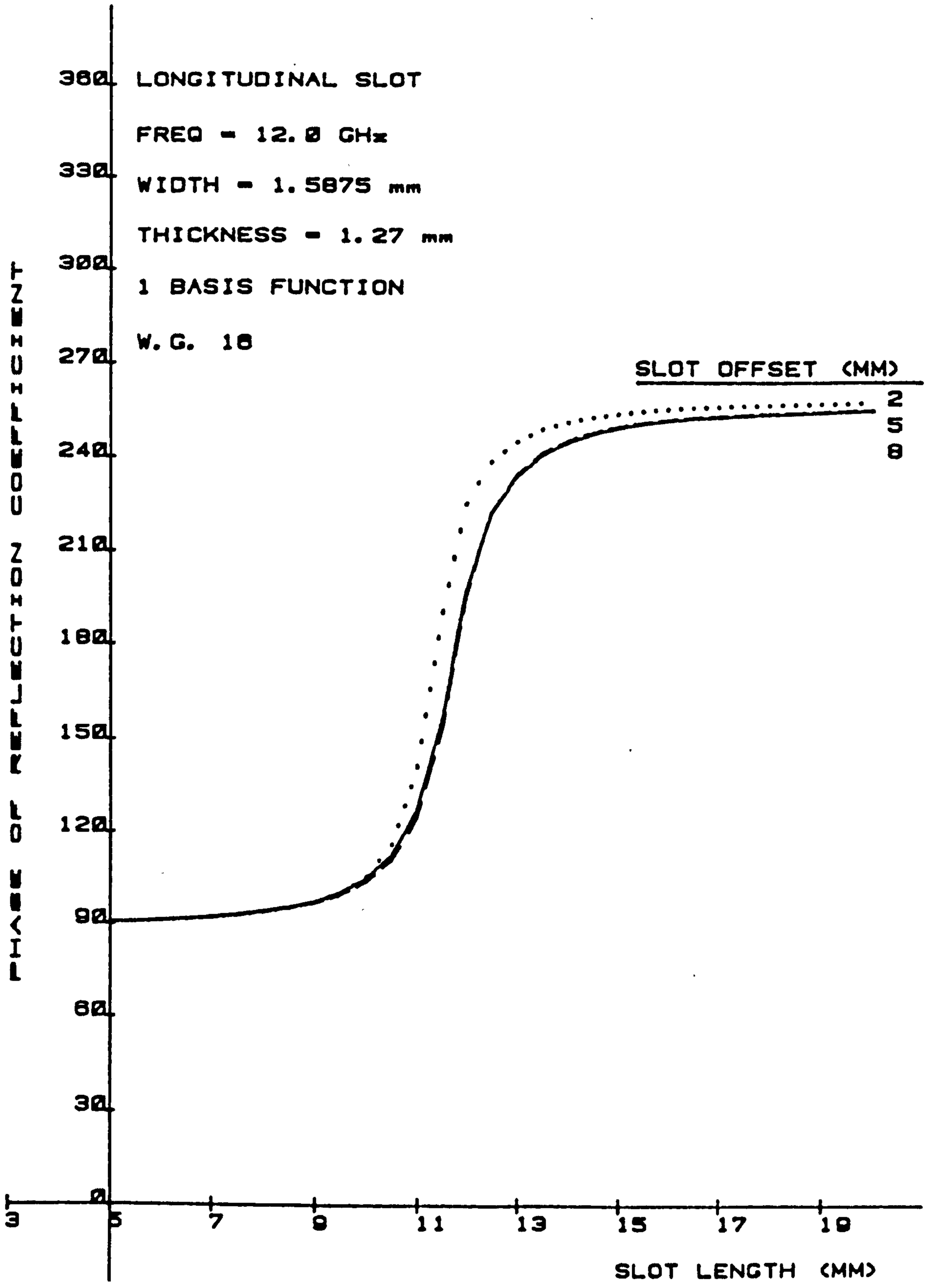

Figure 6.9d

A Graph of the Magnitude of the Reflection Coefficient as a Function of Slot Offset from the Waveguide Centre Line for Various Longitudinal Slots

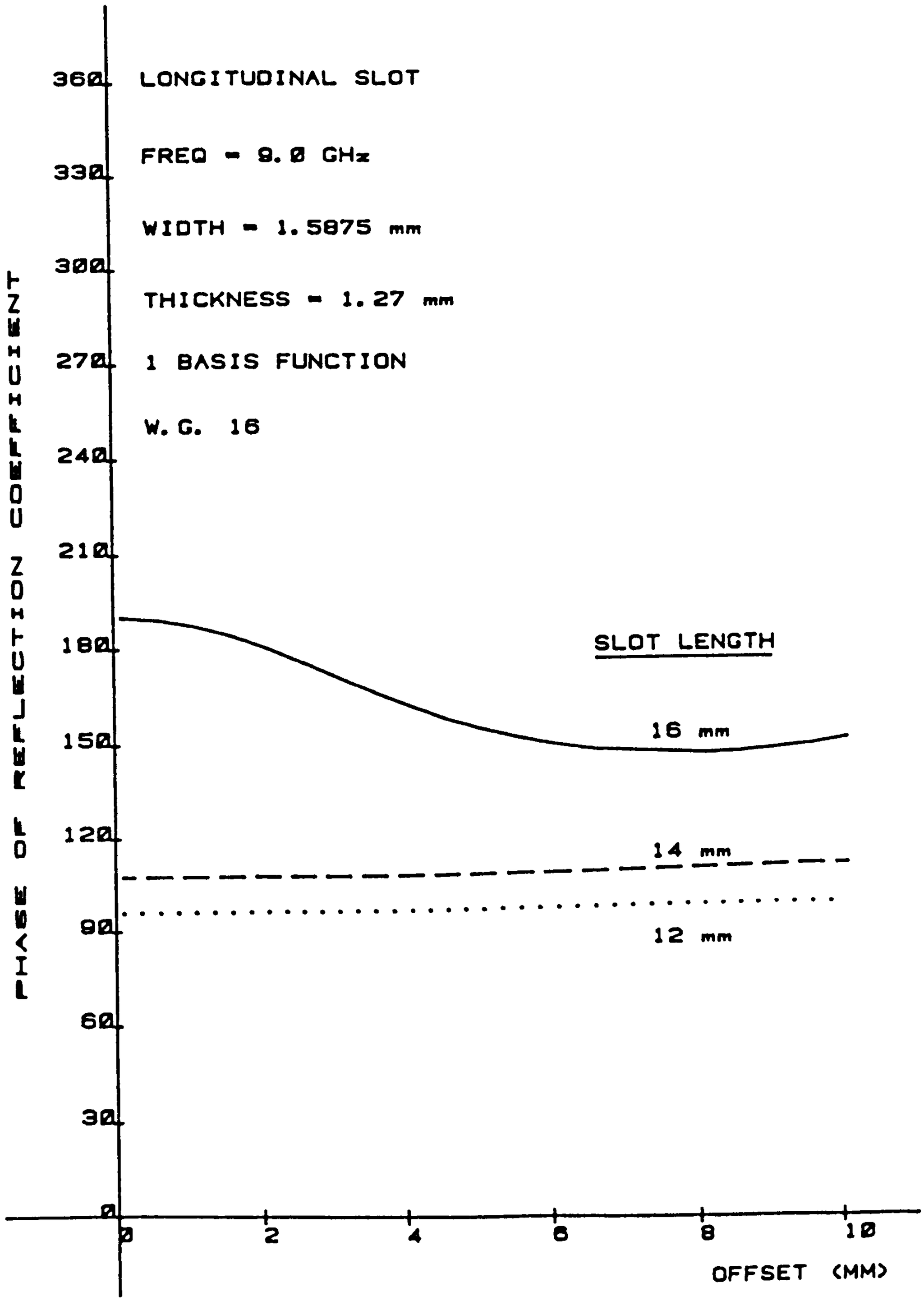

Figure 6.10a

A Graph of the Phase of the Reflection Coefficient as a Function of Slot Offset from the Waveguide Centre Line for Various Longitudinal Slots

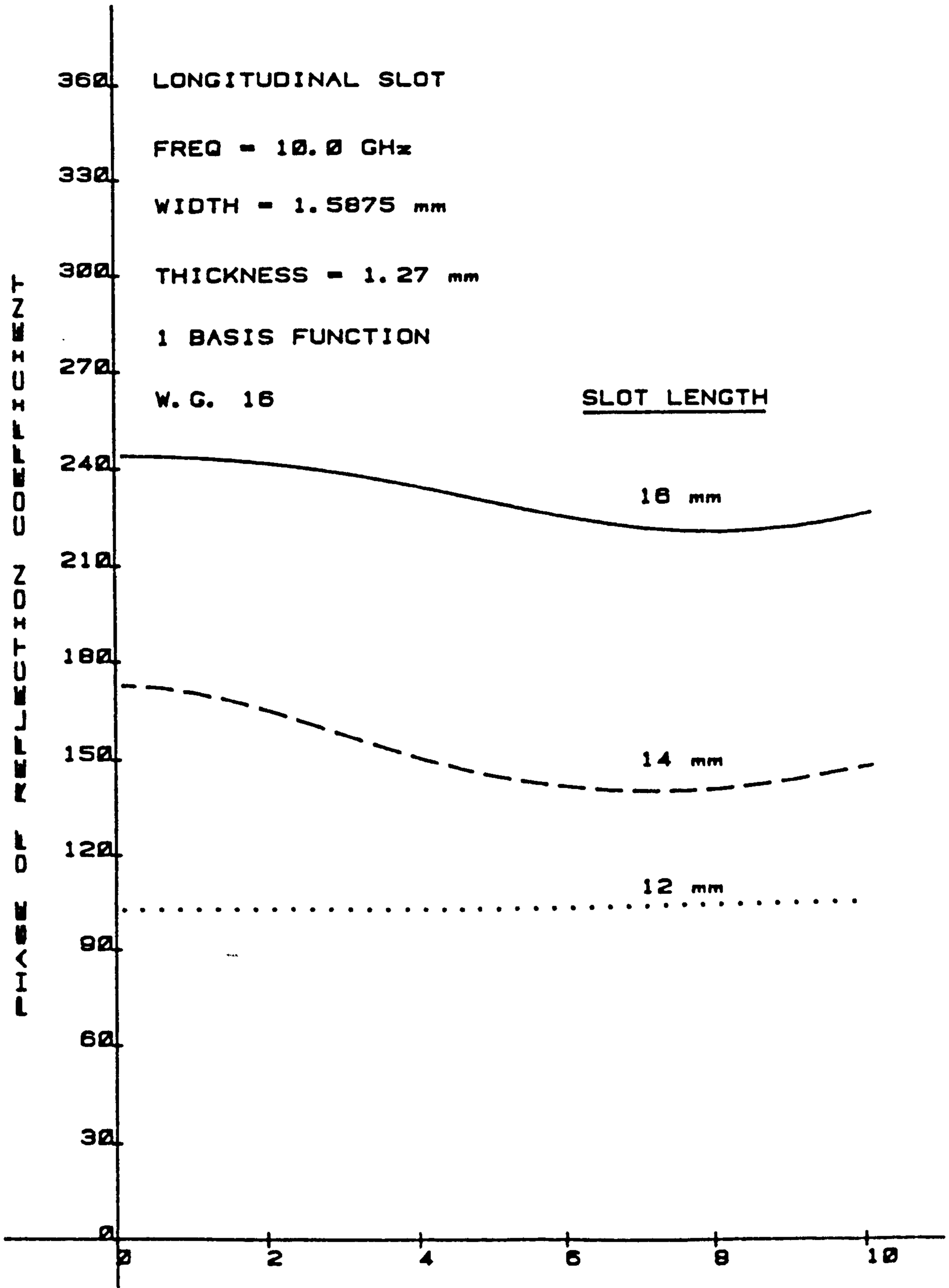

Figure 6.10b

A Graph of the Phase of the Reflection Coefficient as a Function of Slot Offset from the Waveguide Centre Line for Various Longitudinal Slots

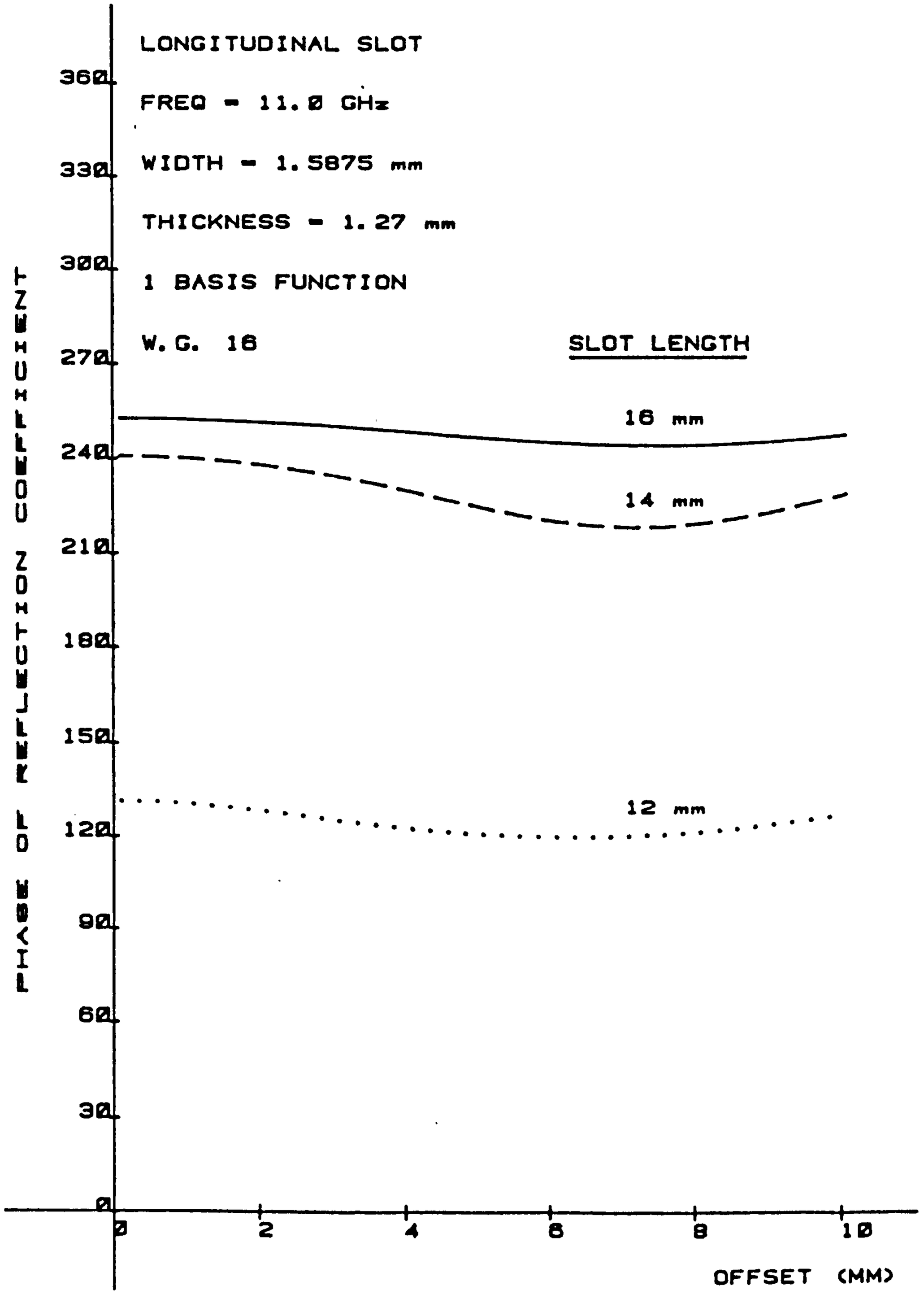

Figure 6.10c

A Graph of the Phase of the Reflection Coefficient as a Function of Slot Offset from the Waveguide Centre Line for Various Longitudinal Slots

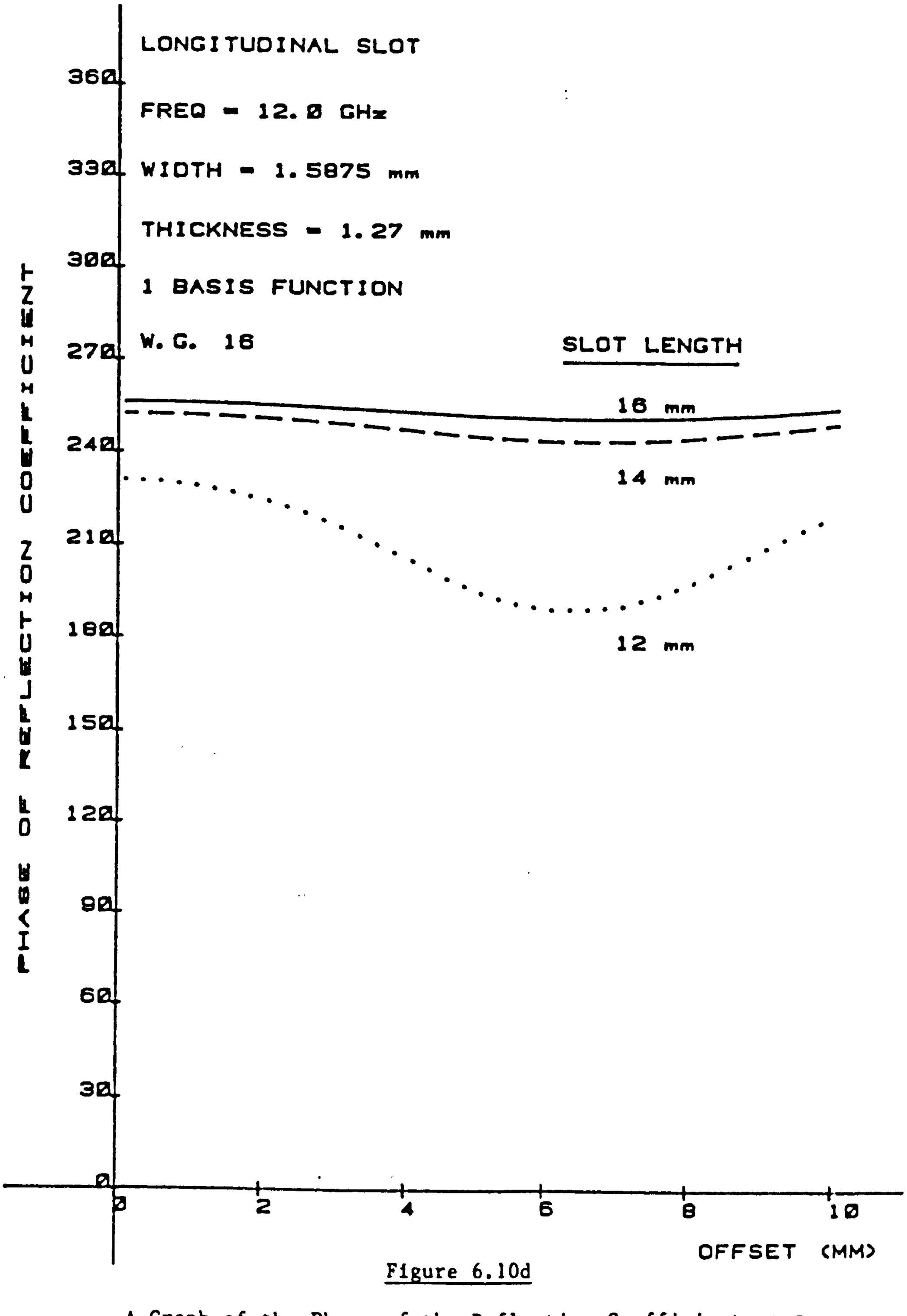

Figure 6.10d

A Graph of the Phase of the Reflection Coefficient as a Function of Slot Offset from the Waveguide Centre Line for Various Longitudinal Slots

α = phase shift passed slot

δ = phase shift through slot

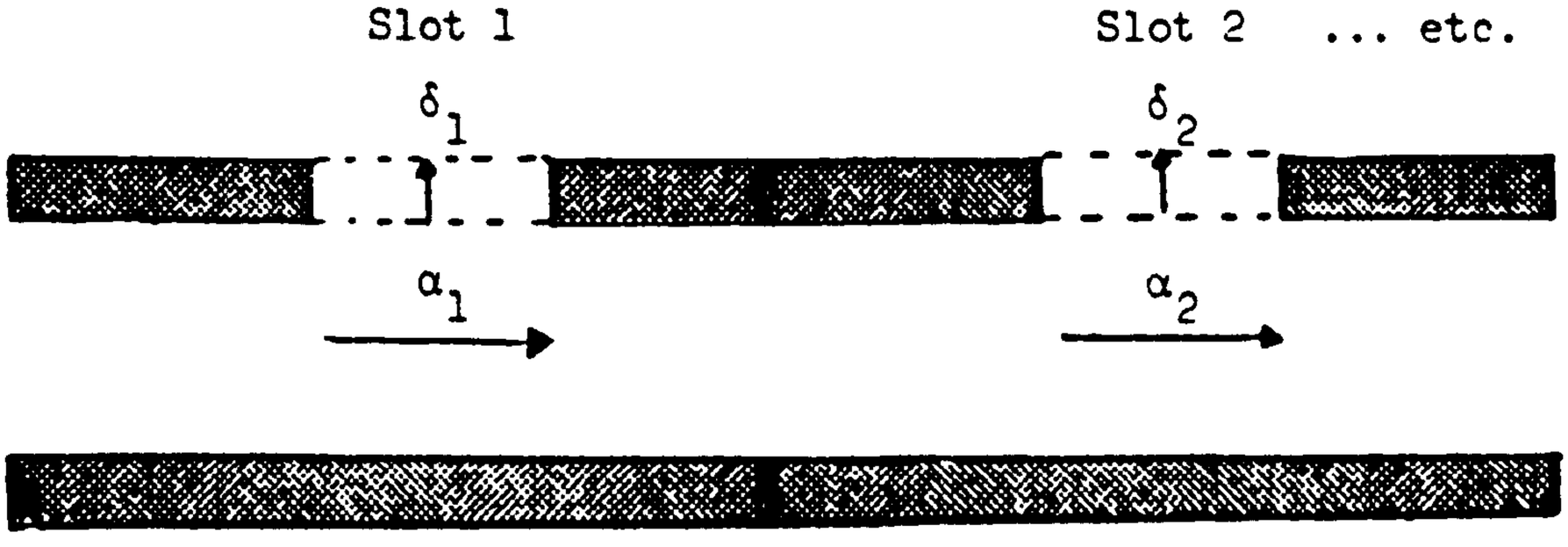

Figure 6.11

Illustration of Radiated and Transmitted Phase Shifts Due to Slots

CHAPTER 7

THEORETICAL AND EXPERIMENTAL ASSESSMENT OF THE CAD SYNTHESIS PACKAGE

A computer aided design/synthesis package for slotted waveguide array antennas has been described in the preceding chapter. This differs from other design procedures presently detailed in the literature [2.63, 2.79, 3.9, 4.4, 6.1, 6.2] in that it uses theoretically evaluated self admittance values, rather than measured self admittances, for the individual slots in the array. This package is assessed in this chapter using two independent tests. Firstly, it has been used to design an array previously detailed by Elliott in [2.80] for which directly comparable results are available. Secondly, to design a 19 element shunt slot array which, once constructed, was comprehensively evaluated on an accurate near field measurement system, courtesy of Ferranti Plc, Edinburgh.

7.1 THEORETICAL ASSESSMENT

Elliott designed a 21 element non-staggered shunt slot travelling wave array using the design procedure described in [2.79, 2.80]. This has been repeated using the CAD package presented in chapter 6. However, before detailing the design it is worth summarising the two design techniques and highlighting the main differences. Two simplified flow charts are presented below to clearly enunciate the respective techniques.

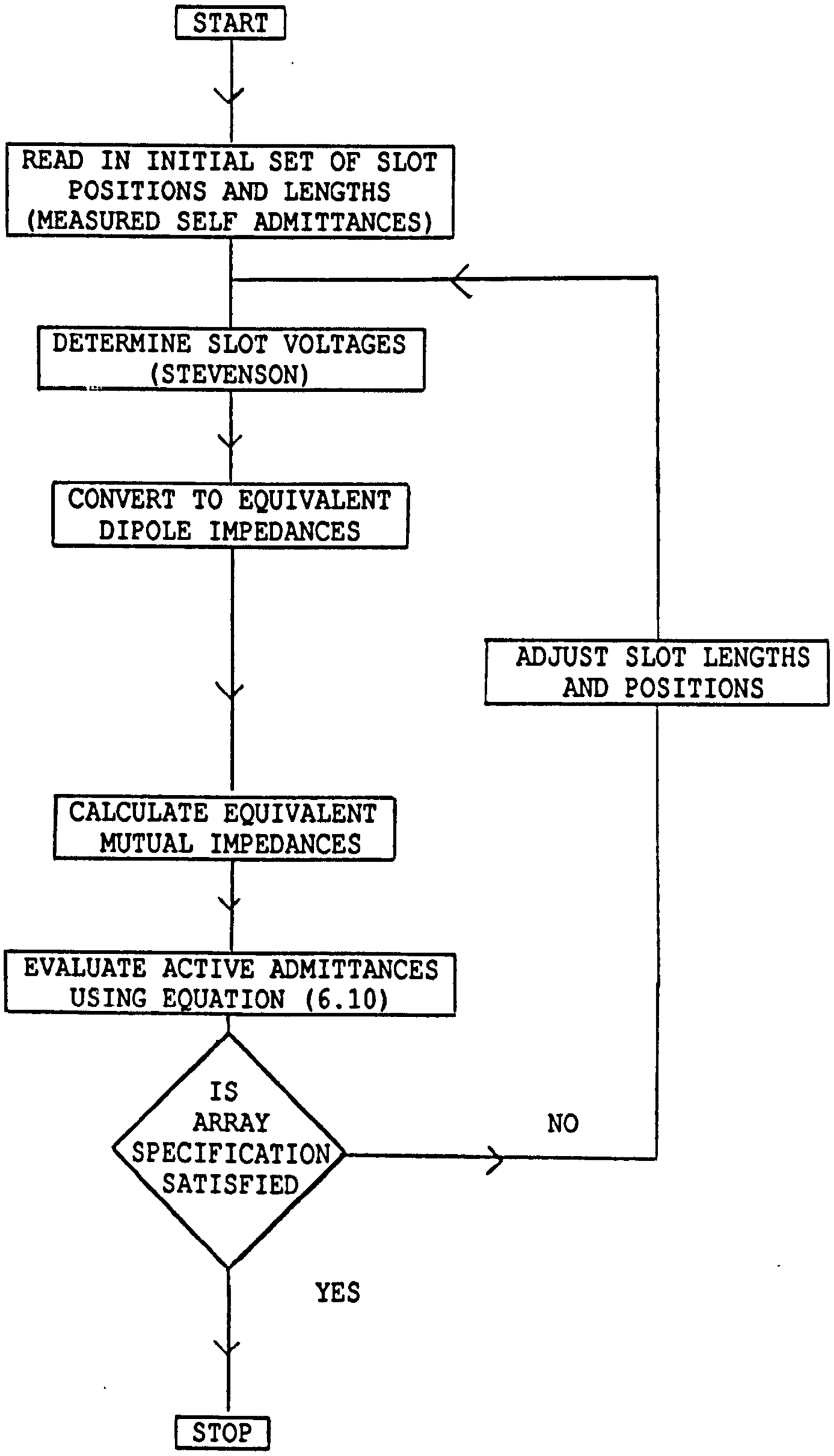
START
READ IN INITIAL SET OF SLOT POSITIONS AND LENGTHS (MEASURED SELF ADMITTANCES)
DETERMINE SLOT VOLTAGES (STEVENSON)
CONVERT TO EQUIVALENT DIPOLE IMPEDANCES
CALCULATE EQUIVALENT MUTUAL IMPEDANCES
EVALUATE ACTIVE ADMITTANCES USING EQUATION (6.10)
IS ARRAY SPECIFICATION SATISFIED
NO
ADJUST SLOT LENGTHS AND POSITIONS
YES
STOP

CAD Synthesis Routine

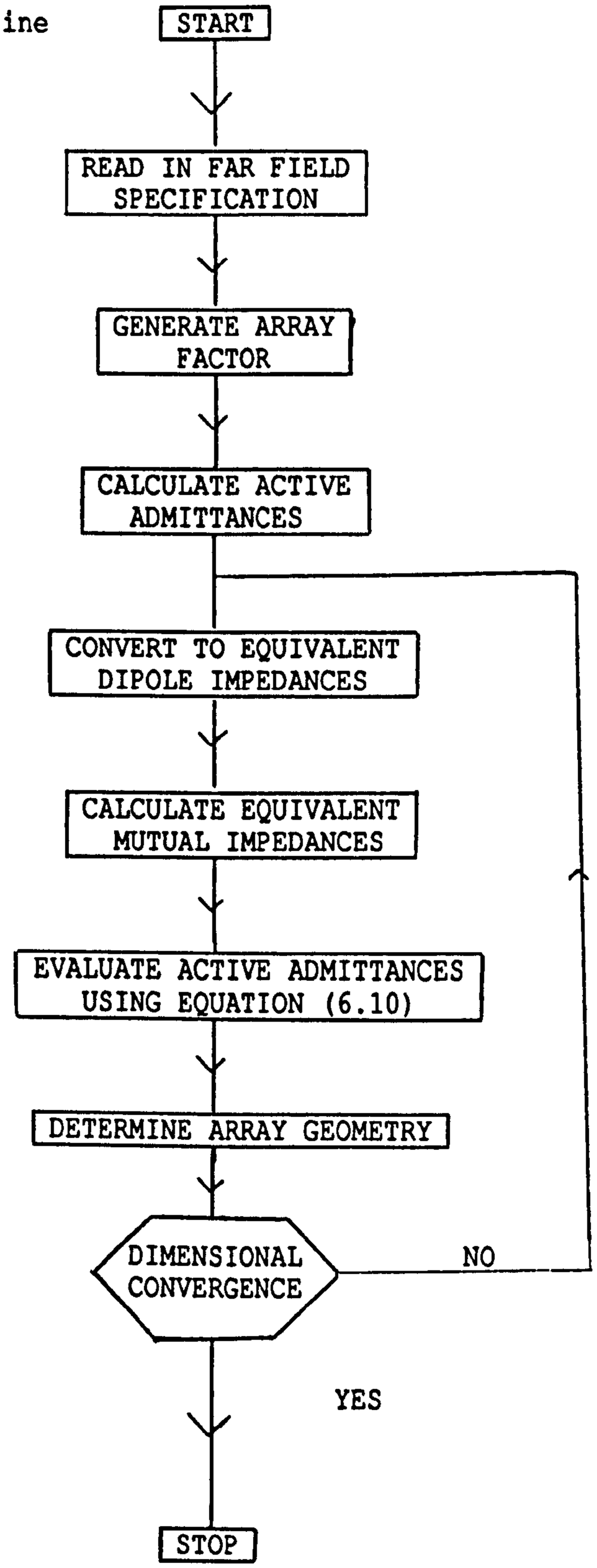

The two techniques differ in that Elliott's starts with a set of measured self admittances for slots whose lengths and offsets are known. Then the active admittances for this array configuration are

determined. These values are compared with the admittance values required to generate the specified far field pattern and the process is repeated, using adjusted self admittance values, until the specification is satisfied. Whereas, the CAD package reverses this and starts by determining the active admittances for the desired far field pattern and subsequently evaluates the self and mutual coupling components. Various root-finding routines are then employed to determine the array configuration and the process is repeated until a satisfactory solution is obtained.

The array designed by Elliott has a Dolph-Chebyshev response with a -30 dB side lobe specification and the main beam is placed at 45 degrees from forward end-fire. The operating frequency is specified as 9.375 GHz. This design has been repeated using the CAD package and the physical array characteristics predicted by the program are reproduced below in table form.

No.	Length (mm)	Offset (mm)	Separation (mm)
1	15.374	1.689	17.40
2	15.214	1.035	17.42
3	15.273	1.474	17.42
4	15.302	1.833	17.42
5	15.306	2.131	17.41
6	15.313	2.315	17.40
7	15.308	2.375	17.39
8	15.296	2.353	17.39
9	15.270	2.273	17.38
10	15.246	2.144	17.38

11	15.212	1.978	17.38
12	15.167	1.794	17.38
13	15.141	1.606	17.38
14	15.123	1.420	17.38
15	15.094	1.236	17.39
16	15.066	1.044	17.39
17	15.040	0.866	17.39
18	14.996	0.715	17.39
19	14.984	0.551	17.40
20	15.013	0.374	17.39
21	14.930	0.562	

Table (7.1)

Predicted Array Geometry for 21 Element Example

Note: The slots are numbered from the load end.

The slot lengths and offsets listed in the above table are substantially in agreement with the corresponding Elliott values when due allowance is made for the fact that Elliott's design uses measured self admittance values for round ended slots and also contains a constraint, which ensures that the resultant slot dimensions are consistent with the data file values. In Figure (7.1) a comparison is made between the theoretical and experimental results for this array. The figure shows the specified pattern (solid curve), a pattern deduced from the theoretical slot offsets and lengths (dotted curve), using Elliott's technique outlined previously with the measured self admittances being replaced by moment method predictions, and a reconstruction of Elliott's measured pattern using

144 data points (chain dotted curve). In connection with this figure it is particularly interesting to note the discrepancy which occurs between the 'ideal' pattern (solid curve) and the deduced pattern (dotted curve). The discrepancy appears predominantly in the side lobe levels which are generally lower than their theoretical value, except for those lobes most remote from the main beam. This error can largely be attributed to the method used to evaluate the mutual coupling between elements which relies on analogy with dipole theory. This analogy necessitates finding a relationship between slot voltages and mode voltages and currently this involves the use of the following approximate expression formulated by Elliott and Kurtz [2.79] based on Stevenson's [2.15] work

$$V_n = \frac{j}{Y_n^A} \left[\frac{8}{\pi^2 \eta} \quad \frac{(a/b)}{(\beta/k)} \right]^{\frac{1}{2}} \sin \frac{\pi x_n}{a} \left(\cos 2\beta L_n - \cos 2kL_n\right) V_n^s \qquad (7.1)$$

where η is the impedance of free space.

A more direct method of evaluating the mutual coupling in the slotted array is required before this weakness in the synthesis program can be eliminated. However, when the synthesised results are compared with Elliott's measurements (chain dotted curve), the degree of agreement is not untypical of synthesised slot array design.

An alternative far field pattern predicted from Elliott's [2.80] array configuration (solid curve), with the slot lengths corrected to compensate for the round ends [3.10] using an equal area rule, is presented in Figure (7.2) along with the measured result (chain dotted curve). The two curves are in reasonable agreement with the

discrepancies mainly appearing in the side lobes. These discrepancies can be predominantly attributed to the following factors.

(a) Inaccuracies in the self admittances predictions, which arise from evaluating the moment method using a single trignometric basis function.

(b) Errors arising from the use of the round end to square end correction factor.

(c) The method of evaluating the mutual coupling between the elements, especially the dependence on the relationship between slot voltage and mode voltage as highlighted previously.

Care must be exercised in interpreting the results in Figure (7.2) and it is difficult to conclude too much. However, this figure demonstrates that some confidence can be placed in the moment method predictions, as they have been used to replace the measured data in [2.80] with theoretical values and the computed far field pattern, using these values, is in reasonable agreement with the measured result.

7.2 EXPERIMENTAL CONFIRMATION

A 19 element shunt slot travelling wave array with staggered slots has also been designed using the CAD synthesis program (see figure (7.3)). The Dolph-Chebyshev response has once again been adopted to characterise the far field pattern with the main beam at 9 degrees

from broadside and -24 dB side lobes. The array was designed to operate at 9.375 GHz and has been constructed in standard X-band waveguide (W.G. 16) using square ended 1.6 mm wide slots. The resultant design has a normalised theoretical input admittance of 1.023 + j 0.0225 and 28 percent of the power is predicted to be dissipated in the load. The physical configuration of the array is tabulated below:

No.	LENGTH (mm)	OFFSET (mm)	SEPARATION (mm)
1	15.171	+ 2.034	18.36
2	15.122	- 1.485	18.34
3	15.109	+ 1.701	18.33
4	15.121	- 2.046	18.31
5	15.157	+ 2.280	18.30
6	15.167	- 2.467	18.29
7	15.189	+ 2.564	18.29
8	15.191	- 2.595	18.29
9	15.185	+ 2.549	18.30
10	15.178	- 2.447	18.31
11	15.159	+ 2.301	18.32
12	15.151	- 2.122	18.34
13	15.150	+ 1.918	18.35
14	15.146	- 1.702	18.36
15	15.133	+ 1.466	18.37
16	15.136	- 1.226	18.38
17	15.158	+ 1.006	18.36

18	15.013	- 0.826	18.38
19	15.206	+ 1.086	

Table (7.2)

Predicted Array Geometry for 19 Element Array

The predicted far field pattern (dotted curve) for this array configuration has been compared with the 'ideal' pattern (solid line) in Figure (7.4). The differences between the two patterns are less than those observed for the Elliott array, and this is due to the lower level of mutual coupling which a staggered array suffers. This in turn means that the approximation in equation (7.1) which has been identified as the primary cause of these theoretical discrepancies is much less significant for this array.

Before discussing the experimental results for this array it is worth digressing slightly and commenting on the suggestion in [2.67, 2.68] that the effect of mutual coupling may be neglected in the design of arrays of this type, as long as the side lobe levels are not lower than -30 dBs. This implies that the mutual effect may be ignored in the above design. Obviously, this has an effect on the predicted array configuration and in order to quantify it the synthesis program has been re-run with the mutual coupling set equal to zero. The resulting configuration is tabulated below:

No.	LENGTH (mm)	OFFSET (mm)	SEPARATION (mm)
1	15.238	+ 1.950	18.38
2	15.188	- 1.197	18.38

3	15.211	+ 1.502	18.38
4	15.234	- 1.784	18.38
5	15.245	+ 2.021	18.37
6	15.279	- 2.190	18.38
7	15.290	+ 2.287	18.38
8	15.290	- 2.306	18.38
9	15.290	+ 2.258	18.38
10	15.287	- 2.158	18.38
11	15.247	+ 2.017	18.38
12	15.247	- 1.855	18.38
13	15.227	+ 1.662	18.38
14	15.227	- 1.476	18.38
15	15.188	+ 1.258	18.38
16	15.188	- 1.069	18.38
17	15.147	+ 0.855	18.38
18	15.147	- 0.691	18.38
19	15.174	+ 1.027	

Table (7.3)

Predicted Array Geometry for 19 Element Array

With Mutual Coupling Set Equal to Zero

It is interesting to note that the values tabulated above differ only slightly from those tabulated in Table (7.2). The predicted far field patterns for the two array configurations have been presented in Figure (7.5). This figure clearly shows that even although the physical differences between the arrays are small, they have a significant effect on the radiation pattern. Therefore, the mutual

coupling must be taken into account in the design, unless the machining tolerances are extremely poor.

The radiation characteristics of the constructed array have been determined experimentally with the array embedded in a ground plane (300 mm x 600 mm) using a near field measurement system which was accurate to approximately ±1 dB. The results obtained using this set-up are presented in Figures (7.6), (7.7) and (7.8). However, in order that the far field pattern may be examined it has been reconstructed from the near field measurements and the phase and magnitude data used to reconstruct the pattern is tabulated below:

No.	Amplitude	Phase (Degrees)
1	21.26	307
2	12.16	269
3	17.30	235
4	17.58	198
5	24.80	184
6	26.60	147
7	29.17	91
8	30.20	67
9	35.10	31
10	28.50	355
11	35.10	333
12	32.36	289
13	27.86	256
14	27.86	207
15	17.00	194

16	22.39	153
17	13.65	127
18	14.29	153
19	13.18	27

Table (7.4)

Measured Near Field Data

Note: The values were read from the appropriate curves at positions equivalent to the centre of each slot.

The reconstructed far field pattern (solid curve), which represents the measured pattern with a fair degree of accuracy, is illustrated along with the 'ideal' pattern (dotted curve) in Figure (7.9). This shows that while the main beam position and width are in good agreement with theory the far out side lobes in particular are considerably in error. The reasons for this error are predominantly due to machining inaccuracies and an inability to produce square ended slots. The machining limitations can clearly be seen in Figure (7.10) where photographs of the individual slots are presented. These effects are also highlighted by near field amplitude and phase patterns for the array in Figures (7.7) and (7.8) which show that slots 10, 15, 18 and 19 are particularly poor. The near field values for these slots have been corrected (see Table (7.5)) and computer predictions of the far field patterns for each adjustment and the overall adjustment are illustrated in Figures (7.11), (7.12), (7.13), (7.14) and (7.15).

SLOT No.	AMPLITUDE	PHASE (Degrees)
10	35.563	Same
15	25.410	Same
18	14.073	90.0
19	21.500	60.0

Table (7.5)

Adjusted Near Field Values

The adjusted pattern (solid curve) presented in Figure (7.15) clearly demonstrates the effect of correcting the slot excitations and shows a significant improvement in the radiation pattern with the far out side lobes falling off.

7.3 CONCLUSION

The computer aided design package for the synthesis of linear travelling wave slotted arrays has been assessed in this chapter. A purely theoretical assessment was initially carried out and the array detailed in [2.80] was redesigned. The predicted array configuration was found to be in substantial agreement with Elliott's configuration. A second and more rigorous assessment was then carried out where the package was used to design a 19 element array, this was constructed and measured on a near field measurement system. The experimental and theoretical results for this array have been shown to be in reasonable agreement once certain constructional limitations are taken into consideration.

The results presented in this chapter demonstrate that it is viable to design arrays of this type using purely theoretical results and therefore, the restriction on the array configurations that may be examined can be relaxed somewhat, as the measured data formerly relied upon can be replaced by theoretically evaluated data. Care, however, must be exercised when using this package as the accuracy is limited due to the simplistic basis function used in the moment method solution and the analogy with dipoles used to evaluate the mutual coupling.

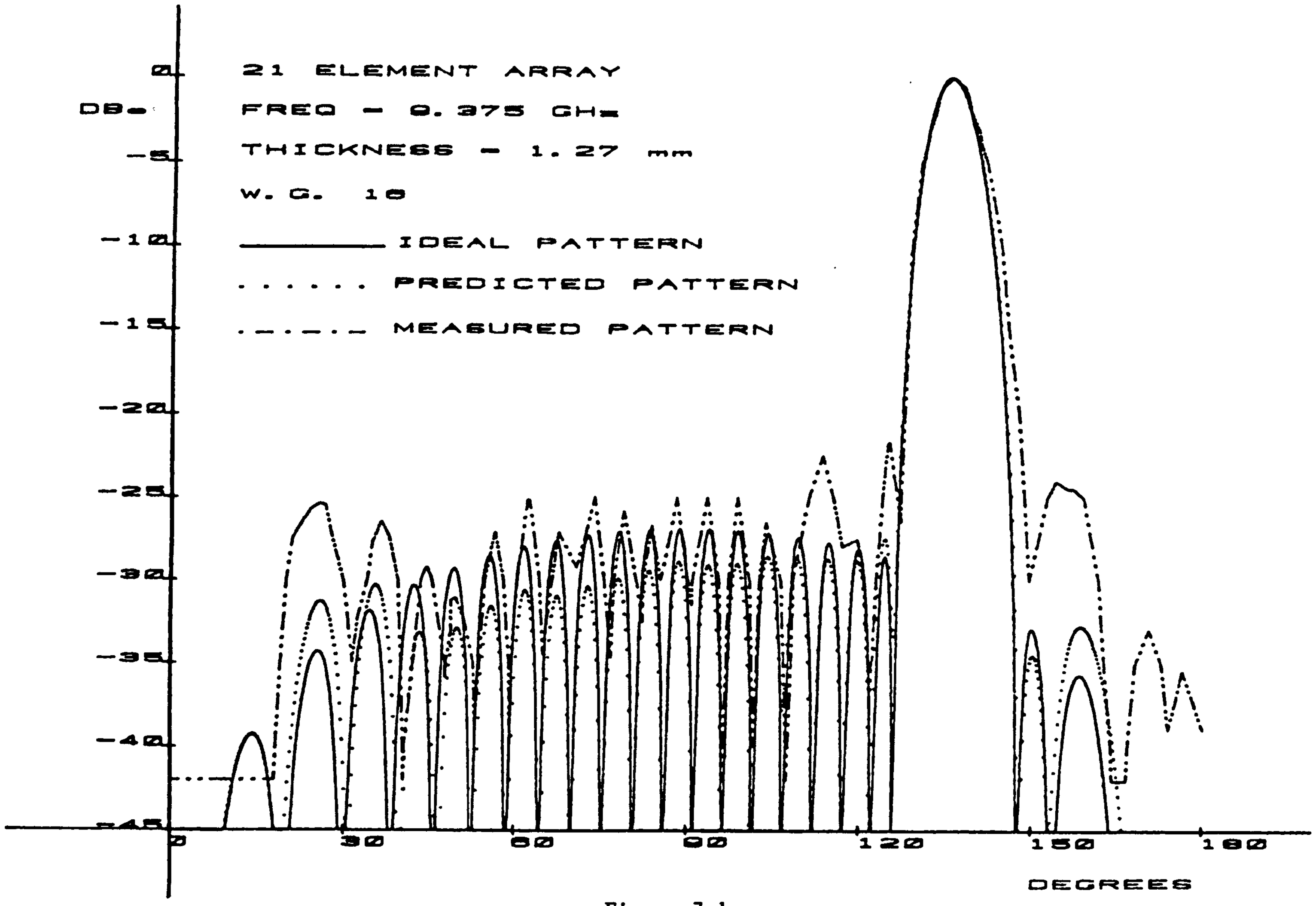

Figure 7.1

Theoretical, Predicted and Measured Far Field Patterns for Elliott's 21 Slot Array

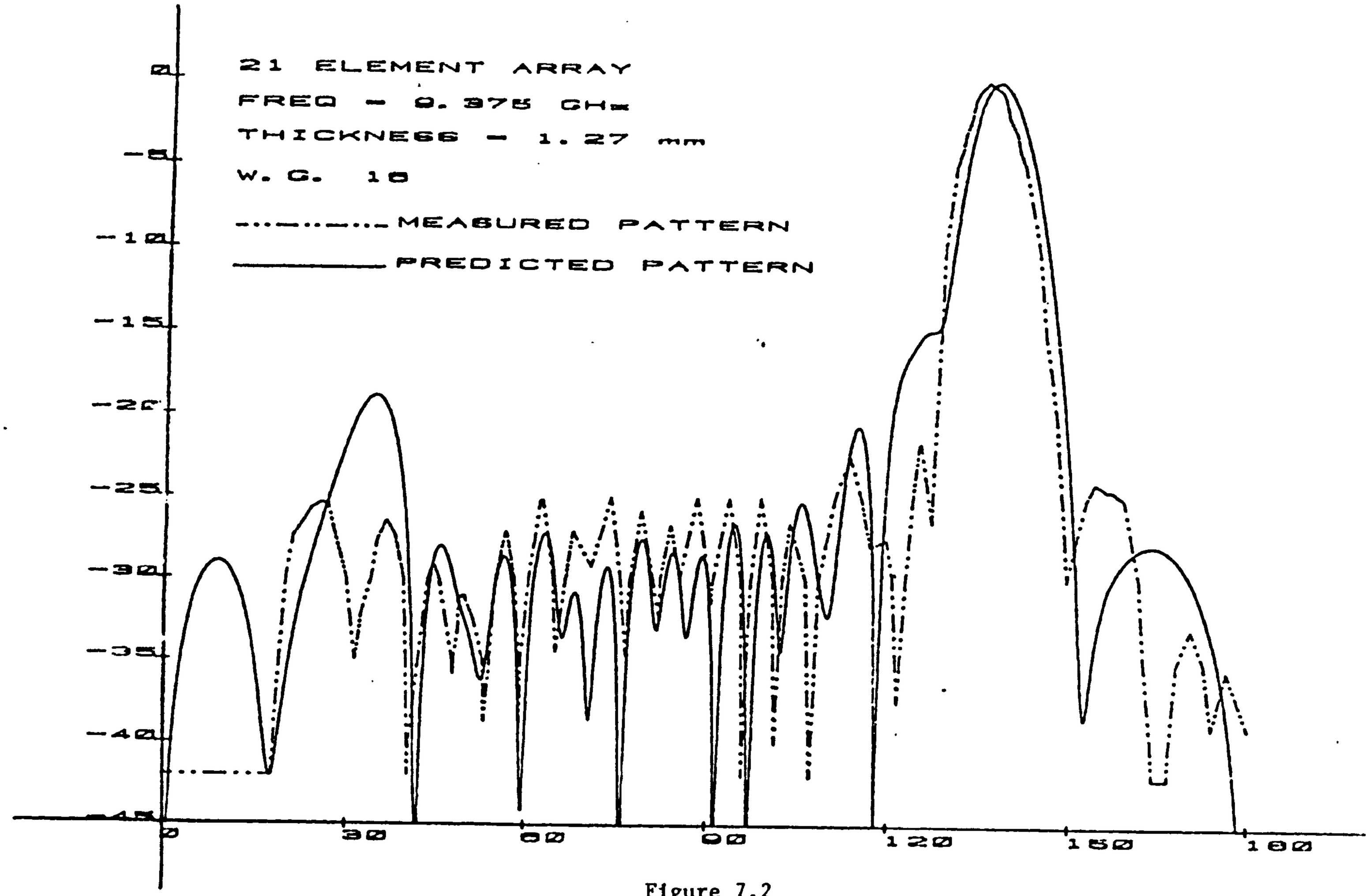

Figure 7.2

Theoretical and Predicted Far Field Patterns for Elliott's 21 Element Array

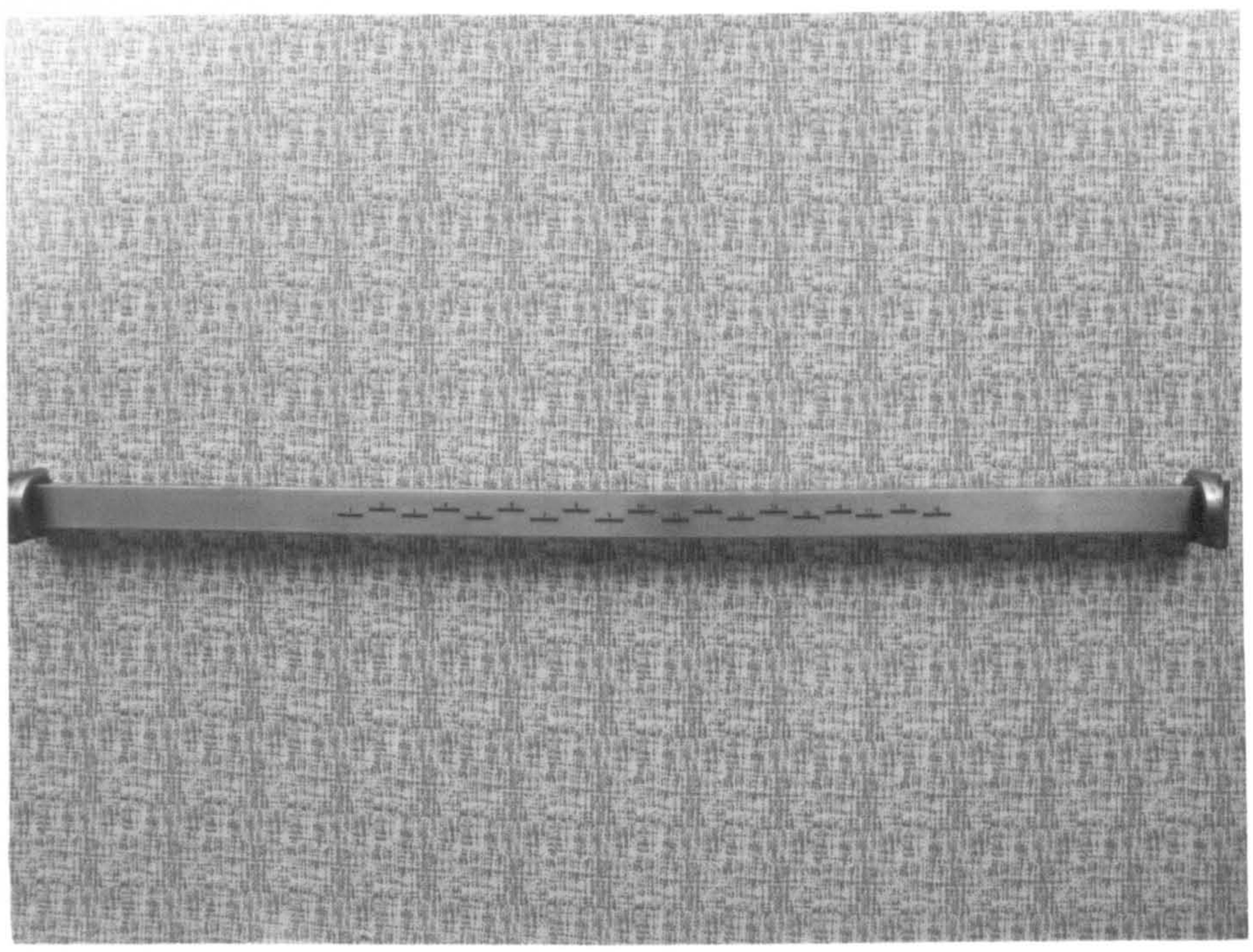

Figure (7.3)

Photograph of 19 Element Array

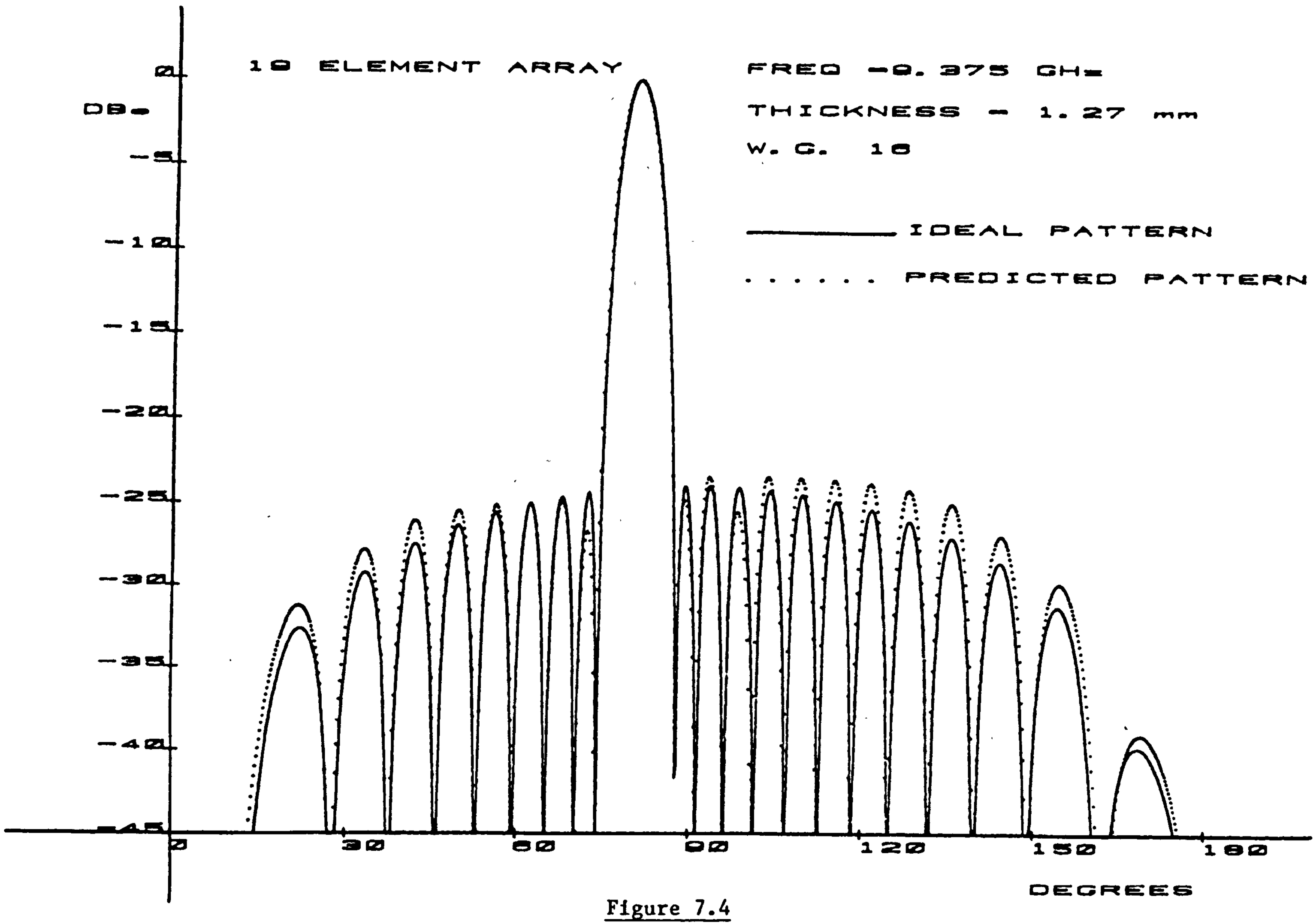

Figure 7.4

Comparison Between Predicted and Ideal Far Field Patterns for 19 Element Array

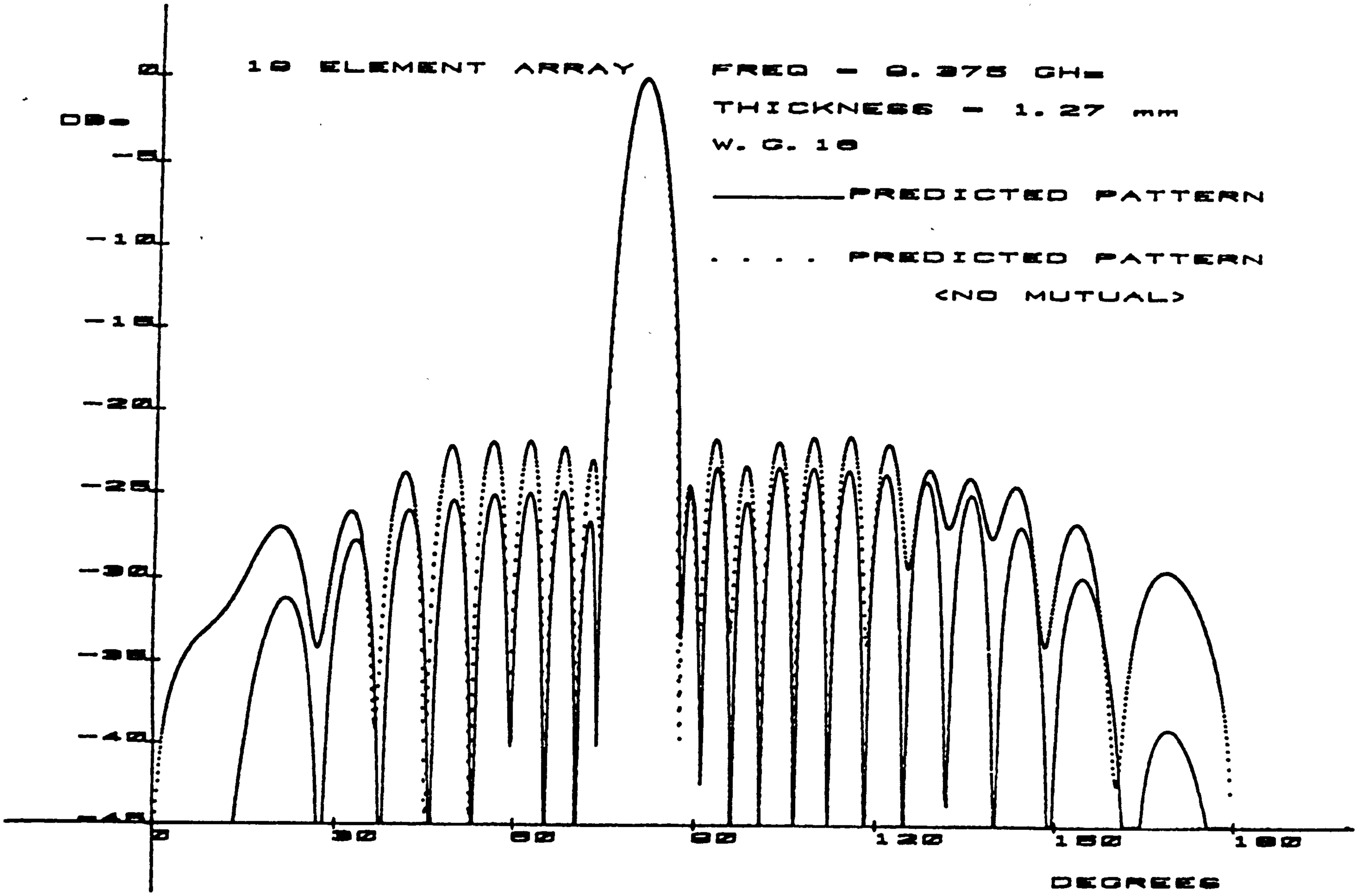

Figure 7.5

Comparison between two Predicted Patterns for 19 Element Array

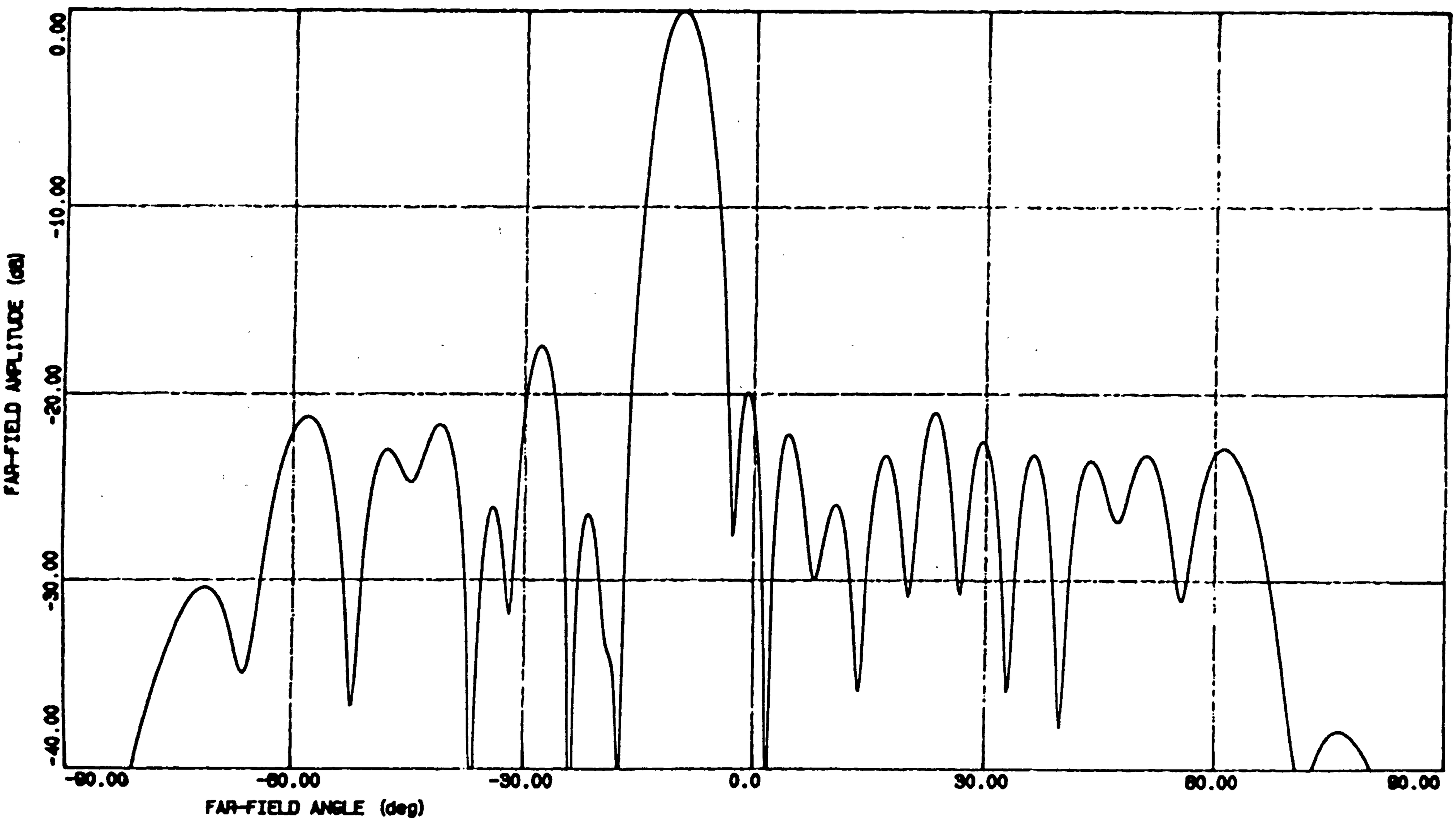

Figure 7.6

Predicted Far Field Pattern Using a Near Field measurement System Courtesy of Ferranti PLc, Edinburgh

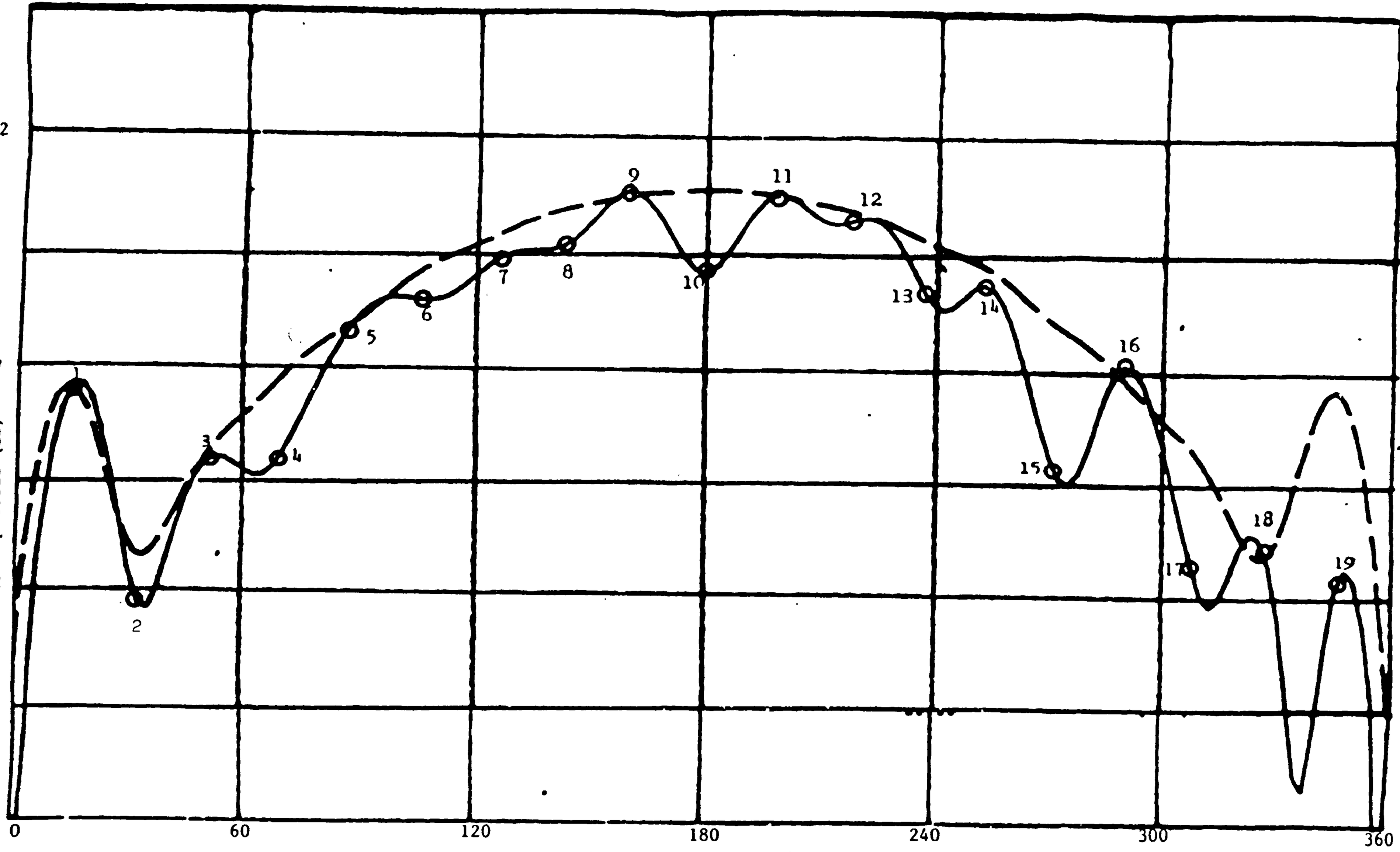

Figure 7.7

Magnitude Comparison of Measured and Theoretical Near Field Patterns

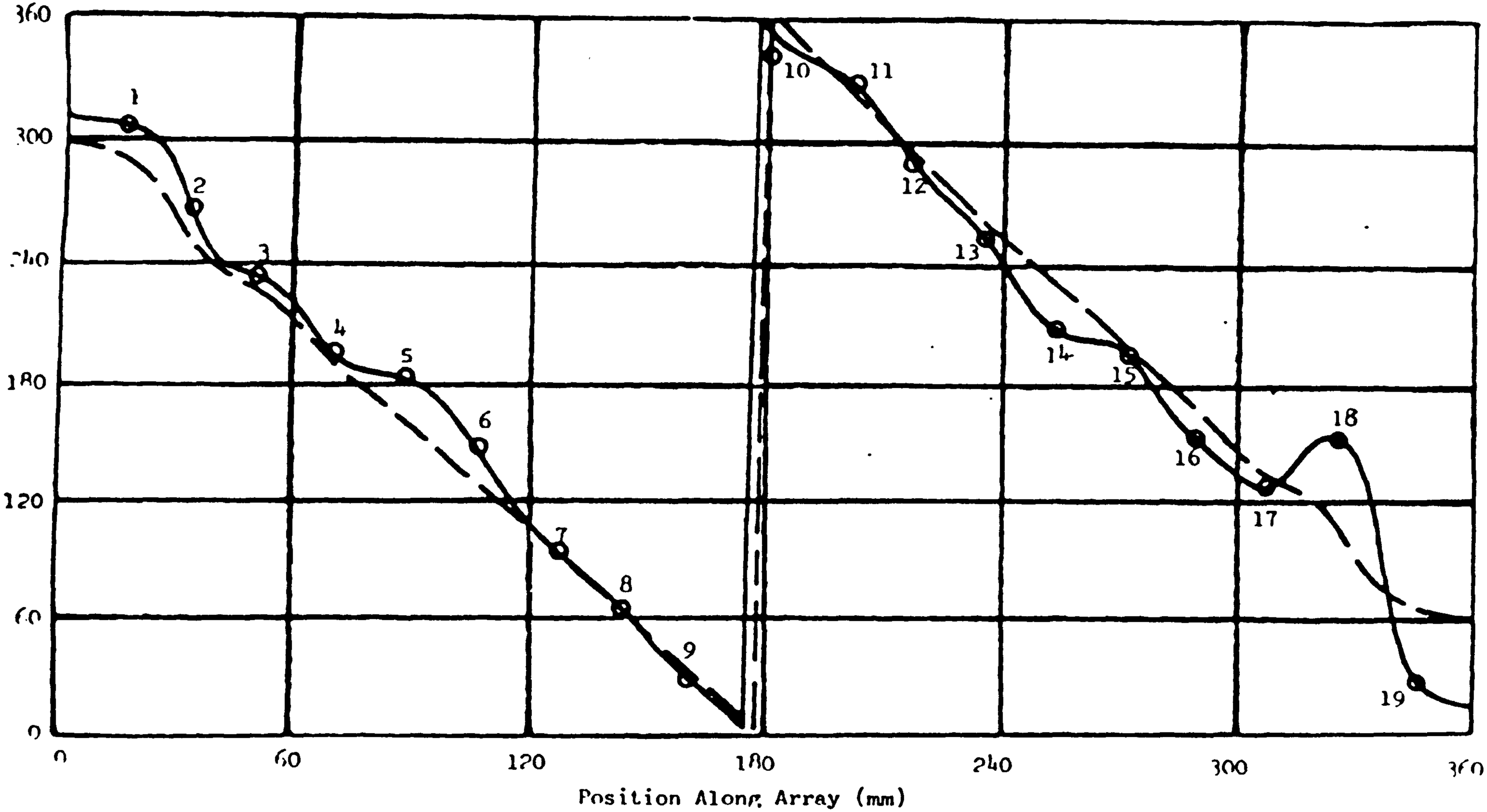

Figure 7.8

Phase Comparison of Measured and Theoretical Near Field Patterns

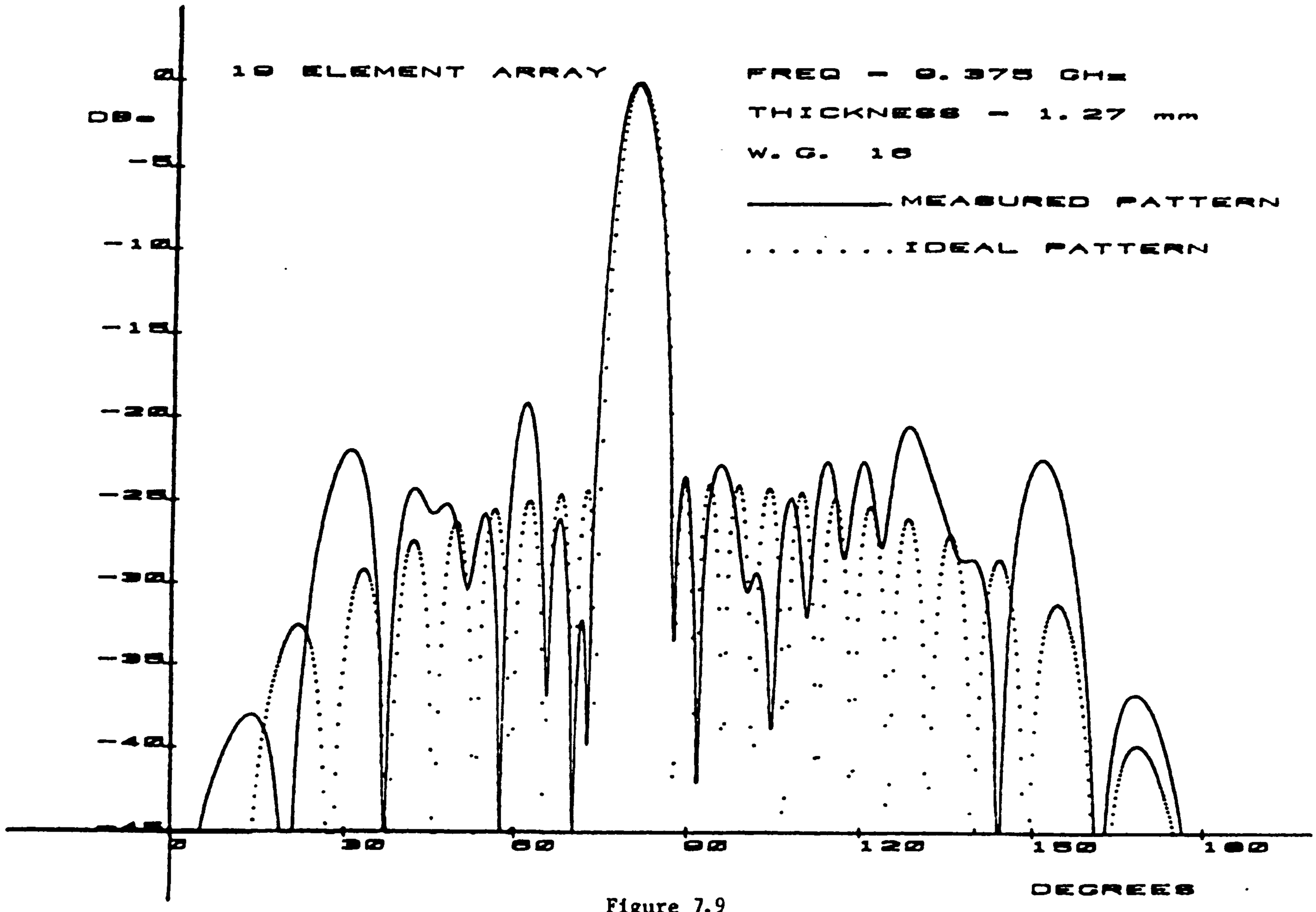

Figure 7.9

Comparison Between Ideal and Measured Far Field Patterns for the 19 Element Array

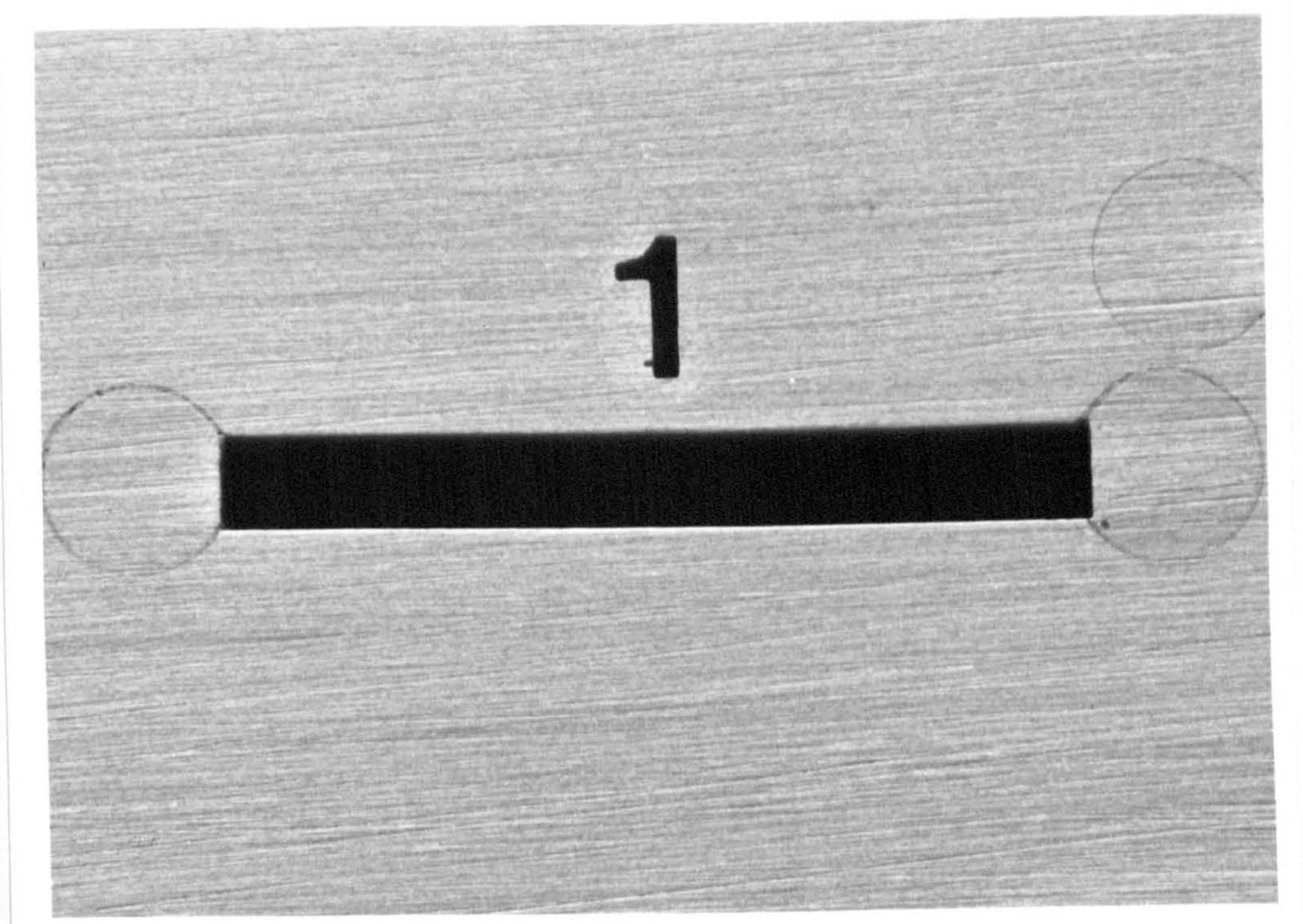

Figure (7.10)

Photographs of Individual Slots in the Array

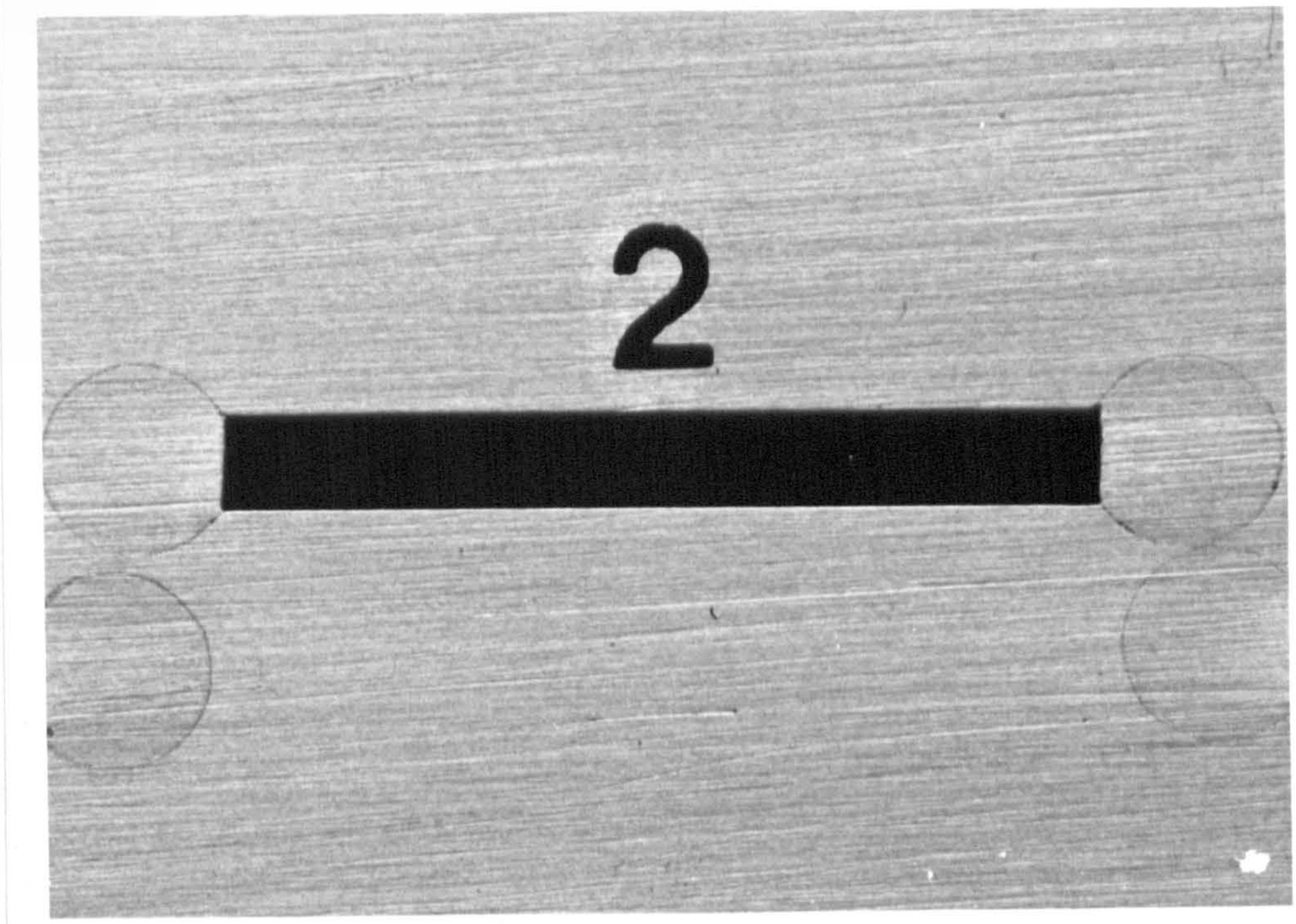
2

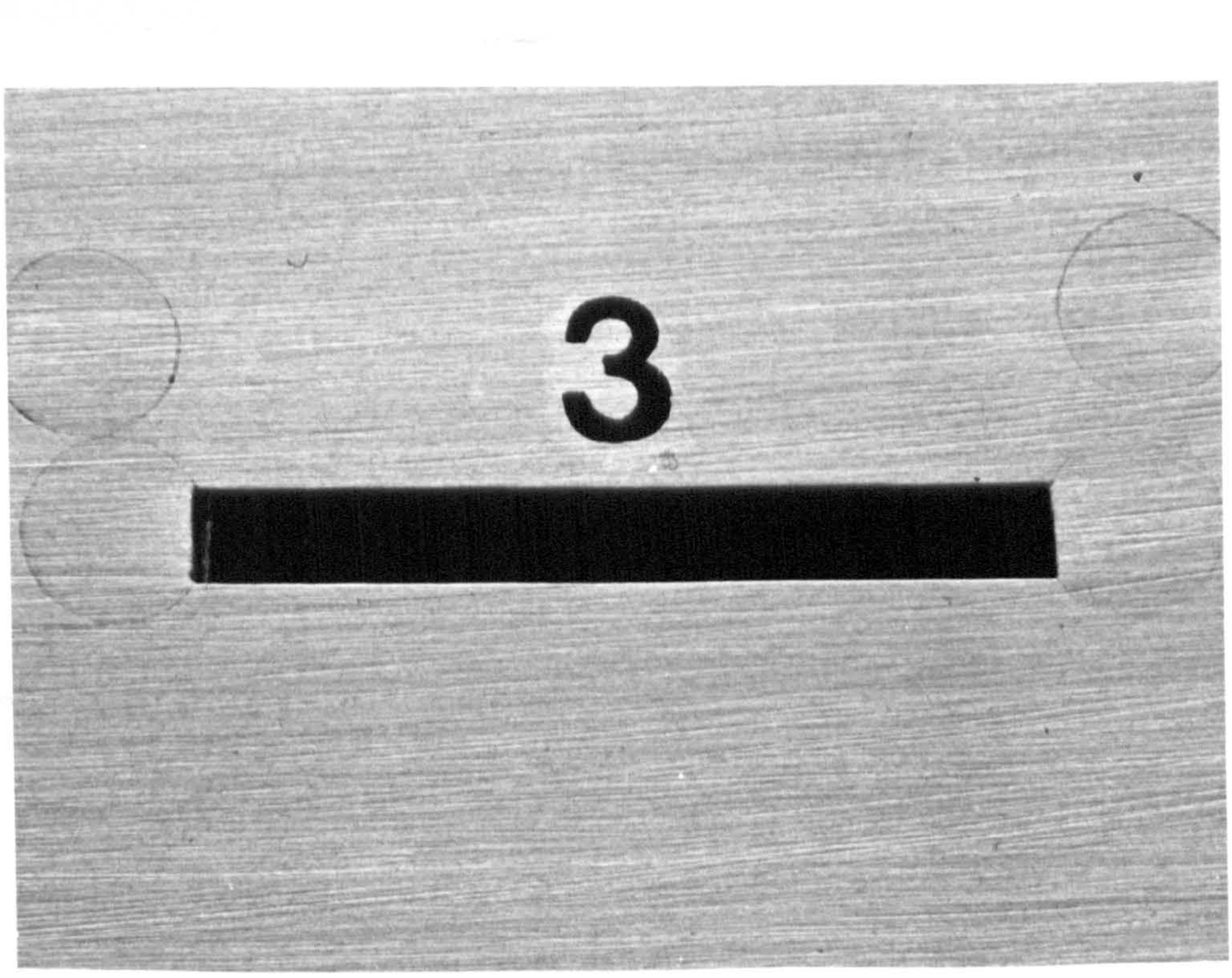
3

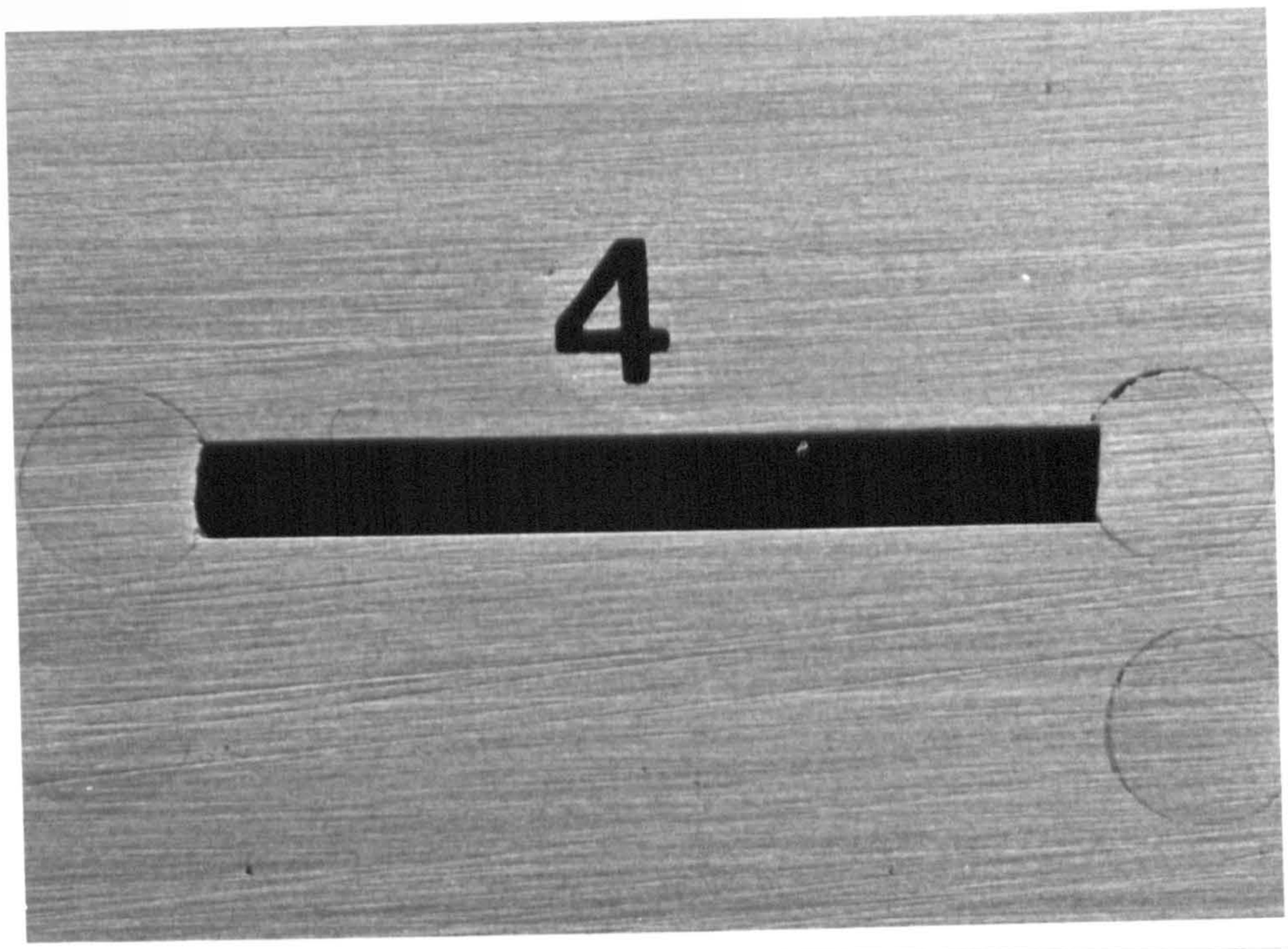
4


5

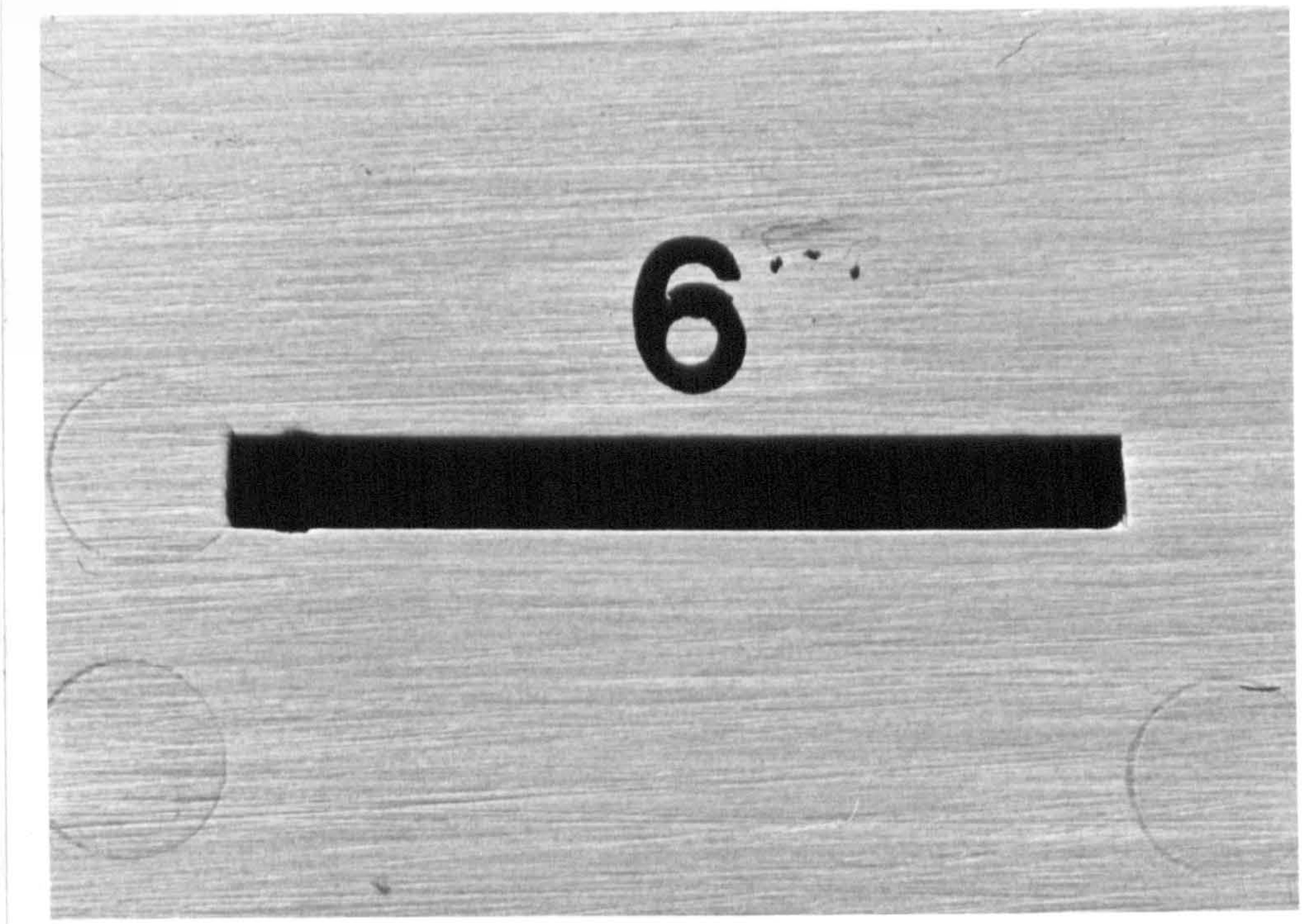
6

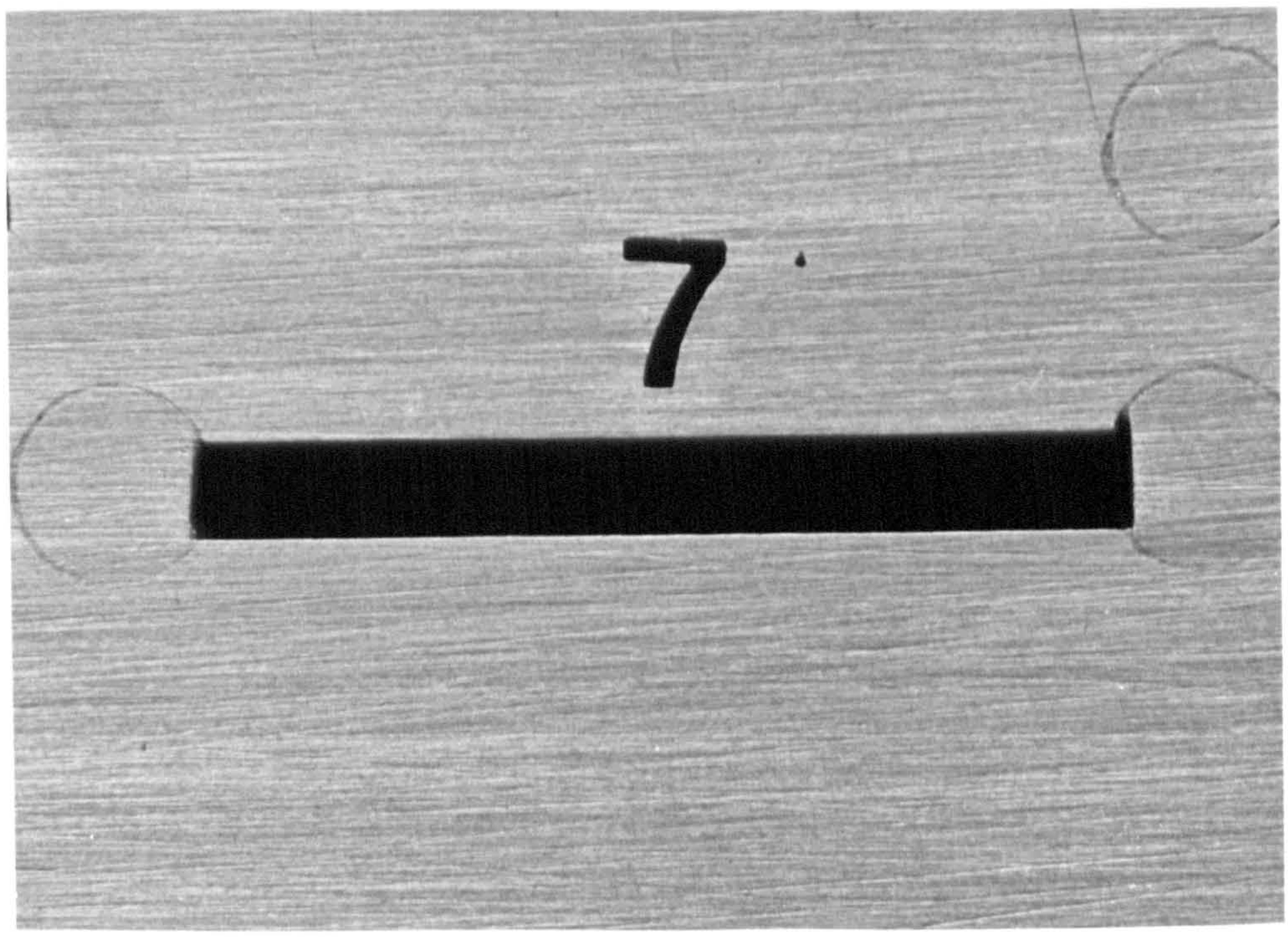
7

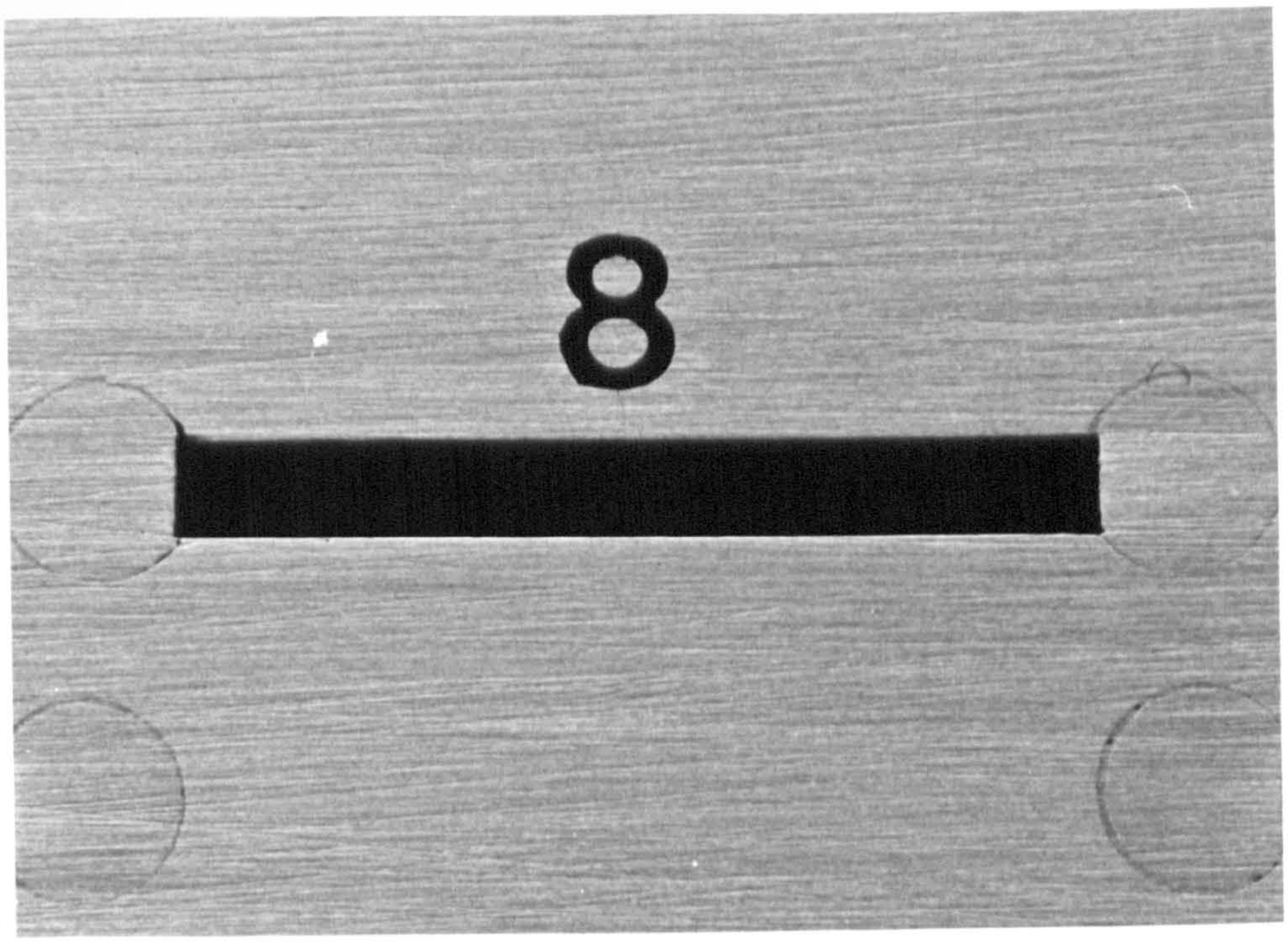
8

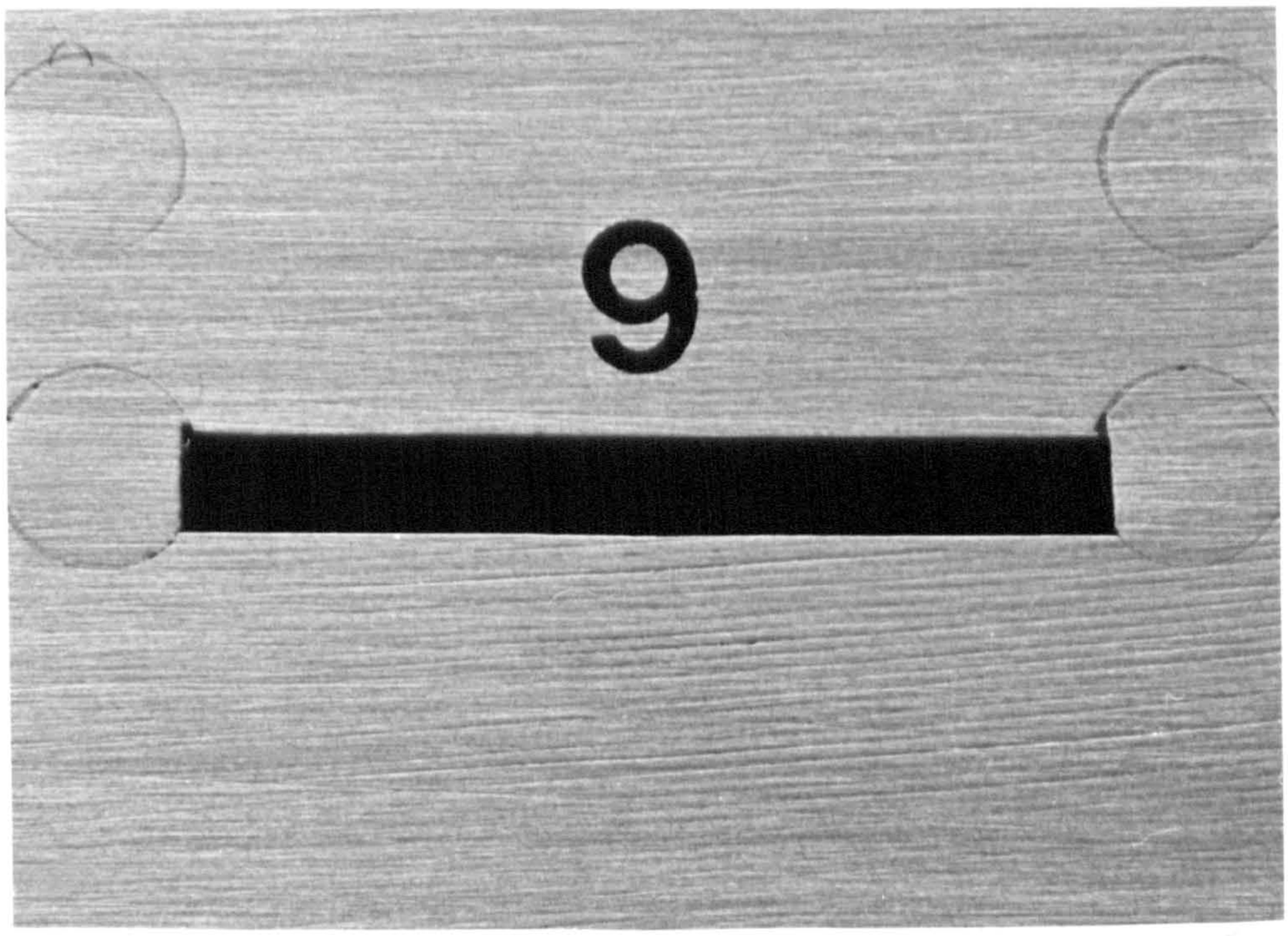
9

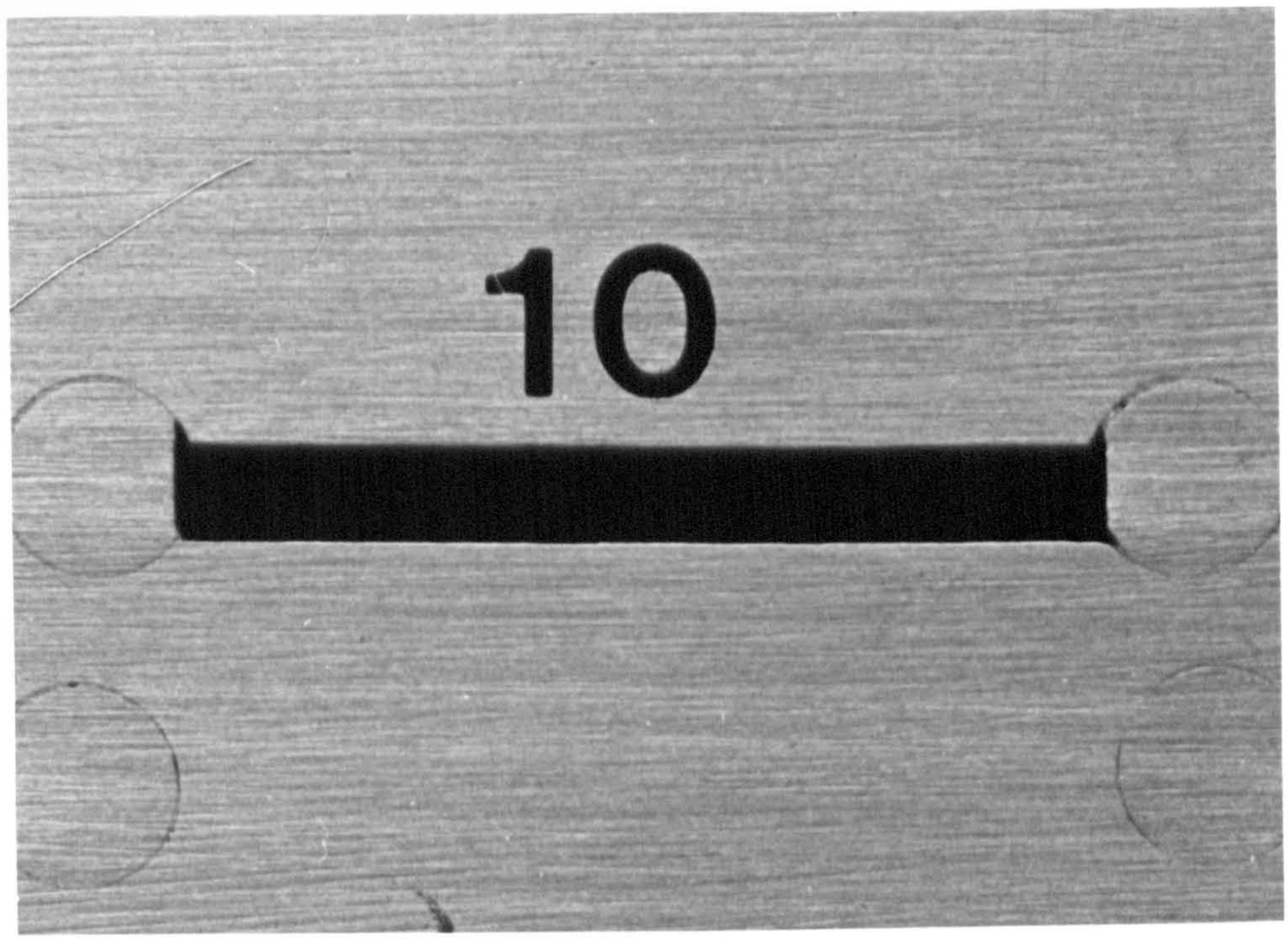
10

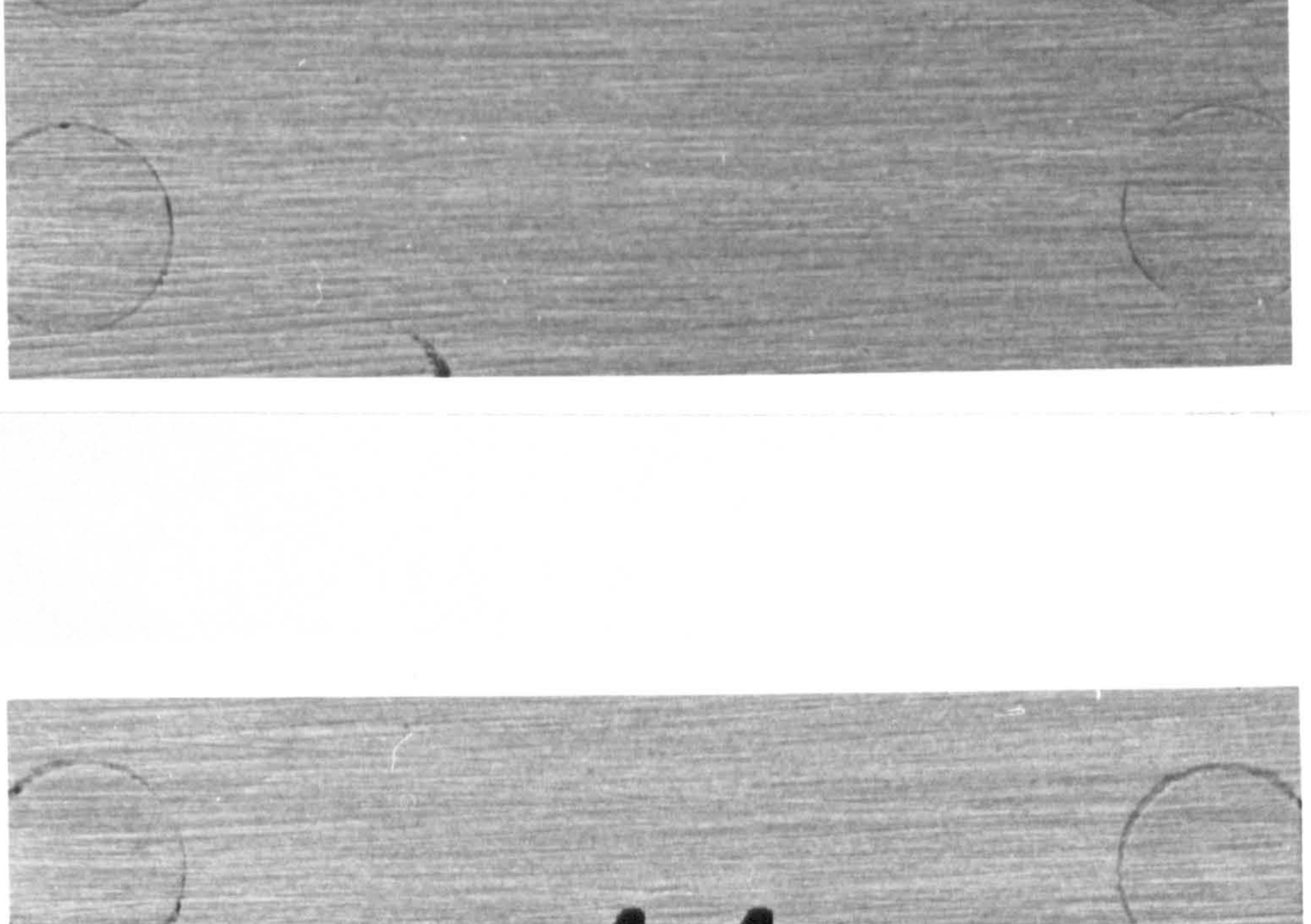
11

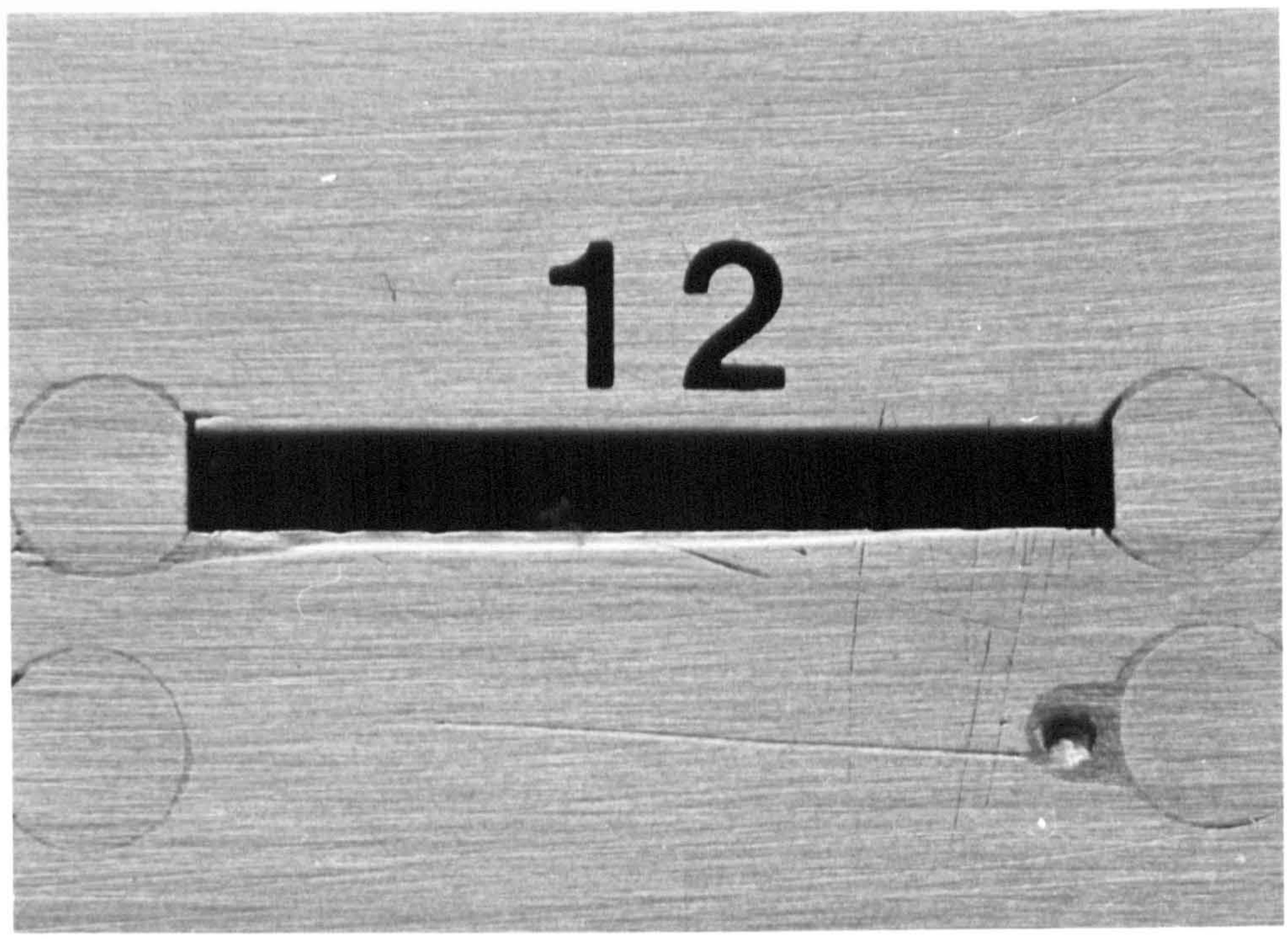
12


13

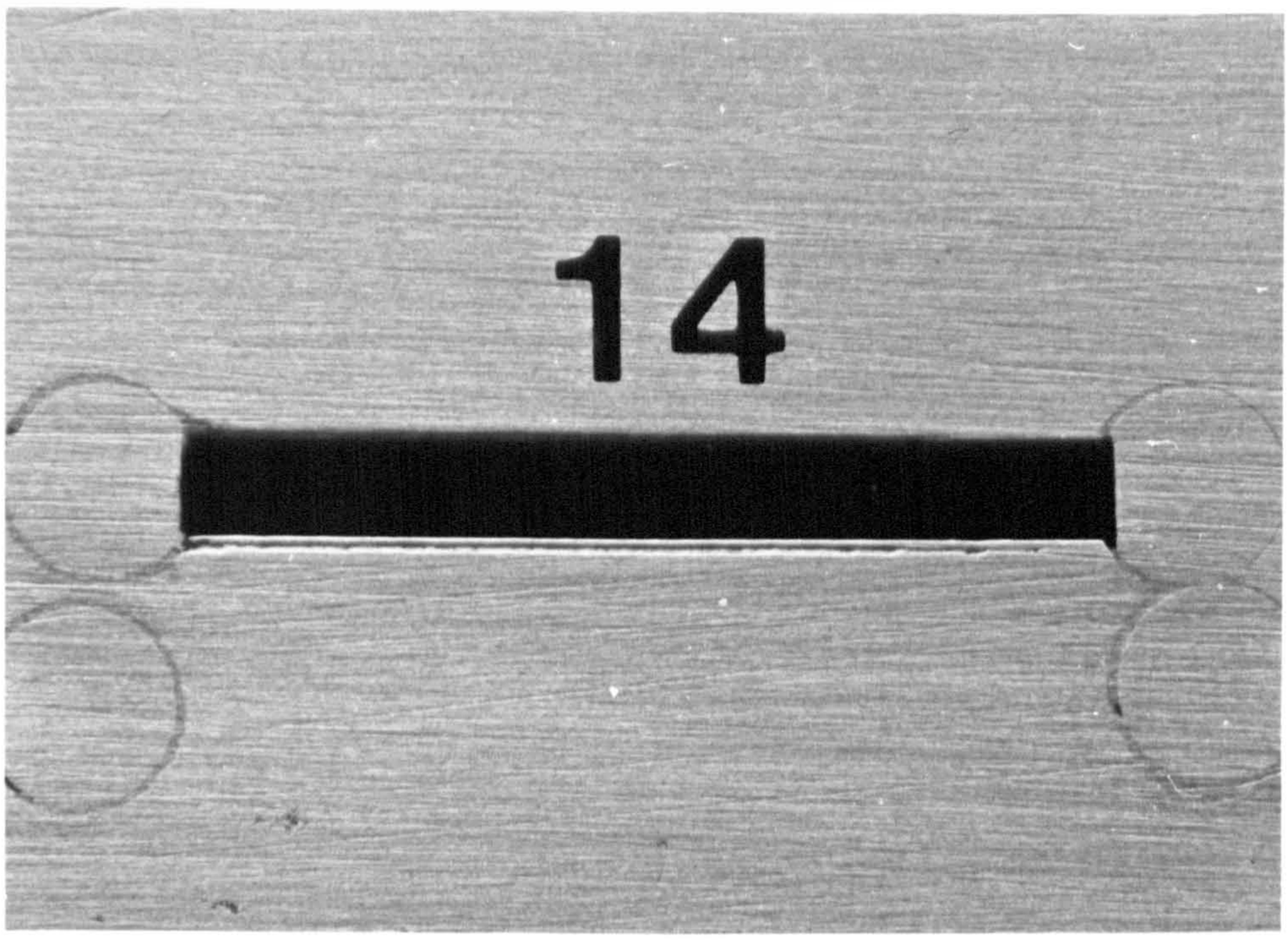
14


15

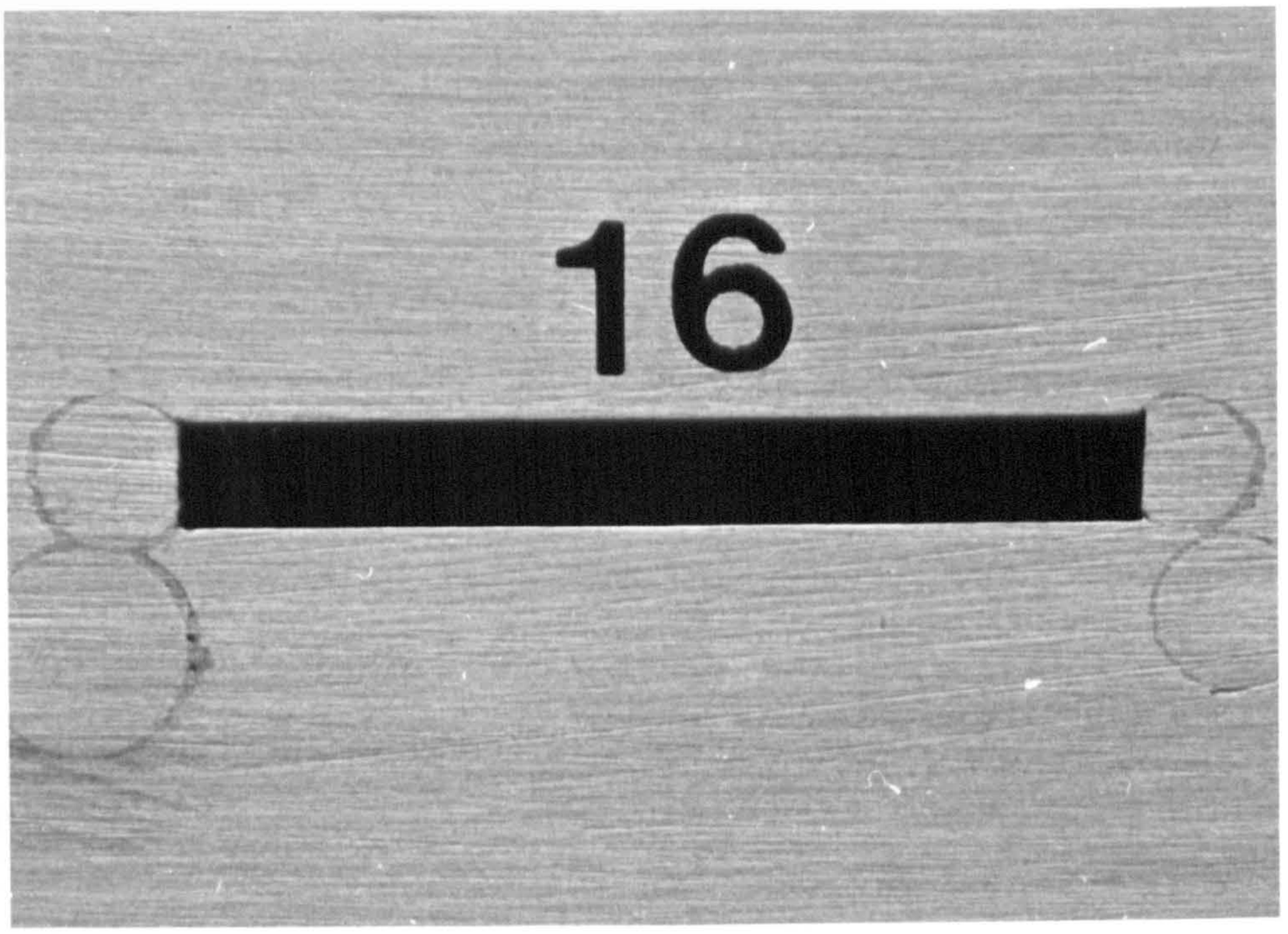
16

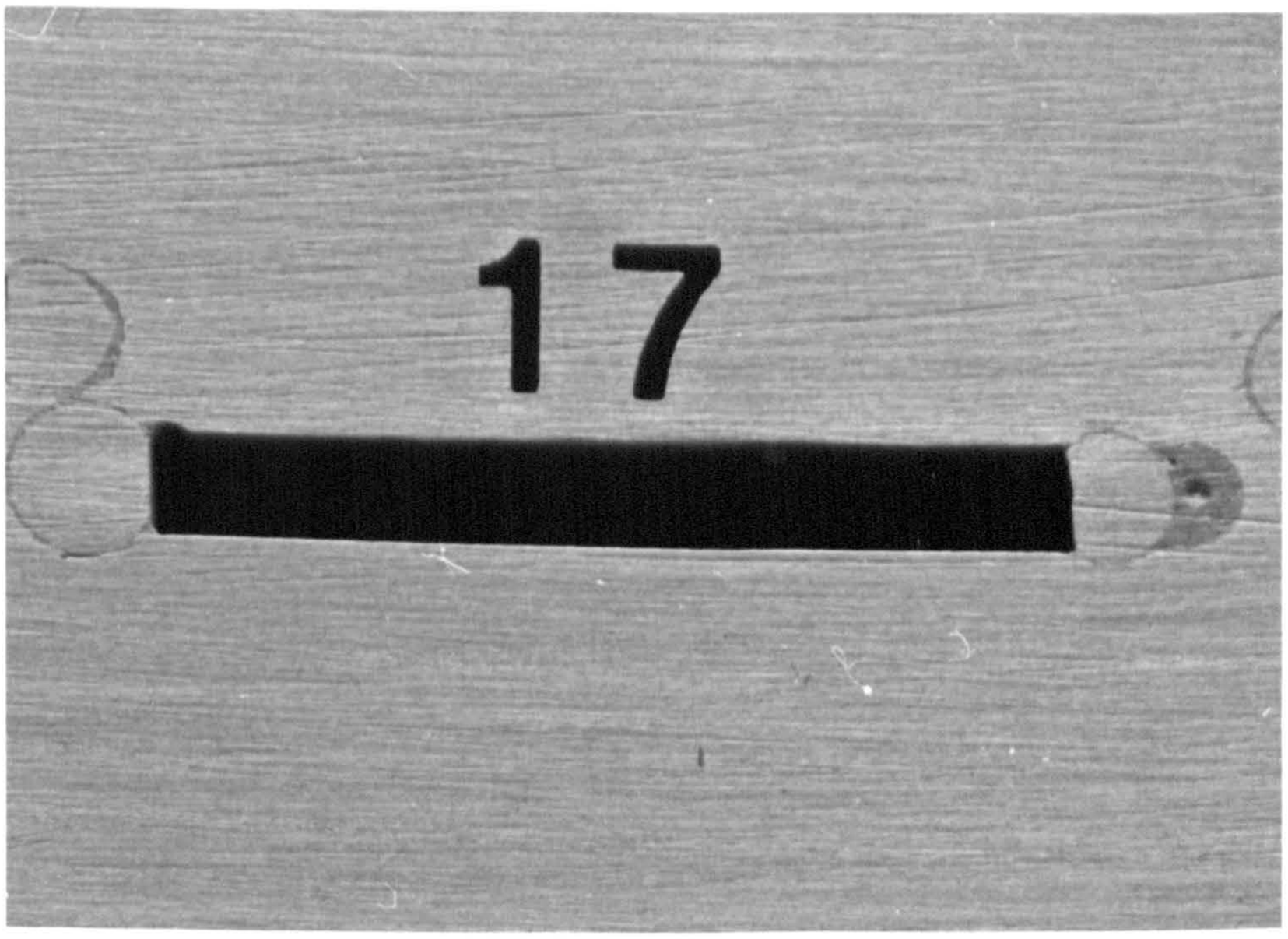
17

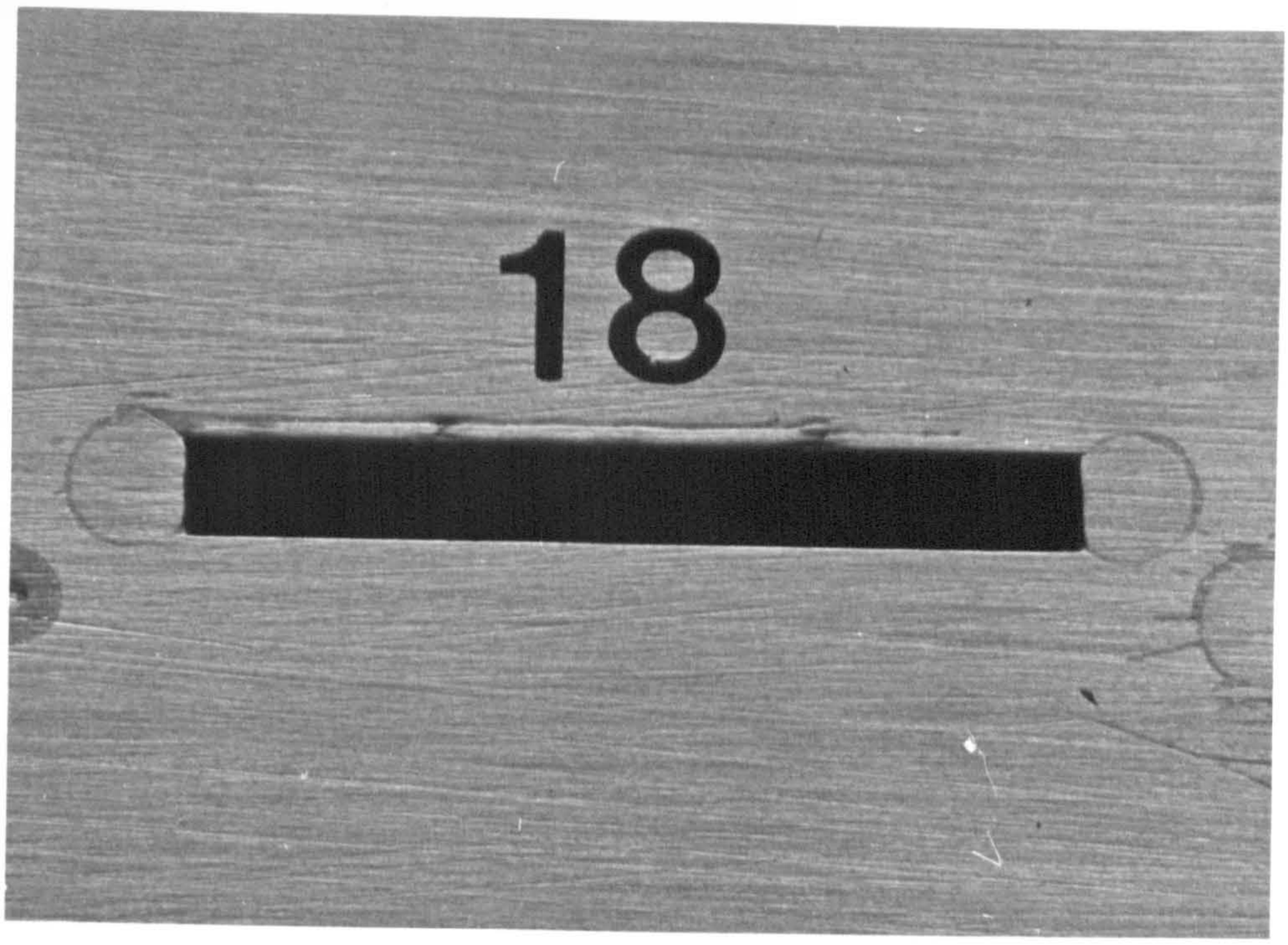
18

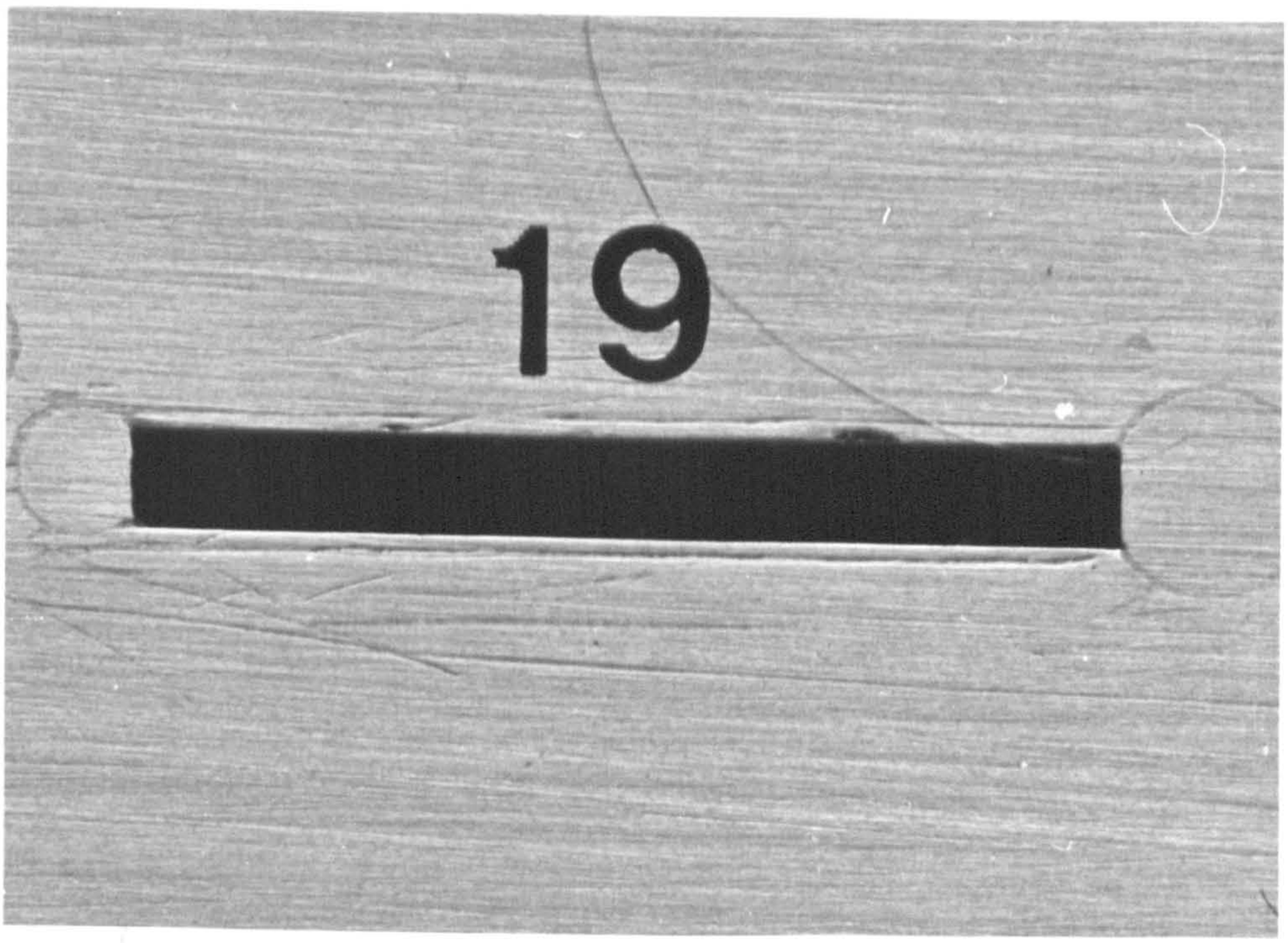
19

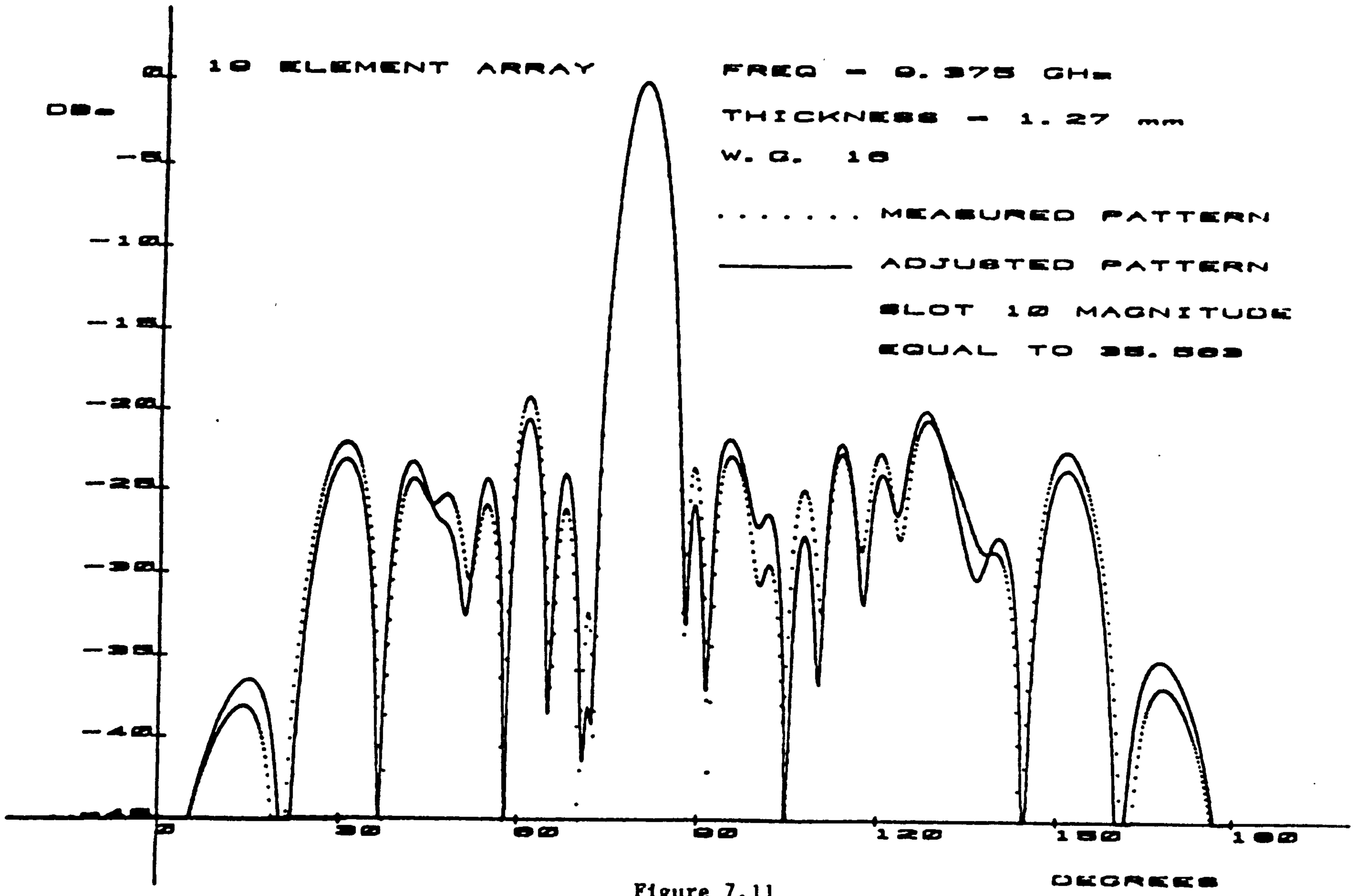

Figure 7.11

Comparison of Adjusted and Measured Far Field Patterns - Slot 10

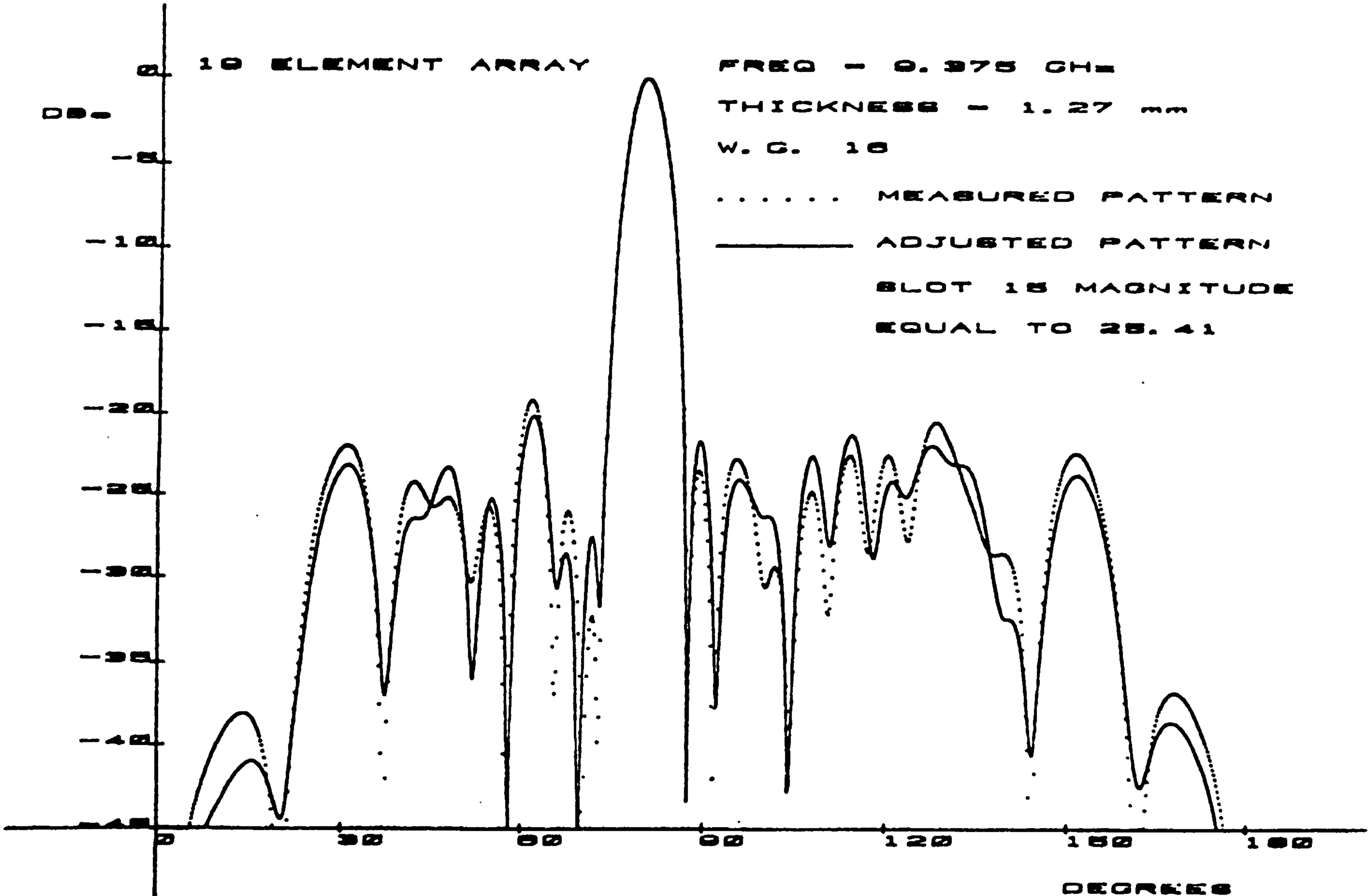

Figure 7.12

Comparison of Adjusted and Measured Far Field Patterns - Slot 15

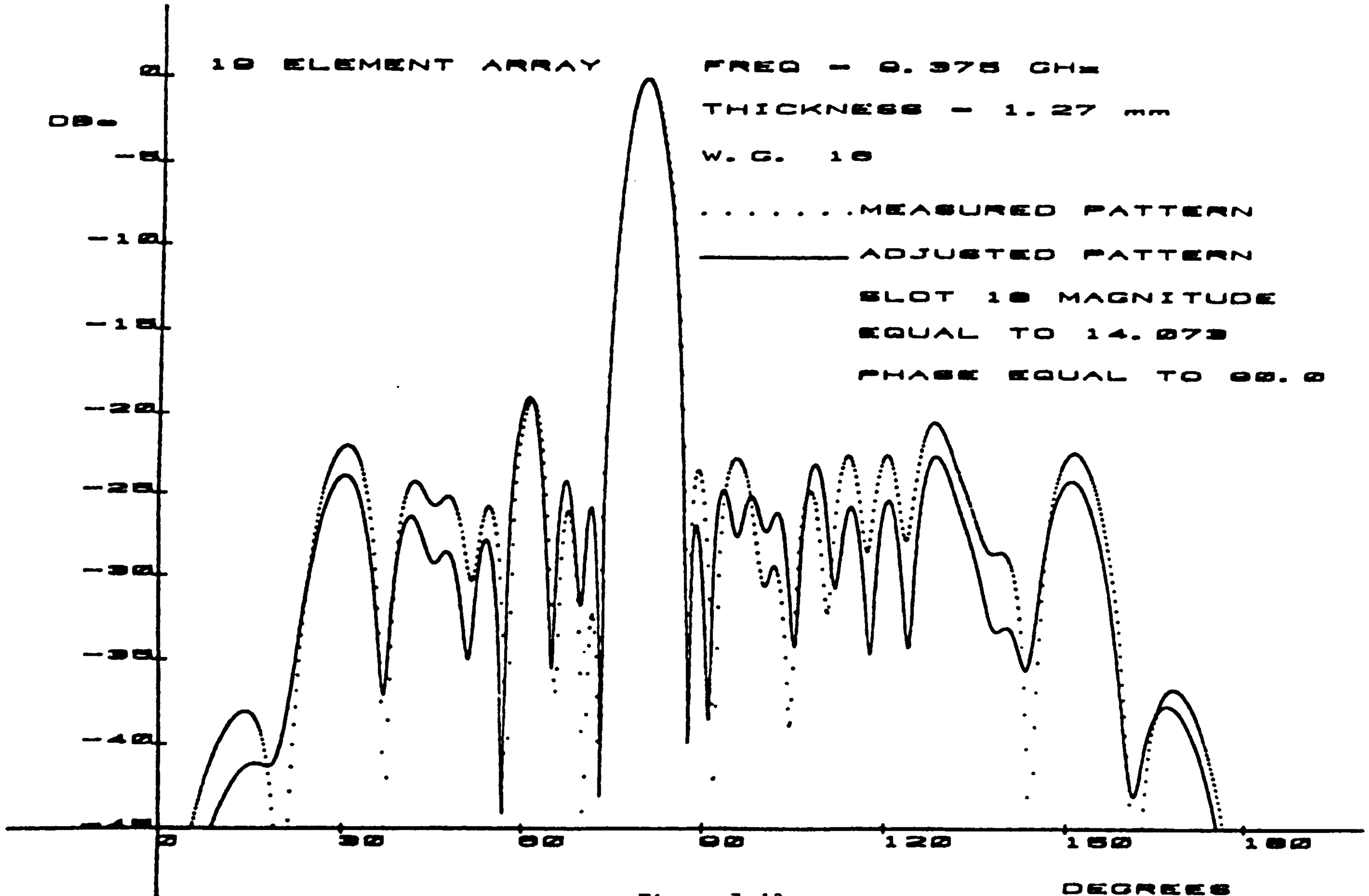

Figure 7.13

Comparison of Adjusted and Measured Far Field Patterns - Slot 18

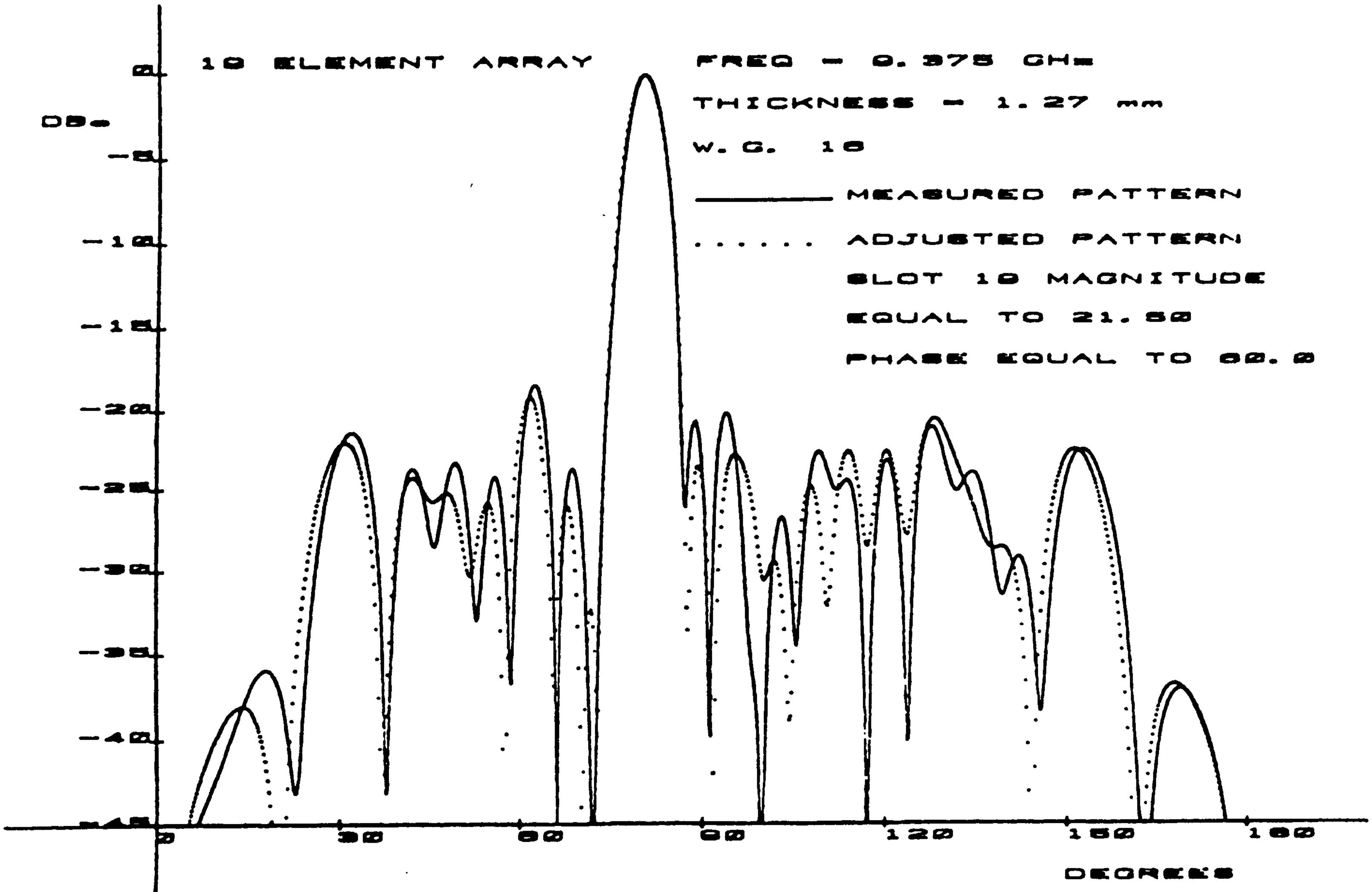

Figure 7.14

Comparison of Adjusted and Measured Far Field Patterns - Slot 19

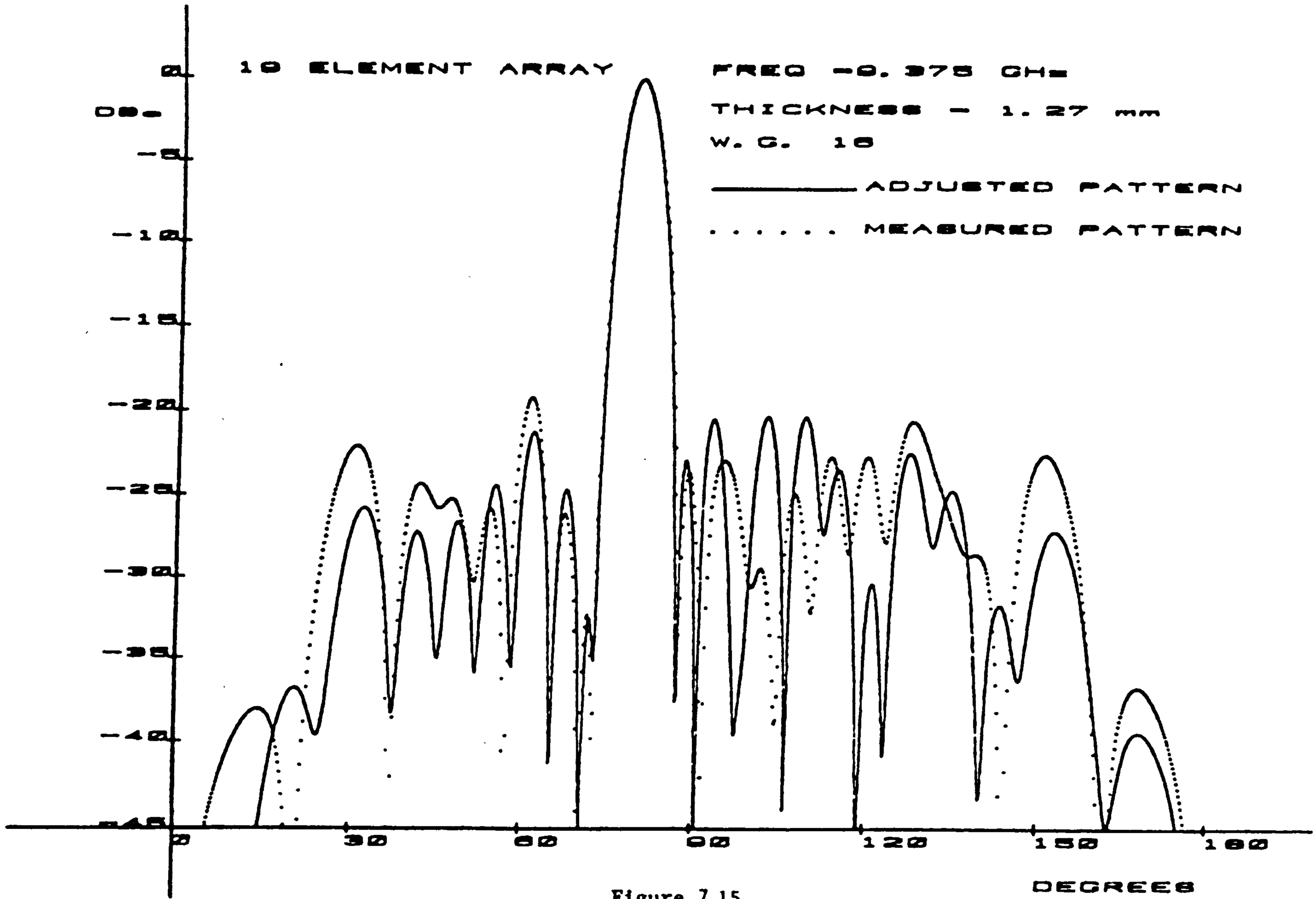

Figure 7.15

Comparison of Adjusted and Measured Far Field Patterns - Slots 10, 15, 18, 19

CHAPTER 8

APPLICATIONS OF CAD SYNTHESIS PROGRAM

A computer aided design procedure to synthesise slotted waveguide array antennas has been developed and assessed in the preceding chapters. This was initially limited to the design of linear travelling wave arrays with the far field pattern being characterised by the Dolph-Chebyshev solution. These restrictions were imposed to demonstrate the principle of slotted waveguide array synthesis using the moment method solution.

The synthesis program, however, can readily be adapted to examine alternative configurations and this chapter indicates how resonant, planar and some unconventional arrays can be designed.

8.1 RADIATION PATTERN SYNTHESIS

The far field pattern may be shaped by suitably tailoring the excitation distribution across the array and the choice of distribution is usually governed by the antenna requirements. For example, ground radar antennas often have a cosecant-shaped elevation pattern to compensate range with elevation and satellite antenna patterns are shaped to fit a geographical area. There are numerous algorithms available to shape the radiation pattern in the literature. Unfortunately, they cannot all be realised by slotted waveguide array antennas due to the interdependence between the slot excitations and the physical array configuration. In practice, the choice is normally restricted to a few standard patterns, four of which have been mentioned below.

Dolph recognised that the Chebyshev polynomial was ideally suited to generate a pattern with side lobes equal in magnitude and consequently, he developed a set of relationships detailed in [2.39] to determine the positions of the roots of the array factor. This solution has been refined over the years and various improved algorithms have evolved [2.40, 2.41, 2.43, 2.44, 2.45, 2.46, 2.47, 2.48, 6.1]. An interesting graph is presented in [2.48], which has been reproduced in Figure (8.1), comparing computer processing times for a number of these and improvements in efficiency in excess of one hundred fold are indicated.

The Taylor solution [2.49], which is widely used in radar antennas, generates a far field pattern where the level of the side lobes close to the main beam is controlled and the far out lobes decay in magnitude as a function of angular displacement from the main beam. An example of this pattern is presented in [8.1] where Elliott and Johnson have detailed the design of a 19 element shunt slot array with the side lobe level being set equal to 20 dB and with the additional feature that the three inner most side lobes are depressed to 30 dB on one side of the main beam.

Woodward [2:50] diversified and developed a solution which shapes the pattern by filling in the nulls. This technique superimposed a family of patterns so that the main beam of each successive partial pattern occurs at the first null of the preceding pattern, with the heights of the main beams being adjusted to fit a desired contour. This technique produces pattern shaping in the 'filled in' region and is often used in land surveillance systems. Consequently, considerable attention has been paid to enhancing this pattern and

more specifically to minimise the ripple etc. in the shaped region [2.51, 2.52, 2.53, 2.54, 2.55, 2.56, 2.57].

The final technique to be mentioned has only recently been implemented as access to a high speed main frame computer is a pre-requisite. This is a direct method which simply adjusts the array configuration until the radiated pattern is within the required specification. Recently this technique has been shown [8.2], when applied to the design of array fed reflectors, to be reasonably efficient in terms of computational effort and it is suggested as a viable alternative to the more traditional techniques mentioned above.

8.2 RESONANT ARRAY

The resonant (standing wave) array is commonly used as an alternative to the travelling wave array and this can readily be synthesised by slightly modifying the CAD program. This array differs from the travelling wave array in that it is designed with the main beam at broadside and all the slots are fed in phase with a slot separation of $\lambda_g/2$. The waveguide is also terminated in a perfect short circuit $\lambda_g/4$ away from the centre of the last slot instead of the matched load. A pictorial representation of the equivalent circuit for this array is presented in Figure (8.2). One disadvantage of this type of array is that it operates over a narrower frequency band than the travelling wave array and the performance deteriorates rapidly as the incident and reflected waves move out of phase. This is primarily due to the distance from the end slot to the short circuit varying from $\lambda_g/4$.

In order to design this type of array an alternative set of equations is required to evaluate the active admittances of the individual slots. These take the following form:

$$Y_T^A = \sum_{n=1}^{N} Y_n^A \qquad (8.1)$$

$$Y_n^A = \sum_{n=1}^{N} K\, C_n^{\,2} \qquad (8.2)$$

$$K \sum_{n=1}^{N} C_n^{\,2} = 1 \qquad (8.3)$$

where Y_T^A is the total active admittance

Y_n^A is the active admittance of the n^{th} slot

C_n is the excitation coefficient of the n^{th} slot

K is a constant.

The region in which these equations should be incorporated into the synthesis program has been highlighted on the flow chart in chapter 6 and they may readily be implemented in place of equations (6.3) to (6.5). This a slightly more efficient solution in terms of computational effort than the travelling wave array as the active admittances are evaluated for a specified input match. Whereas, in the case of the travelling wave array the solution is iterated with the amount of power dissipated in the load being adjusted until an acceptable solution is obtained.

8.3 PLANAR ARRAY

The synthesis program can also be extended to design planar arrays and the additional programming required to implement this is remarkably little. However, it must be stressed that the inclusion of the external mutual coupling is far more significant in the design of planar arrays. As the model currently used to quantify the mutual coupling is known to be inaccurate, some additional caution needs to be exercised in the implementation of the planar array design. Nevertheless, it is worth outlining how this may be done.

The planar array is initially split into two linear arrays, an X directed array and a Z directed array (see Figure (8.3)). The array factors for both arrays are then evaluated and the coefficients of the X directed factor are used to weight the input signals to the Z directed linear arrays. Note, there are many different methods of feeding planar arrays and this area remains to be investigated before the CAD package can provide a complete design of a practical planar array. However, it has been assumed, for the purpose of demonstrating the program, that the Z directed arrays can be fed independently. This assumption enables a design to be obtained and the active admittances of the slots may then be evaluated using the coefficients of the Z directed array factor. The active admittance values of the corresponding slots in the linear arrays are identical and therefore, these values along with the approximate slot positions need only be evaluated for one array.

Once the approximate array configuration is defined then the mutual coupling can be evaluated. This must be calculated for each slot due to the slightly different environment each element sees. The

exception to this is the resonant array, when it is possible to reduce the number of calculations by a factor of two, as the array is symmetrical about the X axis. The self admittances can be evaluated next with the root-finding routines determining the array configuration. Care is required to ensure the trial values for the Gauss-Newton root-finding routine are set up correctly. Particularly in the case of the travelling wave antenna, when the planar array has to be considered as a stack of linear arrays. The trial values for the first slot of each linear array must be either determined using the variational method or from the moment method values obtained from the previous pass. The gradient of $|\rho|$ calculated from the last two slots of the previous array cannot be employed as the offsets of the slots at either end of the array differ considerably and the gradient changes in a non-linear fashion with offset. Consequently, if it was used to estimate the trial value, it would predict an inaccurate value which would impair the efficiency of the root-finding routine and increase the computational effort required to determine the solution.

A 15 element planar array comprising of three linear travelling wave arrays has been designed using the synthesis program with the above modifications incorporated. This was designed to operate at 9.375 GHz in W.G. 16 with a slot width of 1.6 mm. The Dolph-Chebyshev algorithm was once again adopted to characterise the far field pattern and the main beam was positioned at 5 degrees from broadside in the H plane and at broadside in the E plane with the side lobe levels at -22 dB and -10 dB in the respective planes.

The magnitudes of the predicted slot voltages for this design are tabulated below:

Waveguide	Slot	Magnitude of Slot Voltage
1	1	1.00000
	2	1.78188
	3	2.17876
	4	1.78188
	5	1.00000
2	1	1.03899
	2	1.85135
	3	2.26371
	4	1.85135
	5	1.03899
3	1	1.00000
	2	1.78188
	3	2.17876
	4	1.78188
	5	1.00000

Table (8.1)

Table of Magnitudes of Slot Excitations

and the computed array configuration is as follows:

Waveguide	Slot	Length (mm)	Offset (mm)	Separation (mm)
	1	14.93	1.96	19.92
	2	15.49	-3.79	19.59
1	3	15.08	3.52	19.92
	4	15.25	-2.38	19.92
	5	14.95	1.25	
	1	15.23	1.76	19.97
	2	15.37	-2.75	19.99
2	3	15.44	2.96	20.01
	4	15.39	-1.98	19.99
	5	15.40	0.98	
	1	15.28	2.17	19.63
	2	15.03	-3.27	19.91
3	3	15.49	3.75	19.76
	4	14.93	-2.47	19.95
	5	15.11	1.18	

Table (8.2)

Array Configuration for 15 Element Planar Array

It is interesting to note that even although the active admittances of the corresponding slots in the three waveguides are identical the predicted slot lengths and offsets are all different. This is due to the mutual coupling influencing each slot differently with the slots in the centre waveguide experiencing the most severe coupling effect. Also, the computational effort required to process the design of this

array is considerably more than that required to synthesise an equivalent 15 element linear array. The synthesis program had to be iterated 5 times in order to obtain a solution for the planar array, whereas, it only took 3 iterations to design the linear array. The difference in processing requirements can be attributed to the higher level of mutual coupling which a planar array suffers.

8.4 ALTERNATIVE ARRAY CONFIGURATIONS

The synthesis program has so far been employed to design commonly used array configurations. However, it is by no means limited to these and in order to demonstrate the flexibility of the program some rather unusual array configurations have been examined.

The first arrangement to be considered comprises of a linear array with all the slots offset on one side of the waveguide centre line by the same amount and the separation between slots is fixed. The width and length parameters of the slots are adjusted to control the slot excitations. This configuration was selected for two reasons, firstly, to help minimise the machining errors which arise due to incorrectly positioning the slots. Secondly, to eliminate the distortion in the radiation pattern due to a double periodicity error. However, the program soon demonstrated that this was not a practical configuration as the width parameter was unable to provide the required control over the excitations of the individual slots. To help enunciate this the power radiated has been plotted as a function of slot length for various widths in Figure (8.4). This figure clearly demonstrates that the width adjustment does not yield much control over the radiation level, especially for slots close to

resonance. Therefore, it is difficult to develop realistic designs with low side lobes using this configuration.

An alternative to this arrangement is to fix the width parameter and allow the slot separation to vary. This provides good control over the excitation levels of the individual slots. Unfortunately, each time the slot separations are adjusted the roots of the array factor, which control the radiation pattern, are also adjusted which causes distortion in the radiation pattern. Therefore, this configuration can only be implemented for arrays where all the slots are excited by approximately the same amount, otherwise, the separations between the elements vary significantly and the radiation pattern differs from the specification.

The final configuration to be considered is a variation on the above set up. This time the slot widths, offsets and separations are held constant and the lengths are varied. An additional set of capacitive posts are also introduced to provide additional control of the susceptance components of the self admittances to enable the individual slot excitations to be controlled adequately to shape the excitation distribution across the array. The equivalent circuit for a post in the broadwall of rectangular waveguide is illustrated in Figure (8.5). This figure shows that the post is not directly equivalent to a shunt capacitor, however, Marcuvitz [8.3] tabulates values of both X_A and X_B (Table (8.3)) and for the size of posts required for this application the X_B component can be assumed to be zero.

Height of Post / Height of Waveguide	$\frac{X_A}{Z_o}$	$\frac{X_B}{Z_o}$
0.254	-6.204	0.006
0.505	-0.906	0.011
0.756	-0.122	0.017
0.829	-0.028	0.019
0.943	+0.083	0.021
0.961	+0.122	0.022
1.000	+0.277	0.023

Table (8.3)

Reactances of Cylindrical Post (1.5875 mm Diameter)

in W.G. 16

Before redesigning Elliott's example using this configuration it is worth outlining the modification carried out to the program to permit this arrangement to be synthesised. Firstly, the trial values for the Gauss-Newton root-finding routine were obtained in a different manner as the variational solution could not readily be cast into a form which was capable of providing the required.data. A data bank of theoretically evaluated self admittance values was set up instead, using the moment method to provide initial 'trial values' for the root-finding routine. Secondly, this routine searched for the self conductance of the slot instead of the reflection coefficient formerly used. Once a suitable set of slot lengths has been determined then the susceptance compensation required to adjust the self admittances to the desired values can be determined.

The Elliott example was redesigned using the CAD package with the above modifications implemented. The slot width was set equal to 1.5 mm and the offset equal to 2.85 mm from the guide centre line and the resulting array configuration is tabulated below:

Slot	Length (mm)	Compensating Capacitance (x10E-14 Farads)
1	12.97	0.1826
2	12.57	0.1504
3	13.12	0.1953
4	13.53	0.2399
5	13.84	0.2789
6	14.09	0.3103
7	14.28	0.3325
8	14.44	0.3443
9	14.57	0.3466
10	14.67	0.3401
11	14.76	0.3274
12	14.87	0.3038
13	14.94	0.2835
14	14.97	0.2777
15	14.97	0.2799
16	14.94	0.3042
17	14.84	0.3496
18	14.69	0.3758

19	14.46	0.3726
20	14.12	0.3264
21	14.47	0.3810

Table (8.4)

Array Configuration Using Tuning Screws

Note: The values of capacitance tabulated above include compensation for the additional radiated and transmitted phase shifts due to the slots.

This array was not constructed due to time restrictions, however, it appears to be a practical alternative to the more traditional arrangements discussed earlier. The manufacturing of this would be relatively straightforward as the only parameter to be adjusted is the slot length, although, the size and depths of the posts need to be determined before this design can be implemented.

8.5 CONCLUSION

This chapter demonstrates how the synthesis procedure developed in chapter 6 may be extended to permit the design of both resonant and planar arrays comprising of longitudinal shunt slots. The additional programming required to implement these designs is relatively simple and a brief description is given for each case.

Alternative less common array configurations have also been examined to demonstrate the potential of a purely theoretical synthesis/design program. Elliott's 21 slot example has been redesigned using one of these and the predicted array configuration appears to be a practical

alternative to the more traditional arrangements normally implemented. This array was not constructed due to time restrictions. Nevertheless, this theoretical study has helped to demonstrate the flexibility of the design program which is one of its main advantages over the more traditional design techniques which rely on data banks of measured slots.

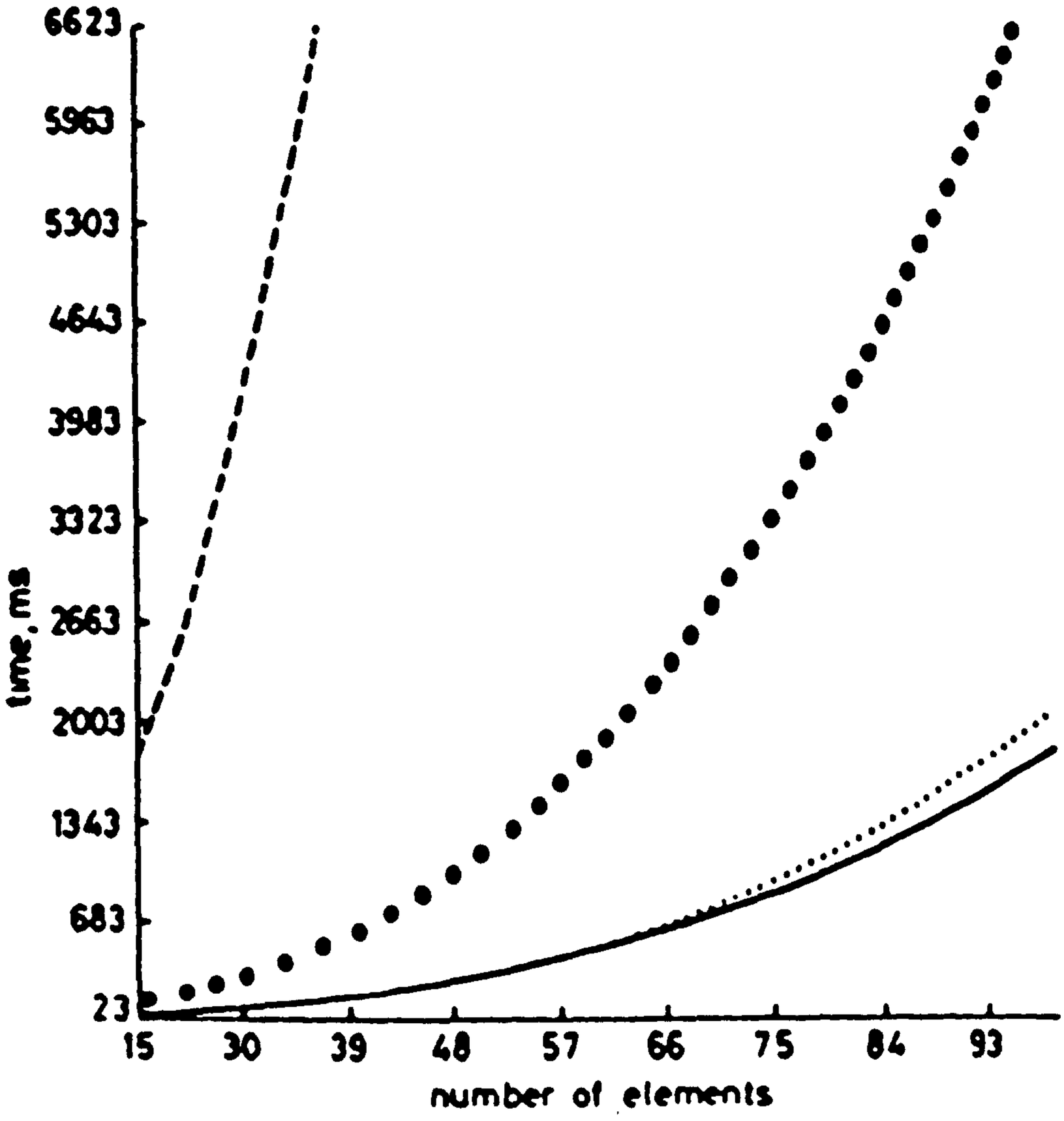

Run-time plotted against array size for four algorithms

Figure 8.1

Processing Times for Various Dolph-Chebyshev Algorithms

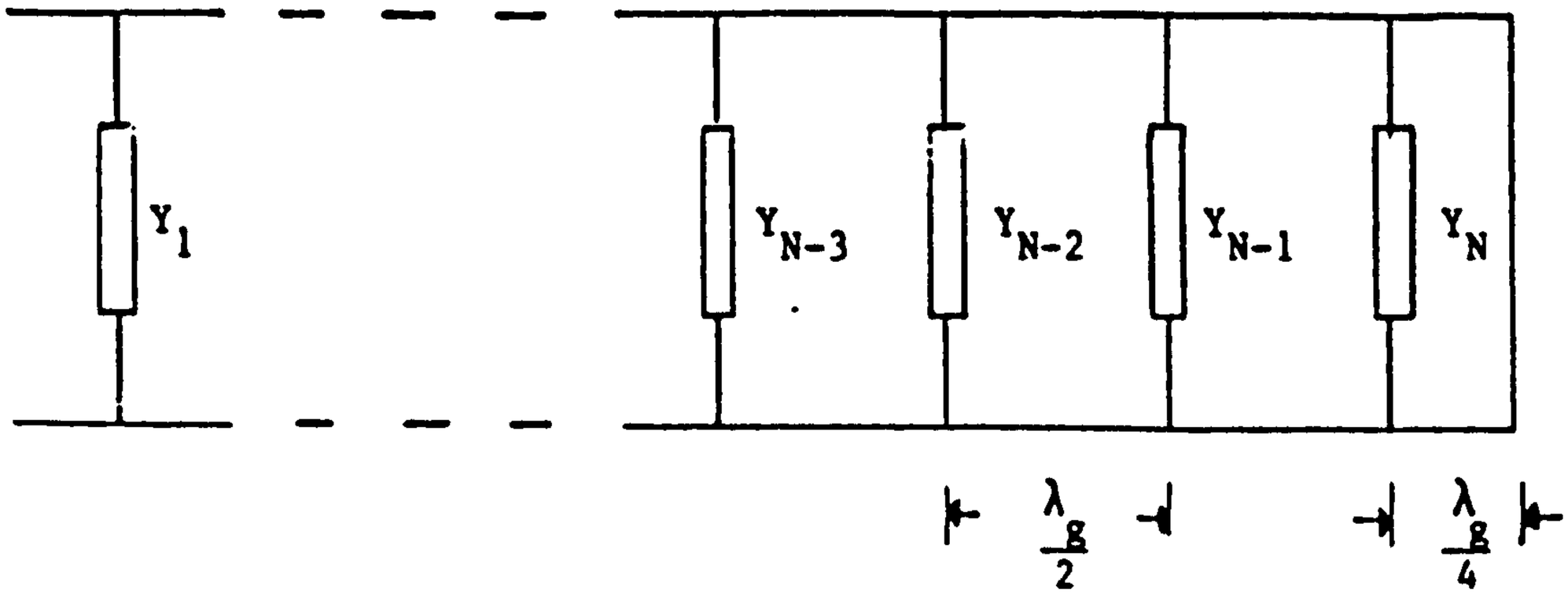

Figure 8.2

Equivalent Circuit for Resonant Array

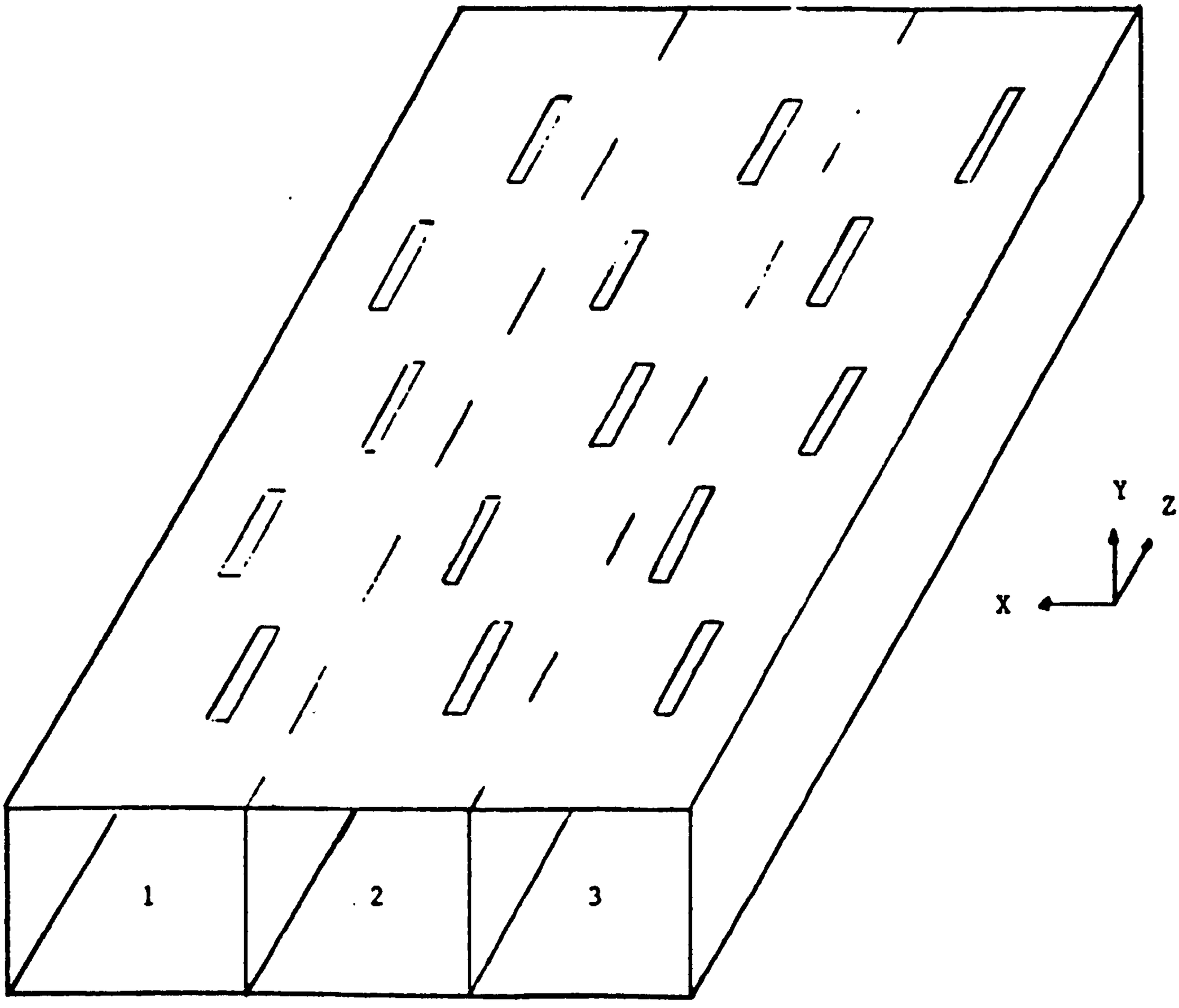

Figure 8.3

Illustration of Planar Array

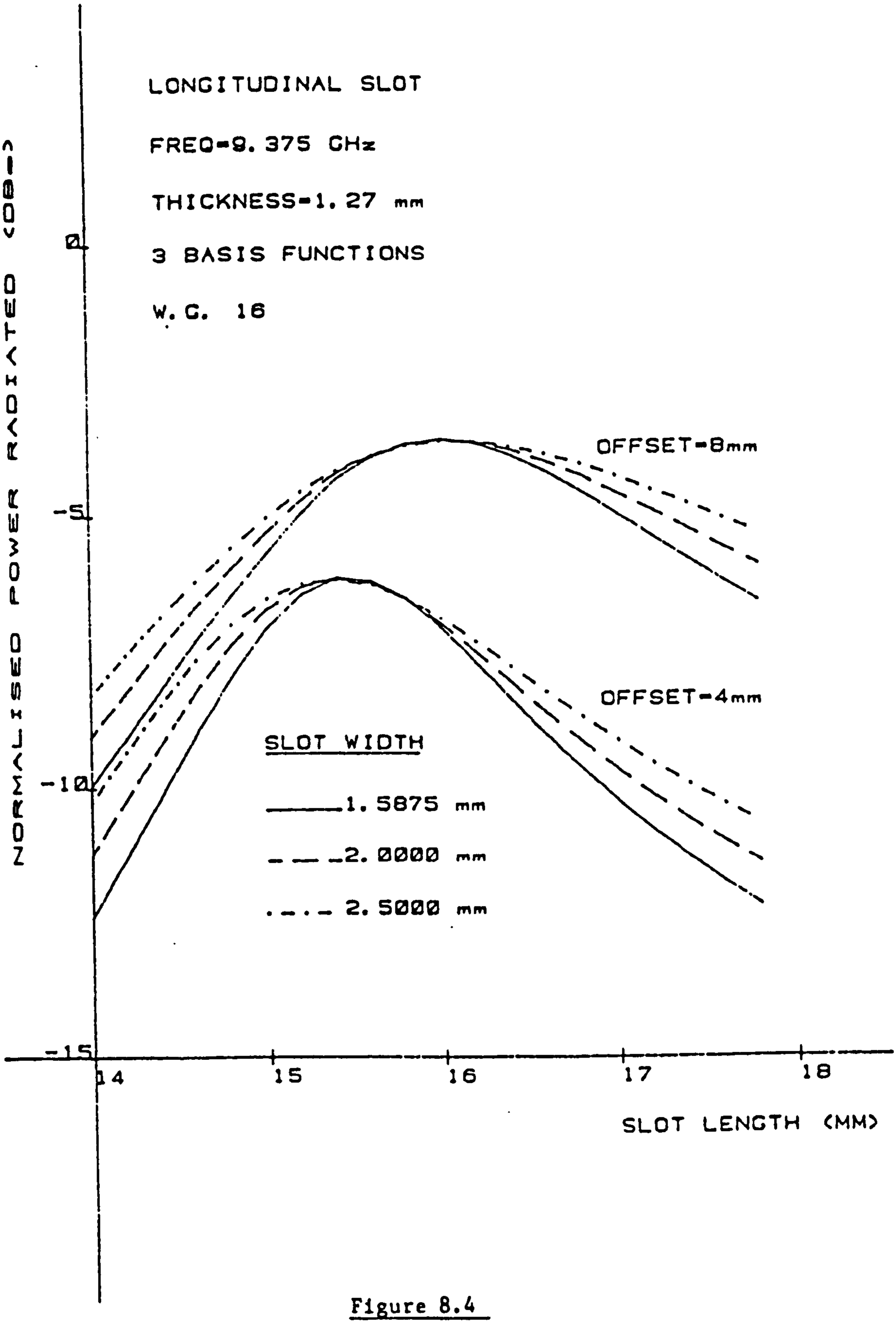

Figure 8.4

Normalised Power Radiated as a Function of Slot Length for a Longitudinal Slot - Thick Walled Case

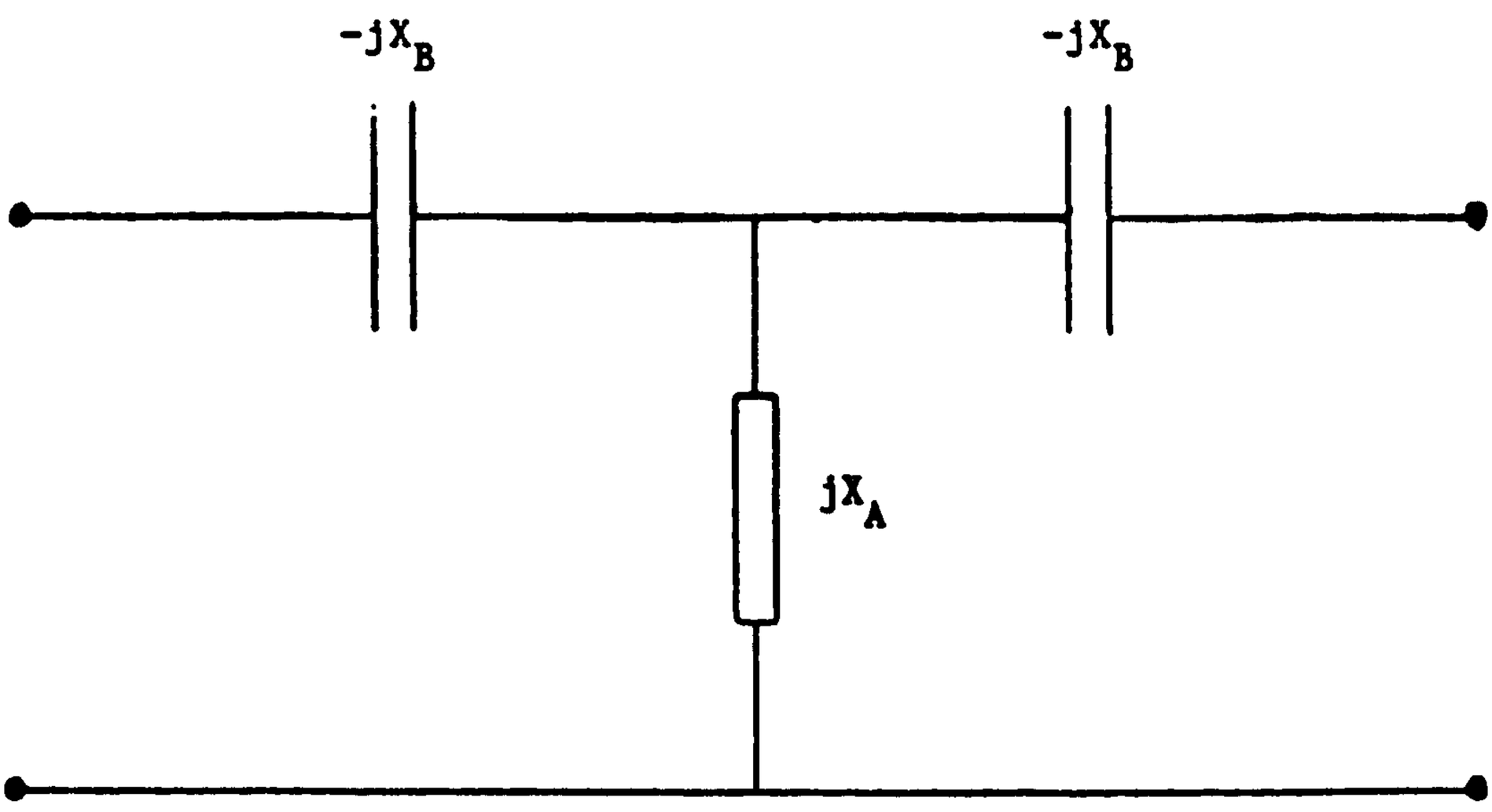

Figure 8.5

Equivalent Circuit for a Post in the Top Wall of a Rectangular Waveguide

CHAPTER 9

CONCLUSION

The aim of this research project has been to develop a theoretical design/synthesis CAD package for slotted waveguide array antennas. The moment method solution has been incorporated into this package to provide theoretical self admittance data on the individual slots in the array. This differs from previous contributions in this field, in that the reliance on measured data has been removed. Preliminary investigations have been carried out to verify that the moment method is capable of accurately characterising a slot. A useful comparison between theoretical and recently reported experimental results has been presented in Figure (3.4) to assist in the assessment of this analysis technique. This figure clearly shows that the theoretical predictions are accurate to within 1% of the measured data. This small residual error can be attributed primarily to inadequate modelling of the field enhancement at the sharp edges within the slot.

This degree of accuracy can only be claimed for narrow square ended slots. For wide slots and round ended slots which are commonly used in practice, there are at least two other sources of error which should be highlighted. The cross-polar or longitudinally directed E field component has not been incorporated into the solution, as the effect is known to be negligible for slots which exhibit large length/width ratios. There are nevertheless some applications which use wide slots and in these instances a more complex basis function is required. The solution is also restricted to characterising square ended slots which gives rise to an additional discrepancy

between theory and practice, as slots of this type are almost never used due to manufacturing difficulties. Round ended slots are far more common and consequently correction factors, based on equal perimeter/area rules, have been introduced to compensate for this error.

The moment method analysis has been extended to address the problem of round ended slots by employing sectioning on the inner surface of the slot with the length of the cavity and outer surface being adjusted to accommodate this modification. This technique is more demanding in terms of computational effort but not excessively so if trignometric basis functions are employed. An improvement of approximately 1% in accuracy has been obtained using this 'improved' model. However, the model has been shown to break down for longitudinal slots exhibiting large offsets due to its crudeness with the sectioning being applied to only the inner surface of the slot. Unfortunately, any attempt to improve the sophistication of the model results in dramatic increases in the computational effort required, which are difficult to justify.

The analysis for the conventional slot has also been used to examine the resonant characteristics of longitudinal shunt slots exhibiting width to length ratios in the range 0.1 to 0.25. The results of this study clearly demonstrate that the relationship between resonant length and slot width differs markedly for slots which are close to the centre of the waveguide and those nearer to the side wall. This difference in behaviour has been explained in terms of slot susceptance.

A series of experiments was conducted using a waveguide bridge measurement system. This set-up was specifically developed for the accurate measurement of the resonant frequency of a radiating slot. Measurements have been carried out on various longitudinal slot examples, each having a different slot width and a different offset from the waveguide centre line. The experimental results confirmed the theoretically predicted relationship between the width parameter and the resonant length of a longitudinal shunt slot.

These investigations into the accuracy of the moment method solution have clearly demonstrated that it may be employed, with some confidence, in a slotted waveguide antenna design procedure. Consequently, such a package has been developed. Considerable care was exercised during the development of this design methodology to generate computationally efficient algorithms, as the moment method does not yield rapidly calculable closed form expressions for the scattering parameters of a slot. The accuracy of the design package is currently limited by the need to achieve practical processor times on presently available computing facilities. Steady improvements in accuracy can consequently be predicted as computational speeds permit. For example, the use of more elaborate basis functions in the moment method solution would clearly improve the basic accuracy of the program, as would a more direct method of calculating the mutual coupling between slots.

The CAD design package was assessed using two independent tests. Firstly, it was used to redesign an example previously detailed in the literature by Elliott and the predicted array configuration was found to be substantially in agreement with the reported

configuration. A second, more rigorous test was also carried out where the package was used to design a 19 element travelling wave antenna. This was constructed and the radiation pattern was measured on an accurate near field measurement system. The experimental and theoretical patterns for this array were compared and the degree of agreement was not untypical of synthesised slot array design. The discrepancies between the patterns were mainly attributed to constructional errors, or more precisely to weaknesses in the method adopted to produce square ended slots.

The flexibility of the program was also examined and various modifications have been discussed to enable other array configurations to be synthesised. A brief description of the additional programming required for both resonant and planar arrays, which was remarkably simple, has been given. Also, some unconventional array configurations have been studied to demonstrate the potential of this design procedure. Elliott's 21 slot example has been redesigned using one of these and the predicted array configuration appears to be a practical alternative to the more traditional arrangements normally implemented. This array was not constructed due to time restrictions. Nevertheless, this theoretical study has helped to demonstrate the flexibility of the design program which is one of its main advantages over the more traditional design techniques which rely on data banks of measured slots.

One obvious refinement to this design package would be to extend it to incorporate the design of the feed system for a planar array. However, the CAD package is a powerful tool as it stands and it has already been employed to design an antenna comprising of two linear

arrays. This antenna has been constructed and is undergoing tests with a view to using it in a marine navigation system. One array, namely a 31 element resonant array of longitudinal shunt slots in a rectangular waveguide was designed conventionally using the CAD package. The second array was less easy to design, since it required an array comprising of 33 inclined slots cut in the narrow wall of a rectangular waveguide to be designed. The inclined slots were accommodated by creating a modified version of the program in which the moment method was replaced by a solution due to Das, Raju and Chakraboty [9.1] for the self admittance of an inclined slot.

The work recorded in this thesis has given rise to two projects which will be commencing shortly. The first of these is aimed at developing a complete electromagnetic solution to the slotted waveguide problem. This will be based on the work of Vu Khac but with his pulse basis functions being replaced by trignometric functions. The second project is directed towards developing a manufacturing procedure for slotted waveguide array antennas using a chemical etching process. This is similar to the method used in making printed circuit boards and a computer will be employed to generate the masks for the array. These masks must be drawn approximately 10 times larger than required, to obtain an accuracy of 0.02 mm and then reduced to the actual size of the array using photographic techniques. The accuracy of this manufacturing procedure is also governed by the etching process and the waveguide wall has to be skimmed to one tenth of its standard thickness if an accuracy of 0.02 mm is to be maintained.

APPENDIX 1

EVALUATION OF THE WAVEGUIDE INTEGRAL FOR THE SECTIONED TRANSVERSE SLOT

The integration of the field across the inner surface of a sectioned transverse slot breaks down into three parts.

(1) The self coupling term for the middle section

(2) The self coupling term for the outer section

(3) The mutual coupling term

which when combined give

$$\sum_{p=1}^{3}\sum_{q=1}^{3} \frac{j\omega\varepsilon_0}{k_c^2 ab} \int_{Z_p-\frac{W_1}{2}}^{Z_p+\frac{W_1}{2}} \int_{x_1-\frac{L_p}{2}}^{x_1+\frac{L_p}{2}} \sin\frac{s\pi(x_0 - x_1 + \frac{L_p}{2})}{L_p}$$

$$\times \int_{Z_q-\frac{W_1}{2}}^{Z_q+\frac{W_1}{2}} \int_{x_1-\frac{L_q}{2}}^{x_1+\frac{L_q}{2}} \sin\frac{s\pi(x_0 - x_1 + \frac{L_q}{2})}{L_q}$$

$$\times \Big(\sum_{n=1}^{\infty}\sum_{m=0}^{\infty} \varepsilon_{om}\, e^{-\Gamma_{nm}|z-z_0|}$$

$$\times \Big[\frac{\Gamma_{nm}}{k^2}\Big(\frac{n\pi}{a}\Big)^2 - \frac{1}{\Gamma_{nm}}\Big(\frac{m\pi}{b}\Big)^2\Big] \sin\frac{n\pi x}{a} \sin\frac{n\pi x_0}{a} \cos\frac{m\pi y}{b} \cos\frac{m\pi y_0}{b}\Big) dx_0 dz_0 dx dz \qquad (A1.1)$$

where $W_1 = W/3$

L_p, L_q are the section lengths dependent on p and q

Z_p, Z_q are the respective displacements from the centre of the slot to the centre of the sections

and $$\varepsilon_{o_j} = \begin{cases} 1 \text{ for } j = 0 \\ 2 \text{ for } j \neq 0 \end{cases}$$

The self coupling term for the middle section will be addressed first as the solution is the same as that for Lyon's single slot [3.1] and the mathematics will be reproduced to clearly enunciate the method of evaluation.

The component of (A1.1) relating to the self coupling of the middle section is as follows

$$j \frac{\omega\varepsilon_o}{k_c^2 ab} \int_{-\frac{W_1}{2}}^{\frac{W_1}{2}} \int_{x_1-\frac{L}{2}}^{x_1+\frac{L}{2}} \sin \frac{i\pi(x - x_1 + \frac{L}{2})}{L} \int_{-\frac{W_2}{2}}^{\frac{W_2}{2}} \int_{x_1-\frac{L}{2}}^{x_1+\frac{L}{2}} \sin \frac{s\pi(x_o - x_1 + \frac{L}{2})}{L}$$

$$\times \sum_{n=1}^{\infty} \sum_{m=o}^{\infty} e^{-\Gamma_{nm}|z-z_o|} \varepsilon_{om} \left[\frac{\Gamma_{nm}}{k^2} \left(\frac{n\pi}{a}\right)^2 - \frac{1}{\Gamma_{nm}} \left(\frac{m\pi}{b}\right)^2 \right] \qquad \text{(A1.2)}$$

$$\times \sin \frac{n\pi x}{a} \sin \frac{n\pi x_o}{a} \cos \frac{m\pi y}{b} \cos \frac{m\pi y_o}{b} \, dx_o dz_o dx dz$$

with $p = q = 2$, $Z_p = Z_q = 0$ and $L_p = L_q = L$ = length of round end slot.

The expression may be simplified considerably if the integrals are evaluated.

Firstly, consider

$$\int_{-\frac{W_1}{2}}^{\frac{W_1}{2}} \int_{-\frac{W_1}{2}}^{\frac{W_1}{2}} e^{-\Gamma_{nm}|z-z_0|} dz_0 dz \qquad (A1.3)$$

this can be solved using a transformation of variables [A1.1] with

$$\Lambda = z - z_0 \qquad \Omega = z + z_0 \qquad (A1.4)$$

$$dz\, dz_0 = \frac{1}{2} d\Lambda d\Omega$$

Hence $$2 \int_0^{W_1} \int_0^{W_1-\Lambda} e^{-\Gamma\Lambda}\, d\Omega d\Lambda \qquad (A1.5)$$

which integrates to give

$$2\left[\frac{W_1}{\Gamma_{nm}} + \frac{1}{\Gamma_{nm}^2}\left(e^{-\Gamma_{nm}W_1} - 1\right)\right] \qquad (A1.6)$$

The second integral is of the form

$$\sigma(i,n) = \int_{x_1-\frac{L}{2}}^{x_1+\frac{L}{2}} \sin \frac{i\pi(x - x_1 + \frac{L}{2})}{L} \sin \frac{n\pi x}{a}\, dx \qquad (A1.7)$$

which may be simplified by the use of trignometric identities and substituting $x = x' + x_1$ to give

$$\sigma(i,n) = \begin{cases} (-1)^{\frac{i}{2}} \int_{-\frac{L}{2}}^{\frac{L}{2}} \sin\frac{i\pi x'}{L} \sin\frac{n\pi(x' + x_1)}{a}\, dx' & (i \text{ even}) \\ (-1)^{\frac{i-1}{2}} \int_{-\frac{L}{2}}^{\frac{L}{2}} \cos\frac{i\pi x'}{L} \sin\frac{n\pi(x' + x_1)}{a}\, dx' & (i \text{ odd}) \end{cases} \qquad (A1.8)$$

The above equations are evaluated in an identical manner therefore only one solution will be outlined with the other simply being quoted. Consider the expression for i even and substitute

$$\theta = \frac{i\pi x'}{L} \qquad (A1.9)$$

into it to produce

$$(-1)^{\frac{i}{2}} \left(\frac{L}{i\pi}\right) \cos\frac{n\pi x_1}{a} \int_{-\frac{i\pi}{2}}^{\frac{i\pi}{2}} \sin\theta \sin\alpha\theta\, d\theta \qquad (A1.10)$$

where

$$\alpha = \frac{nL}{ia} \qquad (A1.11)$$

This integrates to give

$$\sigma(i,n) = \frac{2L}{i\pi} \frac{}{\alpha^2 - 1} \sin\frac{\alpha i\pi}{2} \cos\frac{n\pi x_1}{a} \qquad (A1.12)$$

except when $\alpha = 1$ then

$$\sigma(i,n) = \frac{L}{2} (-1)^{\frac{i}{2}} \cos\frac{n\pi x_1}{a} \qquad (A1.13)$$

and consequently the solution for equation (A1.8) for i odd is

$$\sigma(i,n) = \frac{\frac{2L}{i\pi}}{1-\alpha^2} \cos\frac{\alpha i\pi}{2} \sin\frac{n\pi x_1}{a} \qquad (A1.14)$$

except when $\alpha = 1$ then

$$\sigma(i,n) = \frac{L}{2}(-1)^{\frac{i-1}{2}} \sin\frac{n\pi x_1}{a} \qquad (A1.15)$$

Substituting these back into (A1.2) gives

$$\frac{j2\omega\varepsilon_0}{k_c^2 ab} \sum_{n=1}^{\infty} \sum_{m=o}^{\infty} \varepsilon_{om}\left(1 - \left(\frac{n\pi}{\Gamma_{nm}b}\right)^2\right)\left(W_1 + \frac{1}{\Gamma_{nm}}\left(e^{-\Gamma_{nm}W_1} - 1\right)\right)\sigma(i,n)\sigma(s,n)$$

(A1.16)

which converges slowly due to the m^{-2} and m^{-3} terms. Lyon enhanced the efficiency of this expression by summing these terms analytically. The summation

$$\sum_{m=o}^{\infty} \varepsilon_{mo} W_1\left(1 - \left(\frac{m\pi}{b\Gamma_{nm}}\right)^2\right) \qquad (A1.17)$$

is re-written as

$$W_1\left(1 - 2\sum_{m=1}^{\infty} \frac{\rho_n^2}{m^2 - \rho_n^2}\right) \qquad (A1.18)$$

where

$$\rho_n = b\sqrt{\left(\left(\frac{k}{\pi}\right)^2 - \left(\frac{n}{a}\right)^2\right)} \tag{A1.19}$$

to enable Collin's [3.4] and Vu Khac's [2.7] work be implemented which simplifies this to

$$W_1[U_n] \tag{A1.20}$$

where

$$U_n = \begin{cases} \dfrac{\pi\rho_n \cos\pi\rho_n}{\sin\pi\rho_n} & n = 1 \\ \dfrac{\pi\rho_n \cosh\pi\rho_n}{\sinh\pi\rho_n} & n > 1 \end{cases} \tag{A1.21}$$

The other summation suitable for evaluation is

$$\sum_{m=1}^{\infty} \frac{1}{\Gamma_{nm}^3} \tag{A1.22}$$

which is equivalent to

$$\left(\frac{b}{\pi}\right)^3 \sum_{m=0}^{\infty} \frac{1}{(m^2 - \rho_n^2)^{\frac{3}{2}}} - \left(\frac{b}{\pi}\right)^3 \frac{j}{\rho_n^3} \tag{A1.23}$$

and by applying Hildebrand's [A1.2] results this is reduced to

$$\sum_{m=1}^{\infty} \frac{1}{\Gamma_{nm}^3} = -\left(\frac{b}{\pi}\right)^3 \left(\frac{1}{\rho_n^2}\right)^3 \left(\frac{1}{\rho_n^2} + \frac{1}{2}\frac{j}{\rho_n^3}\right) \tag{A1.24}$$

Therefore the self coupling terms for the middle section may be written as

$$\frac{2j\omega\varepsilon_0}{k^2ab}\sum_{n=1}^{\infty}\sigma(i,n)\sigma(s,n)\left(W_1U_n + \frac{e^{-\Gamma_{no}W_1}-1}{\Gamma_{no}} + \right.$$

$$\left. + 2\Gamma_{no}^2\left(\left(\frac{b}{\pi}\right)^2\left(\frac{1}{\rho_n^2} + \frac{1}{2}\frac{j}{\rho_n^3}\right) + \sum_{m=1}^{\infty}\frac{e^{-\Gamma_{nm}W_1}}{\Gamma_{nm}^3}\right)\right) \qquad \text{(A1.25)}$$

The remaining coupling terms may be evaluated in a similar manner. Differing only in the solutions of the integral (A1.3) due to the Z displacements of the section.

This integral takes the following form for the self coupling of the outer sections.

$$\int_{Z_1-\frac{W_1}{2}}^{Z_1+\frac{W_1}{2}}\int_{Z_1-\frac{W_1}{2}}^{Z_1+\frac{W_1}{2}} e^{-\Gamma_{nm}|Z-Z_0|}\,dZ_0dZ \qquad \text{(A1.26)}$$

and may be evaluated by employing the transformation in (A1.5) giving

$$2\int_{Z_1}^{Z_1+W_1}\int_{Z_1}^{Z_1+W_1-\Lambda} e^{-\Gamma_{nm}\Lambda}\,d\Omega d\Lambda \qquad \text{(A1.27)}$$

and the solution is

$$2\frac{e^{-\Gamma_{nm}Z_1}}{\Gamma_{nm}}\left[Z_1(e^{-\Gamma_{nm}W_1}-1) + W_1 + \frac{1}{\Gamma_{nm}}(e^{-\Gamma_{nm}W_1}-1)\right] \qquad \text{(A1.28)}$$

Substituting this along with equations (A1.12) to (A1.15) into (A1.2) gives the following solution for the self coupling of the outer section

$$\frac{2j\omega\varepsilon_o}{k_c^2 ab} \sum_{n=1}^{\infty} \sigma(i,n)\, \sigma(s,n) \sum_{m=o}^{\infty} \varepsilon_{om}\left[1 - \left(\frac{m\pi}{\Gamma_{nm} b}\right)^2\right] e^{-\Gamma_{nm} Z_1}$$

$$\times \left[Z_1 (e^{-\Gamma_{nm} W_1} - 1) + W_1 + \frac{1}{\Gamma_{nm}} (e^{-\Gamma_{nm} W_1} - 1)\right] \qquad \text{(A1.29)}$$

The solution to (A1.3) for the mutual term is evaluated directly with the modules of $Z-Z_o$ removed as long as $Z \geq Z_o$. This enables the integral to be split as follows

$$\int_{Z_1 - \frac{W_1}{2}}^{Z_1 + \frac{W_1}{2}} e^{-\Gamma_{nm} Z} dZ \int_{Z_2 - \frac{W_1}{2}}^{Z_2 + \frac{W_1}{2}} e^{-\Gamma_{nm} Z_o} dZ_o \qquad \text{(A1.30)}$$

which when solved gives

$$- \frac{1}{\Gamma_{nm}^2} \left[2e^{-\Gamma_{nm}(Z_1 - Z_2)} - e^{-\Gamma_{nm}(Z_1 - Z_2 - W_1)} - e^{-\Gamma_{nm}(Z_1 - Z_2 + W_1)}\right] \qquad \text{(A1.31)}$$

Consequently the solution for the mutual coupling is

$$\frac{j\omega\varepsilon_o}{k_c^2 ab} \sum_{n=1}^{\infty} \sigma(i,n)\, \sigma(s,n) \sum_{m=o}^{\infty} - \frac{\varepsilon_{om}}{\Gamma_{nm}} \left[1 - \left(\frac{m\pi}{\Gamma_{nm} b}\right)^2\right]$$

$$\times \left[2e^{-\Gamma_{nm} Z} - e^{-\Gamma_{nm}(Z+W_1)} - e^{-\Gamma_{mm}(Z - W_1)}\right] \qquad \text{(A1.32)}$$

with $Z = Z_1 - Z_2$

Note the summations in (A1.29) and (A1.32) cannot be solved analytically, therefore these expressions converge more slowly than (A1.25).

APPENDIX 2

EVALUATION OF THE WAVEGUIDE INTEGRAL FOR THE SECTIONED LONGITUDINAL SLOT

The solution for the magnetic field within the waveguide divides into two terms.

(a) The self coupling and mutual coupling term for sections of equal lengths

(b) The mutual coupling term for section of different lengths.

The terms are developed in a similar manner to Lyon's solution for the single slot. The expression for sections of equal lengths is evaluated first as this differs only slightly from Lyon's result.

The magnetic vector potential is calculated from equation (4.11) giving

$$\underline{A}_m = -\varepsilon_o \sum_{n=o}^{\infty} \sum_{m=o}^{\infty} \frac{\varepsilon_{om}\varepsilon_{on}}{2ab\Gamma_{nm}} \cos\frac{n\pi x}{a} \int_{x_a - \frac{W_1}{2}}^{x_a + \frac{W_1}{2}} \cos\frac{n\pi x_o}{a}\, dx_o$$

$$\times \left[e^{\Gamma_{nm} Z} \int_{Z}^{L/2} \sin\frac{s\pi(z_o + L/2)}{L}\, e^{-\Gamma_{nm} Z_o}\, dZ_o \right.$$

$$\left. + e^{-\Gamma_{nm} Z} \int_{-L/2}^{Z} \sin\frac{s\pi(Z_o + L/2)}{L}\, e^{\Gamma_{nm} Z_o}\, dZ_o \right] \qquad (A2.1)$$

On performing the intergrations this reduces to

$$\underline{A}_m = -\frac{\varepsilon_o}{ab}\sum_{n=o}^{\infty}\sum_{m=o}^{\infty}\frac{\varepsilon_{on}\varepsilon_{om}}{\Gamma_{nm}}\cos\frac{n\pi x}{a}$$

$$\begin{cases} W_1 & n=o \\ (\frac{a}{n\pi})(\frac{\sin n\pi(x_a + \frac{W_1}{2})}{a} - \frac{\sin n\pi(x_a - \frac{W_1}{2})}{a}) & n\neq o \end{cases}$$

$$\times \frac{1}{\Gamma nm\ (1 + \frac{s\pi}{\Gamma_{nm}L})^2)}\left[\sin\frac{s\pi(Z + L/2)}{L} + (\frac{s\pi}{\Gamma_{nm}L})\right.$$

$$\left.\times e^{-\Gamma_{nm}L/2}\begin{cases}\cosh\Gamma_{nm}Z & (S\text{ odd}) \\ -\sinh\Gamma_{nm}Z & (S\text{ even})\end{cases}\right]\hat{a}_z \qquad \text{(A2.2)}$$

This is substituted into eqn. (4.10) to obtain H_z.

$$H_z = j\frac{\omega\varepsilon_o}{2ab}\sum_{n=o}^{\infty}\sum_{m=o}^{\infty}\frac{\varepsilon_{om}\varepsilon_{on}}{\Gamma_{nm}}\cos\frac{n\pi x}{a}$$

$$\times \begin{cases} W_1 & n=o \\ (\frac{a}{n\pi})(\sin\frac{n\pi(x_a + \frac{W_1}{2})}{a} - \sin\frac{n\pi(x_a - \frac{W_1}{2})}{a}) & n\neq o \end{cases}$$

$$\times \frac{2}{\Gamma_{nm}(1 + (\frac{s\pi}{\Gamma_{nm}L})^2)}\left[(1 - (\frac{s\pi}{kL})^2)\sin\frac{s\pi(Z + \frac{1}{2})}{L}\right. \qquad \text{(A2.3)}$$

$$\left. + (\frac{s\pi}{\Gamma_{nm}L})(1 + (\frac{\Gamma_{nm}}{k})^2)\begin{cases}\cosh\Gamma_{nm}Z & (s\text{ odd}) \\ -\sinh\Gamma_{nm}Z & (s\text{ even})\end{cases}\right]\hat{a}_z$$

which enables the final integral to be evaluated.

$$\iint_S f_1\,\hat{a}_x \cdot (-\hat{a}_y \times \underline{H}_z)\,dS \qquad \text{(A2.4)}$$

Substituting (A2.3) with (A2.4) gives

$$- j \frac{\omega\epsilon_0}{ab} \sum_{n=0}^{\infty} \sum_{m=0}^{\infty} \frac{\epsilon_{om}\epsilon_{om}}{\Gamma_{nm}} \begin{cases} W_1 & n=0 \\ (\frac{a}{n\pi})(\sin \frac{n\pi(x_a + \frac{W_1}{2})}{a} - \sin \frac{n\pi(x_a - \frac{W_1}{2})}{a}) & n\neq 0 \end{cases}$$

$$\times \int_{x_b - \frac{W_1}{2}}^{x_b + \frac{W_1}{2}} \cos \frac{n\pi x}{a}\, dx \frac{1}{\Gamma_{nm}(1 + (\frac{s\pi}{\Gamma_{nm}L})^2)} ((1 - (\frac{s\pi}{kL})^2)$$

$$\times \int_{-\frac{L}{2}}^{\frac{L}{2}} \sin \frac{s\pi(Z + \frac{L}{2})}{L} \sin \frac{i\pi(Z + \frac{L}{2})}{L}\, dZ$$

$$+ (\frac{s\pi}{\Gamma_{nm}L})(1 + (\frac{\Gamma_{nm}}{k})^2) e^{-\Gamma_{nm}\frac{L}{2}} \int_{-\frac{L}{2}}^{\frac{L}{2}} \sin \frac{i\pi(Z + \frac{L}{2})}{L} \begin{cases} \cosh \Gamma_{nm} Z \text{ (s odd)} \\ -\sinh \Gamma_{nm} Z \text{ (s even)} \end{cases} dZ)$$

(A2.5)

which after integration becomes

$$- j \frac{\omega\epsilon_0}{ab} \sum_{n=0}^{\infty} \sum_{m=0}^{\infty} \frac{\epsilon_{om}\epsilon_{on}}{\Gamma_{nm}}$$

$$\times \begin{cases} W_1 & n=0 \\ [(\frac{a}{n\pi})^2 (\sin \frac{n\pi(x_a + \frac{W_1}{2})}{a} - \sin \frac{n\pi(x_a - \frac{W_1}{2})}{a})(\sin \frac{n\pi(x_b + \frac{W_1}{2})}{a} - \sin \frac{n\pi(x_b - \frac{W_1}{2})}{a}] & n\neq 0 \end{cases}$$

$$\times \frac{1}{\Gamma_{nm}(1 + (\frac{s\pi}{\Gamma_{nm}L})^2)} ((1 - \frac{s\pi}{kL})^2) \frac{L}{2} \delta_{is}$$

$$+ \left(\frac{k_c}{k}\right)^2 \frac{\left(\frac{s\pi}{\Gamma_{nm}L}\right)\left(\frac{i\pi}{\Gamma_{nm}^2 L}\right)}{1 + \left(\frac{i\pi}{\Gamma_{nm}L}\right)^2} e^{-\Gamma_{nm}\frac{L}{2}} \begin{cases} (i - (-1)^i)\cosh \Gamma_{nm} \frac{L}{2} & (s \text{ odd}) \\ (1 + (-1)^i)\sinh \Gamma_{nm} \frac{L}{2} & (s \text{ even}) \end{cases} \quad \text{(A2.6)}$$

This may be simplified somewhat by employing the results on contour integration applied to summing series given by Collin [3.4].

In particular the summation

$$\sum_{m=0}^{\infty} \frac{\varepsilon_{om}\left(1 - \left(\frac{s\pi}{kL}\right)^2\right)L\ \delta_{is}}{\Gamma_{nm}^2 + \left(\frac{s\pi}{L}\right)^2} \quad \text{(A2.7)}$$

when written as

$$\left(\frac{b}{\pi}\right)^2\left(1 - \left(\frac{s\pi}{kL}\right)^2\right)L\ \delta_{is} \sum_{m=0}^{\infty} \frac{\varepsilon_{om}}{m^2 - \left(\frac{b}{\pi}\right)^2\left(k^2 - \left(\left(\frac{s\pi}{L}\right)^2 + \left(\frac{n\pi}{a}\right)^2\right)\right)} \quad \text{(A2.8)}$$

can be reduced to

$$\left(\frac{b}{\pi}\right)^2\left(1 - \left(\frac{s\pi}{kL}\right)^2\right)L\ \delta_{is}\ \Upsilon(n,s) \quad \text{(A2.9)}$$

where

$$\delta(n,s) = -\frac{\pi^2 \cos b\sqrt{k^2 - \left(\left(\frac{s\pi}{L}\right)^2 + \left(\frac{n\pi}{a}\right)^2\right)}}{b\sqrt{k^2 - \left(\left(\frac{s\pi}{L}\right)^2 + \left(\frac{n\pi}{a}\right)^2\right)}\ \sin b\sqrt{k^2 - \left(\left(\frac{s\pi}{L}\right)^2 + \left(\frac{n\pi}{a}\right)^2\right)}} \quad \text{(A2.10)}$$

Incorporating this back into (A2.6) gives

$$- \frac{j\omega\epsilon_o}{2ab} \sum_{n=o}^{\infty} \epsilon_{on}$$

$$\times \begin{cases} W_1 & n=o \\ (\frac{a}{n\pi})^2 (\sin\frac{n\pi(x_a+\frac{W_1}{2})}{a} - \sin\frac{n\pi(x_a-\frac{W_1}{2})}{a})(\sin\frac{n\pi(x_b+\frac{W_1}{2})}{a}) - \sin\frac{n\pi(x_b-\frac{W_1}{2})}{a}) & n\neq o \end{cases}$$

$$\times ((\frac{\delta_{no}}{k^2} - ((\frac{s\pi}{kL})^2 - 1)(\frac{b}{\pi})^2 \delta(n,s))L\ \delta_{is}$$

$$+ (si)(\frac{\pi}{kL})^2 (1 + (-1)^{(i+s)}) \sum_{\substack{m=o \\ m\neq n=o}}^{\infty} \frac{\epsilon_{om}(1 - (-1)^i e^{-\Gamma_{nm}L})(1 + (\frac{k}{\Gamma_{nm}})^2)}{\Gamma_{nm}^3 (1 + (\frac{s\pi}{\Gamma_{nm}L})^2)(1 + (\frac{i\pi}{\Gamma_{nm}L})^2)}$$

(A2.11)

where x_a, x_b are the offsets for the sections in question. Note the contribution of the m=n=o mode is already included in the ψ_o term and therefore it has been omitted from this solution.

The evaluation of the mutual coupling expression for sections of different lengths is more complicated due to the additional terms in the equation for the magnetic vector potential.

$$\underline{A}_m = - \epsilon_o \sum_{n=o}^{\infty} \sum_{m=o}^{\infty} \frac{\epsilon_{on}\epsilon_{om}}{2ab\Gamma_{nm}} \cos\frac{n\pi x}{a} \int_{x_a - \frac{W_1}{2}}^{x_a + \frac{W_1}{2}} \cos\frac{n\pi x_o}{a}\, dx_o$$

$$\times \left[e^{\Gamma_{nm} Z} \int_{Z}^{\frac{L}{2}} \sin \frac{s\pi(Z_0 + \frac{L_1}{2})}{L_1} e^{-\Gamma_{nm} Z_0} dZ_0 \right.$$

$$+ e^{-\Gamma_{nm} Z} \int_{-\frac{L}{2}}^{Z} \sin \frac{s\pi(Z_0 + \frac{L_1}{2})}{L_1} e^{\Gamma_{nm} Z_0} dZ_0$$

$$+ e^{-\Gamma_{nm} Z} \int_{-\frac{L}{2}}^{-\frac{L_1}{2}} \sin \frac{s\pi(Z_0 + \frac{L_1}{2})}{L_1} e^{\Gamma_{nm} Z_0} dZ_0$$

$$\left. + e^{\Gamma_{nm} Z} \int_{\frac{L}{2}}^{-\frac{L_1}{2}} \sin \frac{s\pi(Z_0 + \frac{L_1}{2})}{L_1} e^{-\Gamma_{nm} Z_0} dZ_0 \right] \qquad \text{(A2.12)}$$

where L_1 is the length of the middle section

L is the length of the outer section

The first integration in the equation is trivial, however, the other four require integration by parts and the resulting expressions are detailed below:

$$\int_{Z}^{\frac{L}{2}} \sin \frac{s\pi(Z_0 + \frac{L_1}{2})}{L_1} e^{-\Gamma_{nm} Z_0} dZ_0$$

$$= \frac{1}{\Gamma_{nm}\left[1 + \left(\frac{s\pi}{L_1 \Gamma_{nm}}\right)^2\right]} \left[e^{-\Gamma_{nm} Z} \left[\sin \frac{s\pi(Z + \frac{L_1}{2})}{L_1} + \left(\frac{s\pi}{\Gamma_{nm} L_1}\right) \cos \frac{s\pi(Z + \frac{L_1}{2})}{L_1} \right] \right.$$

$$- e^{-\Gamma_{nm} - \frac{L}{2}}\left[\sin\frac{s\pi(\frac{L}{2} + \frac{L_1}{2})}{L_1} + (\frac{s\pi}{\Gamma_{mn}L_1})\cos\frac{s\pi(\frac{L}{2} + \frac{L_1}{2})}{L_1}\right]] \qquad \text{(A2.13)}$$

$$\int_{-\frac{L}{2}}^{Z} \sin\frac{s\pi(Z_0 + \frac{L_1}{2})}{L_1} e^{\Gamma_{nm}Z_0} dZ_0$$

$$= \frac{1}{\Gamma_{nm}[1 + (\frac{s\pi}{\Gamma_{nm}L_1})^2]}\left[e^{\Gamma_{nm}Z}\left[\sin\frac{s\pi(Z + \frac{L_1}{2})}{L_1} - (\frac{s\pi}{\Gamma_{nm}l_1})\cos\frac{s\pi(Z + \frac{L_1}{2})}{L_1}\right]\right.$$

$$\left. -e^{-\Gamma_{nm}\frac{L}{2}}\left[\sin\frac{s\pi(\frac{L_1}{2} - \frac{L}{2})}{L_1} + (\frac{s\pi}{\Gamma_{nm}L_1})\cos\frac{s\pi(\frac{L_1}{2} - \frac{L}{2})}{L_1}\right]\right] \qquad \text{(A2.14)}$$

$$\int_{-\frac{L_1}{2}}^{-\frac{L}{2}} \sin\frac{s\pi(Z_0 + \frac{L_1}{2})}{L_1} e^{\Gamma_{nm}Z_0} dZ_0$$

$$= \frac{1}{\Gamma_{nm}[1 + (\frac{s\pi}{\Gamma_{nm}L_1})^2]}\left[e^{-\Gamma_{nm}\frac{L}{2}}\left[\frac{\sin s\pi(\frac{L_1}{2} - \frac{L}{2})}{L_1} - (\frac{s\pi}{\Gamma_{nm}L_1})\frac{\cos s\pi(\frac{L_1}{2} - \frac{L}{2})}{L_1}\right]\right.$$

$$\left. + (\frac{s\pi}{\Gamma_{nm}L_1})e^{-\Gamma_{nm}\frac{L_1}{2}}\right] \qquad \text{(A2.15)}$$

and

$$\int_{\frac{L}{2}}^{\frac{L_1}{2}} \sin \frac{s\pi(Z_o + \frac{L_1}{2})}{L_1} e^{-\Gamma_{nm} Z_o} dZ_o$$

$$= \frac{1}{\Gamma_{nm}\left[1 + \left(\frac{s\pi}{\Gamma_{nm} L_1}\right)^2\right]} \left[e^{-\Gamma_{nm} \frac{L}{2}} \left[\frac{\sin s\pi(\frac{L}{2} + \frac{L_1}{2})}{L} + \left(\frac{s\pi}{\Gamma_{nm} L_1}\right) \frac{\cos s\pi(\frac{L}{2} + \frac{L_1}{2})}{L_1}\right]\right.$$

$$\left. -(-1)^s e^{-\Gamma_{nm} \frac{L_1}{2}} \left(\frac{s\pi}{\Gamma_{nm} L_1}\right)\right] \qquad \text{(A2.16)}$$

Therefore the magnetic vector potential becomes

$$\underline{A}_m = -\frac{\varepsilon_o}{2ab} \sum_{n=o}^{\infty} \sum_{m=o}^{\infty} \frac{\varepsilon_{on}\varepsilon_{om}}{\Gamma_{nm}} \cos \frac{n\pi x}{a} \qquad \text{(A2.17)}$$

$$\times \begin{cases} W_1 & n=o \\ \left(\frac{a}{n\pi}\right)\left(\sin \frac{(x_a + \frac{W_1}{2})}{a} - \sin \frac{n\pi(x_a - \frac{W_1}{2})}{a}\right) & n\neq o \end{cases}$$

$$\times \frac{1}{\Gamma_{nm}\left[1 + \left[\frac{s\pi}{\Gamma_{nm} L_1}\right]^2\right]} \left[2 \sin \frac{s\pi(Z + \frac{L_1}{2})}{L_1} + \left(\frac{s\pi}{L_1 \Gamma_{nm}}\right) e^{-\Gamma_{nm}(Z + \frac{L_1}{2})}\right.$$

$$\left. -\left(\frac{s\pi}{L_1 \Gamma_{nm}}\right)(-1)^s e^{\Gamma_{nm}(Z - \frac{L_1}{2})}\right]$$

and H_z is evaluated by substituting this into equation (4.9) giving

$$H_z = \frac{j\omega\varepsilon_0}{2ab} \sum_{n=0}^{\infty} \sum_{m=0}^{\infty} \frac{\varepsilon_{on}\varepsilon_{om}}{\Gamma_{nm}} \cos\frac{n\pi x}{a} \begin{cases} W_1 & n=0 \\ (\frac{a}{n\pi})(\sin\frac{n\pi(x_a + \frac{W_1}{2})}{a} - \sin\frac{n\pi(x_a - \frac{W_1}{2})}{a}) & n\neq 0 \end{cases}$$

$$\times \frac{1}{\Gamma_{nm}[1 + (\frac{s\pi}{\Gamma_{nm}L_1})^2]} [[1 + (\frac{\Gamma_{nm}}{k})^2][(\frac{s\pi}{\Gamma_{nm}L_1})e^{-\Gamma_{nm}(Z+\frac{L_1}{2})} - (\frac{s\pi}{\Gamma_{nm}L_1})(-1)^s e^{\Gamma_{nm}(Z-\frac{L_1}{2})}]$$

$$+ 2[1 - (\frac{s\pi}{kL_1})^2] \sin\frac{s\pi(Z + \frac{L_1}{2})}{L_1}] \qquad \text{(A2.18)}$$

This is then used in (A.24) which gives

$$- \frac{j\omega\varepsilon_0}{2ab} \sum_{n=0}^{\infty} \sum_{n=0}^{\infty} \frac{\varepsilon_{on}\varepsilon_{om}}{\Gamma_{nm}}$$

$$\times \begin{cases} W_1 & n=0 \\ (\frac{a}{n\pi})^2 [\sin\frac{n\pi(x_a+\frac{W_1}{2})}{a} - \sin\frac{n\pi(x_a-\frac{W_1}{2})}{a}] [\sin\frac{n\pi(x_b+\frac{W_1}{2})}{a} - \sin\frac{n\pi(x_b-\frac{W_1}{2})}{a}] & n\neq 0 \end{cases}$$

$$\times [[1 + (\frac{\Gamma_{nm}}{k})^2][\frac{s\pi}{\Gamma_{nm}L_1}]$$

$$\times [\int_{-\frac{L}{2}}^{\frac{L}{2}} e^{-\Gamma_{nm}(Z + \frac{L_1}{2})} \sin\frac{i\pi(Z + \frac{L}{2})}{L} dZ - (-1)^s \int_{-\frac{L}{2}}^{\frac{L}{2}} e^{\Gamma_{nm}(Z + \frac{L_1}{2})} \sin\frac{i\pi(Z + \frac{L}{2})}{L} dZ]$$

$$+ 2[1 - (\frac{s\pi}{kL_1})^2] \int_{-\frac{L}{2}}^{\frac{L}{2}} \sin\frac{i\pi(Z + \frac{L}{2})}{L} \sin\frac{s\pi(Z + \frac{L_1}{2})}{L_1} dZ] \qquad \text{(A2.19)}$$

and the three integrals in this expression are evaluated as follows:

$$\int_{-\frac{L}{2}}^{\frac{L}{2}} e^{-\Gamma_{nm}(Z + \frac{L_1}{2})} \sin \frac{i\pi(Z + \frac{L}{2})}{L} dZ \qquad \text{(A2.20)}$$

$$= \frac{(\frac{i\pi}{L\Gamma_{nm}})}{\Gamma_{nm}[1 + (\frac{i\pi}{L\Gamma_{nm}})^2]} [e^{-\Gamma_{nm}(\frac{L_1}{2} - \frac{L}{2})} - (-1)^i e^{-\Gamma_{nm}(\frac{L}{2} + \frac{L_1}{2})}]$$

$$\int_{-\frac{L}{2}}^{\frac{L}{2}} e^{\Gamma_{nm}(Z - \frac{L_1}{2})} \sin \frac{i\pi(Z + \frac{L}{2})}{} dZ \qquad \text{(A2.21)}$$

$$= \frac{(\frac{i\pi}{L\Gamma_{nm}})}{\Gamma_{nm}[1 + (\frac{i\pi}{L\Gamma_{nm}})^2]} [e^{-\Gamma_{nm}(\frac{L_1}{2} + \frac{L}{2})} - (-1)^i e^{-\Gamma_{nm}(\frac{L_1}{2} - \frac{L}{2})}]$$

and

$$\int_{-\frac{L}{2}}^{\frac{L}{2}} \sin \frac{i\pi(Z + \frac{L}{2})}{L} \sin \frac{s\pi(Z + \frac{L_1}{2})}{L_1} dZ \qquad \text{(A2.22)}$$

$$= \frac{iL_1^2}{s^2\pi L} \frac{[(-1)^i \sin \frac{s\pi(\frac{L}{2} + \frac{L_1}{2})}{L_1} - \sin \frac{s\pi(\frac{L_1}{2} - \frac{L_1}{2})}{L_1}]}{[1 - (\frac{iL_1}{sL})^2]}$$

Substituting (A2.20) to (A2.22) into (A2.19) and employing Collin's work on series gives the final expression as

$$\frac{-j\omega\epsilon_0}{2ab}\sum_{n=1}^{\infty}\begin{cases}W_1\\ \left(\frac{a}{n\pi}\right)^2\end{cases}\left(\sin\frac{n\pi\left(x_a+\frac{W_1}{2}\right)}{a}-\sin\frac{n\pi\left(x_a-\frac{W_1}{2}\right)}{a}\right)$$

$$\times\left(\sin\frac{n\pi\left(x_b+\frac{W_1}{2}\right)}{a}-\sin\frac{n\pi\left(x_b-\frac{W_1}{2}\right)}{a}\right)\begin{cases}\\ \\ \end{cases}\begin{cases}n=0\\ \\ n\neq 0\end{cases}$$

$$\times\left[\frac{2\left(\frac{iL_a^2}{s^2\pi L_b}\right)}{\left[1-\left(\frac{iL_a}{sL_b}\right)^2\right]}\left((-1)^i\sin\frac{s\pi\left(\frac{L_a}{2}+\frac{L_b}{2}\right)}{L_a}-\sin\frac{s\pi\left(\frac{L_a}{2}-\frac{L_b}{2}\right)}{L_a}\right)\right.$$

$$\left.\times\left(\frac{b}{\pi}\right)^2\left[1-\left(\frac{S\pi}{kL_a}\right)^2\right]Y(n,s)\right. \qquad \text{(A2.23)}$$

$$+\left(\frac{si\pi^2}{L_aL_b}\right)\sum_{m=0}^{\infty}\frac{\epsilon_{om}\left[1+\left(\frac{\Gamma_{nm}}{k}\right)^2\right]}{\Gamma_{nm}{}^s\left[1+\left(\frac{s\pi}{\Gamma_{nm}L_a}\right)^2\right]\left[1+\left(\frac{i\pi}{\Gamma_{nm}L_b}\right)^2\right]}\left[\left(e^{-\Gamma_{nm}\left(\frac{L_a}{2}-\frac{L_b}{2}\right)}\right.\right.$$

$$-(-1)^i e^{-\Gamma_{nm}\left(\frac{L_a}{2}+\frac{L_b}{2}\right)})-(-1)^s\left(e^{-\Gamma_{nm}\left(\frac{L_a}{2}+\frac{L_b}{2}\right)}\right.$$

$$\left.\left.-(-1)^i e^{-\Gamma_{nm}\left(\frac{L_a}{2}-\frac{L_b}{2}\right)}\right)\right]\Big]$$

where L_a, L_b are the lengths of the appropriate sections,

and x_a, x_b are the offsets of the appropriate sections for the mutual coupling for sections of different lengths.

APPENDIX 3

PUBLISHED PAPERS

INT. J. ELECTRONICS, 1987, VOL. 62, NO. 5, 641–662

Invited paper

Some observations on the computer-aided design/synthesis of slotted-waveguide antennas

A. J. SANGSTER† and A. H. I. McCORMICK†

Planar array antennas which are formed by stacking together two or more linear slotted-waveguide arrays are widely used in radar systems. These arrays are becoming increasingly amenable to comprehensive computer-aided design and synthesis procedures, since the scattering characteristics of apertures in waveguide can now be predicted to a high degree of accuracy. This paper reviews the three most useful theoretical methods of determining slot characteristics and examines the advantages and disadvantages of the different methods for use in computer-aided design programmes.

1. Introduction

Design, or synthesis, procedures for waveguide fed slot arrays, if they are to provide reliable results are heavily dependent on the availability of accurate values for the self-impedances of slot radiators in waveguide (Elliott 1978). The mutual impedances for arrays of narrow slots can be determined by the method of Baker and Lagrone (1962), if the slot distribution for the planar slot array is known. For planar slotted-waveguide arrays comprising shunt-slotted, or series inclined-slotted waveguides the current design practice is to employ measured results from which self-impedances can be deduced. The array synthesis can then proceed using interpolation where necessary between the measured values.

However this reliance on measured results means that such a synthesis technique is intrinsically inflexible permitting the examination only of those array geometries which comprise slots for which measured results exist. Ideally therefore a synthesis procedure is required which is not measurement based. This in turn means that an analytical method of sufficient accuracy must be constructed to provide the required self-impedance data for slot radiators in waveguide. In this paper the predominant methods which are available for the analysis of apertures in waveguide are examined from the viewpoint of array synthesis. This requirement reduces the examination to three realistic alternatives. These are the diffraction method originally propounded by Bethe (1944), the variational method (Levine and Schwinger 1950, Oliner 1957, Sangster and Hawkins 1972) and the moment method (Harrington 1968, Vu Khac and Carson 1973, Lyon and Sangster 1981).

The diffraction method has the attractive computer-aided design feature that it provides relatively simple closed form expressions for the desired aperture parameters. In its original form it was applicable only to small apertures in an infinitesimally thin conducting wall. However modifications which have been introduced

Received 10 July 1986; accepted 27 October 1986.

† Department of Electrical and Electronic Engineering, Heriot-Watt University, Edinburgh, U.K.

over the intervening years, notably by Cohn (1952a), Levy (1968, 1980), McDonald (1972), Collin (1981) and Van Bladel (1971), have permitted extensions of the method to apertures which are no longer 'small', in waveguide walls of finite thickness. The essential features of the Bethe method are summarized in § 2, which also shows how the various modifications mentioned above have been implemented. Tables and appendices highlighting those formulae which are particularly relevant to the computer-aided design of slot arrays are provided for two typical slot geometries.

The variational method is an intrinsically more general mathematical technique than that of Bethe, and has been used for the analysis of a variety of waveguide obstacles. It was first applied successfully to apertures in waveguide by Oliner (1957). Other significant contributions to the solution of the aperture problem which have employed this technique are given in Sangster and Hawkins (1972) and Das and Sanyal (1970). The variational method also produces closed-form expressions for the scattering parameters of a slot discontinuity in waveguide, and these are presented in equivalent circuit form for two typical slot geometries in Appendices 2 and 3. The primary weakness of this method probably lies in its inability to take account of waveguide wall thickness except through a correction factor similar to that suggested by Cohn (1952a) for small apertures. A correction factor has also been implemented by Oliner for resonant or near-resonant slots but the results are not entirely satisfactory.

The moment method, for the analysis of electromagnetic scattering, is of relatively recent development and much of the early work can largely be attributed to Harrington (1968). It has been applied with some success to waveguide aperture problems (Vu Khac and Carson 1973, Lyon and Sangster 1981). Elliott (1978) has suggested that this method probably provides the most promising route to a synthesis procedure for slot-arrays, particularly when these are required to meet stringent specifications. The method is summarized in § 4.

Finally a quantitiative assessment of the accuracy of the three methods in predicting both the equivalent circuit element values, and also the power radiated, for some typical slot geometries is made in § 5. Some comparisons with measured results are included.

2. Small aperture diffraction theory

The small aperture diffraction theory which was formulated some 40 years ago by Bethe has formed the basis for the design of many microwave devices in the intervening years. Inevitably the method has been modified and improved during this period and it is the purpose of this section to enunciate the significant changes which have been made and thence provide a summary of the formulae which are currently in use for radiating slots in rectangular waveguide.

Apertures in rectangular waveguide have formed the 'building blocks' of microwave filters and couplers, and of microwave antennas when coupled to 'free space'. By the application of an equivalence principle which permits the aperture to be represented by a magnetic current sheet $\mathbf{J}_m$, and by employing the Lorentz reciprocity principle, Collin, using Bethe's basic method, has shown that for small aper-

	$\alpha_{m\xi}$	$\alpha_{m\zeta}$	$\alpha_{e\eta}$
Circular	$(8/3)r^3$	$(8/3)r^3$	$-(4/3)r^3$
Elliptical			
$\epsilon = (1-(w/l)^2)^{1/2}$	$\frac{2\pi}{3}\frac{lw^2\epsilon^2}{(1-\epsilon^2)(F-E)}$	$\frac{2\pi}{3}\frac{lw^2\epsilon^2}{E-(1-\epsilon^2)F}$	$-\frac{2\pi}{3}\frac{lw^2}{E}$
Long narrow			
ellipse ($l \gg w$)	$\frac{2\pi}{3}\frac{l^3}{\left\{\ln\left(\frac{4l}{w}\right)-1\right\}}$	$\frac{2\pi}{3}lw^2$	$-\frac{2\pi}{3}lw^2$

Aperture polarizabilities.

tures internal scattering can be represented by an integral equation of the form

$$\iint_{s_a} \mathbf{H}_n^+ \cdot \mathbf{J}_m \, dA = j\omega[\mu_0 \mathbf{H}_n^+ \cdot \mathbf{M} - \mathbf{E}_n^+ \cdot \mathbf{P}] \tag{1}$$

where $\mathbf{E}_n$ and $\mathbf{H}_n$ are the electric and magnetic field components of the nth normal mode of the waveguide. $\mathbf{M}$ is the magnetic dipole moment for the aperture and is given by

$$\mathbf{M} = -\frac{1}{j\omega\mu_0}\iint_{s_a} \mathbf{r}\nabla \cdot \mathbf{J}_m \, dA \tag{2}$$

where s_a denotes the surface area of the aperture and $\mathbf{r}$ is a vector denoting a point within the aperture. $\mathbf{P}$ is the electric dipole moment for the aperture and is given by

$$\mathbf{P} = -\frac{\epsilon_0}{2}\iint_{s_a} \mathbf{r} \times \mathbf{J}_m \, dA \tag{3}$$

For apertures of regular shape the above integral expressions for $\mathbf{M}$ and $\mathbf{P}$ have been evaluated by a number of authors. These evaluations are normally expressed in the form of aperture electric and magnetic dyadic polarizabilities $\tilde{\alpha}_e$ and $\tilde{\alpha}_m$ respectively. These are generally more useful quantities for defining the coupling strength of an aperture since they are dependent only on aperture shape and size. The relationships between $\mathbf{M}$, $\mathbf{P}$, $\tilde{\alpha}_m$ and $\tilde{\alpha}_e$ are usually expressed in the form

$$\mathbf{M} = \tilde{\alpha}_m \cdot \mathbf{H} \tag{4}$$

$$\mathbf{P} = \epsilon_0 \tilde{\alpha}_e \cdot \mathbf{E} \tag{5}$$

where for apertures in a waveguide wall $\mathbf{E}$ and $\mathbf{H}$ are the fields of the incident waveguide mode at the position of the aperture. For apertures of circular or elliptical shape theoretical values for the components of $\tilde{\alpha}_m$ and $\tilde{\alpha}_e$ are available (Van Bladel 1971). These are tabulated in the Table for an ellipse with its major axis lying along ξ and its minor axis lying along ζ of a ξ, η, ζ coordinate system.

In the Table, r denotes the circular aperture radius, while w and l represent half the width and length of the ellipse respectively. F and E are the complete elliptical

integrals of the first and second kind and are given by

$$F(\epsilon) = \int_0^{\pi/2} \frac{d\phi}{(1 - \epsilon^2 \sin^2 \phi)^{1/2}} \tag{6}$$

$$E(\epsilon) = \int_0^{\pi/2} (1 - \epsilon^2 \sin^2 \phi)^{1/2}\, d\phi \tag{7}$$

ϵ is the eccentricity of the ellipse.

The polarizability values quoted in the Table apply to the problem which is relevant here, namely that of a waveguide fed aperture radiating into a half-space. Values for $\alpha_{m\xi}$, $\alpha_{m\zeta}$ and $\alpha_{e\eta}$ can be found in the literature which disagree with those quoted above usually by a factor of two or four (Collin 1960, Montgomery 1947, Harvey 1963, Rahmat-Samii 1977). However, these differences can usually be attributed to differences in the excitation or radiation conditions (e.g. half-space to half-space rather than waveguide to half-space).

Polarizability values for apertures having shapes which are other than elliptical or circular can be found in Cohn (1951, 1952b) who has produced accurately measured values for a range of useful aperture shapes. These agree with the Bethe/Collin theoretical values where comparison can be made. For waveguide to half-space problems, however, the Cohn polarizability values require to be incremented by a factor of two.

The Bethe/Collin analysis enunciated above has some serious deficiencies when contemplating its use as a design tool for most practical devices. This is because firstly the small aperture requirement is hardly ever maintained in practice and secondly the aperture is never located in a wall of zero thickness. To overcome the first of these difficulties Levy has postulated that, for slots, the magnetic polarisability be modified by the following factor

$$C_f = \frac{\tan \pi f/2f_0}{\pi f/2f_0} \tag{8}$$

where f_0 is the frequency at which the slot resonates. This is given by $2l = \lambda_0/2$. f is the operating frequency.

The influence of wall thickness on aperture polarizability has been studied by several contributors notably Cohn (1952a), Levy (1968) and McDonald (1972). The general approach is to view the aperture as a very short cut-off waveguide operating in its dominant mode. For a slot this implies the TE_{10} mode, and hence the following correction factor can readily be deduced

$$C_T = \exp\left\{\frac{-2\pi t A}{\lambda_c}((1 - \lambda_c^2/\lambda^2))^{1/2}\right\} \tag{9}$$

where t is the wall thickness, λ_c is the cut-off wavelength of the slot-guide, and λ is the free-space wavelength at the operating frequency. For slots and circular holes the correction factor A has been determined to a high accuracy by McDonald. Using these results, Levy has deduced the following simple relationship between A and t for a circular hole of radius r, namely

$$At = 1{\cdot}0064t + 0{\cdot}0819r \quad (t > 0{\cdot}2r) \tag{10}$$

For narrow slots, an equivalently simple relationship has yet to be formulated, and consequently the appropriate value of A requires to be read directly from McDonald's curves, when the correction factor C_f is being used.

In a recent contribution due to Levy (1980) it has been demonstrated that when applied to waveguide or cavity coupling problems the condition of uniform field over the coupling aperture, which is strictly required by the small aperture method, is not usually satisfied. Levy suggests that this difficulty can be greatly minimized by field averaging. This leads to the following correction factors for two typical cases.

(*a*) For a centrally located transverse slot in the broadwall of rectangular waveguide

$$C_{av} = \frac{1}{2}\left[1 + \frac{\sin\dfrac{2\pi l}{a}}{\dfrac{2\pi l}{a}}\right] \tag{11}$$

where $2l$ is the slot length and a is the waveguide width.

(*b*) For an offset longitudinal slot in the broadwall rectangular waveguide

$$C_{av} = \frac{1}{2}\left[1 + \frac{\sin\dfrac{4\pi l}{\lambda g}}{\dfrac{4\pi l}{\lambda g}}\right] \tag{12}$$

where λg is the guide wavelength.

When the correction factors are incorporated into the Bethe analysis the appropriate forms for the slot polarizabilities are

$$\tilde{\alpha}_m^{(c)} = C_f C_T C_{av} \tilde{\alpha}_m \tag{13}$$

$$\tilde{\alpha}_e^{(c)} = C_f C_T C_{av} \tilde{\alpha}_e \tag{14}$$

However for radiation problems, which particularly concern us here, the requirement for power conservation (Collin 1981, Cheng 1982) dictates that the components of the polarizability dyadics be modified in the following way: magnetic polarizability becomes

$$\alpha_{m\xi}^{(p)} = \frac{\alpha_{m\xi}^{(c)}}{\left\{1 + j\,\dfrac{2k_0^3\,\alpha_{m\xi}^{(c)}}{3\pi}\right\}} \tag{15}$$

for the ξ component, and similarly for the ζ component: electric polarizability becomes

$$\alpha_{e\eta}^{(p)} = \frac{\alpha_{e\eta}^{(c)}}{\left\{1 - j\,\dfrac{2k_0^3\,\alpha_{e\eta}^{(c)}}{3\pi}\right\}} \tag{16}$$

for the η component, or any other component if such components occur.

$\tilde{\alpha}_m^{(p)}$ and $\tilde{\alpha}_e^{(p)}$ thus represent the most fully corrected polarizability formulae currently available to us, and they have provided a basis for the synthesis of antenna arrays of moderate capability.

To implement a synthesis procedure for an antenna array of the slotted waveguide type it is generally desirable to express the internal scattering properties of a given slot arrangement by means of an L, R, G, C equivalent circuit. Formulae for the inductance L, series resistance R, parallel conductance G and capacitance C, expressed in terms of aperture polarizabilities and normalized to the waveguide impedance Z_g, have been generated by Van Bladel (1971) for a number of typical slot geometries. Power radiated expressions describing the external behaviour of such slots have also been evolved from small aperture theory by Van Bladel. A summary of these results is produced in Appendix 1.

3. Variational method

In the previous section it was shown that an aperture in waveguide produces electromagnetic scattering both internally and externally and that the scattering into the nth mode can be expressed in terms of integrals of the form

$$\iint_{S_a} \mathbf{J}_m \cdot \mathbf{H}_n^+ \, da = \iint_{S_a} \mathbf{n} \times \mathbf{E}_s \cdot \mathbf{H}_n^+ \, da \tag{17}$$

for scattering in the forward (+ve) direction in the nth mode of the waveguide. $\hat{\mathbf{n}}$ is a unit normal to the aperture surface and $\mathbf{E}_s$ is the unknown electric field in the plane of the aperture. To generate the total scattered field at any position within the waveguide it will obviously be necessary to perform a summation over all possible modes. Such a summation can be achieved by employing an appropriate Green's function for the waveguide. If the magnetic dyadic Green's function for the waveguide, $\tilde{G}_h(\mathbf{r}/\mathbf{r}_0)$, is chosen it is not difficult to show that the above integral, with $\tilde{G}_h(\mathbf{r}/\mathbf{r}_0)$ in place of $\mathbf{H}_n^+(\mathbf{r})$, represents the total magnetic field scattered by the aperture at any position ($\mathbf{r} \rightarrow x, y, z$) within the guide (region 1). More specifically,

$$\mathbf{H}_1(\mathbf{r}) = j\omega\epsilon_0 \iint_{S_a} \mathbf{n} \times \mathbf{E}_s(\mathbf{r}_0) \cdot \tilde{G}_h(\mathbf{r}/\mathbf{r}_0) \, da_0 \tag{18}$$

$\mathbf{r}_0 (\rightarrow (x_0, y_0, z_0))$ denotes position within the aperture. If, alternatively, the magnetic dyadic Green's function for the external half-space (region 2), namely $\tilde{G}_h^{(2)}(\mathbf{r}/\mathbf{r}_0)$, is used, we find that the magnetic field of the externally scattered electromagnetic energy can be expressed as

$$\mathbf{H}_2(\mathbf{r}) = -j\omega\epsilon_0 \iint_{S_a} \mathbf{n} \times \mathbf{E}_s(\mathbf{r}_0) \cdot \tilde{G}_h^{(2)}(\mathbf{r}/\mathbf{r}_0) \, da_0 \tag{19}$$

By applying magnetic field boundary conditions at the surface of the aperture, an integral equation can be formed which is amenable to the variational method (1972). In this way variational expressions can be formulated for any of the scattering parameters of the aperture. Equally, variational expressions for the elements of an equivalent circuit representation of the aperture can similarly be evolved (Oliner 1957, Sangster and Hawkins 1972, Sangster 1965, Stevenson 1948).

These variational formulations invariably contain ratios of the form

$$\frac{\left[\iint_{s_a} \mathbf{H}^{t}_{1o(r)} \cdot \mathbf{n} \times \mathbf{E}_s(\mathbf{r})\, da\right]^2}{\iint_{s_a}\iint_{s_a} \mathbf{n} \times \mathbf{E}_s(\mathbf{r}) \cdot \bar{G}_h(\mathbf{r}/\mathbf{r}_0) \cdot \mathbf{n} \times \mathbf{E}_s(\mathbf{r}_0)\, da\, da_0} \tag{20}$$

If a 'good' approximation is available for the trial field $\mathbf{E}_s$ the variational formulation provides a result for the quantity of interest which is an order more accurate than the original 'trial'. Furthermore if the trial field has a 'simple' functional form which permits direct evaluation of the integrals, closed form expressions for the scattering parameters or equivalent circuit parameters become available. This situation arises when narrow rectangular apertures are employed for which a cosinusoidal field distribution represents an accurate trial form.

Most of the common slot geometries have been investigated using the variational method particularly by Oliner (1957) and by Sangster and Hawkins (1972). Closed form formulae for the equivalent circuit representations of a longitudinal off-set and a transverse slot in the broadwall of rectangular waveguide are presented in Appendices 2 and 3. A closed form power radiated formula for these slot geometries, or for any inclined, off-set broadwall slot in rectangular waveguide, is given in Appendix 4. It should be emphasized here that the variational solution described above is strictly applicable to a two region problem in which the regions are separated by a conducting screen of infinitesimal thickness. In practice, however, the dividing wall in the slotted-waveguide problem is of finite thickness and this must somehow be accommodated within the analysis. It has been found from experience that this can best be done by employing the C_T factor used in small aperture theory and applying it directly to Oliner's 'power radiated' expression. The effect of this modification on the variational formulae for scattering by an aperture in waveguide is indicated in the appendices.

An important criterion which has governed the presentation of the formulae in the Table and Appendices 1–4, has been that demonstrable agreement between the two methods should exist where valid comparisons can be made. For example, for slots for which w/l is small and for which $l \to 0$, the variational solutions should reduce asymptotically to those of diffraction theory. It is not difficult to show that this is in fact so in all cases where direct comparison can be made and when the appropriate definition for aperture polarizability is employed in the Bethe method.

4. Moment method

The moment method (1968) is a relatively new technique for the analysis of electromagnetic boundary value problems of the slotted waveguide (Vu Khac and Carson 1973, Lyon and Sangster 1981) and other types. It exhibits many similarities to the variational method described in the previous section. However, whereas in the variational method use is made of some 'stationary' property of the scattered fields, (when the 'trial field' in the aperture is close to its exact value), to effect a solution to the integral equation which the discontinuity problem generates, in the moment method a more direct approach is employed. This is achieved by postulating that the unknown aperture field can be represented functionally by a series of basis functions. This results in the reduction of the integral equations to a set of

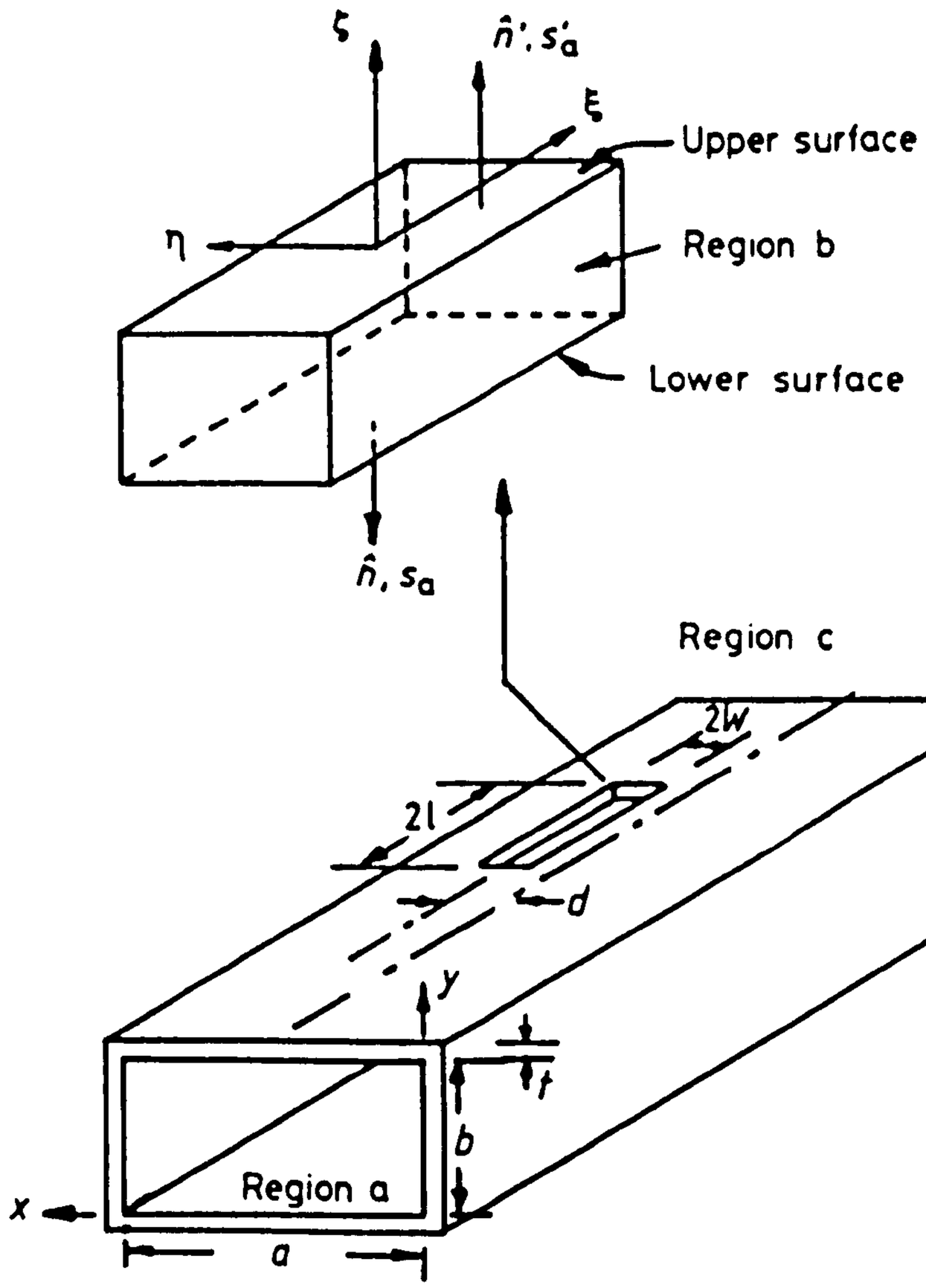

Figure 1. Coordinate system of slotted waveguide with exploded view of slot. (Region a is the waveguide interior, region b is the slot interior, and region c is the half-space into which the slot radiates).

simultaneous equations whose solutions can usually be attained by resorting to matrix manipulation procedures on a high speed digital computer.

A distinct advantage of the moment method over other methods for analysing waveguide aperture problems is that it is not restricted to the two-region problem previously enunciated. Coupling between three or more regions can be considered (Lyon and Sangster 1981) which means that the 'thick wall' problem can be handled in a more natural way.

By employing an equivalence principle the aperture in a thick wall separating a waveguide region and a half-space can be represented as in Fig. 1. If the magnetic dyadic Green's function for each of the three regions shown in this figure is known then, from § 3 we know that the magnetic field scattered by the unknown magnetic currents can be expressed through integrals of the form

$$\mathbf{H}(\mathbf{r}) = j\omega\epsilon_0 \iint_{S_a} \bar{G}_h(\mathbf{r}/\mathbf{r}_0) \cdot \mathbf{J}_m(\mathbf{r}_0)\, da_0 \tag{21}$$

where $\bar{G}_h$ may be $\bar{G}_h^{(a)}$ or $\bar{G}_h^{(b)}$ or $\bar{G}_h^{(c)}$ and $J_m = \pm \mathbf{n} \times \mathbf{E}$ or $\pm \mathbf{n} \times \mathbf{E}'$ as appropriate.

On application of the boundary conditions at the upper and lower surfaces of the aperture the following integral equations result

$$\mathbf{n} \times \mathbf{H}_i(\mathbf{r}) = j\omega\epsilon_0 \mathbf{n} \times \iint_{s_a} [\bar{G}_h^{(a)}(\mathbf{r}/\mathbf{r}_0) + \bar{G}_h^{(b)}(\mathbf{r}/\mathbf{r}_0)] \cdot \mathbf{n} \times \mathbf{E}(\mathbf{r}_0)\, da_0 + j\omega\epsilon_0 \mathbf{n} \times \iint_{s_a'} \bar{G}_h^{(b)}(\mathbf{r}/\mathbf{r}_0) \cdot \mathbf{n}' \times \mathbf{E}'(r_0)\, da_0 \quad (\mathbf{r} \text{ on } s_a) \tag{22}$$

$$0 = j\omega\epsilon_0 \mathbf{n} \times \iint_{s_a'} [\bar{G}_h^{(b)}(\mathbf{r}/\mathbf{r}_0) + \bar{G}_h^{(c)}(\mathbf{r}/\mathbf{r}_0)] \cdot \mathbf{n}' \times E'(\mathbf{r}_0)\, da_0 + j\omega\epsilon_0 \mathbf{n}' \times \iint_{s_a} \bar{G}_h^{(b)}(\mathbf{r}/\mathbf{r}_0) \cdot \mathbf{n}' \times E(\mathbf{r}_0)\, da_0 \quad (\mathbf{r} \text{ on } s_a') \tag{23}$$

where s_a, s_a', $\mathbf{n}$ and $\mathbf{n}'$ are defined in Fig. 1 and $\mathbf{H}_i(\mathbf{r})$ denotes the magnetic field component of the TE_{10} incident wave in the waveguide (region a). A moment method solution to the above integral equations requires, firstly, that the unknown aperture fields $\mathbf{E}$ and $\mathbf{E}'$ be expressed as a series of functionals. For example we may write

$$\mathbf{n} \times \mathbf{E} = \mathbf{n} \times \sum_{s=1}^{N} a_s f_s \mathbf{a}_\eta \quad \text{on } s_a \tag{24}$$

and

$$\mathbf{n}' \times \mathbf{E}' = \mathbf{n}' \times \sum_{s=1}^{N} b_s f_s \mathbf{a}_\eta \quad \text{on } s_a' \tag{25}$$

where $\mathbf{a}_\eta$ is the unit vector in the η-direction of the slot coordinate system. Fig. 1. A suitable form for the functionals $f_s(\xi)$ is (Lyon and Sangster 1981)

$$f_s(\xi) = \sin\left\{\frac{s\pi(\xi + l)}{2l}\right\} \tag{26}$$

Hence by following Galerkin's method which involves the use of testing functions, which are identical to the basis functions, and a suitable 'inner product', the integral equations are converted to the following matrix form

$$\begin{bmatrix} [A] & [C] \\ [B] & [D] \end{bmatrix} \begin{bmatrix} [a] \\ [b] \end{bmatrix} = \begin{bmatrix} [h] \\ [o] \end{bmatrix} \tag{27}$$

where

$$A_{is} = -j\omega\epsilon_0 \iint_{s_a} f_i \mathbf{a}_\eta \cdot \left[\mathbf{n} \times \iint_{s_a} [G_h^{(a)}(\mathbf{r}/\mathbf{r}_0) + G_h^{(b)}(\mathbf{r}/\mathbf{r}_0)] \cdot f_s \mathbf{a}_\xi\, da_0\right] da \tag{28}$$

$$B_{is} = -j\omega\epsilon_0 \iint_{s_a'} f_i \mathbf{a}_\eta \cdot \left[\mathbf{n}' \times \iint_{s_a} [\bar{G}_h^{(b)}(\mathbf{r}/\mathbf{r}_0) + \bar{G}_h^{(c)}(\mathbf{r}/\mathbf{r}_0)] \cdot f_s \mathbf{a}_\xi\, da_0\right] da \tag{29}$$

$$C_{is} = +j\omega\epsilon_0 \iint_{s_a} f_i \mathbf{a}_\eta \cdot \left[\mathbf{n} \times \iint_{s_a'} \bar{G}_h^{(b)}(\mathbf{r}/\mathbf{r}_0) \cdot f_s \mathbf{a}_\xi\, da_0\right] da \tag{30}$$

$$D_{in} = j\omega\epsilon_0 \iint_{s_n'} f_i \mathbf{a}_\eta \cdot \left[\mathbf{n}' \times \iint_{s_n} \bar{G}_h^{(b)}(\mathbf{r}/\mathbf{r}_0) \cdot f_\xi \mathbf{a}_\xi \, da_0 \right] da \tag{31}$$

$$h_i = - \iint_{s_n} f_i \mathbf{a}_\eta \cdot \mathbf{n} \times \mathbf{H}_i(\mathbf{r}) \, da \tag{32}$$

The above matrix equation has been solved for the case of narrow slot radiators, in the broadwall of rectangular waveguides, for which sinusoidal basis and testing functions are appropriate. Expressions for the internal scattering parameters s_{11} and s_{12} and for the radiated power of a transverse and a longitudinal off-set example are presented in Appendices 5 and 6.

It is important to note here that when operating the above system of equations, the waveguide Green's function should contain the ψ = constant mode recently described by Van Bladel (1981) otherwise unexpected errors can occur in the vicinity of resonance for some slot arrangements (Lyon and Hizal 1983).

5. Comparison of some theoretical and experimental results

The three methods of analysis enunciated in preceding sections have been used to provide some computed results depicting the electromagnetic scattering produced by typical slot radiators located in the broadwall of a rectangular waveguide. While these computations give a clear indication of the substantial agreement which exists between the three methods some particular differences are also highlighted.

In Fig. 2, the normalized radiated power is plotted as a function of slot length for a centrally located transverse slot in the broadwall of a rectangular waveguide whose walls are assumed to be infinitesimally thin. The figure clearly shows that in the non-resonant range of slot lengths, namely $2l \leqq 0{\cdot}4\,\lambda$, the small aperture and variational theories are in close agreement. However, while the small aperture theory is obviously limited in its application to slots in this non-resonant range, the variational method is usable up to resonance and beyond. For this zero thickness wall case, the variational method predicts that resonance occurs where $2l = 0{\cdot}465\,\lambda$, whereas the moment method gives a value of $2l = 0{\cdot}445\,\lambda$; a 5% discrepancy. This deviation can largely be attributed to the closed form approximations employed in the variational method which require that the functional form of the slot field be a simple sinusoid. The aperture field in the moment method was formed from three odd-order sinusoidal basis functions. For below resonant slots, Fig. 2 also shows that the moment method predicts lower values of radiated power (of the order of 2 dB down at 6 mm) than does the variational method. This difference is partly due to the closed form simplifications mentioned above but also partly due to the three region nature of the moment method, which prohibits the assumption of a truly zero thickness wall (0·01 mm was used in these calculations).

The above observations are also true for an off-set longitudinal slot in the zero-thickness broadwall of a rectangular waveguide, when the off-set is large. This can be seen from an examination of Fig. 3.

When the above slot examples are now located in a waveguide with walls of finite thickness, namely $t = 1$ mm, the differences between the methods become more

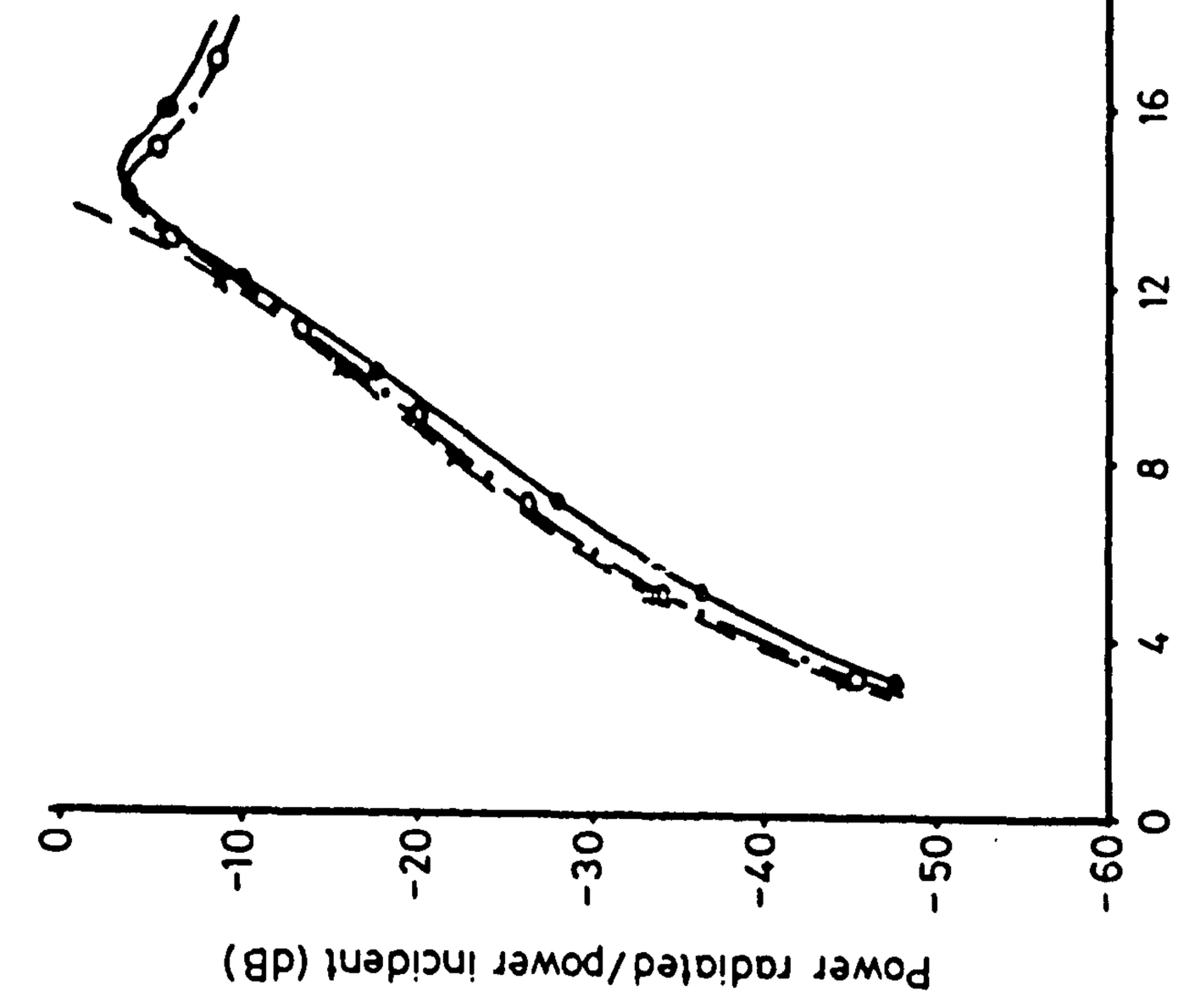

Slot width = 1·5 mm, off-set = 9·43 mm,
wall thickness = 0·0 mm, frequency = 10 GHz.
– – – – Small aperture method
—·— Variational method
——— Moment method

Figure 3. Normalized power radiated versus slot length for a longitudinal slot in the broadwall of a rectangular waveguide.

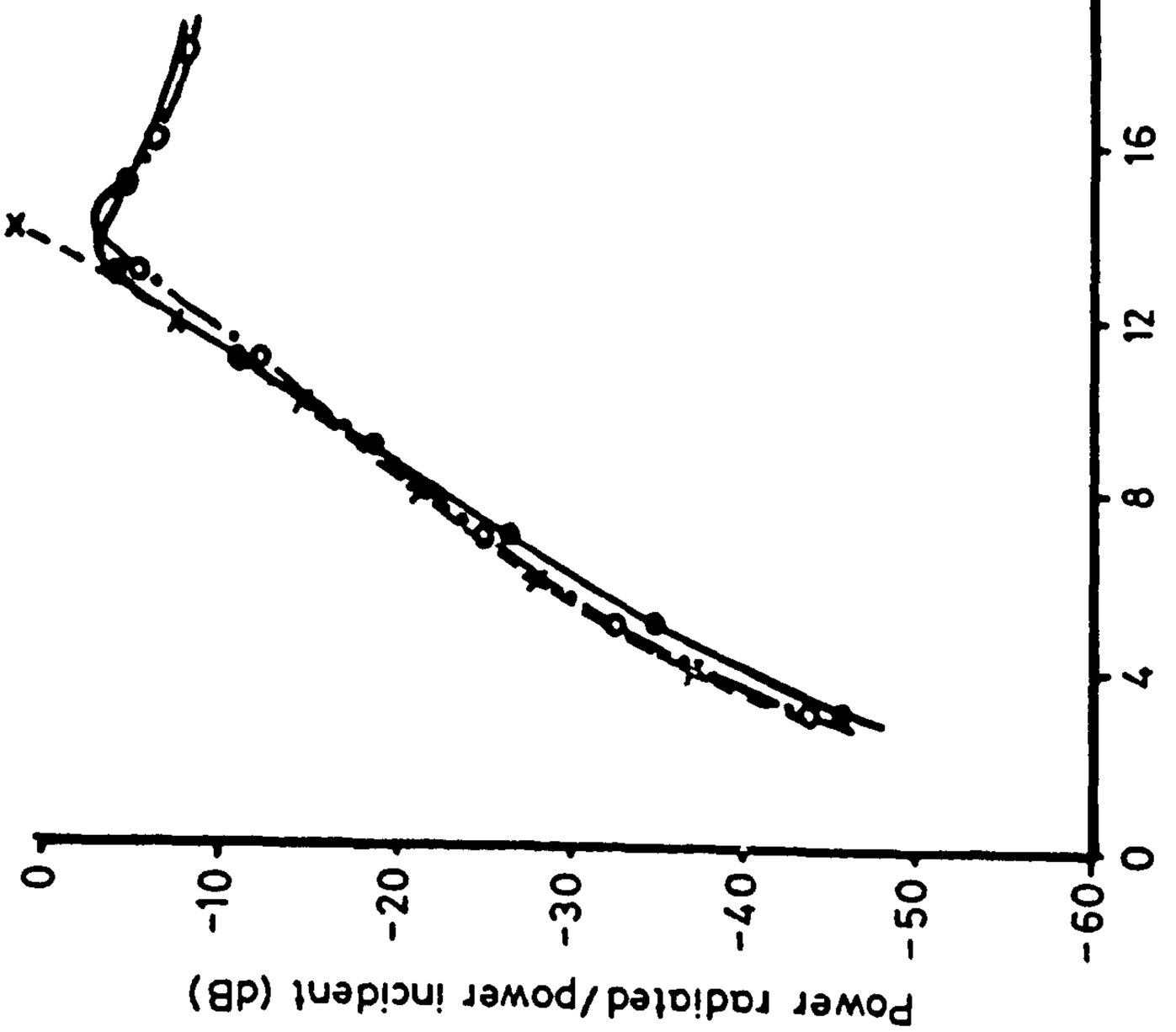

Slot width = 1·5 mm, off-set = 0·0 mm,
wall thickness = 0·0 mm, frequency = 10 GHz.
– – – – Small aperture method
—·— Variational method
——— Moment method

Figure 2. Normalized power radiated versus slot length for a transverse slot in the broadwall of a rectangular waveguide.

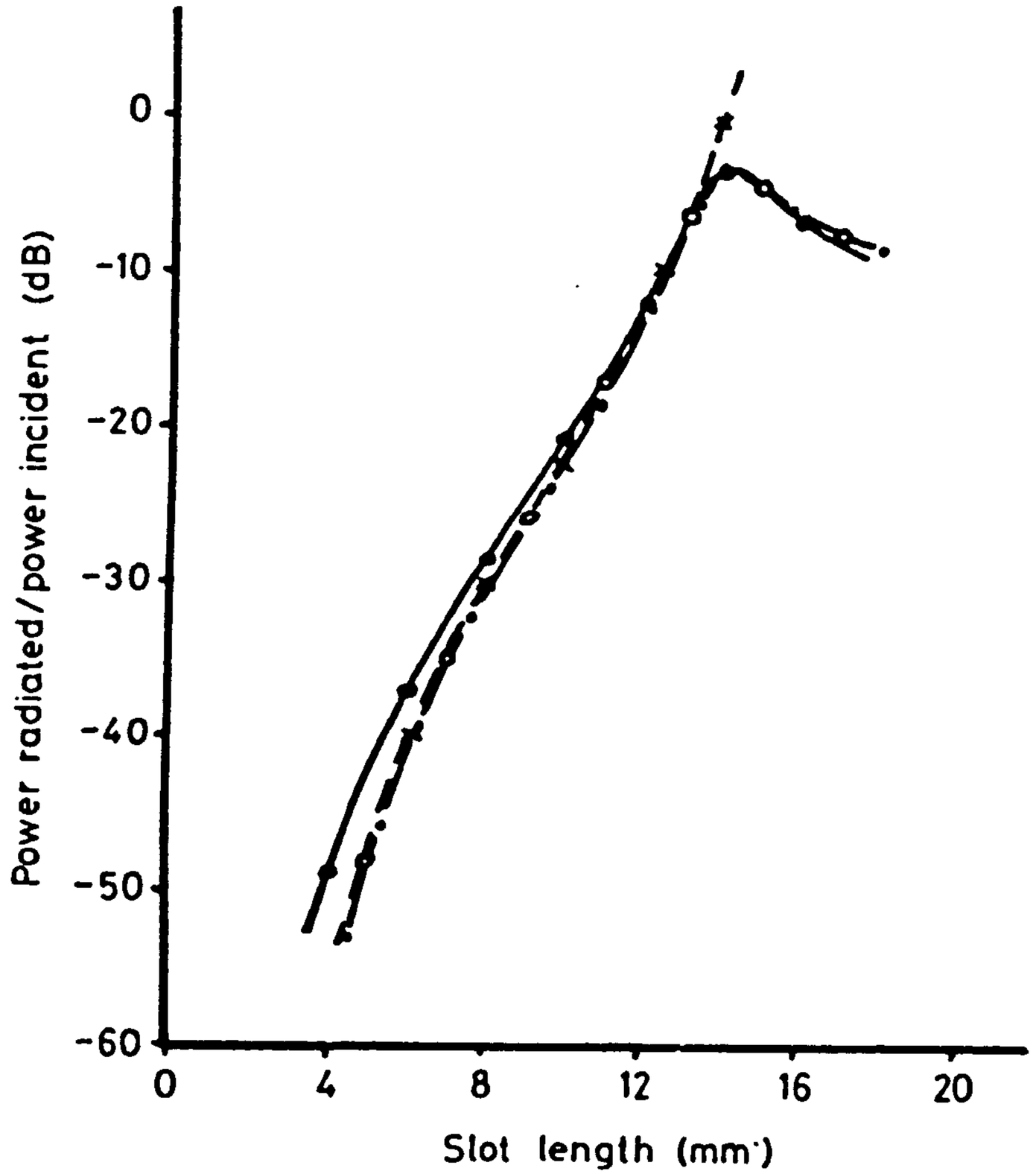

Slot width = 1·5 mm, off-set = 0·0 mm,
wall thickness = 1·0 mm, frequency = 10 GHz.
---- Small aperture method
—·— Variational method
—— Moment method

Figure 4. Normalized power radiated versus slot length for a transverse slot in the broadwall of a rectangular waveguide.

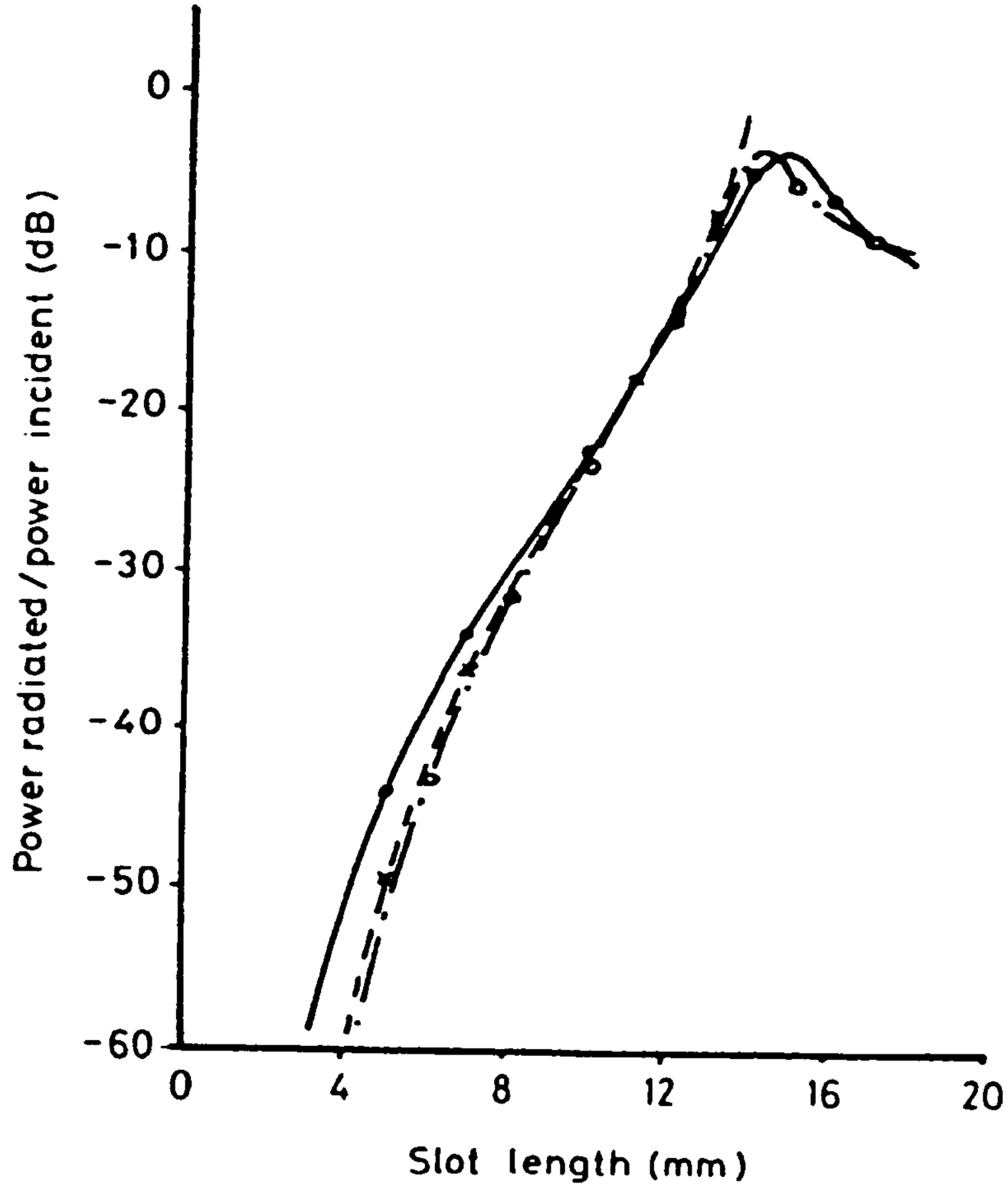

Slot width = 1·5 mm, off-set = 9·43 mm,
wall thickness = 1·0 mm, frequency = 10 GHz.
---- Small aperture method
—·— Variational method
—— Moment method

Figure 5. Normalized power radiated versus slot length for a longitudinal slot in the broadwall of rectangular waveguide.

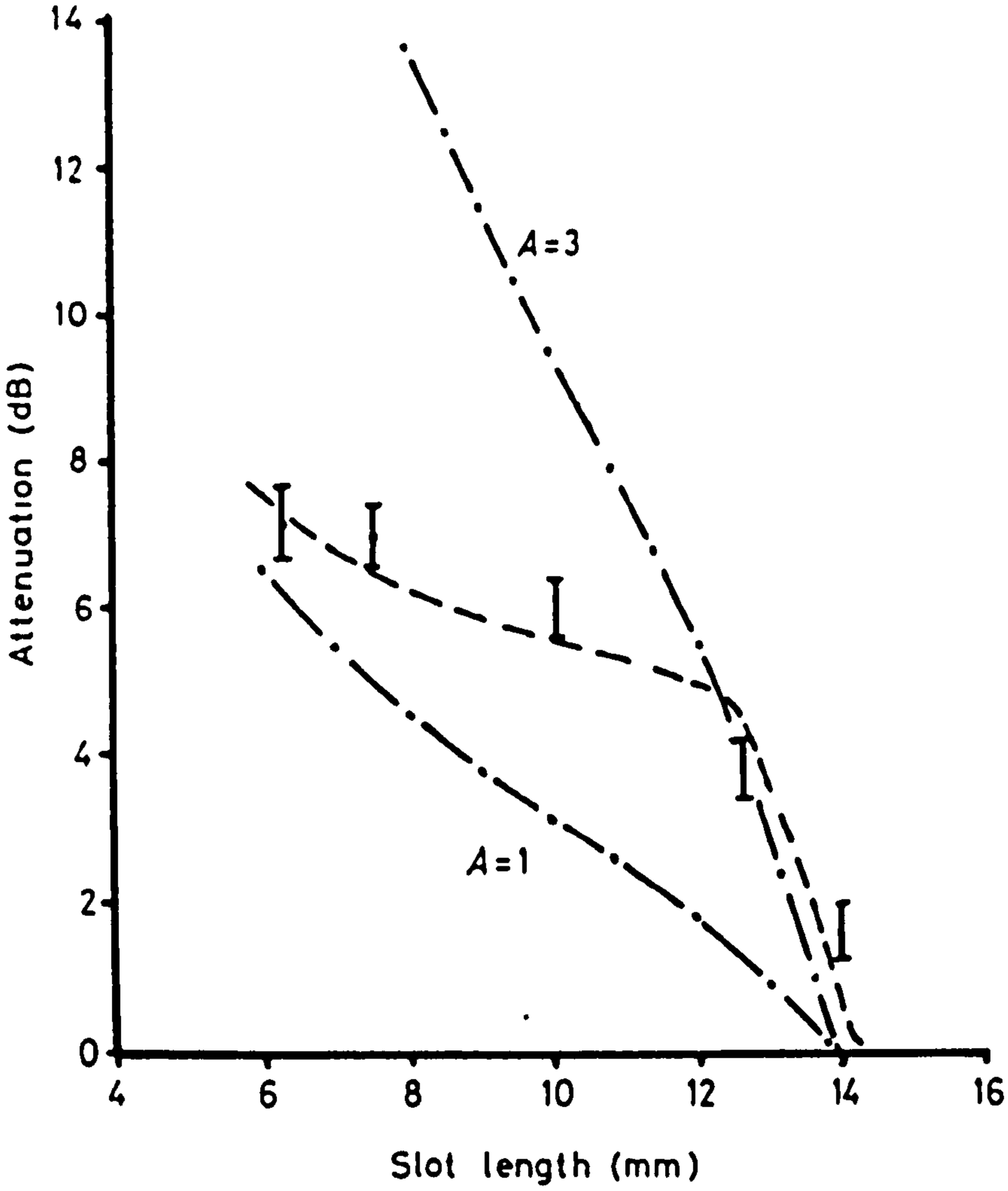

Slot width = 0·0625 in., wall thickness = 0·06 in.,
frequency = 10 GHz.
—·— Cohn estimate
– – – – Moment method
I I I I Measured results

Figure 6. Wall thickness attenuation as a function of slot length.

apparent. For the particular examples chosen, Figs. 4 and 5, the variational and moment methods are now in good agreement near resonance but diverge significantly for slot lengths which are well below resonance. The degree of agreement which was previously noted between the small aperture and variational methods, for slots in the length range $2l \leqq 0{\cdot}4\,\lambda$, is not altered by the introduction of wall thickness. Comparison of Figs. 2 and 4 and Figs. 3 and 5, elicits the result that the moment method predicts less severe wall-thickness attenuation than do the small aperture and variational methods, both of which employ the Cohn formula (eqn. (9)).

The reason for this is clearly demonstrated in Fig. 6. Here wall-thickness attenuation has been plotted as a function of slot length, and it can be seen that when the usual value of 3 is chosen for the Cohn A-factor considerable divergence between the Cohn estimate of wall thickness attenuation and that of the moment method occurs for small slots. This divergence is reflected in the 'power radiated' figures. For small apertures for which wall thickness, t, is not negligible by comparison with slot

length, l. Cohn has suggested that values of A approaching unity may be appropriate. Figure 6 shows that when $A = 1$, Cohn is in much better agreement with the moment method for small slots, but this is obtained at the expense of a deterioration at larger slot lengths. A method of optimizing the value of A at each slot length has been suggested by McDonald (1972). Unfortunately, for narrow rectangular slots, the McDonald technique can be difficult to implement. Some measurements of wall thickness attenuation have also been included in Fig. 6. These were performed using a waveguide 16 jig with 0·06 in. thick walls into which were cut a range of 1/16 in. wide square-ended slots. The results substantially support the moment method predictions.

To improve the confidence of the slotted-waveguide array designer that theoretically predicted slot characteristics can furnish reliable and accurate design information it is necessary to establish good agreement between theory and practice in a regime of slot behaviour which represents a particularly difficult test for any theoretical model. Predicting correctly the manner in which the resonant length of a longitudinal off-set slot is influenced by its off-set represents such a test. This test also has the advantage that very accurate measured results already exist (Stegen 1951). The results are presented in Fig. 7 where the best-fit measured curve, due to Stegen, is compared with both a moment method and a variational method prediction of the same geometry. It can be seen, firstly, that while the predicted curves are generally lower than the Stegen result the moment method demonstrates the correct functionality for change in resonant length with slot off-set. The variational method clearly fails to do this. The 3–4% level difference between the Stegen and the corresponding moment method result can largely be attributed to the fact that the rounded slots of measurement require, at present, to be modelled by square-ended slots in the theory. Other contributory factors, which are not modelled in the theory, are edge effects and resistive losses. Figure 7 also shows that when wall thickness is not allowed for in the analysis the resonant length prediction is in error by approximately 7%.

Recent measurements which have been performed on square-ended longitudinal off-set slots (Stern and Elliott 1985) demonstrate a high level agreement between theory (moment method) and practice. Tabulated results for slots in X-band waveguide, exhibiting off-sets in the range 0·05 in. to 0·35 in., suggest that the discrepancy between theory and experiment is at worst 0·6%. This implies that for square-ended slots, moment method predictions of off-set resonant lengths can justifiably be claimed to be as accurate as the best measured values (typically 0·5–1% experimental error).

6. Conclusions

Three well established methods for predicting theoretically the scattering characteristics of apertures in rectangular waveguide have been examined as potential tools for the synthesis and/or computer-aided design of slotted-waveguide array antennas. Of the three, the moment method has been shown to be the most promising in this regard since, for a wide range of slot geometries, it can provide results which deviate from the best measured results by little more than the experimental error. However it is the most difficult to implement computationally, since this method, unlike the variational and small aperture methods, does not produce closed

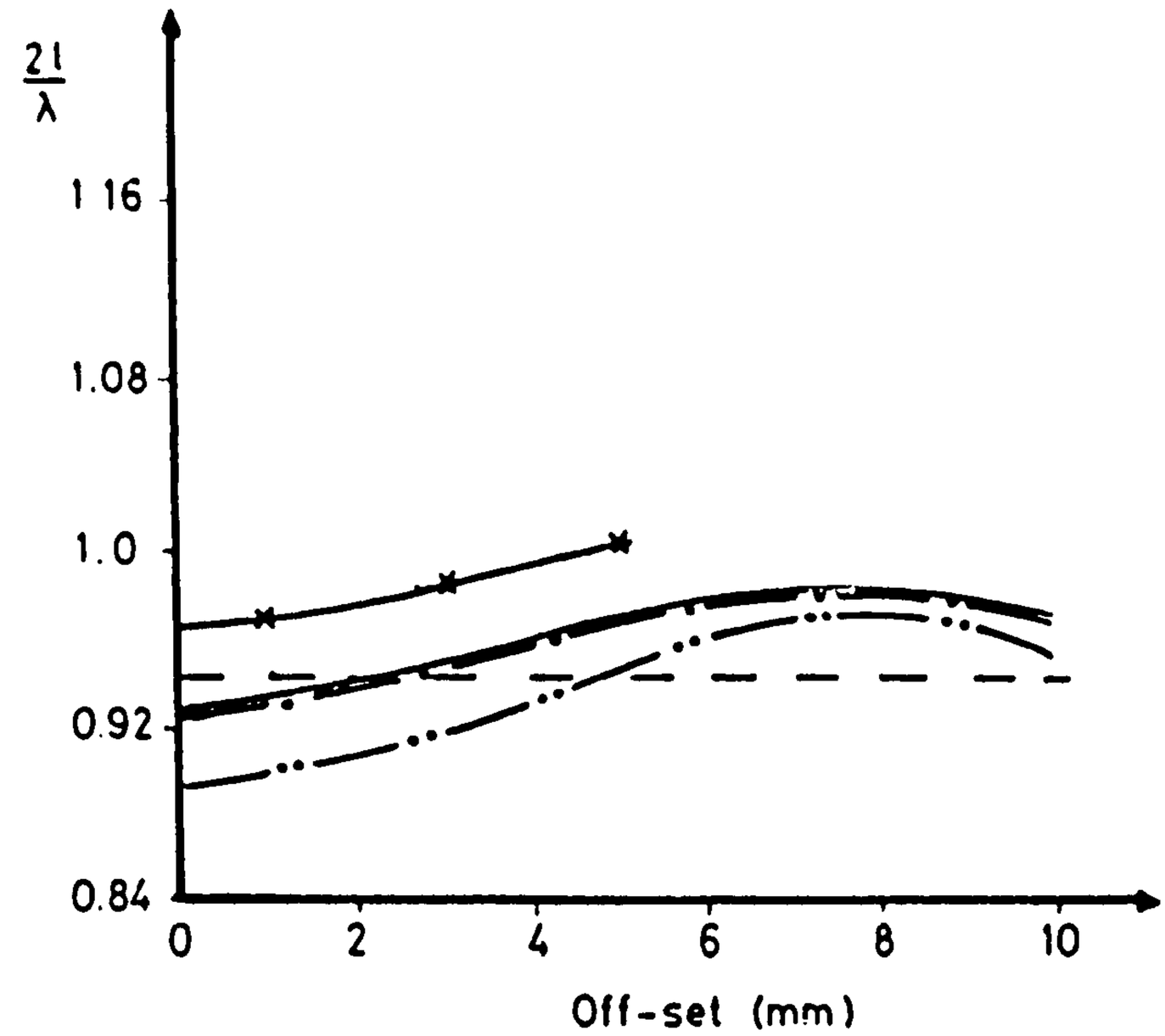

— × — Stegen (wall thickness t = 1·27 mm, $2w$ = 1·5875 mm)
- - - - Oliner (t = 1·0 mm, $2w$ = 1·5 mm)
——— Moment method (t = 1·27 mm, $2w$ = 1·5875 mm)
— - — Moment method (t = 1·0 mm, $2w$ = 1·5 mm)
— · · — Moment method (t = 0·0 mm, $2w$ = 1·5 mm)

Figure 7. Resonant length as a function of off-set for a longitudinal slot in the broadwall of a rectangular waveguide.

form expressions for the slot scattering parameters. Consequently, access to a high speed, high power mainframe computer is a pre-requisite of employing the moment method in any meaningful synthesis role.

When limited computer power is available, such as in a desk top computer, both the variational and small aperture methods can profitably be used. It has been shown that provided some caution is exercised both methods are of sufficient accuracy to at least permit the development of computer-aided design packages for small linear or planar arrays.

The principal caveats which should be noted are as follows:

1. The small aperture method cannot sensibly be used for the design of arrays which may contain resonant slots.
2. Both the variational and small aperture methods require considerable care to be exercised when implementing the wall thickness correction factor.
3. The variational method does not accommodate the Stegen effect for longitudinal off-set slots. This is usually resolved in practice by introducing a correction factor which is based on Stegen's measurements.
4. All three methods are unable to accommodate round-ended slots. In practice this deficiency is usually handled by adopting a rectangular slot whose 'effective length' is the same as the round-ended slot.

Appendix 1. Circuit element and power radiated formulae for typical slot radiators using small aperture theory

Series circuit

Centrally located transverse broadwall slot:

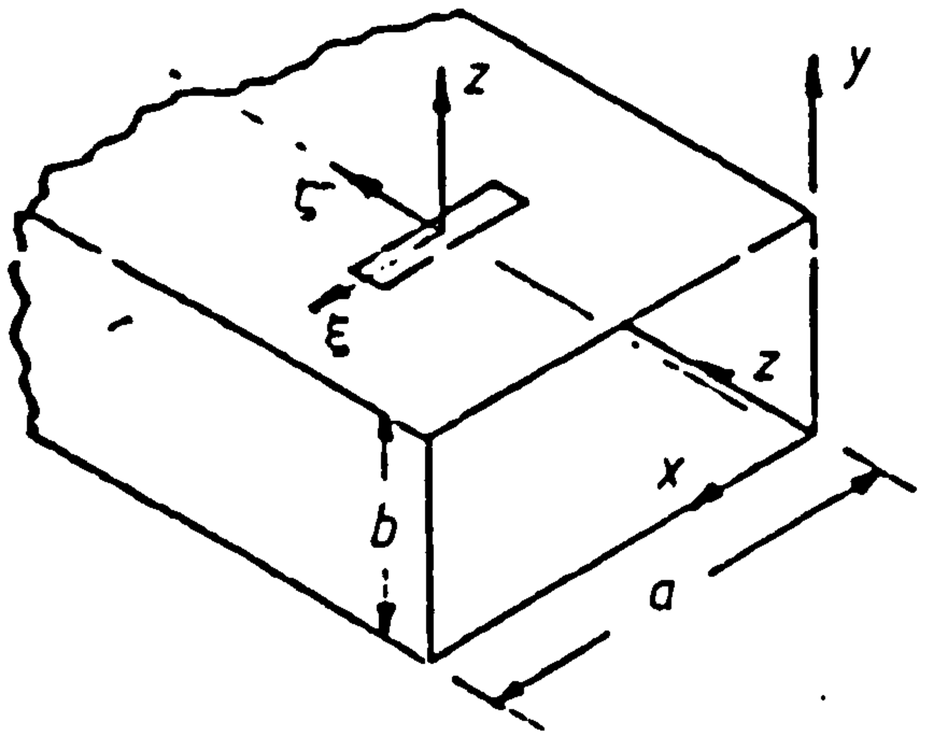

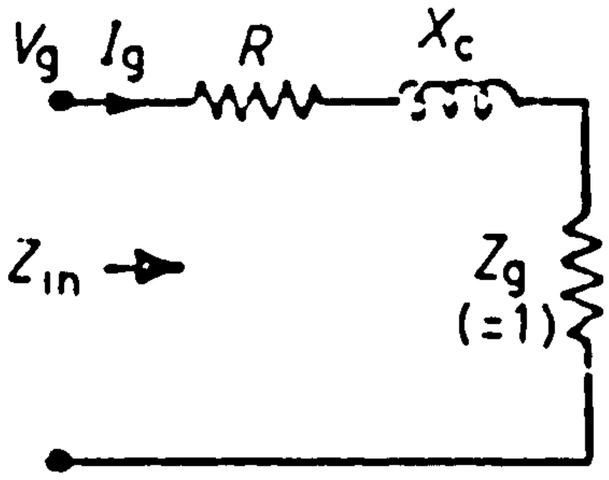

For a narrow slot whose main axis lies in the x-direction:

$$\alpha_{m\zeta} \to \alpha_{mx}; \quad \alpha_{mx} = 0; \quad \alpha_{e\eta} = 0$$

Hence

$$R = \frac{2k_0^3 \beta_{10} [\alpha_{mx}^{(p)}]^2}{3\pi ab}; \quad X_c = \frac{2\beta_{10} \alpha_{mx}^{(p)}}{ab}$$

and

$$\frac{P_{rad}}{P_{inc}} = \frac{2\beta_{10} k_0^3 c^2 \mu_0^2 (\alpha_{mx}^{(p)})^2}{3\pi Z_b^2 ab}$$

These formulae assume excitation by a TE_{10} mode whose field components are normalized such that the power flowing in the guide $P_{inc} = 1/2 \text{ Re} \iint_A \mathbf{E}_{inc} \times \mathbf{H}_{inc}^* \cdot \mathbf{dA} = 1/2$ in magnitude, and also $P_{inc} = V_g I_g/2$.

Shunt circuit

Longitudinal off-set slot in broadwall of waveguide:

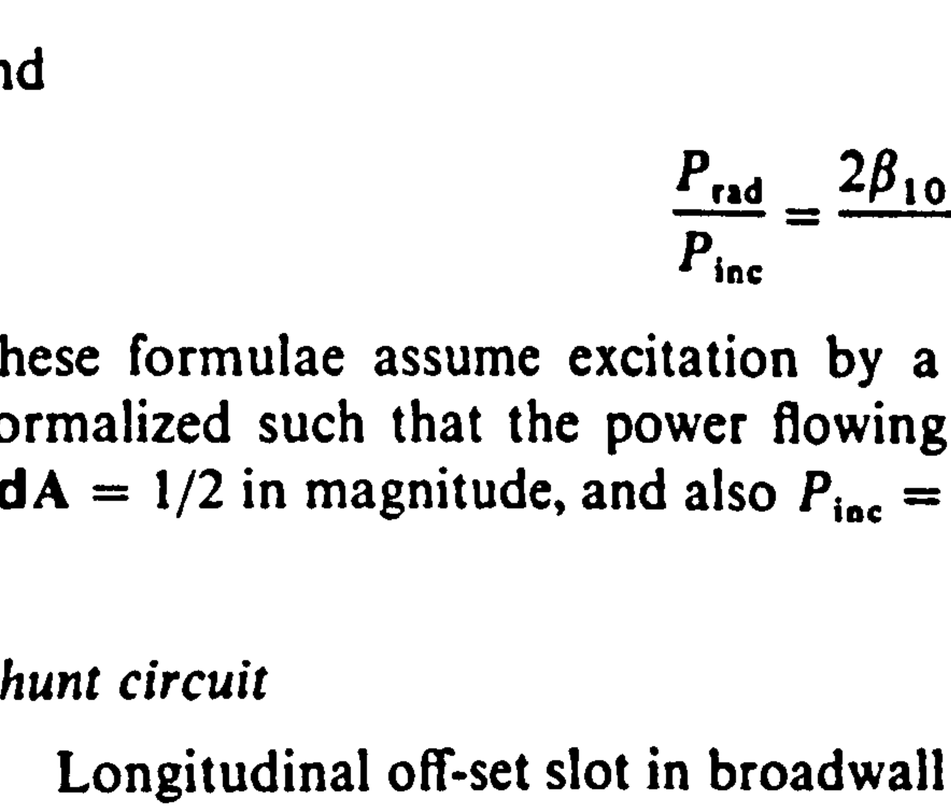

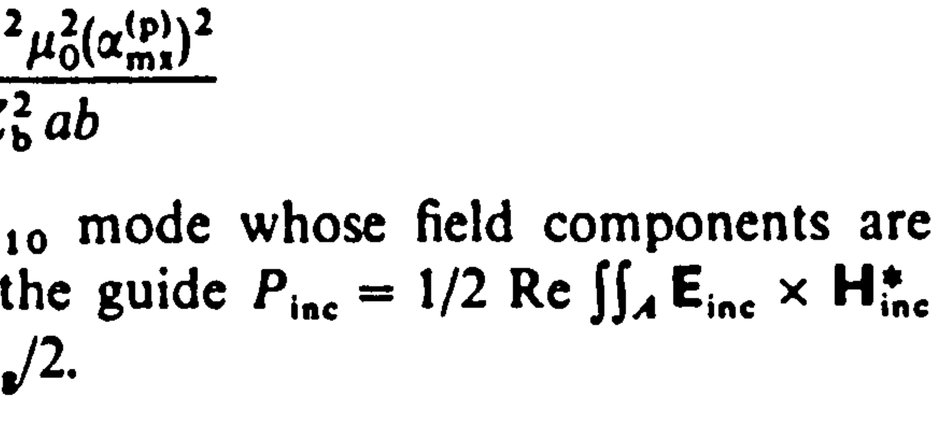

For a narrow slot whose major axis lies in the z-direction

$$\alpha_{m\xi} \to \alpha_{mz}; \quad \alpha_{m\zeta} = 0; \quad \alpha_{e\eta} = 0$$

Hence from Van Bladel:

$$G = \frac{2\pi k_0^3 [\alpha_{mz}^{(p)}]^2}{3\beta_{10} b a^3} \sin^2 \frac{\pi d}{a}; \quad B = \frac{2\pi^2 \alpha_{mz}^{(p)}}{\beta_{10} a^3 b} \sin^2 \frac{\pi d}{a}$$

and

$$\frac{P_{rad}}{P_{inc}} = \frac{2\pi k_0^3 \mu_0^2 c^2 [\alpha_{mz}^{(p)}]^2}{3\beta_{10} Z_0^2 a^3 b} \sin^2 \frac{\pi d}{a}$$

Appendix 2. Circuit element formulae for an off-set transverse slot in the broadwall of waveguide, using the variational method

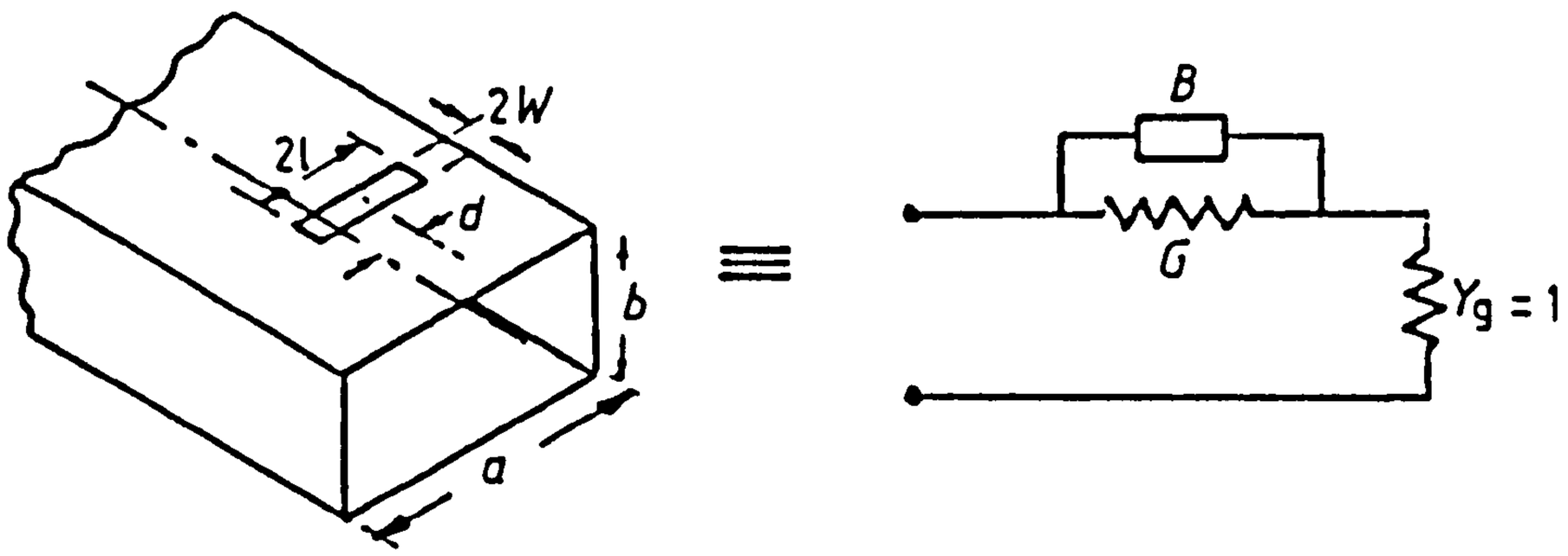

$$G = \frac{\lambda_g}{\lambda_0^3} \cdot \frac{32ab}{3\pi} \left[\frac{\pi}{4} \frac{1 - \left(\frac{2l}{a}\right)^2}{\cos\left(\frac{\pi l}{a}\right)} \right]^2 \left\{ 1 - 0{\cdot}374 \left(\frac{2l}{\lambda_0}\right)^2 + 0{\cdot}13 \left(\frac{2l}{\lambda_0}\right)^4 \right\} \sec^2 \frac{\pi d}{a} C_T^2$$

$$B = \tfrac{1}{2} B_t + \frac{B_{rj}}{n_j^2} + \frac{2b}{\lambda_g} \left[\ln 2 + \frac{\pi w}{3b} + \frac{3}{2} \left(\frac{b}{\lambda_g}\right)^2 \right]$$

where G and B are normalized to Y_0 the characteristic admittance of the waveguide and C_T is defined in § 2. Also

$$B_t = \frac{4b}{\lambda_g} \left\{ -\ln \left[\sin\left(\frac{\pi w}{b}\right) \right] + \frac{1}{2} \left(\frac{b}{\lambda_g}\right)^2 \cos^4 \left(\frac{\pi w}{b}\right) \right\}$$

$$- \frac{4b}{\lambda_g} \left(\frac{\lambda_g}{\lambda_{g3}}\right)^2 \left[\frac{\cos\left(\frac{3\pi l}{a}\right)}{\cos\left(\frac{\pi l}{a}\right)} \cdot \frac{1 - \left(\frac{2l}{a}\right)^2}{1 - 9\left(\frac{2l}{a}\right)^2} \right]^2 \left[1 + \frac{\pi d}{(\lambda_{g3})^2} \right] \ln \left(\frac{2\lambda_{g3}}{\pi \gamma w} \right)$$

$$\frac{1}{n_j^2} = \frac{ab}{4wl} \left[\frac{\pi}{4} \frac{1 - \left(\frac{2l}{a}\right)^2}{\cos\left(\frac{\pi l}{a}\right)} \right]^2$$

$$B_{r1} = \frac{4w\lambda_g}{\lambda_0^2}$$

$$\left\{\left(\frac{k^1}{k_0}\right)^2 [C + \tfrac{1}{2} - \ln(\gamma | k^1 | w)] + \frac{\sin 2k_0 l}{2k_0 l} + \left[1 + \left(\frac{\lambda_0}{4l}\right)^2\right] S - \frac{2}{3}\frac{w}{l}\left(\frac{\lambda_0}{4l}\right)^2\right\}$$

Also

$$k^1 = \left(k_0^2 - \left(\frac{\pi}{2l}\right)^2\right)^{1/2}; \quad k_0 = \frac{2\pi}{\lambda_0}; \quad \gamma = 1{\cdot}781$$

$$\lambda_{g3} = \frac{\lambda_0}{\sqrt{\left|1 - \left(\frac{3\lambda_0}{2a}\right)^2\right|}}$$

and

$$C = \frac{Ci(2k_0 l + \pi) + Ci|2k_0 l - \pi|}{2}$$

where Ci is the cosine integral;

$$Ci(x) = \int_{\infty}^{x} \frac{\cos t}{t}\, dt$$

and

$$S = \frac{Si(2k_0 l + \pi) - Si(2k_0 l - \pi)}{2\pi}$$

where Si is the sine integral:

$$Si(x) = \int_{0}^{x} \frac{\sin t}{t}\, dt$$

It is assumed that for the incident mode in the waveguide $\int_0^a \int_0^b \mathbf{E}_{10} \times \mathbf{H}_{10}^* \cdot da = 1$.

Appendix 3. Circuit element formulae for an off-set longitudinal slot in the broadwall of waveguide, using variational method

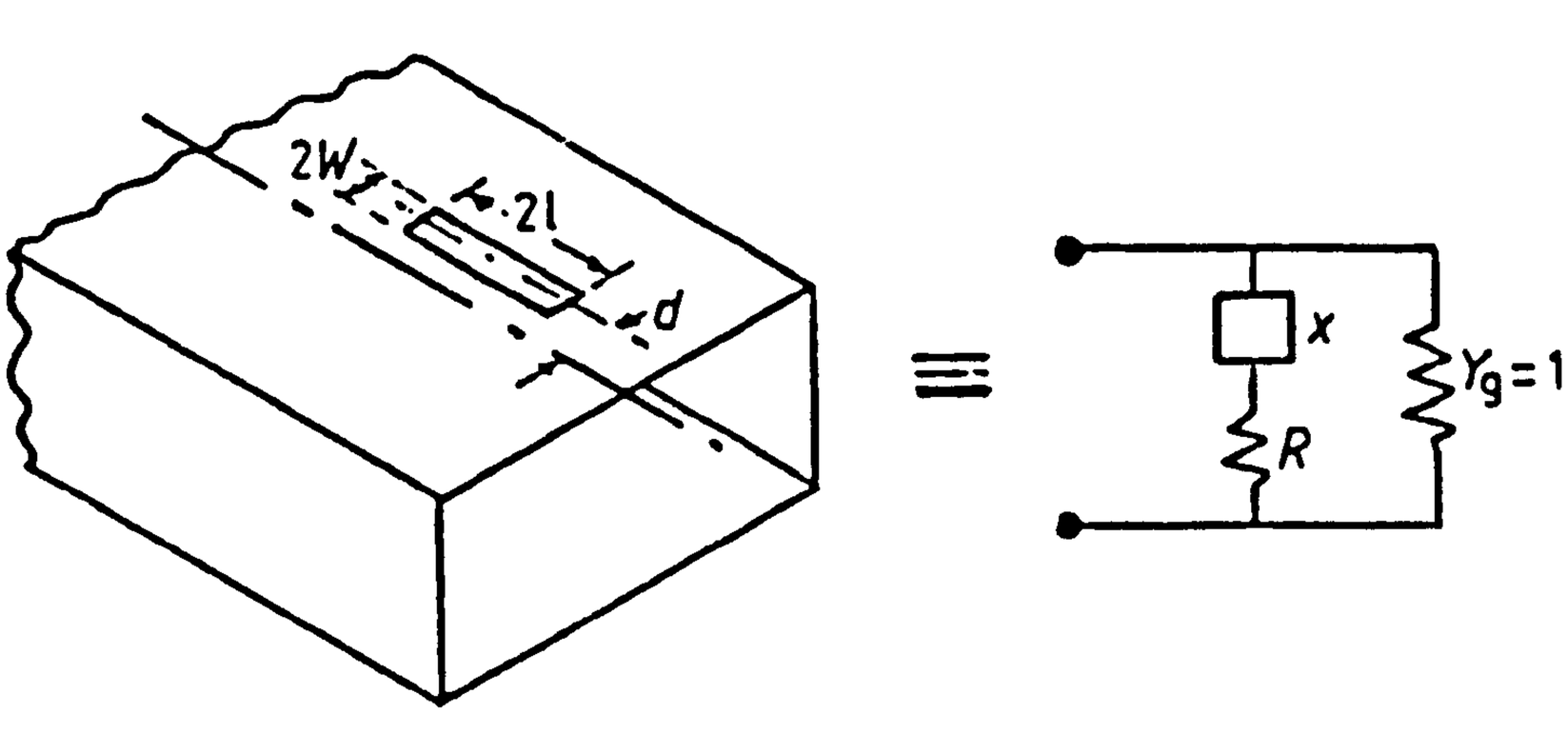

$$R = \frac{\dfrac{8\pi a^3 h}{3\lambda_0^3 \lambda_g}\left[1-\left(\dfrac{4l}{\lambda_g}\right)^2\right]^2\left[1-0{\cdot}374\left(\dfrac{2l}{\lambda_0}\right)^2+0{\cdot}130\left(\dfrac{2l}{\lambda_0}\right)^4\right]C_T^2}{\sin^2\left(\dfrac{\pi d}{a}\right)\cos^2\left(\dfrac{2\pi l}{\lambda_g}\right)}$$

$$X = \left(\frac{2a}{\lambda_g}\right)^2\left[\frac{\cos\dfrac{\pi l}{a}\left(1-\left(\dfrac{4l}{\lambda_g}\right)^2\right)}{\cos\dfrac{2\pi l}{\lambda_g}\left(1-\left(\dfrac{2l}{a}\right)^2\right)}\right]^2 \operatorname{cosec}^2\left(\frac{\pi d}{a}\right)\cdot B$$

where B is defined in Appendix 2.

Appendix 4. Closed form formulae for the power radiated by an off-set inclined slot in the broadwall of rectangular waveguide

$$\frac{\text{Power radiated}}{\text{Power incident}} = \frac{2\dfrac{Z}{Y}(M^2+N^2)}{\left\{1+\dfrac{Z}{Y}(M^2+N^2)\right\}^2+\left(\dfrac{X}{Y}\right)^2}$$

where

$$X = \frac{B\cdot 6\pi Z_0}{abk_0^2}\left[\frac{\cos\left(\dfrac{\pi l}{a}\right)}{1-\left(\dfrac{2l}{a}\right)^2}\right]^2$$

where B is defined in Appendix 2 and $Z_0 = 377\,\Omega$. Also

$$Y = \left\{1-0{\cdot}374\left(\frac{2l}{\lambda_0}\right)^2+0{\cdot}130\left(\frac{2l}{\lambda_0}\right)^4\right\}\cdot C_T^2$$

$$Z = \frac{0{\cdot}75\beta_{10}\pi}{abk_0^3}$$

$$M = \left[J(\theta)\sin(\theta)+\frac{\pi}{a\beta_{10}}I(\theta)\cos\theta\right]\sin\frac{\pi d}{a}$$

$$N = \left[I(\theta)\sin(\theta)+\frac{\pi}{a\beta_{10}}J(\theta)\cos\theta\right]\cos\frac{\pi d}{a}$$

$$\left.\begin{matrix}I(\theta)\\J(\theta)\end{matrix}\right\} = \frac{\cos\dfrac{\pi P}{2}}{1-P^2}\pm\frac{\cos\dfrac{\pi Q}{2}}{1-Q^2}$$

$$\left.\begin{matrix}P\\Q\end{matrix}\right\} = \frac{2l}{a}\sin\theta\pm\frac{2l\beta_{10}}{\pi}\cos\theta$$

Where θ is the slot inclination to the guide axis ($=0^0$ for longitudinal slot).

Appendix 5. Scattering parameter formulae for an off-set transverse slot in rectangular waveguide using the moment method

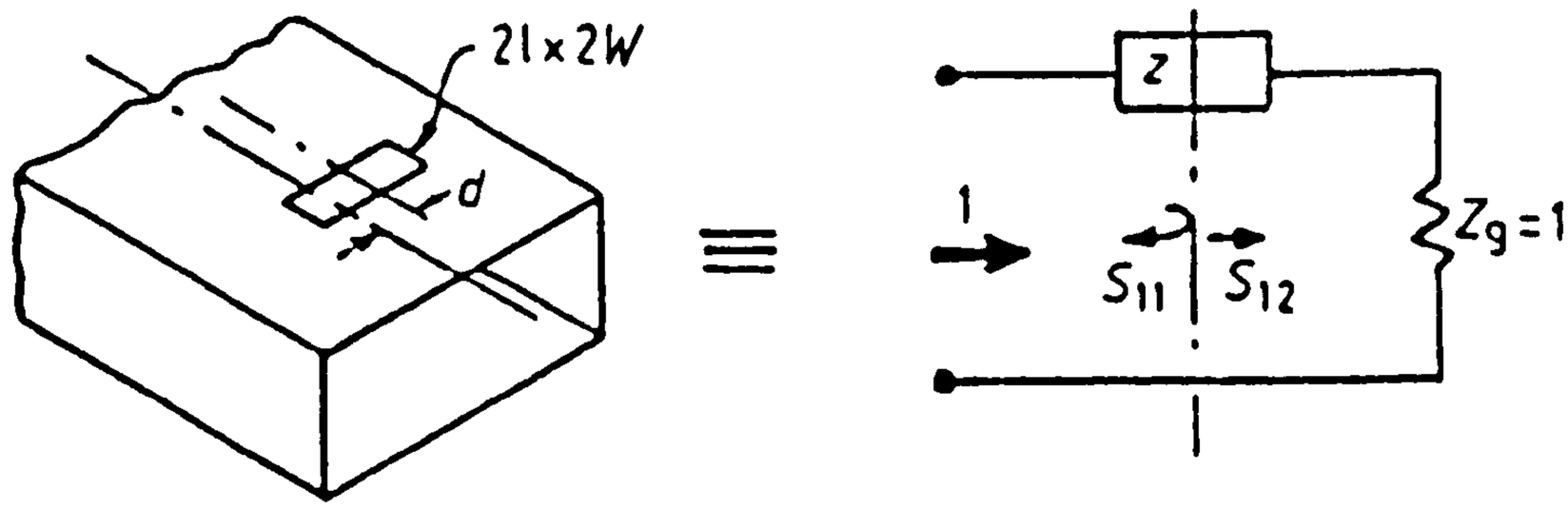

$$S_{11} = \frac{A_{10}\sqrt{2\pi}}{a} \sin(\beta_g w) \sum_{s=1}^{N} a_s \sigma(s, 1)$$

$$S_{12} = 1 - S_{11}$$

where a_s are the coefficients of the basis function series obtained by solving matrix eqn. (27)

$$A_{10} = j\left[\frac{2}{\omega\mu_0 \beta_g k_c^2 ab}\right]^{1/2}; \quad \beta_g = \frac{2\pi}{\lambda_g}; \quad k_c = \frac{\pi}{a}$$

and

$$\sigma(s, 1) = \begin{cases} \dfrac{\dfrac{4l}{s\pi}}{\left[\left\{\dfrac{2l}{s\pi a}\right\}^2 - 1\right]} \sin\left(\dfrac{\pi l}{a}\right) \sin\left(\dfrac{\pi d}{a}\right) \\ (-1)^{s/2} l \sin\left(\dfrac{\pi d}{a}\right) \end{cases} (s \text{ even})$$

$$\begin{cases} \dfrac{\dfrac{4l}{s\pi}}{\left[1 - \left\{\dfrac{2l}{s\pi a}\right\}^2\right]} \cos\dfrac{\pi l}{a} \cos\dfrac{\pi d}{a} \\ (-1)^{((s-2)/2)} l \cos\dfrac{\pi d}{a} \end{cases} (s \text{ odd})$$

Also from power conservation

$$\frac{P_{rad}}{P_{inc}} = 10 \log_{10}\left[1 - (s_{11}^2 + s_{12}^2)\right] dB$$

Appendix 6. Scattering parameter formulae for an off-set longitudinal slot in rectangular waveguide using the moment method

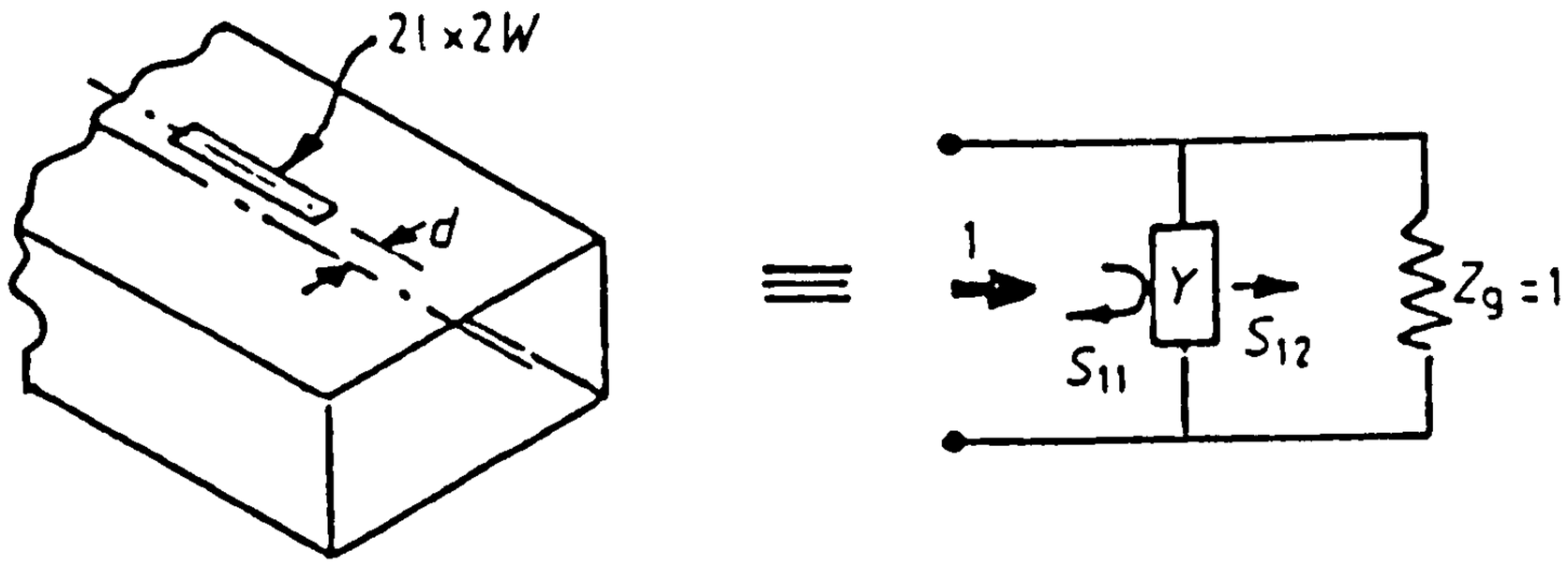

$$S_{11} = \frac{A_{10}\pi}{j\sqrt{2a}} \cdot \left\{\sin\frac{\pi}{a}(d+w) - \sin\frac{\pi}{a}(d-w)\right\} \times$$

$$\sum_{s=1}^{N} a_s \frac{\frac{s\pi}{2l}}{\left[\left\{\frac{s\pi}{2l}\right\}^2 - \beta_g^2\right]} \times \begin{cases} 2\cos\beta_g l & (s \text{ odd}) \\ 2j\cos\beta_g l & (s \text{ even}) \end{cases}$$

$$S_{12} = 1 - (-1)^s S_{11}$$

The power radiated by the aperture can be calculated from power conservation (Appendix 5).

References

Baker, H. C., and Lagrone, A. H., 1962, Digital implementation of the mutual impedance between thin dipoles. *I.R.E. Transactions*, **AP-10**, 172–178.

Bethe, H. A., 1944, Theory of diffraction by small holes. *Physical Review*, **66**, 163–182.

Cheng, D. K., 1982, Generalised hybrid network parameters for electromagnetic coupling between dissimilar regions through a small aperture. *I.E.E. Proceedings*, **129**, Pt. H, 325–332.

Cohn, S. B., 1951, Determination of aperture parameters by electrolytic tank measurements. *I.R.E. Proceedings*, **39**, 1416–1421.

Cohn, S. B., 1952a, Microwave coupling by large apertures. *Proceedings of the I.R.E.*, **40**, 696–699.

Cohn, S. B., 1952b, Electric polarisability of apertures of arbitrary shape. *I.R.E. Proceedings*, **40**, 1069–1071.

Collin, R. E., 1960, Field theory of guided waves. (New York: McGraw-Hill Book Co.).

Collin, R. E., 1981, Rayleigh scattering and power conservations. *I.E.E.E. Transactions*, **AP-29**, 795–798.

Das, B. N., and Sanyal, G. S., 1970, Network parameters of a waveguide broadwall slot radiator. *Proceedings of the I.E.E.*, **117**, 41–44.

Elliott, R. S., 1978, The design of small slot arrays. *I.E.E.E. Transactions*, **AP-26**, 214–219.

Harrington, R. F., 1968, *Field Computation by Moment Method* (London: Macmillan).

Harvey, A. F., 1963, *Microwave Engineering* (New York: Academic Press).

Levine, H., and Schwinger, J., 1950, On the theory of electromagnetic wave diffraction by an aperture in an infinite plane conducting screen. *Symposium on the theory of e.m. waves*, p. 355.

Levy, R., 1968, Analysis and synthesis of waveguide multi-aperture directional couplers. *I.E.E.E. Transactions*, **MTT-16**, 995–1006.

LEVY, R., 1980, Improved single and multi-aperture waveguide coupling theory. *I.E.E.E. Transactions*, **MTT-28**, 331–338.

LYON, R. W., and HIZAL, A., 1983, A moment method analysis of narrow dielectric covered rectangular slots in the broadwall of waveguide. *Proceedings of International Conference on Antennas & Propagation*, pp. 150–153.

LYON, R. W., and SANGISTER, A. J., 1981, Efficient moment method analysis of radiating slots in a thick-walled waveguide. *Proceedings of the I.E.E.*, **128**, Pt. H, 197–205.

MCDONALD, N. A., 1972, Electric and magnetic coupling through small apertures in shield walls of any thickness. *I.E.E.E. Transactions*, **MTT-20**, 689–695.

MONTGOMERY, C. G., 1947, *Radiation laboratory series*, Vol. 8. (New York: McGraw-Hill).

OLINER, A. A., 1957, The impedance properties of narrow radiating slots in the broadface of rectangular waveguide. *I.R.E. Transactions*, **AP-5**, 4–20.

RAHMAT-SAMII, 1977, Electromagnetic coupling through small apertures. *I.E.E.E. Transactions*, **AP-25**, 180–187.

SANGSTER, A. J., 1965, Variational methods for the analysis of waveguide coupling. *I.E.E. Proceedings*, **112**, 2171–2179.

SANGSTER, A. J., and HAWKINS, D. C., 1972, Scattering parameters of an arbitrarily shaped aperture in waveguide. *Proceedings of the I.E.E.*, **119**, 1465–1466.

STEGEN, R. J., 1951, Longitudinal shunt slot characteristics. Hughes Technical Memo. 261, Hughes Aircraft Co., U.S.A.

STERN, G. J., and ELLIOTT, R. S., 1985, Resonant length of longitudinal slots and validity of circuit representation: theory and experiment. *I.E.E.E. Transactions*, **AP-33**, 1264–1271.

STEVENSON, A. F., 1948, Theory of slots in rectangular waveguide. *Journal of Applied Physics*, **19**, 24–38.

VAN BLADEL, J., 1971, Small holes in a waveguide wall. *Proceedings of the I.E.E.*, **118**, 43–50.

VAN BLADEL, J., 1981, Contribution of the ψ = constant mode to the modal expansion in waveguide. *I.E.E. Proceedings*, **128**, Pt. H, 247–251.

VU KHAC, T., and CARSON, C. T., 1973, Impedance properties of a longitudinal slot antenna in the broadface of rectangular waveguide. *I.E.E.E. Transactions*, **AP-21**, 708–710.

Moment method applied to round-ended slots

A.J. Sangster, MSc, PhD, CEng, FIEE
A.H.I. McCormick, MEng

Indexing terms: Antennas (slot), Antennas (theory)

Abstract: Round-ended slot radiators in waveguides remain difficult to analyse accurately using conventional techniques because these are, in general, incapable of accommodating other than square-ended slot models. This paper shows that a sectional-slot model can provide some improvement in theoretical performance for the moment method analysis of such slots

1 Introduction

The electromagnetic boundary value problem formed by a radiating aperture in a rectangular waveguide has received considerable attention in the literature over the past 40 years. The solution to this problem presents formidable analytical difficulties which have normally been eased by the adoption of certain simplifying assumptions. These simplifications have led to the evolution of three predominant methods of analysis. These are the diffraction method [1], the variational method [2] and the moment method [3].

The progressive sophistication contained in these methods has permitted increasingly more realistic models to be analysed so that today the behaviour of a slot of any length, located with little restriction, in a wall of any thickness, can be predicted with some accuracy. For example the moment method, which uses a largely numerical approach to solve the integral equations, when applied to a longitudinal offset slot in the broad wall of a rectangular waveguide, predicts a resonant length which is only a few percent lower than the accurately measured value [4]. This residual inaccuracy can be attributed to three main factors.

(*a*) inadequate modelling of field enhancement at sharp edges within the slot

(*b*) inadequate modelling of rounded ends

(*c*) neglection of the 'cross-polar' component of field in the slot.

Some of these factors have already been addressed by other investigators. For example, the edge effect has been examined by Park [5] and Stern and Elliott [6], whereas correction factors to improve the correspondence between the square-ended slots which are used in theory and the round-ended slots which are used in practice have been suggested by Yee [7] and Josephsson [8]. For narrow slots which have large length-to-width ratios (such slots are almost always used in practical antennas) the cross-polar, or longitudinally directed, E-field component within the slot is so small that it can safely be neglected [2].

In this paper, the round-ended slot is reconsidered and an 'improved' theoretical model is postulated. It comprises an axially sectioned slot geometry in which the sections can have different lengths. This model is then analysed using a moment method and if trigonometrical rather than pulse basis junctions are used, it is found that computation times on a mainframe computer (Burroughs B6930) can be kept within reasonable bounds. For example, the calculation of the scattering parameters of a single slot at one frequency requires approximately 5 min of processor time when three basis functions and three sections are used.

2 Mathematical formulation: square ended slot

To enunciate the analytical procedures adopted to achieve an adequate mathematical description of the round ended-slot most clearly, it is convenient, first, to restate the integral equations (in matrix form) which are generated when the moment method is applied to the conventional square ended slot [3, 9]. It should be noted that trigonometrical basis functions have been preferred for the reasons given in the introduction. The results are:

$$\begin{bmatrix} [A] & [C] \\ [D] & [B] \end{bmatrix} \begin{bmatrix} [a] \\ [b] \end{bmatrix} = \begin{bmatrix} [h] \\ [0] \end{bmatrix} \tag{1}$$

where

$$A_{i,s} = -j\omega\varepsilon_0 \iint_S f_i \hat{a}_\eta \cdot \left\{ \hat{n} \times \iint_S [G_a(r/r_0) + G_b(r/r_0)] \cdot f_s \hat{a}_\xi \, dS_0 \right\} dS \tag{2a}$$

$$B_{i,s} = -j\omega\varepsilon_0 \iint_{S'} f'_i \hat{a}_\eta \cdot \left\{ \hat{n}' \times \iint_{S'} [G_b(r/r_0) + G_c(r/r_0)] \cdot f'_s \hat{a}_\xi \, dS_0 \right\} dS \tag{2b}$$

$$C_{i,s} = j\omega\varepsilon_0 \iint_S f'_i \hat{a}_\eta \cdot \left\{ \hat{n} \times \iint_{S'} G_b(r/r_0) \cdot f_s \hat{a}_\xi \, dS_0 \right\} dS \tag{2c}$$

$$D_{i,s} = j\omega\varepsilon_0 \iint_{S'} f_i \hat{a}_\eta \cdot \left\{ \hat{n} \times \iint_S G_b(r/r_0) \cdot f'_s \hat{a}_\xi \, dS_0 \right\} dS \tag{2d}$$

$$h_i = -\iint_S f_i \hat{a}_\eta \cdot \{\hat{n} \times H_i(r)\} \, dS \tag{2e}$$

$G_{a,b,c}$ are the Greens functions of the waveguide, cavity and half-space, respectively, as illustrated in Figs. 1 and 2,

Paper 5340H (E11), first received 11th November 1986 and in revised form 16th February 1987

The authors are with the Department of Electrical and Electronic Engineering, Heriot-Watt University, 31-35 Grassmarket, Edinburgh EH1 1HT, United Kingdom

and f_i and f_s are the basis functions. H_i is the magnetic field component of the TE_{10} incident wave in the waveguide.

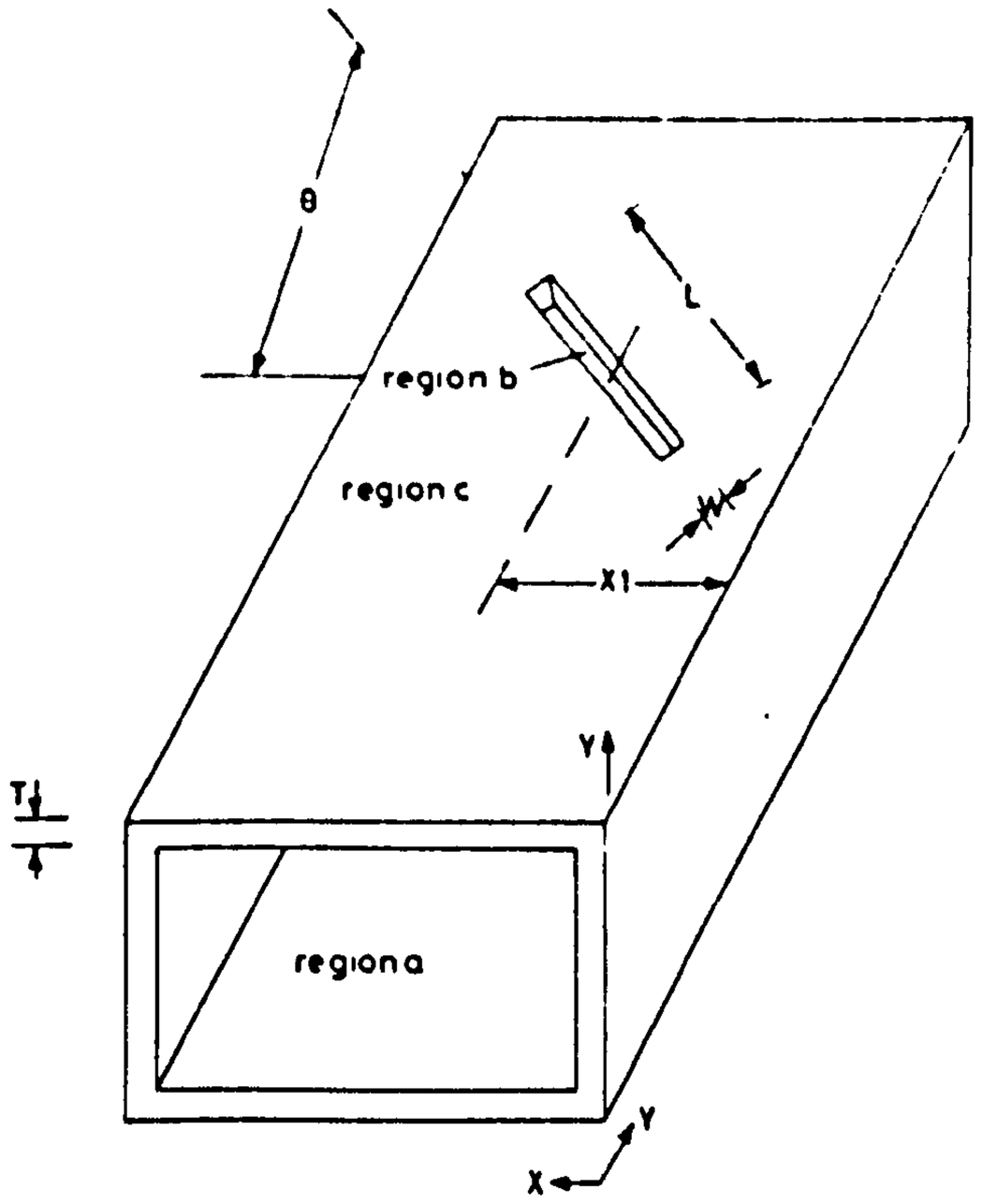

Fig. 1 *Co-ordinate system of slotted waveguide*

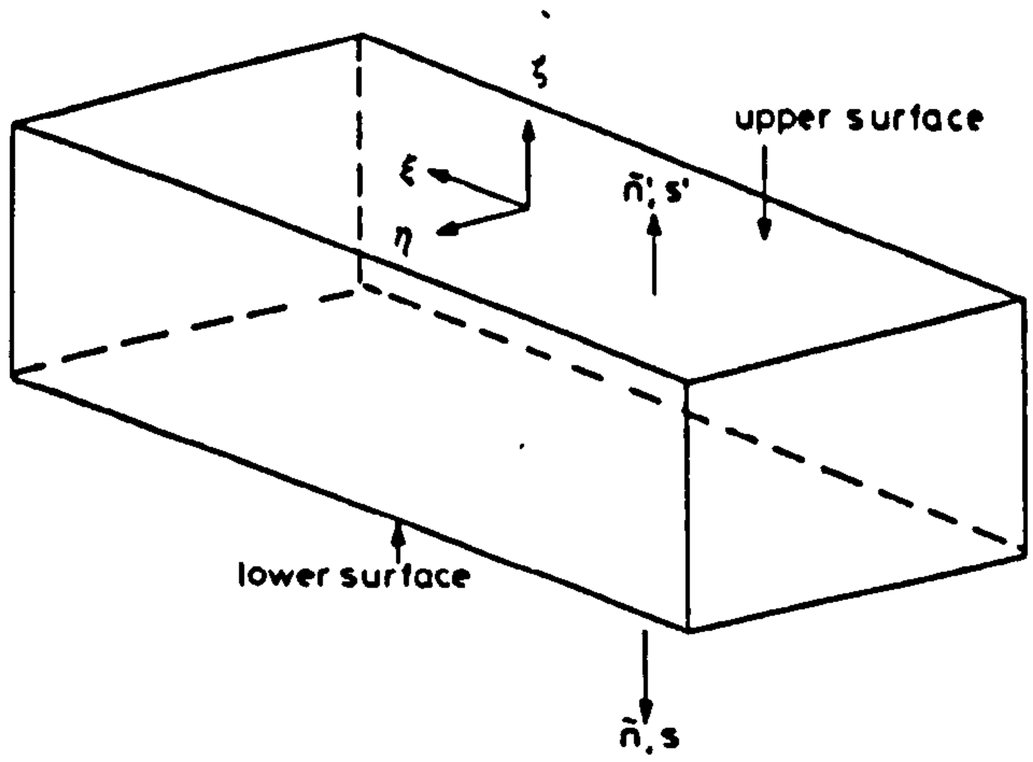

Fig. 2 *Expanded view of slot*

3 Modified formulation for round ended slot

A round-ended slot can be modelled using the moment method by considering that the slot comprises the rectangular slices as illustrated, for $n = 3$, in Fig. 3*c*. The

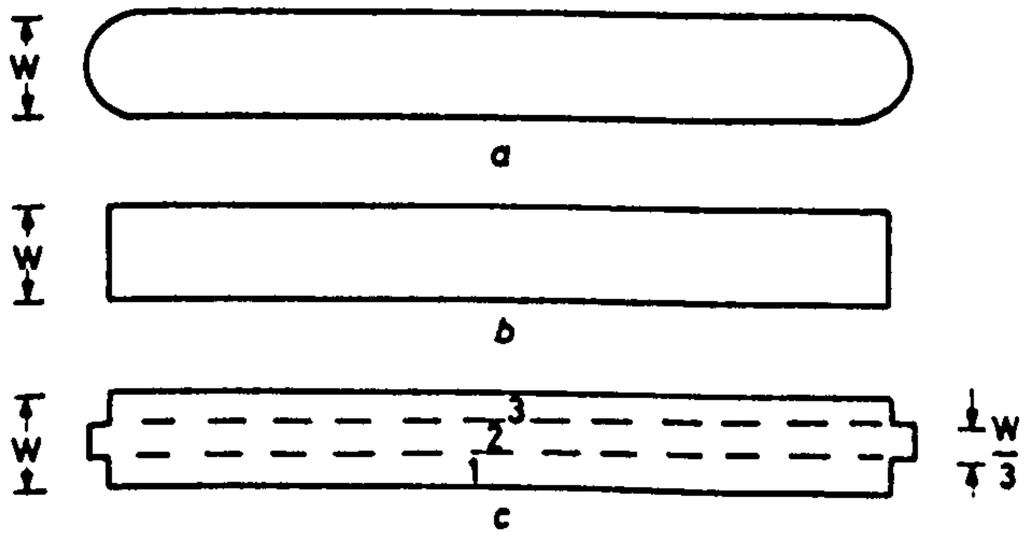

Fig. 3 *Views of slots*
a Rounded ended slot
b Equivalent length rectangular slot
c Sectioned slot

essence of the modification in mathematical terms then lies in calculating the self coupling for each section and the mutual coupling between the sections.

Before detailing the development of the mathematics, the algorithm for determining the section lengths shall be stated:

(*a*) set the length of the middle section equal to the length of the rounded slot

(*b*) calculate the remaining length by setting the section width equal to w/3 and matching the area to that of the round-ended model

(*c*) calculate the length of the equivalent square-ended slot having the same width (*w*) and perimeter as the given round-ended slot.

From the above, the following formulas are obtained:

$$\text{length of section 1, 3} = L \text{ equivalent} + \left(\frac{1}{2} - \frac{\pi}{8}\right)w \quad (3)$$

$$\text{length of section 2} = L \text{ equivalent} + \left(2 - \frac{\pi}{2}\right)w \quad (4)$$

In the current analysis the above split slot modification is applied to the inner surface of the slot only (see Fig. 2). The cavity and its outer surface are set equal to the length of the middle section. This minimises the computation yet provides sufficient evidence to demonstrate the effectiveness of this procedure. In principle, however, the modification could be applied to both inner and outer surfaces of the slot 'cavity' and to the cavity itself, in a 'thick' wall example.

Eqn. 49 of Reference 9 gives the mathematical relationships describing the self-coupling processes within a single (i.e. individual) slot. For a divided slot comprising three equal width elements, this term can be re-expressed as

$$\sum_{p=1}^{3}\sum_{q=1}^{3}\iint_{S_{p,q}} f_i \hat{a}_z \cdot (-\hat{a}_r \times H_{s_{p,q}})\, ds \quad (5)$$

where

$$H = -j\omega_s A_m + \frac{\nabla\nabla \cdot A_m}{j\omega\mu_0\varepsilon_0} \quad (6)$$

$$A_m = \varepsilon_0 \iint_{S_{p,q}} J_m(r) \cdot G_m(r/r_0)\, dS_0 \quad (7)$$

$$J_m = -\hat{a}_z \sin\left\{\frac{s\pi\left(z_0 + \frac{L}{2}\right)}{L}\right\} \quad (8)$$

and

$$G_m = \sum_{n=0}^{\infty}\sum_{m=0}^{\infty} \frac{\varepsilon_{0n}\varepsilon_{0m}}{2ab\Gamma_{nm}} e^{-\Gamma_{nm}|z - z_0|} \times \cos\frac{n\pi x}{a}\cos\frac{n\pi x_0}{a}\sin\frac{m\pi y}{b}\sin\frac{m\pi y_0}{b} \quad (9)$$

The integrals in eqn. 5 can be evaluated following procedures previously outlined in Reference 9 (see Appendix 7).

4 Discussion of results

A computer program has been written to accommodate the analysis described in preceding Sections, and this program is capable of providing estimates of the radi-

ation or scattering characteristics, in S-matrix or equivalent circuit form, of any longitudinal or transverse slot in the broadwall of rectangular waveguide. To demonstrate the effectiveness of the program the particularly interesting case of the resonance behaviour of a longitudinal offset slot in a rectangular waveguide has been examined in some detail.

In Fig. 4, computer predictions are presented of the resonant length of a square-ended longitudinal slot as a

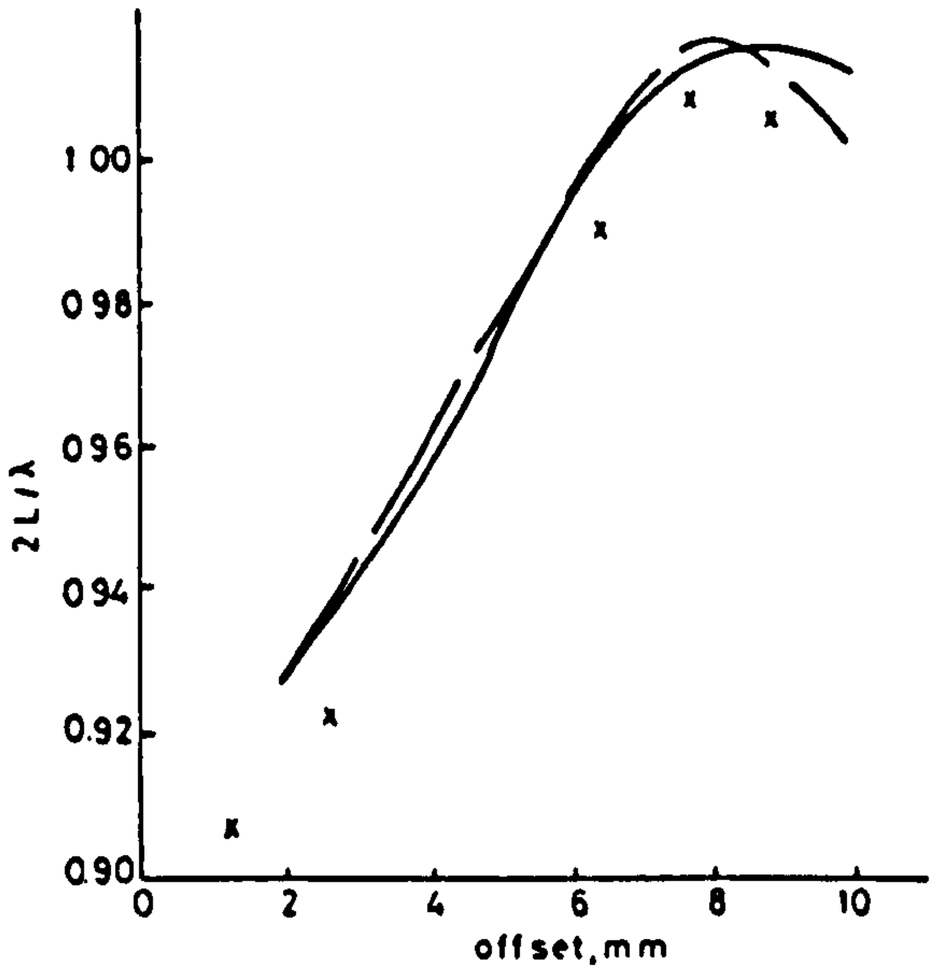

Fig. 4 *Resonant length as a function of offset for a rectangular longitudinal slot*

× Stern & Elliott's experimental results
——— moment method
- - - - moment method (sectioned slot)
frequency = 9 GHz, width = 1.5875 mm, thickness = 0.127 mm

function of its offset from the guide centre line. Two cases are presented, namely a conventional result and a sectioned slot result. Both cases use three trigonometrical basis functions. It can be seen that for this square-ended slot, example slot sectioning has very little effect on the computed results except for very large offsets. Clearly, therefore, there is little to be gained by sectioning for square-ended slots. Both curves show an approximate 1% deviation from the measured results of Stern & Elliott [6]. Agreement of a similar quality has also been demonstrated for transverse slot radiators in the broadface of rectangular waveguide.

Moment methods using pulse [11] rather than trigonometric basis functions are equally accurate. It has been found that three trigonometric basis functions provide results which are of essentially the same accuracy as 20 pulse functions (Fig. 5).

However, in practical slotted waveguide antennas square-ended slots are almost never used. Round-ended slots are much more common. It is pertinent, therefore, to attempt to model the round-ended slots, as discussed earlier, and some results from this modelling are shown in Fig. 6. This Figure also contains some measured results due to Stegen [4] to assist in the assessment of the computer predictions. Two theoretical cases are shown each of which is intended to model the Stegen experiment. These are, first, a square-ended slot model, and secondly a three-section slot model.

The Figure quite clearly demonstrates that the sectioned-slot model is an improvement, by as much as 2%, on the conventional square-ended slot model, even for this relatively crude 3-section case moving the computed result to within 2–3% of the measured result. That sectioning can provide more accurate theoretical predictions is thus not in doubt. Unfortunately, increased sectioning (beyond three sections) produces only small

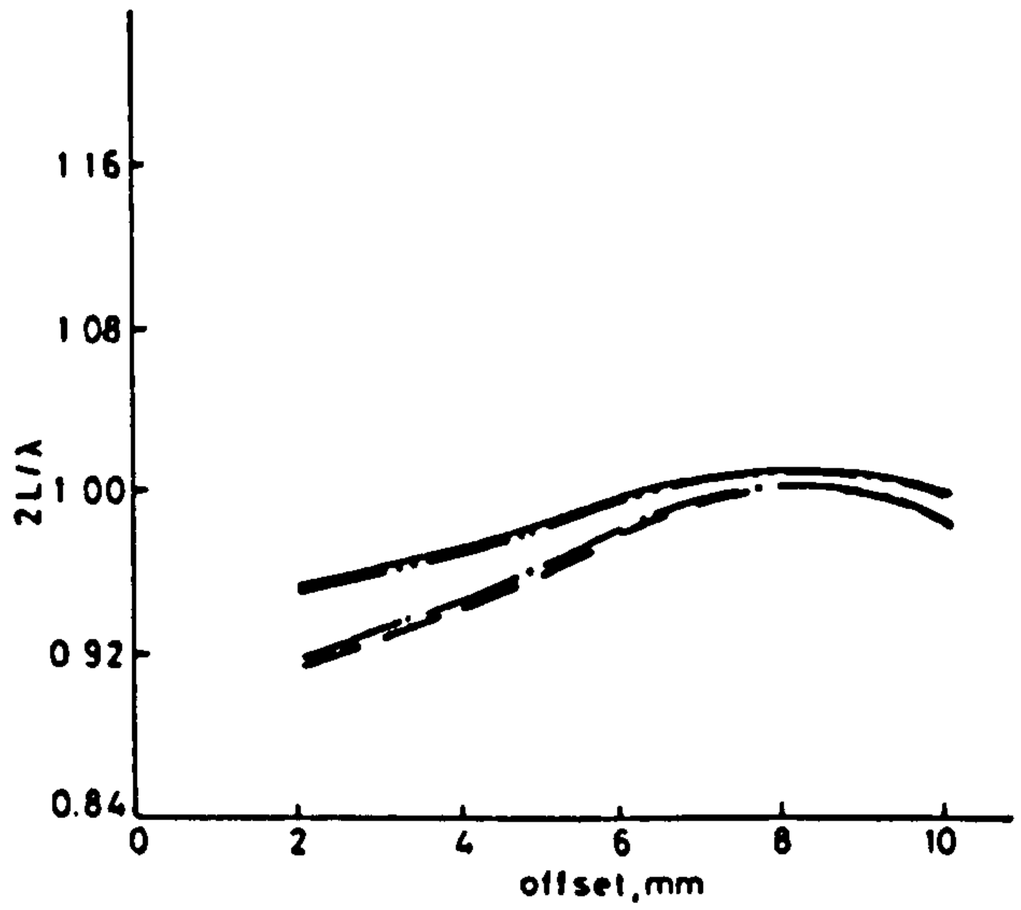

Fig. 5 *Resonant length as a function of offset for various longitudinal slots*

——— Vu Khac (T = 1.27 mm)
- - - - Vu Khac (T = 0 mm)
—··— moment method (T = 1.27 mm)
—·—· moment method (T = 0 mm)

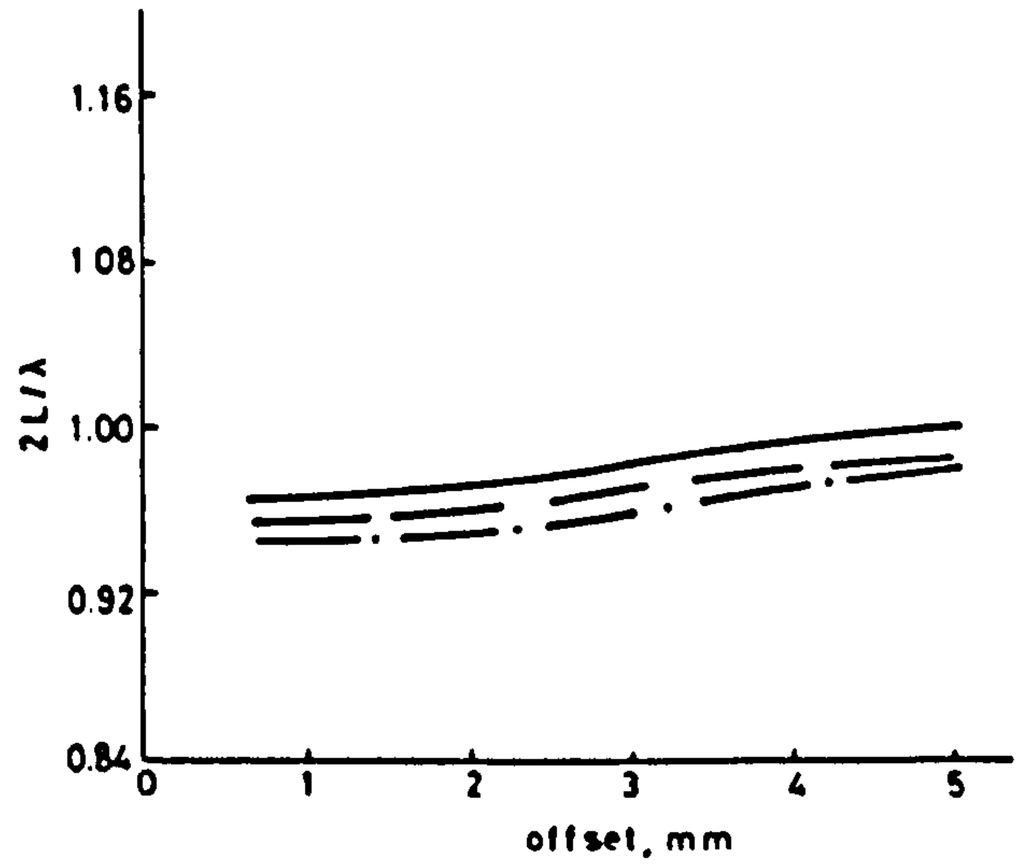

Fig. 6 *Resonant length as a function of offset for various longitudinal slots*

——— Stegen's experimental results
—·—· square ended slot
- - - - 3-section slot
frequency = 9.375 GHz, width = 1.5875 mm, thickness = 1.27 mm

additional improvements at the expense of disproportionate increases in computational effort.

5 Conclusions

The moment method of analysis of radiating slots in rectangular waveguides has conventionally been applied to square-ended slots in thin-walled waveguides. This paper extends the analysis to round-ended slots in thick-walled waveguides by using slot sectioning on the inner surface of the slot. The slot cavity and the outer-slot surface are adjusted to accommodate this modification. The technique is clearly more demanding in computational terms but not excessively so if trigonometrical basis functions are used. Improvements in accuracy of the order of 2% are observed for the predicted resonant lengths of longitudinal offset slots in thick-walled rectangular waveguides.

6 References

1 BETHE, H.A.: 'Theory of diffraction by small holes', *Phys. Rev.*, 1944, 66, pp. 161–182
2 OLINER, A.A.: 'The impedance properties of narrow radiating slots in the broadface of rectangular waveguide', *IRE Trans.*, 1957, AP-5, pp. 4–20
3 HARRINGTON, R.F.: 'Field computation by moment methods' (Macmillan 1968)
4 STEGEN, R.J.: 'Longitudinal shunt slot characteristics', Hughes Technical Memo 261, Hughes Aircraft Co., USA, 1951
5 PARK, P.K.: 'Characterization of slots in rectangular waveguide by method of moments with proper edge condition', IEEE International Symposium on Antennas and Propagation, 1982, pp. 572–574
6 STERN, G.T., and ELLIOTT, R.S.: 'Resonant length of longitudinal slots and validity of circuit representation: theory and experiment', *IEEE Trans.*, 1985, AP-33, (11), pp. 1264–1271
7 YEE, H.Y.: 'Impedance of a narrow longitudinal shunt slot in a slotted waveguide array', *IEEE Trans.*, 1974, AP-22, pp. 589–592
8 JOSEFSSON, L.: 'Analysis of longitudinal slots in rectangular waveguides'. Proceedings of URSI International Symposium EM wave theory, Budapest, Hungary, 1986, pp. 367–369
9 LYON, R.W., and SANGSTER, A.J.: 'Efficient moment method analysis of radiating slots in a thick-walled rectangular waveguide', *IEE Proc. H, Microwaves, Opt. & Antennas*, 1981, 128, (4), pp. 197–205
10 BUTLER, C.M., RAHMAT-SAMII, Y., and MITTRA, R.: 'Electromagnetic penetration through apertures in conducting surfaces', *IEEE Trans.*, 1978, AP-26, pp. 82–93
11 VU KHAC, T.: 'Studies of slot discontinuities in rectangular waveguides'. PhD Thesis, Monash University, 1974
12 VAN BLADEL, J.: 'Contribution of the ψ = constant mode to the modal expansion in waveguide', *IEE Proc. H, Microwave, Opt. & Antennas*, 1981, 128, (5), pp. 247–251
13 VU KHAC, T.V., and CARSON, C.T.: '$m = 0$, $n = 0$ mode and rectangular-waveguide slot discontinuity', *Electron. Lett.*, 1973, 9, (18), pp. 431–432

7 Appendix

The integrals involved in expr. 5 are conveniently divided into two types; those associated with the self coupling terms and the mutual coupling terms for sections of equal length, and those associated with the mutual coupling terms for sections of unequal length.

In the former case, eqn. 5 may be solved for the first sections in conjunction with eqns. 6–9 to give, after some mathematics, terms of the following form:

for $n = 0$

$$-\frac{j\omega\varepsilon_0}{ab}\left[W_1^2\left\{\left(\frac{1}{k^2}+\left(1-\left(\frac{s\pi}{kL}\right)^2\right)\left(\frac{b}{\pi}\right)^2\gamma(n,s)\right)\right\}\right.$$
$$\times L\delta_{is}+(si)\left(\frac{\pi}{kL}\right)^2\{1+(-1)^{(i+s)}\}$$
$$\left.\times\sum_{m=1}^{\infty}\frac{\varepsilon_{0m}(1-(-1)^i e^{-\Gamma_{nm}L})\left\{1+\left(\frac{k}{\Gamma_{nm}}\right)^2\right\}}{\Gamma_{nm}^3\left\{1+\left(\frac{s\pi}{\Gamma_{nm}L}\right)^2\right\}\left\{1+\left(\frac{i\pi}{\Gamma_{nm}L}\right)^2\right\}}\right] \quad (10a)$$

and for $n \neq 0$

$$-\frac{j\omega\varepsilon_0}{2ab}\sum_{n=1}^{\infty}\left[\left(\frac{a}{n\pi}\right)^2\left(\sin\frac{n\pi\left(x_a+\frac{W_1}{2}\right)}{a}\right.\right.$$
$$\left.-\sin\frac{n\pi\left(x_a-\frac{W_1}{2}\right)}{a}\right)\left(\sin\frac{n\pi\left(x_b+\frac{W_1}{2}\right)}{a}\right.$$
$$\left.\left.-\sin\frac{n\pi\left(x_b-\frac{W_1}{2}\right)}{a}\right)\left\{\left(1-\left(\frac{s\pi}{kL}\right)^2\right)\left(\frac{b}{\pi}\right)^2\gamma(n,s)\right\}L\delta_{is}\right.$$
$$+(si)\left(\frac{\pi}{kL}\right)^2\{1+(-1)^{(i+s)}\}$$
$$\left.\times\sum_{m=1}^{\infty}\frac{\varepsilon_{0m}(1-(-1)^i e^{-\Gamma_{nm}L})\left\{1+\left(\frac{k}{\Gamma_{nm}}\right)^2\right\}}{\Gamma_{nm}^3\left\{1+\left(\frac{s\pi}{\Gamma_{nm}L}\right)^2\right\}\left\{1+\left(\frac{i\pi}{\Gamma_{nm}L}\right)^2\right\}}\right] \quad (10b)$$

where

$$\gamma(n,s)=\frac{-\pi^2\cos b\sqrt{k^2-\left\{\left(\frac{s\pi}{L}\right)^2+\left(\frac{n\pi}{a}\right)^2\right\}}}{b\sqrt{k^2-\left\{\left(\frac{s\pi}{L}\right)^2+\left(\frac{n\pi}{a}\right)^2\right\}}}$$
$$\times\sin b\sqrt{k^2-\left\{\left(\frac{s\pi}{L}\right)^2+\left(\frac{n\pi}{a}\right)^2\right\}}$$

and x_a and x_b are the offsets for the sections in question and $W_1 = W/3$.

In the latter case eqn. 5 is solved with different limits of integration due to the differing section lengths, and produces terms which are typically of the form:

for $n = 0$

$$-\frac{j\omega\varepsilon_0}{ab}W_1^2\left[\frac{2\left(\frac{iL_a^2}{s^2\pi L_b}\right)}{\left[1-\left(\frac{iL_a}{sL_b}\right)^2\right]}(-1)^i\sin\frac{s\pi\left(\frac{L_a}{2}+\frac{L_b}{2}\right)}{L_a}\right.$$
$$-\sin\frac{s\pi\left(\frac{L_a}{2}-\frac{L_b}{2}\right)}{L_a}\left[\frac{1}{k^2}+\left(\frac{b}{\pi}\right)^2\left[1-\left(\frac{s\pi}{kL_a}\right)^2\right]\gamma(n,s)\right]$$
$$+\left(\frac{si\pi^2}{L_aL_b}\right)\sum_{m=1}^{\infty}\frac{\varepsilon_{0m}\left[1+\left(\frac{\Gamma_{nm}}{k}\right)^2\right]}{\Gamma_{nm}^5\left[1+\left(\frac{s\pi}{\Gamma_{nm}L_a}\right)^2\right]\left[1+\left(\frac{i\pi}{\Gamma_{nm}L_b}\right)^2\right]}$$
$$\times\left[\left\{\exp\left[-\Gamma_{nm}\left(\frac{L_a}{2}-\frac{L_b}{2}\right)\right]\right.\right.$$
$$-(-1)^i\exp\left[-\Gamma_{nm}\left(\frac{L_a}{2}+\frac{L_b}{2}\right)\right]\}$$
$$-(-1)^s\left\{\exp\left[-\Gamma_{nm}\left(\frac{L_a}{2}+\frac{L_b}{2}\right)\right]\right.$$
$$\left.\left.\left.-(-1)^i\exp\left[-\Gamma_{nm}\left(\frac{L_a}{2}-\frac{L_b}{2}\right)\right]\right\}\right] \quad (11a)$$

and for $n \neq 0$

$$-\frac{j\omega\varepsilon_0}{2ab}\sum_{n=1}^{\infty}\left(\frac{a}{n\pi}\right)^2\left(\left(\sin\frac{n\pi\left(x_a+\frac{W_1}{2}\right)}{a}\right.\right.$$
$$\left.\left.-\sin\frac{n\pi\left(x_a-\frac{W_1}{2}\right)}{a}\right)\right.$$
$$\times\left(\sin\frac{n\pi\left(x_b+\frac{W_1}{2}\right)}{a}-\sin\frac{n\pi\left(x_b-\frac{W_1}{2}\right)}{a}\right)$$

$$\times \left[\frac{2\left(\frac{iL_a^2}{s^2\pi L_b}\right)}{\left[1-\left(\frac{iL_a}{sL_b}\right)^2\right]} \left((-1)^i \sin \frac{s\pi\left(\frac{L_a}{2}+\frac{L_b}{2}\right)}{L_a} \right.\right.$$

$$\left.\left. - \sin \frac{s\pi\left(\frac{L_a}{2}-\frac{L_b}{2}\right)}{L_a} \right) \left(\frac{b}{\pi}\right)^2 \left[1-\left(\frac{s\pi}{kL_a}\right)^2\right] \gamma(n,s) \right.$$

$$\left. + \left(\frac{si\pi^2}{L_a L_b}\right) \sum_{m=0}^{n} \frac{\varepsilon_{0m}\left[1+\left(\frac{\Gamma_{nm}}{k}\right)^2\right]}{\Gamma_{nm}^5 \left[1+\left(\frac{s\pi}{\Gamma_{nm}L_a}\right)^2\right]\left[1+\left(\frac{i\pi}{\Gamma_{nm}L_b}\right)^2\right]} \right.$$

$$\times \left[\left\{ \exp\left[-\Gamma_{nm}\left(\frac{L_a}{2}-\frac{L_b}{2}\right)\right] \right.\right.$$

$$\left. - (-1)^i \exp\left[-\Gamma_{nm}\left(\frac{L_a}{2}+\frac{L_b}{2}\right)\right]\right\} - (-1)^s$$

$$\times \left\{ \exp\left[-\Gamma_{nm}\left(\frac{L_a}{2}+\frac{L_b}{2}\right)\right] \right.$$

$$\left.\left. \left. - (-1)^i \exp\left[-\Gamma_{nm}\left(\frac{L_a}{2}-\frac{L_b}{2}\right)\right]\right\}\right] \right] \quad (11b)$$

where L_a and L_b are the lengths of the appropriate sections.

The ψ = constant mode must also be included in the complete solution for the longitudinal slot. This mode may be modified as follows for the sectional slot:

$$-\frac{3W_1^2(1-(-1)^i)(1-(-1)^s)\times(L_1+2L_2)}{j\omega\mu_0 abis\pi^2} \quad (12)$$

where L_1 and L_2 are the lengths of the middle section and outer section, respectively.

The complete solution for integral expression 5 is

$$\sum \text{term (eqn. 10)} + \sum \text{term (eqn. 11)} + \text{term (eqn. 12)} \quad (13)$$

The summation of eqn. 10 includes all self coupling terms and mutual coupling terms for sections with the same length. The eqn. 11 summation includes all mutual coupling terms for differing lengths.

The contribution of the incident field remains to be calculated for the new slot arrangement, which is given by

$$h_i = -\iint_S f_i \hat{a}_z \cdot \{n \times H_i(r)\}\, ds \quad (14)$$

and which depends on the slot orientation. The incident fields are given by

$$E_y^+ = -j\omega\mu_0 \phi \sin\frac{\pi x}{a} e^{-j\beta_\theta z}\hat{a}_y \quad (15)$$

$$H_x^+ = j\beta_\theta \phi \sin\frac{\pi x}{a} e^{-j\beta_\theta z}\hat{a}_x \quad (16)$$

$$H_z^+ = \frac{\pi}{a}\phi \cos\frac{\pi x}{a} e^{-j\beta_\theta z}\hat{a}_z \quad (17)$$

where

$$\phi = (kZ_0\beta_\theta ab)^{-1/2} \quad (18)$$

and $\hat{a}_x$, $\hat{a}_y$ and $\hat{a}_z$ are unit vectors.

Substituting eqns. 15–17 into eqn. 14 gives, for a longitudinal slot

$$h_i = \sum_{D=1}^{3} \phi \left[\sin\frac{\pi\left(X_D+\frac{W_1}{2}\right)}{a} - \sin\frac{\pi\left(X_D-\frac{W_1}{2}\right)}{a} \right]$$

$$\times \frac{\overline{L_D}}{\left(\frac{i\pi}{L_D}\right)^2-\beta_\theta^2} \begin{cases} 2\cos\beta_\theta L_D/2 & i \text{ odd} \\ 2j\sin\beta_\theta L_D/2 & i \text{ even} \end{cases} \quad (19)$$

where X_D is the offset to the centre line of the section, and L_D is the length of the section.

References

Number

2.1 Bethe, H.A., "Theory of diffraction by small holes", Physical Review, Vol. 66, pp. 163-182, 1944.

2.2 Levine, H., & Schevinger, J., "On the theory of electromagnetic wave diffraction by an aperture in an infinite plane conducting screen", Symp. of the theory of e.m. waves, p. 355, 1950.

2.3 Oliner, A.A., "The impedance properties of narrow radiating slots in the broadface of rectangular waveguide", IRE Trans., Vol. AP-5, pp. 4-20, 1957.

2.4 Sangster, A.J. & Hawkins, D.C., "Scattering parameters of an arbitrarily shaped aperture in waveguide", Proc. IEE, Vol. 119, pp. 1465-1466, 1972.

2.5 Das, B.N., & Sanyal, G.S., "Network parameters of a waveguide broadwall slot radiator", Proc. IEE, Vol. 117, No. 1, pp. 41-44, 1970.

2.6 Harrington, R.F., "Field computation by moment methods", Macmillan 1968.

2.7 Vu Khac, T., "Studies of slot discontinuities in rectangular waveguides", Ph.D. Thesis, Monash University, 1974.

2.8 Lyon, R.W. & Sangster, A.J., "Efficient moment method analysis of radiating slots in a thick-walled waveguide", Proc. IEE, Vol. 128, Pt.H, No. 4, pp. 197-205, 1981.

2.9 Sangster, A.J. & McCormick, A.H.I., "Some observations on the computer aided design/synthesis of slotted waveguide antennas", Int. J. Electronics, Vol. 62, No. 5, pp. 641-662, 1987.

2.10 Lord Rayleigh, "On the incidence of aerial electric waves upon small obstacles in the form of ellipsoids or elliptic cylinders, and on the passage of electric waves through a circular aperture in a conducting screen", phil. Mag., Series 5, Vol. 4, pp. 28-52, 1897.

2.11 Stratton, J.A., "Electromagnetic theory", (McGraw-Hill, 1941).

2.12 Bouwkamp, C.J., "On Bethe's Theory of Diffraction by Small Holes", Philips Res. Rep. 5, pp. 321-332, 1950.

2.13 Levine, H. and Schwinger, J., "On the Theory of Diffraction by an Aperture in an Infinite Plane Conducting Screen", Symposium on the Theory of Electromagnetic Waves, June, 1950.

2.14 Watson, W.H., "Resonant Slots", IEE Journal Vol 93, Part 3A, pp. 747-777, 1946.

2.15 Stevenson, A.F., "Theory of slots in rectangular waveguide", Jour. App. Phys., Vol. 19, pp. 24-38, 1948.

2.16 Marcuwitz, N. & Schwinger, J., "On the Representation of the Fields Produced by Currents and Discontinuities in Waveguides", Jrnl. Appl. Phys., Vol. 22, pp. 806-819, 1951.

2.17 Lewin, L., "Advanced Theory of Waveguides", Iliffe and Sons, 1951.

2.18 Marcuwitz, N., "The Representation, Measurement and Calculation of Equivalent Circuits for Waveguide Discontinuities With Application to Rectangular Slots", Poly. Inst. of Brooklyn Rept., 1949.

2.19 Larson, R.W. & Powers, V.M., "Slots in dielectrically loaded waveguide", Radio science, vol 1 (New series), pp. 31-35, 1966.

2.20 Bailey, M.C., "The impedance properties of dielectric covered narrow radiating slots in the broad face of a rectangular waveguide", IEEE Trans, vol A-18, pp. 96-603, 1970.

2.21 Sangster, A.J. & Hawkins, D.C., "Radiating Apertures in Corrugated Rectangular Waveguide", Electronic Letters, Vol. 15, pp. 329-331, 1973.

2.22 Harrington, R.F., "Time-Harmonic electromagnetic fields", (McGraw-Hill, 1961).

2.23 Vu Khac, T., "Solution of some waveguide discontinuities by the method of moments", IEEE Trans., Vol. MTT-20, pp416-417, 1972.

2.24 Vu Khac, T. & Carson, C.T., "Coupling by slots in rectangular waveguide with arbitrary wall thickness", Electronic Letters, Vol. 8, pp456-458, 1972.

2.25 Vu Khac, T. & Carson, C.T., "Impedance properties of longitudinal slot antenna in the broadface of rectangular waveguide", IEEE Trans., Vol. AP-21, pp. 708-710, 1973.

2.26 Sangster, A.J. & Lyon, R.W., "Moment method analysis of a T-shaped slot radiator in bifurcated waveguide", IEE Proc. Vol. 129, Pt. H, No. 6, pp299-306, 1982.

2.27 Lyon, R.W. & Hizal, A., "A moment method analysis of narrow dielectric covered rectangular slots in the broadwall of waveguide", Proceedings of International Conference on Antennas & Propagation, pp. 150-3, 1983.

2.28 Stern, G.T. & Elliott, R.S., "Resonant length of longitudinal slots and validity of circuit representation: theory and experiment". IEEE Trans., Vol. AP-33, No. 11, pp. 1264-1271, 1985.

2.29 Park, P.K., "Characterization of slots in rectangular waveguide by method of moments with proper edge condition", IEEE Int. Symp. AP-S 1982, pp. 572-574.

2.30 Van Bladel, J., "Small hole coupling of resonant cavities and waveguides", IEE Proc., Vol. 117, pp1098-1104, 1970.

2.31 Van Bladel, J., "Small holes in a waveguide wall", Proc. IEE, Vol. 118, No. 1, pp. 43-50, Jan. 1971.

2.32 Levy, R., "Analysis and synthesis of waveguide multi-aperture directional couplers", IEEE Trans., Vol. MTT-16, pp. 995-1006, 1968.

2.33 Cohn, S.B., "Electric polarisability of apertures of arbitrary shape", IRE Proc., Vol. 40, pp. 1069-1071, 1952.

2.34 McDonald, N.A., "Electric and magnetic coupling through small apertures in shield walls of any thickness", IEEE Trans., Vol. MTT-20, pp. 689-695, 1972.

2.35 Levy, R., "Improved single and multi-aperture waveguide coupling theory", IEEE Trans., Vol. MTT-28, No. 4, pp. 331-338, 1980.

2.36 Collin, R.E., "Rayleigh scattering and power conservations", IEE. Trans., Vol. AP-29, No. 5, pp795-798, Sept. 1981.

2.37 Cheng, D.K., "Generalised hybrid network parameters for electromagnetic coupling between dissimilar regions through a small aperture", IEE Proc., Vol. 129, Pt. H, No. 6, pp. 325-332, 1982.

2.38 Schelkunoff, S.A., "A mathematical theory of linear arrays", BSTJ, 22, pp80-107, 1943.

2.39 Dolph, C.L., "A current distribution for broadside arrays which optimizes the relationship between beam width and side-lobe level", Proc. IRE 34, pp. 335-348, 1946.

2.40 Balakrishnan, N. & Sethuraman, R., "Easy generation of Dolph-Chebyshev excitation coefficients", Proc. IEEE, 1981, 69, (11), pp. 1508-1509.

2.41 Zielinski, A., "Matrix formulation for Dolph-Chebyshev beam-forming", Proc. IEEE, 74, (12), pp. 1799-1800.

2.42 Barbiere, D., " A method of calculating the current distribution of Tchebyscheff arrays", J. Appl. Phys., 1954, 25, (1), pp.121-124.

2.43 Van der Maas, G.J., "A simplified calculation for Dolph-Tchebyscheff arrays", J. Appl. Phys., 1954, 25, (1), pp. 121-124.

2.44 Salzer, H.E., "Note on the Fourier coefficients for Chebyshev patterns", Proc. Inst. Elec. Eng. (London), 1956. 103C, pp. 286-288.

2.45 Brown, J.L., Jr, "A simplified derivation of the Fourier coefficients for Chebyshev patterns", Proc. Inst. Elec. Eng. (London), 1957, 105C, pp. 167-168.

2.46 Brown, J.L. Jr, "On the determination of excitation coefficients for a Tchebyscheff pattern", IRE Trans. Antennas Propagat., 1962, 10, pp. 215-216.

2.47 Bresler, A.D., "A new algorithm for calculating the current distribution of Dolph-Chebyshev arrays", IEEE Trans. Antennas Propagat, 1980, 28, (6), pp. 951-952.

2.48 Ares, F. & Moreno, E. "New Methods for Computing Dolph-Chebyshev arrays and its comparison with other methods", IEE. Proc Vol 135. Pt H, No 2, 1988.

2.49 Taylor, T.T., "Design of line-source antennas for narrow beamwidth and low side lobes.'", IRE Trans. Antennas Propogat. 3, 16-28 (1955).

2.50 Woodward, P.M., "A method of calculating the field over a plane aperture required to produce a given polar diagram", J. Inst. Elec. Eng., (London), pt. IIIA, vol. 93, pp. 1554-1558, 1947.

2.51 Schell, A.C. and Ishimaru, A., "Antenna pattern synthesis", in Antenna Theory, Part I, Collin, R. and Zucker, F., Eds. New York: McGraw-Hill, 1969.

2.52 Steyskal, H., "On antenna power pattern synthesis", IEEE Trans. Antennas Propagat., vol. Ap-18, pp. 123-124, Jan., 1970.

2.53 Stutzman, W.L., "Synthesis of shaped-beam radiation patterns using the iterative sampling method", IEEE Tans. Antennas Propagat., vol. AP-19, pp. 36-41, Jan., 1971.

2.54 Fong, T.S. & Birgenheier R.A., "Method of conjugate gradients for antenna pattern synthesis", Radio Sci., vol. 6, pp. 1123-1130, Dec., 1971.

2.55 Chakraborty, A., Das, B.N. & Sanyal, G.S., "Determination of phase functions for a desired on-dimensional pattern", IEEE Trans. Antennas Propagat., vol. AP-29, pp. 505-506, May, 1981.

2.56 Chakraborty, A., Das, B.N. & Sanyal, G.S., "Beam shaping using nonlinear phase distribution in a uniformly spaced array", IEEE Trans. Antennas Propagat., vol. AP-30, pp. 1031-1034, Sept, 1982.

2.57 Elliott, R.S., & Stern, G.J., "A new technique for shaped beam synthesis of equispaced arrays", IEEE Trans. Antennas Propagat., vol. AP-32, No. 10, pp. 1129-1133, 1984.

2.58 Tsunoda, Y. & Goto, N., "Non uniformly spaced slot area antenna with low side lobe pattern", IEE Proc. vol. 133 Pt. H, No. 2 pp. 155-158, 1986.

2.59 Fry, D.W., "Slotted linear arrays", J. Inst. Elec. Eng., Part 3 93, pp. 43-45, 1946.

2.60 Kaminow, L.P. & Stegen, R.J., "Waveguide Slot Array Design", Tech. Memo. No. 348 (AD 63 600), pp. 64-66. Hughes Aircraft Co., ASTIA, Airlington, Virginia, 1954.

2.61 Dion, A., "Nonresonant slotted arrays", IRE Trans. Antennas Propagat. 6, pp. 360-365, 1958.

2.62 Jasik, H., "Antenna Engineering Handbook", McGraw-Hill, 1961.

2.63 Collin, R.E. & Zucker, F.J., "Antenna Theory", Pt. 1, McGraw-Hill, 1969.

2.64 Young, L., "Advances in Microwaves", Academic Press, 1971.

2.65 Edelberg, S. & Oliner, A.A., "Mutual coupling in large antenna arrays, Pt. 1 slot arrays", IRE Trans. Antennas Propagat. vol. AP-8, pp. 286-297, May, 1960.

2.66 Edelberg, S. & Oliner, A.A., "Mutual coupling in large antenna arrays, Pt. 2 compensation effects", IRE Trans. Antennas Propagat. vol AP-8, pp. 360-367, July, 1960.

2.67 Ehrlich, J.J. & Short, J., "Mutual coupling considerations in linear slot array design, Proc. IRE, vol. 42, pp. 956-961, June, 1954.

2.68 Kay, A.F. & Simmons, A.J., "Mutual coupling of shunt slots", IRE Trans. Antennas Propagat. vol. AP-8, pp. 389-400, July, 1960.

2.69 Elliott, R.S. & O'Loughin, W., "The design of slot arrays including internal mutual coupling", IEEE Trans. Antenna Propagat. vol. AP-34, No. 9, pp. 1149-1154, 1986.

2.70 Das, B.N. & Sanyal, G.S., "Mutual impedance between two resonance slot radiators", IEE Proc. vol. 118, No. 11, pp. 1535-1538, 1971.

2.71 Booker, H.G., "Slot aerials and their relationship to complementary wire aerials (Babinet's Principle)", JIEE (London), 93, Part IIIA, pp. 620-626, 1946.

2.72 Carter, P.S., "Circuit relations in radiating systems and applications to antenna problems", Proc. IRE, Vol. 20, pp. 1004-1041, June 1932.

2.73 Brown, G.H., "Directional antennas", Proc. IRE, Vol. 25, pp. 78-145, January 1937.

2.74 Cox, C.R., "Mutual impedance between vertical antennas of unequal heights", Proc. IRE, Vol. 35, pp. 1367-1370, November 1947.

2.75 King, H.E., "Mutual impedance of unequal length antennas in echelon", IRE Trans. on Antennas and Propagation, Vol. AP-5, pp. 306-313, July 1957.

2.76 Baker, H.C. & Lagrone, A.H., "Digital implementation of the mutual impedance between thin dipoles", IRE Trans., Vol. AP-10, pp. 172-178, 1962.

2.77 Hansen, R.C., "Formulation of echelon dipole mutual impedance for computation", IEEE Trans., Vol. AP-20, pp780-781, 1972.

2.78 Hansen, R.C. & Brunner, G., "Dipole mutual impedance for design of slot arrays", Microwave Journal, pp54-56, Dec. 1979.

2.79 Elliott, R.S. & Kurtz, L.A., "The design of small slot arrays", IEEE Trans., Vol. AP-26, No. 2, pp. 214-219, 1978.

2.80 Elliott, R.S., "On the design of travelling wave-fed longitudinal shunt slot arrays", IEEE Trans., Vol. AP-27, No. 5, pp. 717-720, 1979.

2.81 Elliott, R.S., "An improved design procedure for small arrays of shunt slots", IEEE Trans., AP-31, No. 1, pp. 48-53, 1983.

2.82 Malherbe, J.A.G. & Davidson, D.B., "Mutual impedance for half-cosinusoid slot voltage distribution: an evolution", IEEE Trans., Vol. AP-32, No. 9, pp. 990-991, 1984.

3.1 Lyon, R.W., "An investigation of apertures in dual mode rectangular waveguide for variable polarisation arrays", PhD thesis, Heriot Watt University, 1979.

3.2 Kantorovich, L.V. & Krylov, V.I., "Approximate methods of higher analysis", Fourth edition (translated Benster, C.D.) John Wiley & Sons Inc., New York, 1959.

3.3 Jones, D.S., "A critique of the variational method in scattering problems", IRE Trans. Antennas Propagat. vol. AP-4 No. 3, pp. 297-301, 1956.

3.4 Collin, R.E., "Field theory of guided waves", McGraw Hill Book Co., 1960.

3.5 Collin, R.E., "On the incompleteness of E and H modes in waveguides", Can. J. Phys., vol. 51, pp. 1135-1140, 1973.

3.6 Rahmat-Samii, Y., "On the question of computation of dyadic Green's function at the source region in waveguides and cavities", IEEE Trans., vol. MTT-23, pp. 762-765, 1975.

3.7 Vu Khac, T. & Carson, C.T., "m = 0, n = 0 mode and rectangular-waveguide slot discontinuity", Electron. Lett., 1973, 9, pp. 431-432.

3.8 Van Bladel, J., "Contribution of the ψ = constant mode to the modal expansion in waveguide", IEE Proc., Vol. 128, Pt. H, pp. 247-251, 1981.

3.9 Silver, S., "Microwave antenna theory and design", Dover Publication Inc., New York, 1965.

3.10 Josefsson, L., "Analysis of longitudinal slots in rectangular waveguides", Proc. URSI Int. Symp. EM Wave Theory, Budapest pp. 367-369, 1986.

3.11 Sinha, S.N., "A generalised network formulation for a class of waveguide coupling problems", Proc. IEE, Vol. 134, Pt.H, No. 6, pp. 502-508, 1987.

3.12 Yee, H.Y., "Impedance of a narrow longitudinal shunt slot in a slotted waveguide array", IEEE Trans. Antennas Propagat., AP-22, 1974, pp. 589-592.

3.13 Wang, H. & Wan, W., "Moment method analysis of a feeding system in a slotted-waveguide antenna", IEE Proc. Pt. H, (to be published).

4.1 Sangster, A.J. & McCormick, A.H.I., "The moment method applied to round-ended slots", Proc. IEE, Vol. 134, Pt. H, No. 3, pp. 310-314, 1987.

4.2 Putman, J.L., "Input impedances of centre fed slot aerials near half-wave resonance"., Jour IEE, Vol. 95, pt. IIIA, pp. 290-294, 1948.

4.3 Crompton, J.W., "Impedance/frequency characteristics of some slot aerials", Jour. IEE, Vol. 96, pt. IIIA, pp. 39-44, 1949.

4.4 Watson, W.H., "The physical principles of waveguide transmission and antenna systems", (Clarendon Press, 1947).

4.5 Sangster, A.J. & McCormick, A.H.I., "Resonance characteristics of waveguide slot radiators with moderate width to length ratios", Proc. IEE, Pt. H, (To Be Published).

4.6 Stegen, R.J., "Longitudinal shunt slot characteristics", Hughes Tech. Memo. 261, Hughes Aircraft Co., U.S.A., 1951.

5.1 Wong, N.F., Tang, R. & Okubo, G.A., "Investigation of characteristics and practical implementation of arbitrary polarised radiators in slot arrays", Hughes Aircraft Co., Ground Systems Group, Fullerton, California, U.S.A., Feb. 1971.

5.2 McGrane, A., "Characterisation of slots in waveguide using a resonant cavity technique", Plessey Radar Ltd, Radar and Environmental Systems Unit Report, IWR 3070, Isle of Wight, 1979.

6.1 Elliott, R.S., "Antenna theory and design", (Prentice Hall Inc., 1981).

6.2 Rudge, A.W., "The handbook of antenna design", Vol.2, (Peter Peregrinus Ltd., London, 1983).

6.3 Mautz, J.R. & Harrington, R.F., "Computational methods for antenna pattern synthesis", IEEE Trans., Vol. AP-23, No. 4, pp. 507-512, July 1975.

6.4 Narasimhan, M.S., Varadarangan, K. & Christopher, S., "A new technique of synthesis of near or far-field patterns of arrays", IEEE Trans., Vol., AP-34, No. 6, pp. 773-778, June 1986.

6.5 Ng, T.S., "Generalised array pattern synthesis using the projection matrix", Proc. IEE, Vol. 132, Pt. H, No. 1, pp. 44-46, February, 1985.

6.6 Elliott, R.S., "Longitudinal shunt slots in rectangular waveguide: Pt. 1, Theory", Rantec, Calabasa, California, Rantec Report No. 72022 - TN - 1.

6.7 Sangster, A.J. & Hawkins, D.C., "The design of the AR3D antenna", Plessey Radar Ltd., Isle of Wight laboratory, IWR 2603, 1972.

8.1 Elliott, R.S. & Johnson, R.N., "Experimental results on a linear array for asymmetric side lobes", IEEE Trans. Antennas Propagat., vol. AP-26, pp. 351-352, 1978.

8.2 Bergmann, J., Brown, R.C., Clarricoats, P.J.B. & Zhou, H. "Synthesis of shaped beam reflector antenna patterns", IEE Proc. Pt. H, vol. 135, No. 1, pp. 48-53, Feb., 1988.

8.3 Marcuvitz, N., "Waveguide handbook", McGraw-Hill Inc., 1951.

9.1 Das, B.N., Raju, G.S.N. & Chakraborty, A., "Investigation on a new type of inclined slot coupled T-junction", IEE Proc.

Pt. H, vol. 134, No. 5, pp. 473-476, 1987.

A1.1 Sangster, A.J. & Hawkins, D.C., "Analysis of a non resonant slot in waveguide", Plessey Radar Ltd., Isle of Wight laboratory, IWR 2503, 1971.

A1.2 Hildebrand, F.B., "Introduction to numerical methods", McGraw-Hill, 1956.